Argonne NATIONAL LABORATORY

ANL-10/06
ISSN 1931-5015
May 2010

APS Science 2009

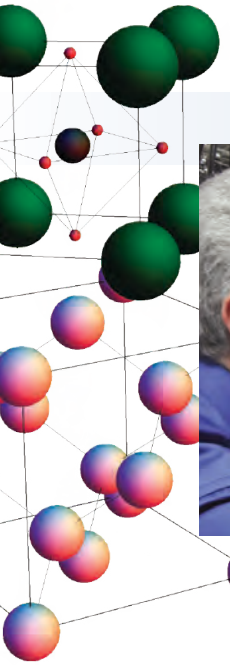

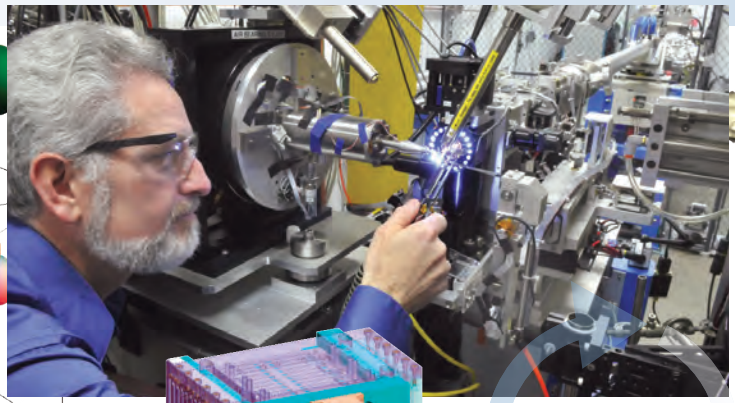

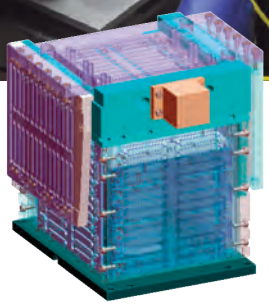

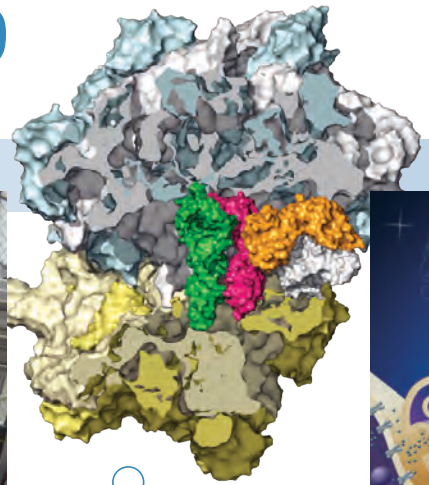

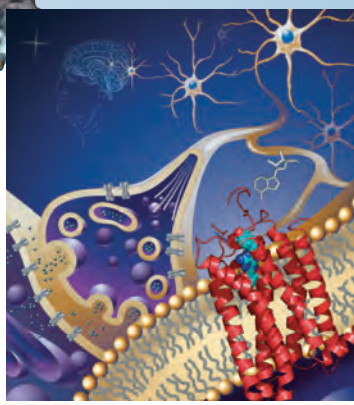

Research and Engineering Highlights
from the Advanced Photon Source
at Argonne National Laboratory

ANL-10/06
ISSN 1931-5015
May 2010

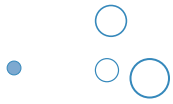

The Advanced Photon Source at Argonne National Laboratory is supported by the U.S. Department of Energy, Office of Science, Office of Basic Energy Sciences, under Contract No. DE-ACO2-06CH11357

About Argonne National Laboratory

Argonne is a U.S. Department of Energy laboratory managed by UChicago Argonne, LLC under contract DE-ACO2-06CH11357. The Laboratory's main facility is outside Chicago, at 9700 South Cass Avenue, Argonne, Illinois 60439. For information about Argonne and its pioneering science and technology programs, see www.anl.gov.

Availability of This Report

This report is available, at no cost, at http://www.osti.gov/bridge. It is also available on paper to the U.S. Department of Energy and its contractors, for a processing fee, from:

U.S. Department of Energy
Office of Scientific and Technical Information
P.O. Box 62
Oak Ridge, TN 37831-0062
phone (865) 576-8401
fax (865) 576-5728
reports@adonis.osti.gov

Disclaimer

ANL-10/06
ISSN 1931-5015
May 2010

APS Science 2009

The Annual Science Report
of the Advanced Photon Source
at Argonne National Laboratory

Argonne is a U.S. Department of Energy laboratory managed by UChicago Argonne, LLC
The Advanced Photon Source is funded by the U.S. Department of Energy, Office of Science, Office of Basic Energy Sciences

Welcome from the Director

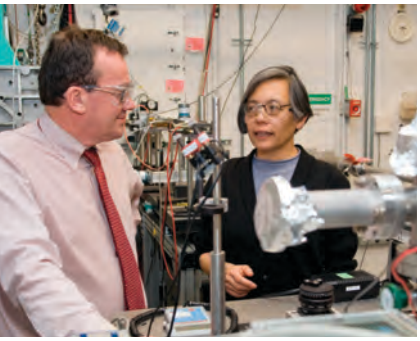

Murray Gibson (left), Argonne Associate Laboratory Director for Photon Sciences, and X-ray Science Division Director Linda Young in the 7-ID research station on the APS experiment hall floor.

It is my pleasure to introduce the 2009 annual report of the Advanced Photon Source. This was a very good year for us. We operated with high reliability and availability, despite growing problems with obsolete systems, and our users produced a record output of publications. The number of user experiments increased by 14% from 2008 to more than 3600. We congratulate the recipients of the 2009 Nobel Prize in Chemistry—Venkatraman Ramakrishnan (Cambridge Institute for Medical Research), Thomas Steitz (Yale University), and Ada Yonath (Weizmann Institute) - who did a substantial amount of this work at APS beamlines.

Thanks to the efforts of our users and staff, and the ongoing counsel of the APS Scientific Advisory Committee, we made major progress in advancing our planning for the upgrade of the APS (APS-U), producing a proposal that was positively reviewed. We hope to get formal approval in 2010 to begin the upgrade. With advocacy from our users and the support of our sponsor, the Office of Basic Energy Sciences in the Department of Energy (DOE) Office of Science, our operating budgets have grown to the level needed to more adequately staff our beamlines. We were also extremely fortunate to have received $7.9 M in American Recovery and Reinvestment Act ("stimulus") funding to acquire new detectors and improve several of our beamlines. The success of the new Linac Coherent Light Source at Stanford, the world's first x-ray free-electron laser, made us particularly proud since the undulators were designed and built by the APS.

Among other highlights, we note that more than one-quarter of the 46 Energy Frontier Research Centers, funded competitively across the U.S. in 2009 by the DOE, included the Advanced Photon Source in their proposed work, which shows that **synchrotron radiation, and the APS in particular, are central to energy research**. While APS research covers everything from fundamental to applied science (reflected by the highlights in this report), the challenge of sustainable energy provides an opportunity for expanded involvement with industrial research.

We were privileged to recruit several outstanding new leaders at the APS. Linda Young, from Argonne's Chemical Sciences Division, became the new Director of the X-ray Science Division (XSD). Chris Jacobsen (from Stony Brook University) has been added to Linda's team as an XSD Associate Division Director, joining George Srajer. Alexander (Sasha) Zholents (formerly of Berkeley Lab) became Director of the Accelerator Systems Division. Sasha is the inventor of the short-pulse x-ray scheme that we plan to implement in the APS-U to obtain very high average brightness, broadband, 1-ps x-ray pulses. Walter Lowe (formerly of Howard University) has taken a new position as senior advisor for outreach and development of the user community. Walter's role is to increase the diversity of the user community (with diversity read broadly to include

users, institutions, and technical disciplines that are underrepresented at APS). Walter is also leading an effort to increase access for industrial users. I am confident that we have in place a great team to help our users and the APS take fullest advantage of the APS-U opportunity.

In planning with users for the proposed APS-U, we focused on the need to study "real materials under real conditions in real time" on spatial and temporal scales unavailable today. Only by studying materials as they are made—or as they perform—in difficult environments can we solve the grand challenge of higher-performance, sustainable materials for energy and health. The proposed APS-U will improve the brightness of penetrating x-rays produced by the APS over 100 times, and support our efforts in developing state-of-the-art instruments to address these challenges. Take a look at the potential impact of the APS-U as spelled out in our "Proposal for approval of Conceptual Design" (http://www.aps.anl.gov/Upgrade/Documents/aps_cdzero.pdf). **The next few years promise to be an exciting time**.

J. Murray Gibson
(jmgibson@aps.anl.gov)

The APS Scientific Advisory Committee

Photographed at the APS January 21, 2010

***Front row**: Seated in chairs (left to right): Miles V. Klein (University of Illinois at Urbana-Champaign), William Stirling, Chair (European Synchrotron Radiation Facility), J. Murray Gibson (Argonne National Laboratory). **Second row**: Seated on chair arms (left to right): Soichi Wakatsuki (High Energy Accelerator Research Organization), Janos Kirz (Lawrence Berkeley National Laboratory), Louise N. Johnson, DBE, (University of Oxford Laboratory of Molecular Biophysics), Ka Yee C. Lee (The University of Chicago). **Third row**: Standing (left to right): Glenn Waychunas (Lawrence Berkeley), John Corlett (Lawrence Berkeley National Laboratory), Tom Irving, PUC Chair, **ex officio** (Illinois Institute of Technology), Roger A. Leach (E.I. DuPont de Nemours & Company), Philip H. Bucksbaum (Stanford University), Howard M. Einspahr (Bristol-Myers Squibb, retired), Dan Neumann (National Institute of Standards and Technology), Paul Fuoss, APSUO Chair, **ex officio** (Argonne National Laboratory), Britt Hedman (Stanford Synchrotron Radiation Lightsource). **Not pictured**: J. Friso Van der Veen (Paul Scherrer Institut).*

The APS Upgrade – A Report from the Upgrade Steering Committee

The Path to Becoming a DOE Project

A considerable amount of effort has gone into the development and refinement of a plan to enhance and expand the capabilities of the Advanced Photon Source since the last issue of *APS Science* (2008), including a name change for this effort. This project, originally called the APS Renewal, is now known as the APS Upgrade Project, or APS-U for short. The APS submitted a white paper to the Department of Energy (DOE) Office of Basic Energy Sciences (BES) in November 2008 making the broad case for investment in the facility to maintain its leadership capabilities for the next decade and beyond. Working closely with the DOE, the APS then developed a "Proposal for Approval of Conceptual Design (CD-0)" in May 2009 (http://www.aps.anl.gov/Upgrade/Documents/aps_cdzero.pdf). That document was organized around two themes ideally suited for study with the upgraded APS: “Mastering Hierarchical Structures through Imaging” and “Real Materials under Real Conditions in Real Time.” A BES-conducted peer evaluation of the proposal for the APS-U provided strong support for the decision to proceed toward Critical Decision Zero–Approval of Mission Need (CD-0). To further develop the case for Mission Need, BES assembled an integrated project team from Argonne, the DOE Office of Science, and the DOE Argonne Site Office. The APS Scientific Advisory Committee (SAC) met at the APS in October 2009 to hone the scientific case for the APS-U and provide guidance on project scope (i.e., identify the “flagship” beamlines) for the CD-0. Their advice was folded into a briefing book that provided more detailed information regarding our upgrade plans to assist the DOE in their planning process.

The APS Upgrade Steering Committee

Photographed at the APS April 5, 2010

Left to right: *Michael Borland, Bob Fischetti, Paul Fuoss, Denny Mills, John Maclean, George Srajer, and Rod Gerig.*
Not pictured: *Tom Irving, Dan Neumann.*

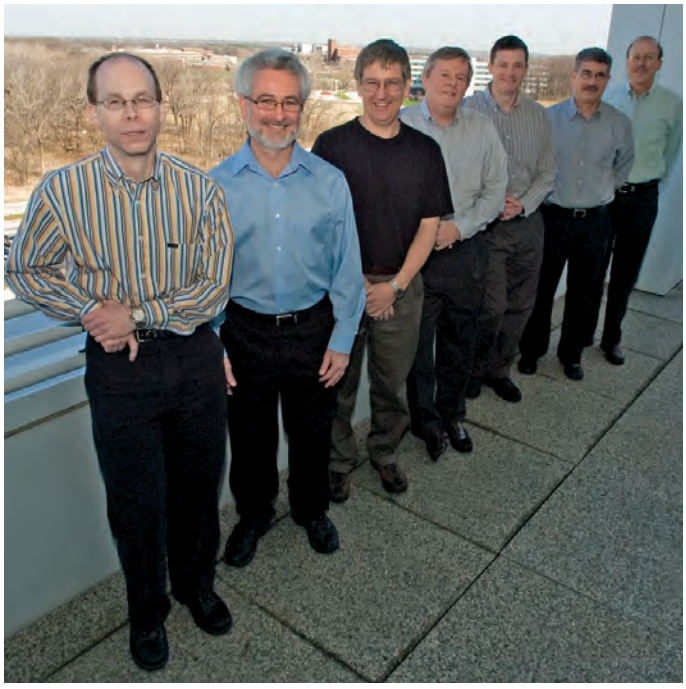

"Strawman" Beamline Configuration Map

In addition to providing information to the DOE as described above, the APS began to formulate a beamline configuration map that captured the essence of the upgrade plans. The Upgrade Steering Committee felt that it would be important to get a draft, or “strawman,” version of the roadmap out to the user community for comment before it would be discussed at the next APS SAC meeting scheduled for January 19-21, 2010. Unfortunately, even in late December 2009, it was not clear which of the various configurations for distribution of long straight sections (LLSs) would be possible from an accelerator operations point of view. In fact, APS accelerator physicists arranged to get access to Argonne supercomputers over the 2009-2010 holiday break to work on this problem; only at the beginning of January 2010 was a clearer picture emerging as to which LLS configurations might be feasible. Therefore, the strawman beamline configuration that was developed had to be done in a very short time by a small group of APS staff to allow for distribution of a plan to the community before the SAC meeting. The purpose in developing and releasing the roadmap was twofold: (1) to lay out a single possible beamline arrangement that would accommodate the flagship upgrades called out in previous documents, and (2) to stimulate engagement of the APS user community through comment and discussion of the strawman beamline configuration.

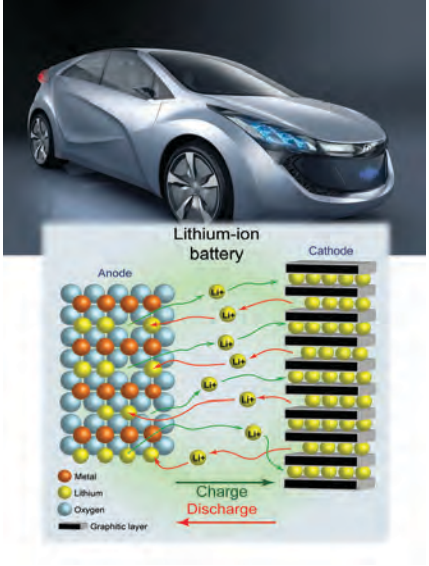

Real Materials under Real Conditions in Real Time: The complex process of charge transfer and storage in batteries limits performance. Improvements are expected by observing the electrochemistry in action with hard x-rays.

The Next Steps

At the time of this writing (March 2010) we are planning—in anticipation of a positive CD-0 determination by the DOE—the process for the next very important step in the proposed APS Upgrade: development of a Conceptual Design Report (CDR). In the conceptual design we will describe the capabilities that we propose to build, showing that these choices flow from the scientific vision we have articulated in our proposal. The CDR is one of the most important components needed to reach Critical Decision 1 and proceed with the preliminary engineering design phase of the project. The CDR will connect more explicitly the proposed instrumentation to the science drivers for each of the six beamline areas we identified:

Imaging and Coherence; Extreme Conditions; Ultrafast Dynamics; Interfaces in Complex Systems; High-Resolution Spectroscopy; Proteins to Organisms.

During development of the CDR it will not be practical or necessary to identify the location of each of the possible beamline upgrades that are proposed. However, the APS is planning to meet with all the user groups who have expressed concern about this draft roadmap and work to optimize the map further in 2010. We need such a roadmap soon in order to make more precise resource and schedule estimates, and get as close as reasonably possible to the final configuration at the time we submit the CDR. Much of this will be presented and discussed at the next APS User Meeting in May 2010, where the focus of the meeting will be the upgrade.

The Role of the Steering Committee

Since this message is from the APS Upgrade Steering Committee, you might ask, “What is the role of this committee?” The APS Upgrade Steering Committee was chartered by APS Director Murray Gibson to provide the upgrade project team with:

- Guidance and advice on strategic direction for the project;
- Input from the APS user communities;
- Support in the development of workshops, meetings, etc., regarding the APS Upgrade; and
- Feedback on draft proposals, plans, designs, etc.

The members of the Steering Committee, which meets weekly, are advocates for the APS user community, providing advice to the upgrade team on the process for insuring that user ideas and comments are heard, guidance and suggestions for forums and meetings where information regarding the upgrade can be exchanged, and comments on various documents developed by the upgrade team.

For up-to-date information go to the APS-U Web site at:
http://www.aps.anl.gov/Upgrade/

APS Upgrade Contacts

Contact Denny Mills, *Chair*, ANL-PSC (APS, dmm@aps.anl.gov), or any of the other APS Steering Committee members (listed below) if you have comments, suggestions, or concerns regarding the APS Upgrade process.

Michael Borland, ANL-ASD (APS, borland@aps.anl.gov)

Bob Fischetti, GM/CA-CAT and ANL-BIO (APS Life Sciences Council Representative, rfischetti@anl.gov)

Paul Fuoss, ANL-MSD (APS Users Organization Representative, fuoss@anl.gov)

Rod Gerig, ANL-PSC (APS, rod@aps.anl.gov)

Tom Irving, IIT and Bio-CAT (APS Partner User Council Representative, irving@iit.edu)

John Maclean, ANL-AES (APS, jfm@aps.anl.gov)

Dan Neumann, NIST (APS Scientific Advisory Committee Member, dan@nist.gov)

George Srajer, ANL-XSD (APS, srajerg@aps.anl.gov)

The Advanced Photon Source Facility at Argonne National Laboratory

The APS occupies an 80-acre site on the Argonne campus, about 25 miles from downtown Chicago, Illinois. For directions to Argonne, see www.anl.gov/Administration/visit.html.

Access to Beam Time at the APS

Beam time at the APS can be obtained either as a general user (a researcher not associated with a particular beamline) or as a partner user: a member of a collaborative access team [CAT], a partner user proposer, or a member of a collaborative development team. If you are a CAT member, contact your CAT for instructions on applying for CAT beam time. At minimum, 25% of the time at all operating beamlines is available to general users, but many offer considerably more general user time—up to 80% on X-ray Operations and Research beamlines, for example. APS general users get more than 50% of all the available beam time at the APS.

How General Users Can Apply for Beam Time at the APS

1) First-time users should read the information for new users found on our Web site at http://www.aps.anl.gov/Users/Prospective/ before applying for beam time. Also, certain administrative requirements must be completed. In particular, a user agreement between the APS and each research-sponsoring institution must be in place.

2) To choose the appropriate technique(s) and beamline(s), see the beamlines directory in the “Data” section of this volume or at https://beam.aps.anl.gov/pls/apsweb/beamline_display_pkg.beamline_dir.

3) Submit a proposal via the Web-based system. Proposals are evaluated before each user run.
For more information see the proposal system overview at:
www.aps.anl.gov/Users/Scientific_Access/General_User/General_User_Proposal/Instructions/Proposer/.

Contact Us

For more information about the Advanced Photon Source or to order additional copies of this, or previous, issues of APS Science, send an e-mail to apsinfo@aps.anl.gov, or write to APS info, Bldg. 401, Rm. A4115, Argonne National Laboratory, 9700 S. Cass Ave., Argonne, IL 60439. Visit the APS on the Web at www.aps.anl.gov.

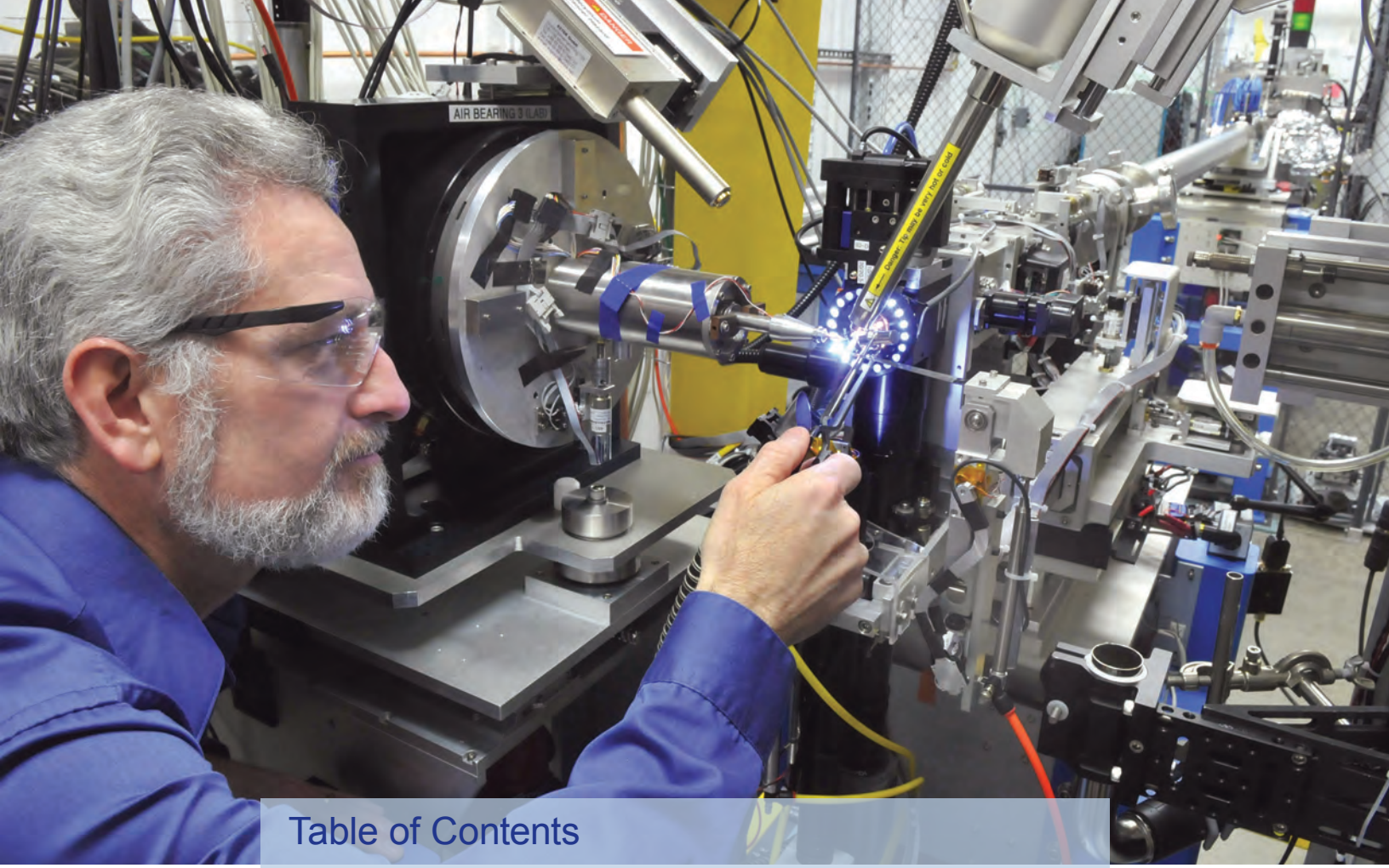

Table of Contents

APS Sectors

Sectors 1-4: XOR 1-4
X-ray Operations and Research (XOR)

Sector 5: DND-CAT
DuPont-Northwestern-Dow Collaborative Access Team (CAT)

Sector 6: MU/XOR
Midwest Universities/XOR

Sector 7: XOR 7

Sector 8: XOR 8

Sector 9: XOR/CMC
XOR/Complex Materials Consortium

Sector 10: MR-CAT
Materials Research CAT

Sectors 11 and 12: XOR/BESSRC
XOR/Basic Energy Sciences Synchrotron Radiation Center

Sectors 13 through 15: CARS
Center for Advanced Radiation Sources:
> GeoSoilEnviroCARS—sector 13
> BioCARS—sector 14
> ChemMatCARS—sector 15

Sector 16: HP-CAT
High Pressure CAT

Sector 17: IMCA-CAT
Industrial Macromolecular Crystallography Association CAT

Sector 18: Bio-CAT
Biophysics CAT

Sector 19: SBC-CAT
Structural Biology Center CAT

Sector 20: XOR/PNC
XOR/Pacific Northwest Consortium

Sector 21: LS-CAT
Life Sciences CAT

Sector 22: SER-CAT
Southeast Regional CAT

Sector 23: GM/CA-CAT
General Medicine and Cancer Institutes CAT

Sector 24: NE-CAT
Northeastern CAT

Sector 26: CNM/XOR
Center for Nanoscale Materials/XOR

Sector 30: XOR/IXS
XOR/Inelastic X-ray Scattering

Sector 31: LRL-CAT
Lilly Research Laboratories

Sector 32: XOR 32

Sectors 33 and 34: XOR/UNI
XOR/University-National Laboratory-Industry

The Advanced Photon Source (APS), a national synchrotron radiation research facility at the U.S. Department of Energy's (DOE's) Argonne National Laboratory in Illinois, provides this nation's brightest x-ray beams for science. Research by APS users extends from the center of the Earth to outer space, from new information on combustion engines and microcircuits to new drugs and nanotechnologies whose scale is measured in billionths of a meter. The APS, which is funded by the DOE Office of Science, Office of Basic Energy Sciences, enhances America's competitiveness in such areas as superconductors, semiconductors, pharmaceuticals, polymers, and catalysts, and promises to have far-reaching impact on our technology, economy, health, and fundamental knowledge of the materials that make up our world.

At the APS, a "sector" comprises the radiation sources (potentially one of the two bending magnets, and one insertion device, although the number of insertion devices in the straight sections of the storage ring can vary), and the beamlines, enclosures, and instrumentation that are associated with a particular storage ring sector. The APS has 35 sectors, 34 of which are dedicated to user science and experimental apparatus. The 35th has limited space for instrumentation and is used primarily for accelerator-related studies.

X-ray Operations and Research (XOR) sectors comprise those beamlines operated by the APS. Some XOR sectors have historic CAT origins, e.g., XOR/PNC.

Collaborative Access Team (CAT) sectors comprise beamlines operated by independent groups made up of scientists from universities, industry, and/or research laboratories.

To access the APS as **general users** (GUs), researchers submit proposals that can be active for up to two years. These proposals are reviewed and rated by one of nine proposal review panels comprising scientific peers, generally not affiliated with the APS. Beam time is then allocated by either of two APS Beam Time Allocation Committees.

Those users who propose to carry out research programs beyond the scope of the GU program may apply to become **partner users** on any beamline operated by the APS. Prospective Partner User Proposals are peer reviewed by a subset of the APS Scientific Advisory Committee. Final decisions on the appointment of partner users are made by APS management.

Beamlines, sector designations, disciplines, techniques, radiation sources, and general-user status for particular beamlines are displayed with the science highlights that follow.

This information can be viewed in whole at: http://beam.aps.anl.gov/pls/apsweb/beamline_display_pkg.beamline_dir.

APS Sector Allocations & Disciplines – Source Configuration

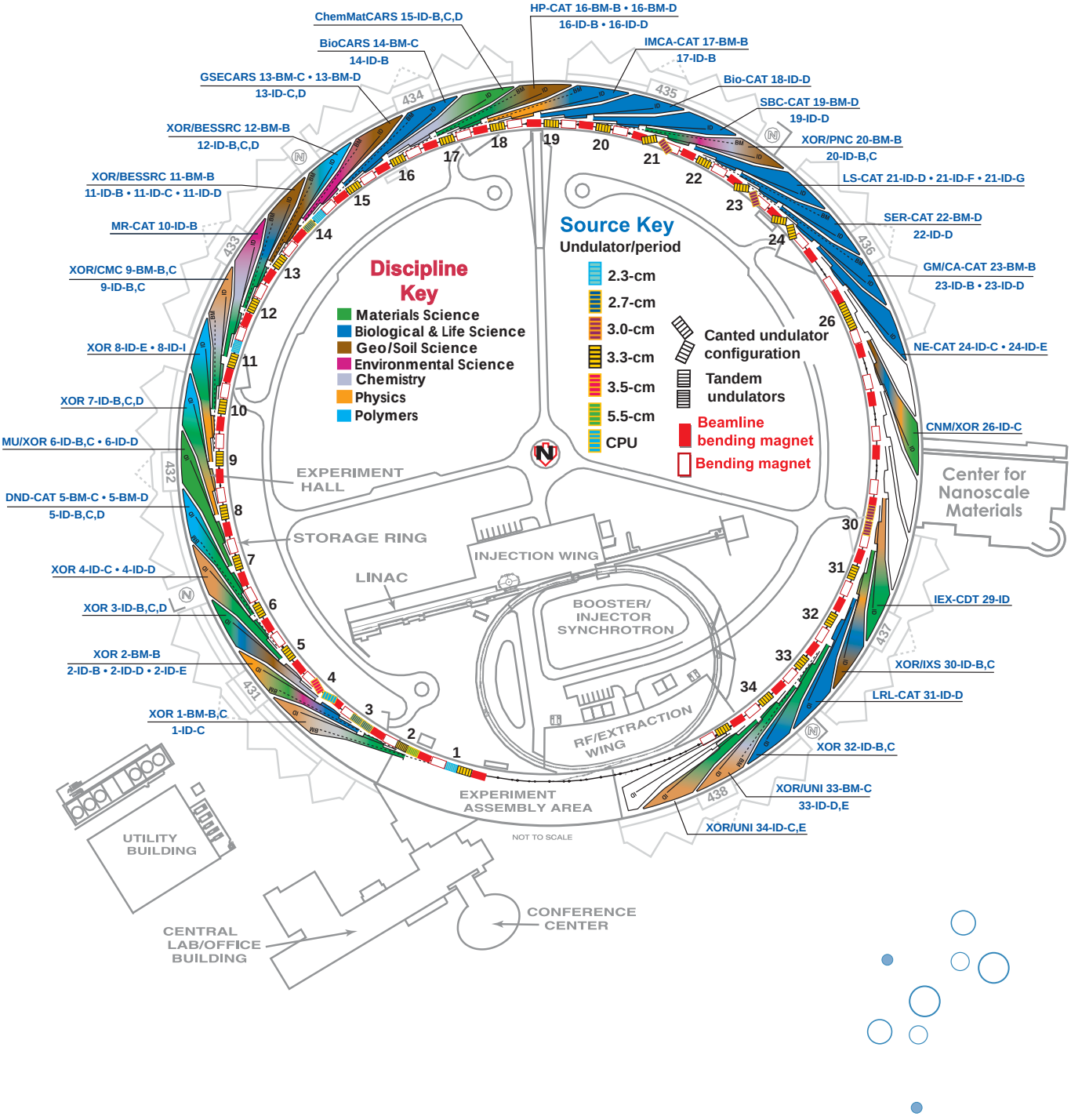

Giving Silicon a Longer-Lasting Memory

IN SHORT > Silicon has one major drawback when it comes to storing the 1s and 0s of computer memory. Without a constant source of power, silicon quickly loses its electric charge. A research team used the XOR/UNI 33-BM beamline at the APS to help them figure out how to give silicon a better memory by coating it in a thin film of strontium titanate. The team's x-ray studies confirmed that the atoms of the strontium titanate become slightly compressed in the process, which gives them the property of ferroelectricity—the same property that allows modern subway and bus fare cards to store information without drawing power. With any luck, the material, or something like, it could be used to make computers that start up much faster after being switched off.

MORE > In the standard random access memory (RAM) found in home computers, microscopic zones of silicon represent 1 or 0 depending on whether they are full of electrons or not. Because these zones rapidly leak electrons, the memory has to be constantly refreshed, which uses power. If the computer is rebooted, it needs time to reload the RAM from the hard drive. Ferroelectric materials are better suited to storing information because they are polarized, meaning they have a slight positive charge on one end and a negative charge on the other. By applying a voltage to a patch of ferroelectric material, its polarization can be flipped like a switch. The trick is how to incorporate silicon, the workhorse of modern electronics. In the past, researchers have placed layers of ferroelectric material on silicon, but these devices have all required a separate insulating layer in between the ferroelectric and the silicon.

A research team including members from Cornell University; the University of Pittsburgh; the National Institute of Standards and Technology; Pennsylvania State University; Northwestern University; Motorola, Inc.; Ames Laboratory; Intel Corporation; and TricornTech wanted to see if they could create a ferroelectric material from strontium titanate, which is related to materials used in ferroelectric fare cards, by applying it directly to silicon. Although strontium titanate is not itself ferroelectric, prior calculations indicated that if the two materials came together gently enough, the atoms making up strontium titanate would squeeze together to fit with the more closely spaced silicon atoms (see Fig. 1), thus becoming ferroelectric in the process.

To fuse the materials cleanly, the group developed a method of spray-painting strontium, titanium, and oxygen atoms (the ingredients of strontium titanate) onto silicon at low temperature. X-ray diffraction studies carried out beamline 33-BM confirmed that in extremely thin films of the material, consisting of alternating layers of strontium and titanium, the strontium atoms had squeezed themselves together to match the pattern of silicon atoms. In films that were five strontium layers thick, the strontium atoms had squeezed themselves from their usual spacing of 3.90 Å to a tighter spacing of 3.84 Å. In thicker films made of 20 strontium layers, the atoms had adopted their usual spacing.

The researchers then used an atomic force microscope, which applies a small electric voltage to one or a few atoms at a time, to create a set of microscopic polarized patches in the strontium titanate films. Consistent with the x-ray findings, all of the samples except the thickest one were able to support polarization. In the best performing film—six atomic layers thick—the patches remained polarized for 72 h at room temperature.

The researchers say it might be hard to turn their material into the kind of device found in real computer memory, where the silicon itself would deliver the voltage to switch the polarization of strontium titanate. But the payoff would be significant. By doing away with the insulating layer used in previous designs, a smaller electric voltage would accomplish the same switching, which could save not only precious time spent waiting for the computer to power up, but energy, too.

— JR Minkel

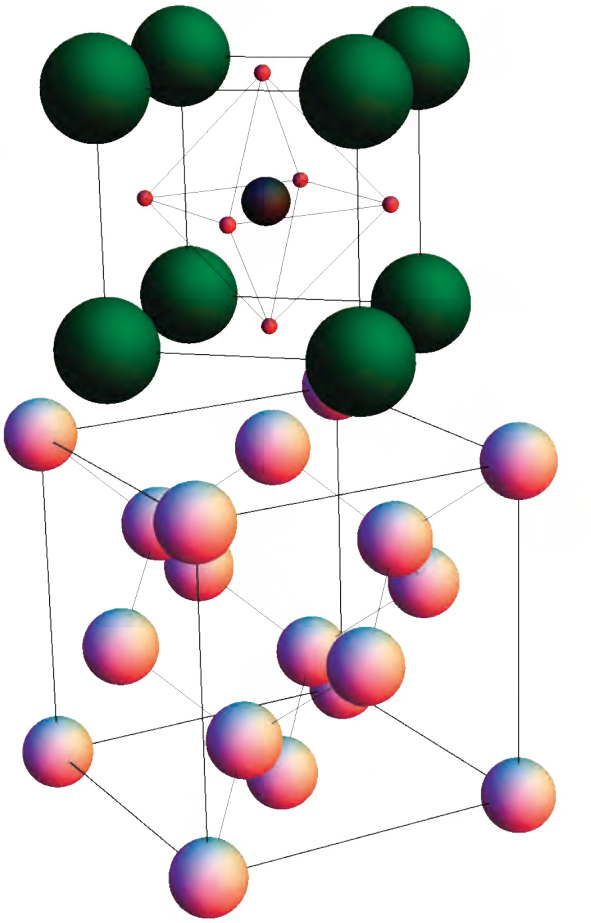

*< Fig. 1 The atomic structure of a film of strontium titanate fused with silicon, shown schematically **(left)** and as measured by atomic force microscopy **(below)**. Strontium titanate consists of alternating layers of strontium atoms (left; green) and titanium atoms (black), with oxygen (red) mixed in. Researchers found that when they carefully deposited these atoms onto silicon (pink), the strontium atoms squeezed together closer than usual, resulting in ferroelectricity.*

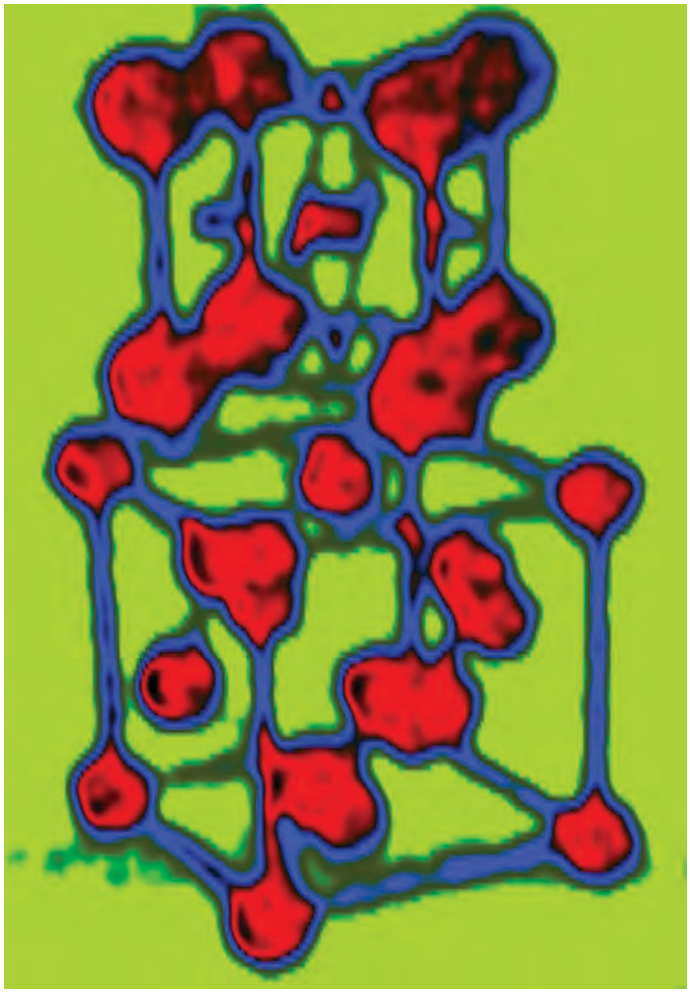

See > Maitri P. Warusawithana[1], Cheng Cen[2], Charles R. Sleasman[2], Joseph C. Woicik[3], Yulan Li[4], Lena Fitting Kourkoutis[1], Jeffrey A. Klug[5], Hao Li[6], Philip Ryan[7], Li-Peng Wang[8,9], Michael Bedzyk[5], David A. Muller[1], Long-Qing Chen[4], Jeremy Levy[2], Darrell G. Schlom[1]*, "A Ferroelectric Oxide Made Directly on Silicon," Science **324**(17), 367 (April 2009). DOI: 10.1126/science.1169678

Author affiliations >
[1]Cornell University, [2]University of Pittsburgh, [3]National Institute of Standards and Technology, [4]Pennsylvania State University, [5]Northwestern University, [6]Motorola Inc., [7]Ames Laboratory, [8]Intel Corporation, [9]TricornTech

Correspondence >
*schlom@cornell.edu

> This work was supported by Office of Naval Research grant N00014-04-1-0426 (M.P.W., L.F.K., D.A.M., and D.G.S.), National Science Foundation grants DMR-0507146 and DMR-0704022, Materials Research Science and Engineering Center program grants DMR-0520404, DMR-0520513, and DMR-0820404. Use of the Advanced Photon Source was supported by the U.S. Department of Energy, Office of Science, Office of Basic Energy Sciences, under Contract No. No. DE-AC02-06CH11357.

> 33-BM • XOR/UNI • Materials science, physics, chemistry • Anomalous and resonant scattering (hard x-ray), diffuse x-ray scattering, powder diffraction, x-ray reflectivity, general diffraction, grazing incidence diffraction • Bending magnet • Accepting general users

The Importance of Magnetism and Structural Distortions in Arsenide Superconductors

IN SHORT > Iron pnictide compounds—which are based on conducting layers of iron (Fe) and arsenic (As)—were discovered in 2008 to possess superconducting properties while under pressure and also upon doping. A subset of these iron-based superconductors, called 122 iron arsenides, became important to condensed-matter physicists because relatively large and high-quality single crystals can be grown. To learn more about the properties of these 122 iron arsenides, researchers using the MU/XOR 6-ID-D beamline at the APS studied the magnetic and structural properties of the compound $BaFe_2As_2$ doped with cobalt (Co). Their research will help science gain a further understanding of how superconductivity arises in high-temperature superconductor (high-T_c) materials, and may help point the way to a yet-to-be established high-T_c theory.

MORE > The 122 iron arsenides AFe_2As_2, where "A" denotes the alkaline-earth metals of the elements barium (Ba), calcium (Ca), or strontium (Sr), display complicated structural, magnetic, and superconducting properties in and around the boundary between an antiferromagnetic (AFM) phase and a superconductivity (SC) phase. The experiment with these 122 iron arsenides led the research group to discover that, instead of a simultaneous first-order transition from a tetragonal (T) phase into an antiferromagnetic ordered orthorhombic (AFM-O) phase, which occurs without doping, Co-doping causes the single simultaneous transition to split into two transitions, with the transition to the orthorhombic (O) phase occurring before the antiferromagnetic (AFM) transition while cooling (Fig. 1). In addition, superconductivity appears as the transition to the O and AFM phases is increasingly suppressed with additional doping. The researchers made first-ever microscopic observations that confirmed both the structural and magnetic changes taking place at each transition.

X-ray diffraction and neutron scattering analyses were performed on the 122 iron arsenide superconductor based on single crystals of the composition $Ba(Fe_{1-x}Co_x)_2As_2$. The experiment was focused on a Co-doped composition of 4.7% (x = 0.047), called an underdoped composition, where an emergent superconducting phase coexists with a state of weak AFM order (Fig. 2). In their experiments, the scientists from Iowa State University were able to verify that the AFM and O transitions separated, and were able to identify the structural and magnetic phases in the underdoped region. A first-order transition from a tetragonal phase to a orthorhombic phase occurs for $Ba(Fe_{0.953}Co_{0.047})_2As_2$ at the structural transition temperature (T_S) = 60K, and a second-order transition to an AFM state takes place at the magnetic ordering (Néel) temperature (T_N) = 47K. In the process, they succeeded in making microscopic observations of this transition, showing for the first time the specific structural and magnetic changes taking place. The x-ray diffraction studies carried out at the 6-ID-D high-energy beamline at the APS verified that a single-phase orthorhombic structure existed throughout the crystal, verifying the neutron scattering measurements performed at the High Flux Isotope Reactor at Oak Ridge National Laboratory.

As Co doping suppressed both the O and AFM phases, a superconducting state evolved. In fact, superconductivity occurred within the orthorhombic and antiferromagnetic state below the superconducting transition temperature (T_c) = 17K. Below the superconducting temperatures at 17K, the researchers found a substantial reduction in magnetic moments, along with a gap in low-energy spin excitations. With the observed redistribution of spin excitations and reduced magnetic moment under these temperatures, it is clear that competition occurs

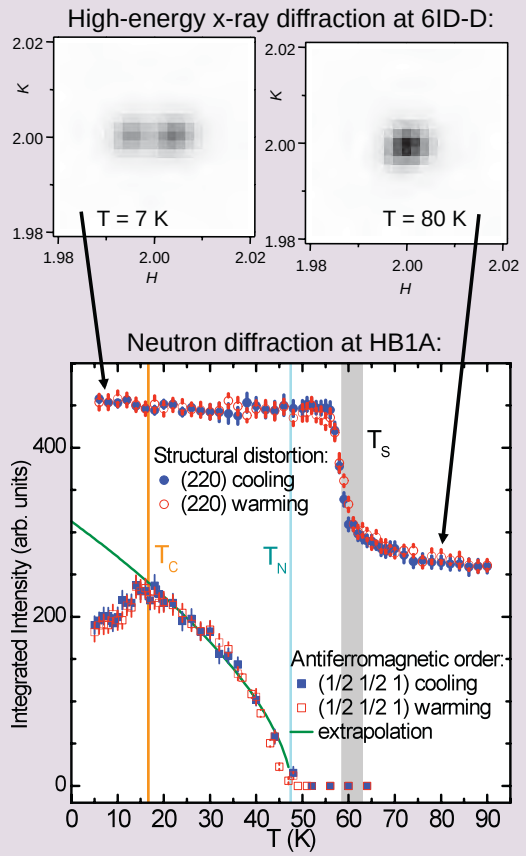

> *Fig. 1 X-ray and neutron diffraction data on a single crystal of $Ba(Fe_{1-x}Co_x)_2As_2$. The upper panels show x-ray diffraction data measured on MU/XOR beamline 6-ID-D on a single crystal with x = 3.8%. At low temperatures (T = 7K, below T_S), the (220) nuclear Bragg peak is split by the orthorhombic distortion. At 80K (above T_S), the single (220) peak indicates the tetragonal structure. The lower panel shows neutron scattering data on a single crystal with x = 4.7%. The structural transition is indicated by the change of intensity of the (220) nuclear reflection. The magnetic Bragg peak at (1/2 1/2 1) appears as $T_N < T_S$. Below T_C, the magnetic Bragg peak is suppressed.*

between the co-existing AFM and SC states. Such actions emphasize the important interrelationship between magnetism, structural distortions, and superconductivity within the iron arsenides.

— William Arthur Atkins and Patricia Panatier

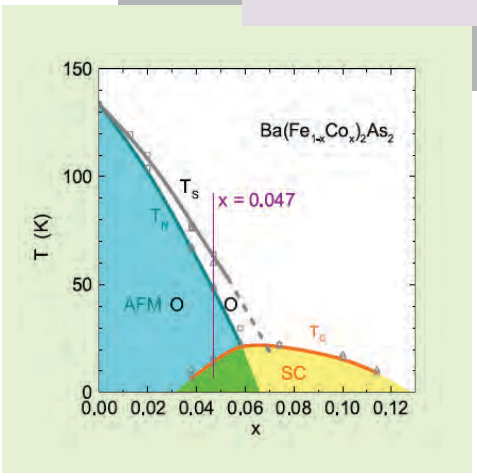

< *Fig. 2 Phase diagram for $Ba(Fe_{1-x}Co_x)_2As_2$ showing paramagnetic tetragonal (T), paramagnetic orthorhombic (O), AFM ordered orthorhombic (AFM O), and superconducting (SC). AFM O and SC phases coexist between x = 4% and 6%. The vertical line shows the position of the x = 4.7% sample studied here.*

See > Daniel Keith Pratt, W. Tian, A. Kreyssig, J.L. Zarestky, S. Nandi, N. Ni, S.L. Bud'ko, P.C. Canfield, A.I. Goldman, and Robert John McQueeney*, "Coexistence of Competing Antiferromagnetic and Superconducting Phases in the Underdoped $Ba(FE_{0.953}Co_{0.047})_2As_2$ Compound Using X-ray and Neutron Scattering Techniques," Phys. Rev. Lett. **103**, 087001 (2009). DOI:10.1103/PhysRevLett. 103.087001
*Note: similar results have been described by Christianson et al., Phys. Rev. Lett. **103**, 087002 (2009).*

Author affiliation >
Iowa State University

Correspondence >
*mcqueeney@ameslab.gov

> Work at the Ames Laboratory and the MU/XOR is supported by the U.S. Department of Energy Office of Science under Contract No. DE-AC02 07CH11358. Use of the Advanced Photon Source at Argonne National Laboratory was supported by the U.S. Department of Energy, Office of Science, Office of Basic Energy Sciences, under Contract No. DE-AC02-06CH11357.

> 6-ID-D • MU/XOR • Materials science, physics • High-energy x-ray diffraction, magnetic x-ray scattering, pair distribution function, powder diffraction • 3.3-cm Undulator A • Accepting general users

Charge Excitation from Stripes in Nickelate and Superconducting Cuprates

IN SHORT > Within high-temperature superconductor (HTS) compounds of cuprates, charge stripe order appears when holes are doped because of strong repulsive electron-electron correlations. For a better understanding of the charge dynamics within stripes, researchers using an APS beamline observed, for the first time, charge excitations occurring from the charge stripe-ordered state in 214-type nickelate and cuprate superconductors. This research advances our understanding of strongly correlated electron systems, including the high-temperature superconductor compounds, and helps scientists better understand the behavior of collective electrons under strong correlations, which has been a long-standing puzzle.

MORE > Charge stripes are defined as doped holes —separated by insulated regions not containing holes—that are confined to parallel lines of copper atoms in copper-oxygen planes. And, importantly, a dynamical collective motion of these stripes is thought by scientists to help bring about superconductivity.

For their study of charge excitation from stripes, the scientists from the Japan Atomic Energy Agency, Tohoku University, the Advanced Institute for Materials Research, and Argonne researched the nickelate compound $La_{5/3}Sr_{1/3}NiO_4$ —part of the 214 nickelate family: $La_{2-x}Sr_xNiO_4$(LSNO). They also studied the superconducting cuprate compounds $La_{15/8}Ba_{1/8}CuO_4$, $La_{1.92}Ba_{0.08}CuO_4$, and $La_{1.88}Sr_{0.12}CuO_4$ —part of the 214 cuprate family La_{2-x}(Ba or Sr)$_xCuO_4$ (LBCO and LSCO, respectively). For their experiments, the researchers used hard x-ray resonant inelastic x-ray scattering (RIXS) to measure charge excitation within these compounds. The method permits the probing of a stripe possessing a characteristic momentum transfer (q_s) that measures its spatial period. Their measurements show an approximate 1-eV charge excitation for both the nickelate stripes, which propagate diagonally along the plane containing the NiO_2 square lattice, and the cuprate stripes, which propagate vertically or horizontally along the CuO_2 plane.

Hard x-rays were used for this RIXS study in order to excite electrons from the 1s orbital to the $4p_\pi$ orbital, with a specific incident photon energy of 8,347 eV for the nickelate and 8,993 eV for the three cuprates. The nickelate measurement was performed at a temperature of 10K, using the MERIX spectrometer installed on the XOR/IXS 30-ID beamline at the APS. Likewise, the cuprate measurements were performed at 8K with an inelastic x-ray spectrometer installed on the BL11XU beamline at the SPring-8 light source in Japan.

The researchers prepared single crystals of the nickelate LSNO with x = 1/3, and the cuprates LBCO with x = 0.125, LBCO with x = 0.08, and LSCO with x = 0.12. LSNO and LBCO (x = 0.125) produced strong charge stripe order below 180K and 55K, respectively (Fig. 1). LBCO (x = 0.08) did not result in charge stripe order, and the researchers could not verify charge stripe order in LSCO. They observed three peaks from the RIXS spectra at all but one [$q_s = (4\pi/3, 2\pi/3)$] of the different momentum transfer positions for LSNO. The three peaks consisted of an "elastic" peak at zero energy transfer (0 eV), an "in-gap" peak at ~1.5 eV, and a "CT" peak at ~4.5 eV (where CT refers to charge transfer, involving the charge excitation across the CT gap).

RIXS data from LBCO found that all spectra contained two peaks: the elastic peak and the CT peak at ~4 eV. However, the cuprates did not show a defined in-gap peak below the CT gap energy, while the nickelate did, because the cuprates are not insulators like the nickelate.

According to this study, the charge stripe state results in additional RIXS signals at energy transfer 1 eV and characteristic momentum transfer, regardless of

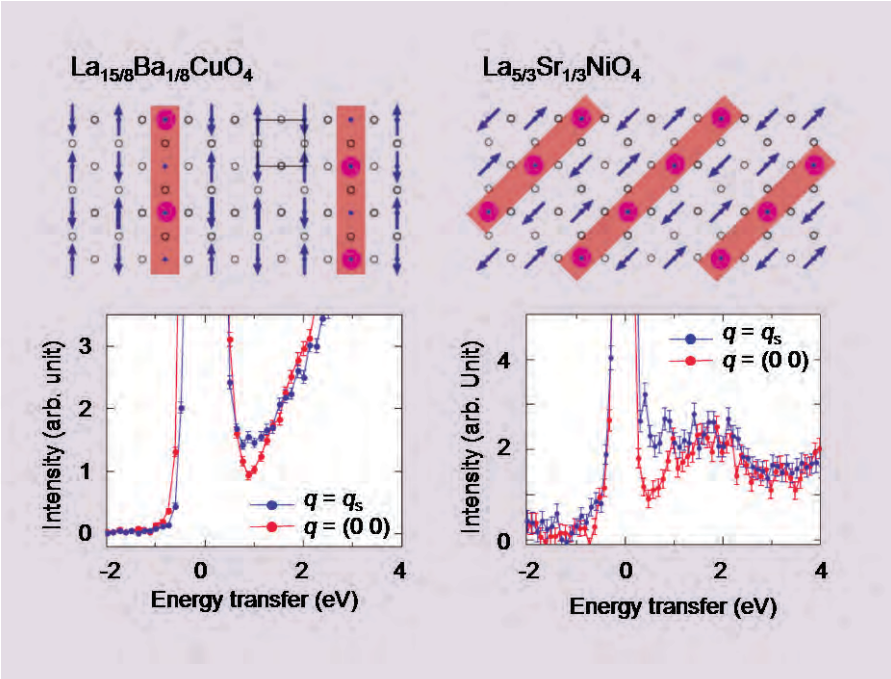

^ *Fig. 1 Upper panels show charge stripe ordered states for $La_{15/8}Ba_{1/8}CuO_4$ and $La_{5/3}Sr_{1/3}NiO_4$ on planes consisting of Cu (or Ni) and oxygen atoms. Arrows show spins of electrons and red circles show doped holes that extinguish spins. Lower panels show comparison between scattered x-ray intensity with momentum transfer q_s corresponding to the spatial period of charge stripes (blue data) and that without q_s (red data). An additional signal of charge excitation from the stripe state is observed around the energy transfer of 1 eV in the scattering x-ray intensity with q_s in both materials, regardless of the geometry of the stripes.*

the stripe geometry. The charge stripe excitations appear in all of the diagonal nickelate stripes and the vertical cuprate stripes. The researchers state that because the charge stripe excitations appear even in the insulating LSNO, they may not be directly related to superconductivity, although they may be necessary for the superconductivity—that is, they could be interpreted as collective stripe excitations. In another possibility, the observed anomaly at the characteristic momentum transfer might be caused by the in-gap state of the striped system. That is, the anomaly may result from softening in the charge excitonic modes of the in-gap states.

— William Arthur Atkins

See > Shuichi Wakimoto[1]*
H. Kimura[2], K. Ishii[3], K. Ikeuchi[3], T. Adachi[4], M. Fujita[5], K. Kakurai[1], Y. Koike[4], J. Mizuki[3], Y. Noda[2], K. Yamada[5,6], A.H. Said[7], and Yu. Shvyd'ko[7], "Charge Excitations in the Stripe-Ordered $La_{5/3}Sr_{1/3}NiO_4$ and $La_{2-x}(Ba, Sr)_xCuO_4$ Superconducting Compounds," Phys. Rev. Lett. **102**, 157001 (2009). DOI:10.1103/PhysRevLett.102.157001

Author affiliations >
[1]Japan Atomic Energy Agency, [2]Tohoku University, [3]Japan Atomic Energy Agency, [4]Tohoku University, [5]Tohoku University, [6]Advanced Institute for Materials Research, [7]Argonne National Laboratory

Correspondence >
*wakimoto.shuichi@jaea.go.jp

> This work is supported by a Grant-In-Aid from the Ministry of Education, Culture, Sports, Science, and Technology, Japan. The synchrotron radiation experiments at SPring-8 were performed under the Common-Use Facility Programme of JAEA. Use of the Advanced Photon Source at Argonne National Laboratory was supported by the U.S. Department of Energy, Office of Science, Office of Basic Energy Sciences, under Contract No. DE-AC02-06CH11357.

> 30-ID • XOR/IXS • Geoscience • life science • materials science • physics • Inelastic x-ray scattering • 3.0 undulator (US), 3.0 undulator (DS) • Accepting general users

Putting the Squeeze on Magnetic Semiconductors

IN SHORT > The interest in spintronic devices has fueled many directions in materials research, in particular research into the properties of ferromagnetic-semiconductor EuX monochalcogenides. Their ferromagnetic ordering temperature (T_c) can be increased from 70K to values near room temperature by subjecting them to hydrostatic pressure, thereby opening the door for many potential bulk applications. But a detailed understanding of the way pressure compresses the lattice isotropically, changes the electronic structure, and strengthens the ferromagnetism in these materials remains elusive. Researchers using the APS obtained direct spectroscopic evidence that electronic mixing in a particular monochalcogenide is significantly enhanced by the application of external pressure, the first measurements to establish the definite, key role played by this orbital mixing in increasing the ferromagnetic ordering temperature.

MORE > Most models that have been suggested for monochalcogenides EuX (where X can denote either Te, Se, S, or O) hinge on f-d, s-f, or p-f orbital mixing, and there is significant experimental evidence pointing to the fact that Eu 4f-5d mixing plays a key role in the ferromagnetic enhancement. Researchers from Argonne, Northwestern University, and the Commissariat à l'énergie atomique, working at XOR beamline 4-ID-D at the APS, carried out both x-ray absorption near edge structure (XANES) and x-ray magnetic circular dichroism (XMCD) experiments, and obtained direct spectroscopic evidence that Eu 4f-5d electronic mixing is significantly enhanced by the application of external pressure.

This initial direct evidence is tantalizing, and could potentially affect future experimental work aimed at investigating other mechanisms that have also been found to enhance ferromagnetic ordering, such as interfacial strain in epitaxial films, or chemical substitution. The former is of particular interest because, while it is true that biaxial strain is less effective than hydrostatic pressure at raising T_c, symmetry breaking at the interfaces of strained films could potentially raise the value of T_c beyond the value of the electron-delocalization limit in bulk EuO.

The group exploited the element and orbital selectivity of Eu *L*-edge x-ray absorption in the electric dipole (2p to 5d) and electric quadrupole (2p to 4f) channels to probe the spin polarization of the valence (4f) and conduction (5d) states of the EuX lattice as pressure was applied in a diamond anvil cell. The results they obtained on the Eu 4f-5d mixing were supported by density functional theory calculations. The researchers also investigated the effect of anion substitution and found that while such a substitution gives rise to a lattice contraction much larger than the one obtained by the application of hydrostatic pressure, the concomitant enhancement of ferromagnetism was not as significant. At the onset of absorption, theory suggests the photoexcitation process is dominated by the weak quadrupolar (2p to 4f) interaction, while the dipolar contributions (2p to 5d) take over as the absorbed energies become higher. Indeed, the spectral weight transfer from high to low energies is observed in both XMCD and XANES data, indicating charge transfer from the Eu 4f to the Eu 5d states. Density functional theory band structure calculations indicate that empty 4f states come from predominantly spin-up states that lie slightly below the Fermi level at atmospheric pressure, but they become chemically active through hybridization with empty 5d states in the conduction band as the lattice is

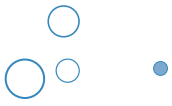

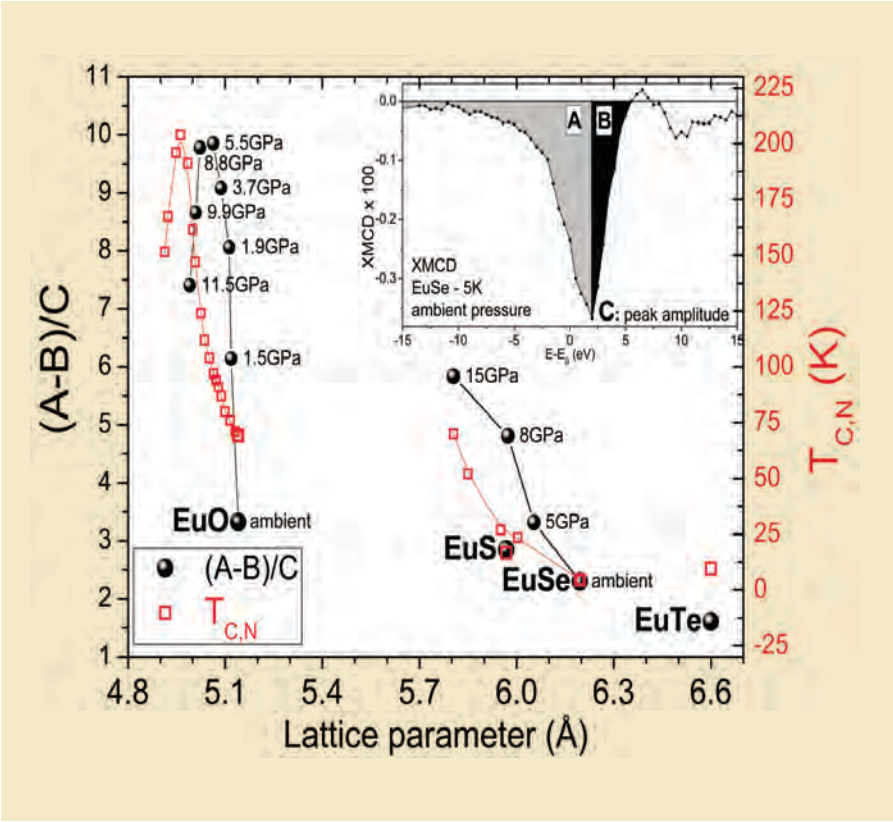

^ *Fig. 1 Mixing fraction, (A-B)/C, as a function of the lattice parameter. A is the area to the left, and B to the right of the peak amplitude C. The strong correlation between the Mixing fraction (dots) and the Ferromagnetic ordering temperature (boxes) is readily apparent. (Copyright © 2009 The American Physical Society)*

contracted by the applied pressure. To quantify this enhancement of quadrupolar contributions (and hence the reduction of the dipolar contribution) in the absorption as a result of the lattice contraction, the mixing fraction was calculated, as shown in Fig. 1. It can be seen that the mixing fraction grows for contracted lattices as 4f levels cross the Fermi level, and that a strong correlation exists between the mixing fraction and the value of T_c in these compounds, again demonstrating that f-d mixing is the primary cause of T_c enhancement under pressure.

— Luis Nasser

See > Narcizo M. Souza-Neto*[1], Daniel Haskel**[1], Yuan-Chieh Tseng[2,1], and Gerard Lapertot[3], "Pressure-Induced Electronic Mixing and Enhancement of Ferromagnetic Ordering in EuX (X = Te, Se, S, O) Magnetic Semiconductors," Phys. Rev. Lett. **102**, 057206 (6 February 2009). DOI:10.1103/PhysRevLett.102.057206

Author affiliations >
[1]Argonne National Laboratory,
[2]Northwestern University,
[3]Institut Nanosciences et Cryogénie

Correspondence >
*narcizo@aps.anl.gov
**haskel@aps.anl.gov

> Use of the Advanced Photon Source at Argonne National Laboratory was supported by the U.S. Department of Energy, Office of Science, Office of Basic Energy Sciences, under Contract No. DE-AC02-06CH11357.

> 4-ID-D • XOR • Physics, materials science • Anomalous and resonant scattering (hard x-ray), magnetic x-ray scattering, magnetic circular dichroism (hard x-ray) • 3.5-cm undulator • Accepting general users

Better Switching through Chemistry in Thin Ferroelectrics

IN SHORT > Because the atomic structure and polarity of ferroelectric materials respond dramatically to an applied electric field, they have found increasing application in such areas as electromechanical actuators, nonvolatile computer memories, and advanced radio-frequency electronics. But what if there were another way to make ferroelectric materials do their thing—not electrically by applying a voltage, but through another mechanism? A group of experimenters from Argonne, the University of Pennsylvania, and Northern Illinois University has managed to do just that, proving that not just electricity but also a little bit of chemistry can flip the structure and thus the polarity of a ferroelectric film.

*> Fig. 1 Hysteresis in L scans through the 304 Bragg peak of a 10-nm $PbTiO_3$ film at 644K, at various oxygen partial pressures pO_2. Plots **(a)** and **(b)** are for pO_2 decreasing from a high value and increasing from a low value, respectively. Redder hues indicate higher intensity (log scale). Plots **(c)** and **(d)** show peak position and intensity; closed and open symbols are for decreasing and increasing pO_2, respectively. To fully switch the sample at low pO_2 (not shown), oxygen flow was set to zero, resulting in $pO_2 < 10^{-7}$ mbar. (Copyright © 2009 The American Physical Society)*

MORE > The researchers studied very thin lead titanate ($PbTiO_3$) films, 2 to 21 nm in thickness, grown on $SrRuO_3$ films on $SrTiO_3$ substrates. While varying the oxygen partial pressure (pO_2) on the top surface of the lead titanate film at temperatures from 550K to 950K, the team used synchrotron x-ray scattering at the XOR/BESSRC 12-1D beamline at the APS. By using 28-keV x-rays to penetrate the reactive atmosphere and chamber walls, the structural changes in the thin films could be monitored *in situ* as they occurred, providing more direct information than had been available (Fig.1).

As the pO_2 was altered, hysteresis was evident in the film structure, indicating polarization changes. All of the unit cells in the lead titanate changed their structure when the surface was exposed to a different pO_2. At a high pO_2, their polarization pointed up. By changing to low pO_2, it could be switched and made to point down. The switching was reversible and could be cycled back and forth repeatedly. During the polarization switching process, scattering interference patterns showed that domains of both directions were present.

The team's finding—that the chemically-induced polarization switching could be reproduced and repeated under control—is quite significant because it indicates that the chemical environment in which these ultrathin ferroelectrics operate is more important and influential than previously believed. It is a phenomenon that needs to be taken into account as these materials are created and used. Not only are the electronic properties of the interface important, but so is the chemistry: whether there are extra ions of one sign or another.

The changes in the $PbTiO_3$ surface resulting from equilibration with the atmosphere were confirmed by x-ray experiments showing a new surface structure and by *ab initio* calculations based on density functional theory. The team thinks that the outermost atomic layer is losing 1 out of every 4 oxygens at low oxygen pressure.

That discovery has implications both for the future design of devices based on these film structures and for the development of new applications. Although the team emphasizes that they are still at the fundamental research stage, and so the applications are not very certain or direct, the researchers speculate that this awareness of chemical

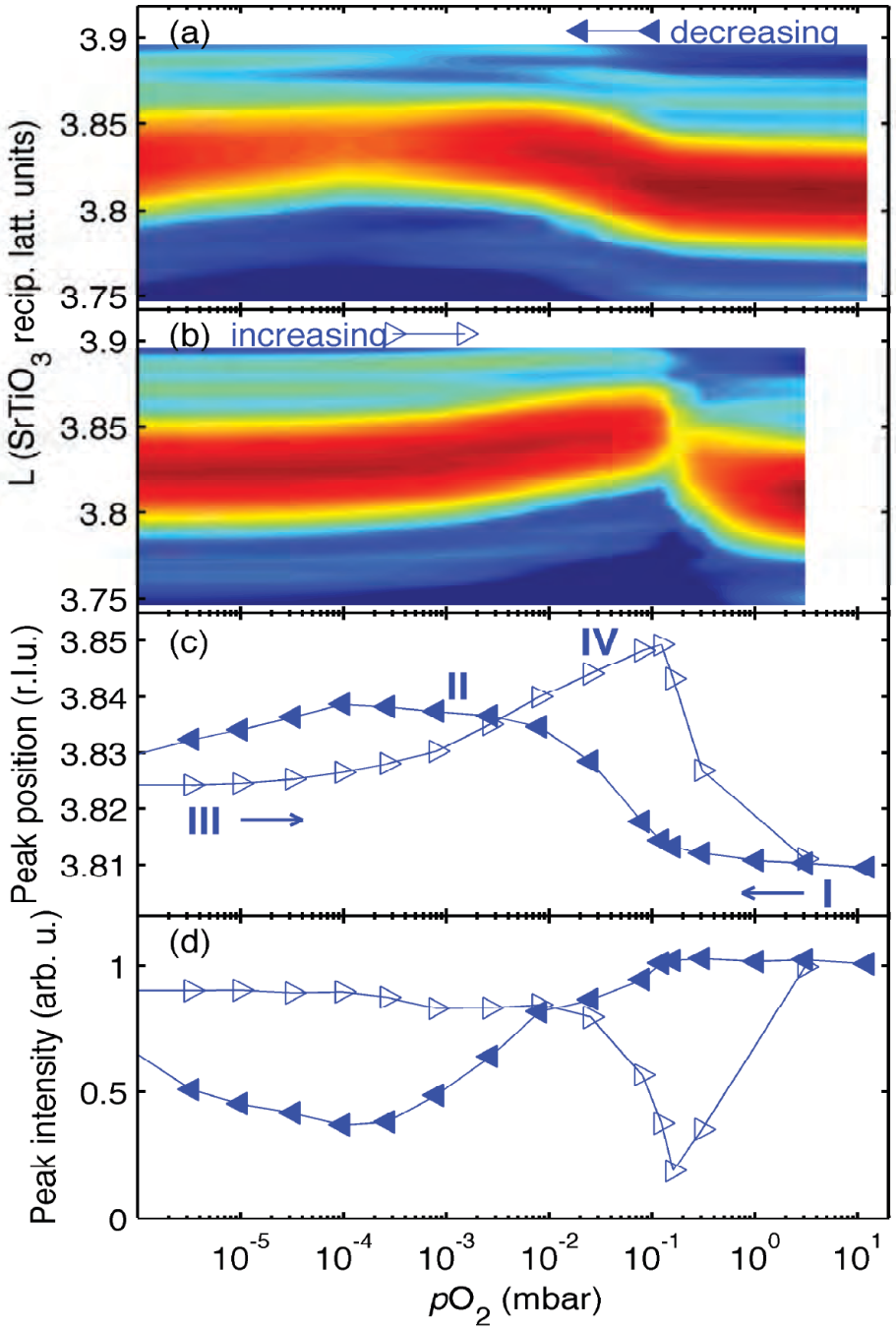

ferroelectric switching and the ability to manipulate it could lead to new types of catalysts and chemical actuators for nanoelectronics.

For now, the team plans to continue to investigate chemical ferroelectric switching, including the use of different chemistries and the precise details of the mechanisms involved. Achieving ferroelectric switching chemically rather than electrically is a new capability, opening fascinating possibilities for the study of new basic scientific phenomena.

— Mark Wolverton

See > R.V. Wang[1§], D.D. Fong[1], F. Jiang[1§§], M.J. Highland[1], P.H. Fuoss[1], Carol Thompson[2], A.M. Kolpak[3§§§], J.A. Eastman[1], S.K. Streiffer[1], A.M. Rappe[2], and G.B. Stephenson[1]*, "Reversible Chemical Switching of a Ferroelectric Film," Phys. Rev. Lett. **102**, 047601 (2009). DOI: 10.1103/PhysRevLett.102.047601

Author affiliations >
[1]Argonne National Laboratory,
[2]Northern Illinois University,
[3]University of Pennsylvania
[§]Present address: Numonyx Corp.,
[§§]Present address: Ohio University,
[§§§]Present address: Yale University

Correspondence >
*stephenson@anl.gov

> This work was supported under Contract No. DEAC02-06CH11357 between UChicago Argonne LLC and the Department of Energy. A. M. K. and A. M. R. acknowledge the support of the Department of Energy under Grant DE-FG02-07ER15920, the Air Force Office of Scientific Research under Grant FA9550-07-1-0397, and a Challenge Grant from the HPCMO of the Department of Defense. Use of the Advanced Photon Source at Argonne National Laboratory was supported by the U.S. Department of Energy, Office of Science, Office of Basic Energy Sciences, under Contract No. DE-AC02-06CH11357.

> 12-ID • XOR/BESSRC • Chemistry, physics, materials science • Small-angle x-ray scattering, wide-angle x-ray scattering, grazing incidence small-angle scattering, surface diffraction • 3.3-cm Undulator A • Accepting general users

Avoiding Short Circuits by a Whisker

IN SHORT > Whiskers are generally associated with shaving cream commercials and grizzled old prospectors from western movies. But when whiskers of tin (Sn) form on coatings of that metal when it is used to plate and solder copper (Cu) microelectronic components, the whiskers can grow and create electrical connections where none are meant to be, causing short circuits that damage and destroy delicate equipment. It has happened in satellites, computers, even pacemakers, wreaking great havoc, and all caused by a whisker of tin that might be only a few micrometers thick by a couple of millimeters long. Even after 50 years of research, a definite explanation for the cause of the whiskers has proven maddeningly elusive. Now, a team of researchers used an APS beamline to achieved a crucial new insight into how and why these tin whiskers form and grow.

MORE > Researchers from Germany's Max Planck Institute for Metals Research, Robert Bosch GmbH, Oak Ridge National Laboratory, and Argonne used the XOR/UNI 34ID-E beamline at the APS to study how differences in mechanical stress in an Sn plating cause the whiskers to form. Using a technique known as white-beam micro-Laue diffraction, they were able to measure extremely fine differences in stress distribution around the whisker root during ongoing growth, revealing the forces driving the growth for the first time.

The experimenters electrodeposited pure Sn thin films with an approximate thickness of 3 μm onto pure Cu substrates, and aged them at room temperature. About four days later, the first Sn whiskers began to form. (For comparison purposes, some whisker-free specimens were also prepared by annealing the Sn films at 150° C for 1 h.) The researchers first determined the stress differences between the base and the surface of the tin film by performing x-ray diffraction measurements in the laboratory. Then, in order to precisely measure and spatially resolve the stress distribution in the surface plane around a growing whisker, they used the micro-Laue diffraction method at the APS (Fig. 1). A very fine x-ray beam with a diameter of about 300 nm was used to scan in 0.5-μm steps the region around the whisker root. In combination with a very-high-resolution charge-coupled device detector, Laue diffraction patterns were captured from each probed position. Finally, the local stresses of each probed position were derived directly from the measured Laue patterns.

Previous work on whisker formation in Sn coatings on Cu surfaces had shown that compressive stress in the Sn layer plays an important role, but the experimenters in this study revealed for the first time that this is not a necessary condition for whisker formation. Based on state-of-the-art laboratory and synchrotron x-ray diffraction stress investigations of unprecedented accuracy during whisker growth, the researchers have shown that a negative nature of the stress *gradients* viewed from the whisker root, not a possibly compressive nature of the stress, is decisive for whisker formation.

Thus, the following model for whisker formation emerges: During room-temperature ageing, Cu atoms from the substrate diffuse into the Sn film above and form the intermetallic compound Cu_6Sn_5 along Sn grain boundaries at the Cu/Sn interface. Due to this compound formation, compressive stress is generated at the

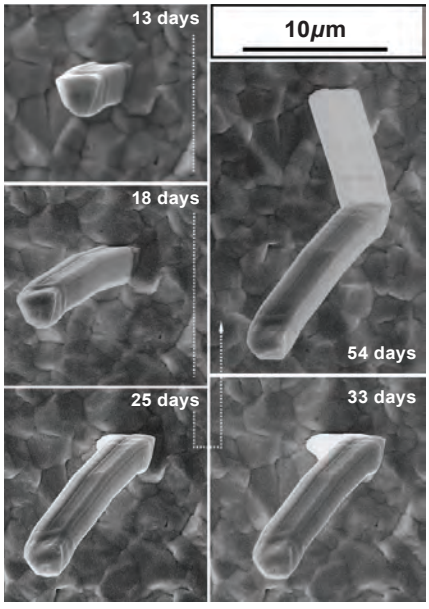

> Scanning electron micrographs of the same Sn whisker taken at different ageing times at room temperature.

interface, and tensile stress forms at the surface of the Sn film. At the locations where this compound formation is most significant at the interface with the substrate, tensile stress is also most significant at the Sn surface. Consequently, both negative out-of-plane stress gradients from the Sn surface to the interface region and negative in-plane stress gradients from the site of the forming whisker toward its surrounding area develop. These stress gradients move Sn atoms to the whisker formation site, and the whisker continues to grow outward as more Sn atoms are added to the base. Whisker growth continues as long as the stress gradients persist.

In essence, Sn atoms are forced toward the whisker root by the nature of the surrounding stress field, much as pressure on the end of a toothpaste tube forces toothpaste out the other end. This model is confirmed by examination of the whisker-free samples, which showed none of the in-plane or out-of-plane negative stress gradients in the Sn layer.

Interestingly, the experimenters found that whiskers do not form at every location with a significant amount of Cu_6Sn_5 beneath the Sn surface. They speculate that this is likely due to the anisotropy of physical properties (as the diffusion coefficients) of Sn.

The next step will be to find ways to prevent the formation and propagation of these negative stress gradients that lead to whisker formation and growth in Sn/Cu films. That will be the key to solving the hairy problem of metallic whisker formation in microelectronic circuits.

— Mark Wolverton

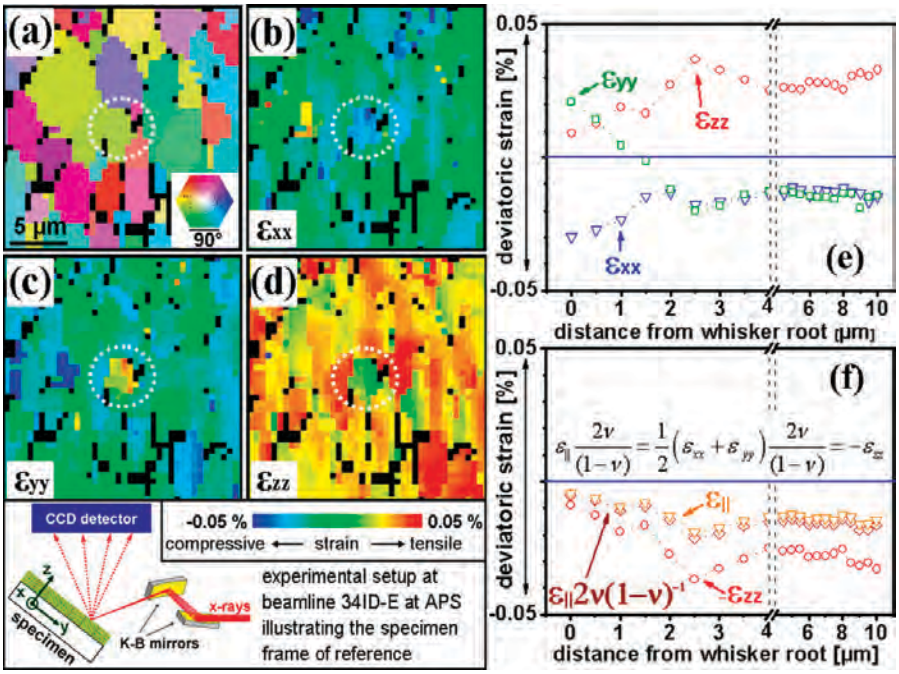

^ *Fig. 1 Two-dimensional micro-diffraction (area of ~20 × 20 × μm²) data taken around the root (white dotted circle) of a growing Sn whisker. The regions colored black correspond to non-indexed data points.* ***(a)*** *The orientation image displays the corresponding (RGB) color-coded crystallographic orientations of the [001] axis of the Sn grains with respect to the [001] pole (which has the white color code).* ***[(b)–(d)]*** *Color-coded diagonal (deviatoric) strain tensor components ε_{xx}, ε_{yy}, and ε_{zz} (see the illustration of the beamline setup and indication of the specimen frame of reference at the bottom of the figure). The scale bar displays the color-coded deviatoric strains.* ***(e)*** *Radially, in the plane of the surface, averaged values of all diagonal (deviatoric) strain tensor components (ε_{xx}, ε_{yy}, and ε_{zz})as a function of the distance from the whisker root.* ***(f)*** *Radially averaged inplane strain $\varepsilon_{\parallel}$ as function of the distance from the whisker root in comparison with the radially averaged values of $\varepsilon_{\parallel}2\nu(1-\nu)^{-1}$ and $-\varepsilon_{zz}$. (Copyright © 2009 American Institute of Physics)*

See > M. Sobiech[1,2]*, M. Wohlschlögel[1], U. Welzel[1], E.J. Mittemeijer[1]**, W. Hügel[2], A. Seekamp[2], W. Liu[3]***, and G.E. Ice[4], "Local, submicron, strain gradients as the cause of Sn whisker growth," Appl. Phys. Lett. **94**, 221901(2009). DOI: 10.1063/1.3147864

Author affiliations >
[1]Max Planck Institute for Metals Research, [2]Robert Bosch GmbH, [3]Argonne National Laboratory, [4]Oak Ridge National Laboratory

Correspondence >
*m.sobiech@mf.mpg.de
**e.j.mittemeijer@mf.mpg.de
***wjliu@anl.gov

> The authors are much obliged to the company Hans Heimerdinger Oberflächentechnik in Pforzheim, Germany, for specimen preparation. G.E.I. was supported by the U.S. Department of Energy Division of Material Sciences and Engineering, Office of Basic Energy Sciences. Use of the Advanced Photon Source was supported by the U.S. Department of Energy, Office of Science, Office of Basic Energy Sciences, under Contract No. DEAC02-06CH11357.

> 34-ID • XOR/UNI • Materials science, physics • Coherent x-ray scattering, microdiffraction • 3.3-cm Undulator A • Accepting general users

Accentuating the Positive by Cation Ordering in Manganite Superlattices

IN SHORT > Heterostructures are indispensable in the manufacture of semiconductor devices and other critical applications, and the quest to improve their capabilities and characteristics is of great importance. One approach is to attain greater control over the creation of these structures, ideally down to the level of a single unit-cell. Such capabilities could allow control over useful properties such as the ferromagnetic (or antiferromagnetic) ordering of a material by altering the atomic structures in ways that would adjust its Curie or Néel temperatures. Argonne researchers at the Materials Science Division (MSD), Center for Nanoscale Materials (CNM) and the APS, using the MU/XOR 6-ID-B,C and XOR/UNI 33-BM beamlines at the APS and neutron scattering at Oak Ridge National Laboratory, have demonstrated just such a capability.

MORE > Using molecular beam epitaxy approaches similar to those used for semiconductors, researchers from Argonne and the University of Illinois at Urbana-Champaign were able to interweave single unit-cell layers of undoped $LaMnO_3$ and $SrMnO_3$ in a superlattice structure, thus eliminating disorder at La/Sr cation sites. With this method, which the researchers call "digital synthesis," they were able to adjust the Néel temperature (T_N) of the films. Compared to a compositionally-equivalent, randomly-doped manganese film, $La_{1}/_{3}Sr_{2}/_{3}MnO_3$, the team enhanced the T_N by approximately 70K, a substantial increase.

Previous experimental work had already demonstrated that lattice disorder can affect the ferromagnetic characteristics of complex oxides, but the effects of disorder on antiferromagnetism remain largely unexplored. Because the various order parameters—such as charge, spin, orbitals, etc.—in these materials can be closely coupled to one another, altering one parameter via doping can affect others, sometimes creating potentially useful effects. The researchers created $(LMO)_m(SMO)_{2m}$ structures in superlattices in which La/Sr cations were arranged in ordered two-dimensional layers while still preserving the La/Sr ratio found in similar random alloys. They used x-ray diffraction at the APS beamlines neutron scattering at Oak Ridge National Laboratory to probe the effects of cation-site order on randomly-oriented $La_{1}/_{3}Sr_{2}/_{3}MnO_3$ films and $(SMO)_2$-$(LMO)_1$ superlattices that were grown under similar conditions (Fig. 1).

Neutron scattering studies show that both types of films displayed A-type antiferromagnetism, with in-plane, double-exchange-mediated, ferromagnetic sheets coupled in the out-of-plane direction along the c axis antiferromagnetically. In the superlattices, the A-type AF order propagates coherently in the direction of growth, with the m = 1 superlattices maintaining long-range order up to a temperature of 320K, and the m = 2 superlattices up to 285K. This amounts to a Néel temperature approximately 70K higher than seen in the $La_{1}/_{3}Sr_{2}/_{3}MnO_3$ films. X-ray scattering shows that this is the result of an in-plane structural modulation in the superlattices. The cation ordering drives this modulation to longer wavelengths, improving charge itinerancy and the ordering temperature, and thus increasing the Néel temperature.

The ability to increase the Néel temperature of complex oxides to above room temperature displayed in this work opens up some intriguing possibilities for the design and development of various similar materials. The digital synthesis process demonstrated here can be used with many other oxides, promising new materials with enhanced characteristics for a wide range of applications.

— Mark Wolverton

v *Fig. 1* ***(a)*** *Antiferromagnetic $La_{2/3}Sr_{1/3}MnO_3$ with random La/Sr cations and ordered La/Sr cations in $(LaMnO_3)_m(SrMnO_3)_{2m}$ superlattices. The magnetic moment on the Mn atoms align antiferromagnetically (blue arrows) at low temperatures* ***(b)*** *The magnetic order, as measured with neutron scattering, is lost upon warming up above the Néel temperature T_N, which is 70K higher when the cations are ordered* ***(c)*** *Superlattice fringes about the main (22δ) peak indicate a periodic in-plane modulation in the lattice that is strongest in the material with the randomly arranged La/Sr cations, which also has the lowest T_N. The modulation shifts to longer wavelengths as T_N increases.*

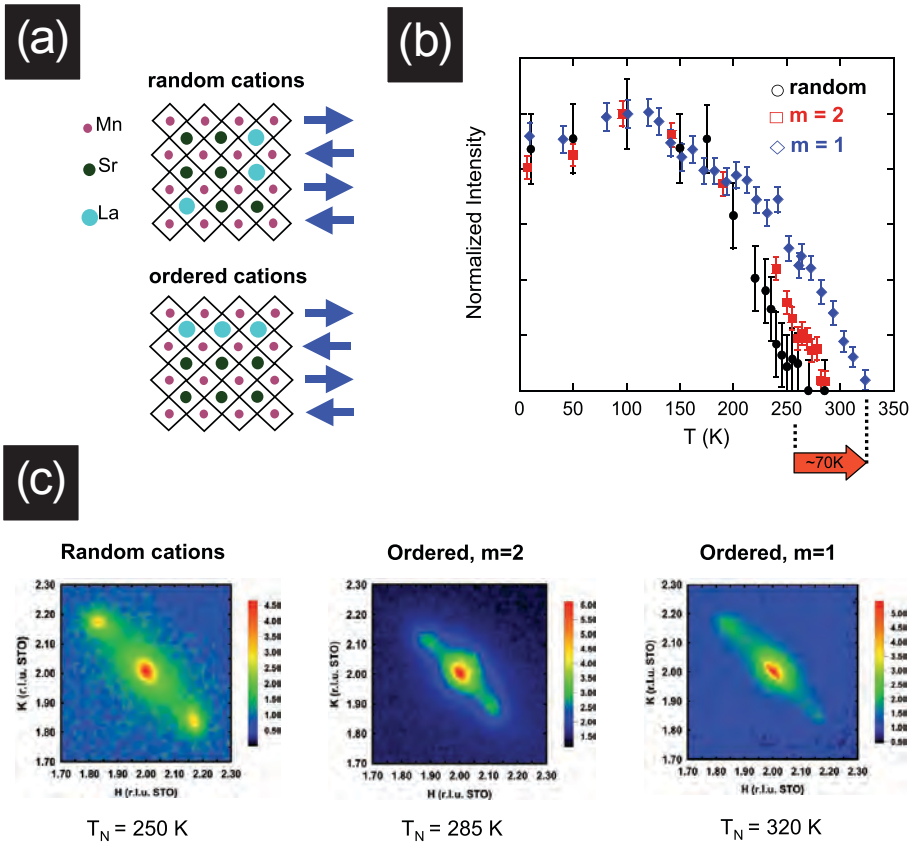

See > S.J. May[1], P.J. Ryan[2], J.L. Robertson[3], J.-W. Kim[1], T.S. Santos[1], E. Karapetrova[1], J.L. Zarestky[4], X. Zhai[5], S.G.E. te Velthuis[1], J.N. Eckstein[5], S.D. Bader[1], and A. Bhattacharya[1]*, "Enhanced ordering temperatures in antiferromagnetic manganite superlattices," Nat. Mater. **8**, 892 (November 2009). DOI:10.1038/NMAT2557

Author affiliations > [1]Argonne National Laboratory, [2]Ames Laboratory, [3]Oak Ridge National Laboratory, [4]Ames Laboratory and Iowa State University, [5]University of Illinois at Urbana-Champaign

Correspondence > *anand@anl.gov

> Work at Argonne, including use of the Advanced Photon Source and the Center for Nanoscale Materials, was supported by the U.S. Department of Energy, Office of Science, Office of Basic Energy Sciences, under contract No DE-AC02-06CH11357. Work at Oak Ridge National Laboratory's High Flux Isotope Reactor was sponsored by the Scientific User Facilities Division, Office of Basic Energy Sciences, U.S. Department of Energy.

> 6-ID-B,C • MU/XOR • Materials science, physics • Anomalous and resonant scattering (hard x-ray), general diffraction, grazing incidence diffraction, liquid scattering, magnetic x-ray scattering, surface diffraction (UHV) • 3.3-cm Undulator A • Accepting general users

> 33-BM • XOR/UNI • Materials science, physics, chemistry • Anomalous and resonant scattering (hard x-ray), diffuse x-ray scattering, powder diffraction, x-ray reflectivity, general diffraction, grazing incidence diffraction • Bending magnet • Accepting general users

Linking Surface Structure and Magnetism

IN SHORT > Manganites have been extensively studied for many years because of their rich array of intriguing electronic, magnetic, and structural properties arising from strongly competing internal interactions that can lead to unexpected ground states. For example, the broken translational symmetry at the surface of such a material can be enough to produce distinct functionality there due to the changing balance of charge, lattice, orbital, and spin degrees of freedom. With the help of the XOR 4-ID-C beamline at the APS, researchers from Louisiana State University, Northwestern University, the University of Tennessee, Oak Ridge National Laboratory, the Royal Institute of Technology, Charles University, and Argonne investigated the origin of a nonferromagnetic phase present at the surface of $La_{2-2x}Sr_{1+2x}Mn_2O_7$ manganites with hole doping levels corresponding to bulk ferromagnetic order (x = 0.36 and 0.40), using a combined experimental and theoretical analysis.

MORE > A quantitative study of surface structure was undertaken using low-energy electron diffraction (LEED) to determine geometric and chemical ordering, and the full-potential linearized augmented plane-wave (FLAPW) theoretical approach was employed in calculating the electronic structure of the $La_{2-2x}Sr_{1+2x}Mn_2O_7$ system for the two doping levels. Electronic and magnetic characterizations of *in situ* cleaved (001) surfaces were also performed using x-ray resonant magnetic scattering.

The LEED structural analyses revealed a LaSrO rocksalt-terminated surface that showed no sign of surface reconstruction (Fig. 1c). This indicates that the changes in the physical properties at the surface must not be due to a change of symmetry, but could be due to a change of lattice parameters at the surface. This finding was consistent with a detailed comparison of the electronic properties of manganese at the surface and in the bulk material using x-ray absorption spectroscopy, showing that the surface had the same composition as the bulk material.

To probe the details of the surface structure, a quantitative analysis of the experimental and theoretical LEED $I(V)$ curves was conducted, showing that the main structural changes at the (001) surface pertain to three different manganese-oxygen (Mn-O) distances in the top half of the surface bilayer. The most significant change was in the spacing between manganese and the top/bottom oxygen, designated as Mn-O(II). The other two Mn-O spacings basically keep their bulk values. The reduction of Mn-O(II) is consistent with a change in orbital occupancy and, consequently, the magnetic order at the surface. Specifically, the surface relaxation was seen to produce a collapse in the c axis, decreasing the Jahn-Teller lattice distortion. Bulk theoretical calculations revealed that, even at fixed doping level, the relaxation of the Jahn-Teller distortion at the surface is consistent with the stabilization of an A-type state with moments aligned ferromagnetically within the layer and antiparallel between the double layers.

This theoretical finding was supported by directly measuring the magnetic state at the surface using x-ray resonant magnetic scattering (XRMS) on XOR beamline 4-ID-C at the APS (Fig. 1a). The key observation from the XRMS measurements is that a change of sign of the XRMS signal occurs and can be connected to a single surface bilayer that displays no net magnetism and is therefore not ferromagnetic (Fig. 1b). Such a sign change would be absent if ferromagnetism was present in the surface bilayer.

— Vic Comello

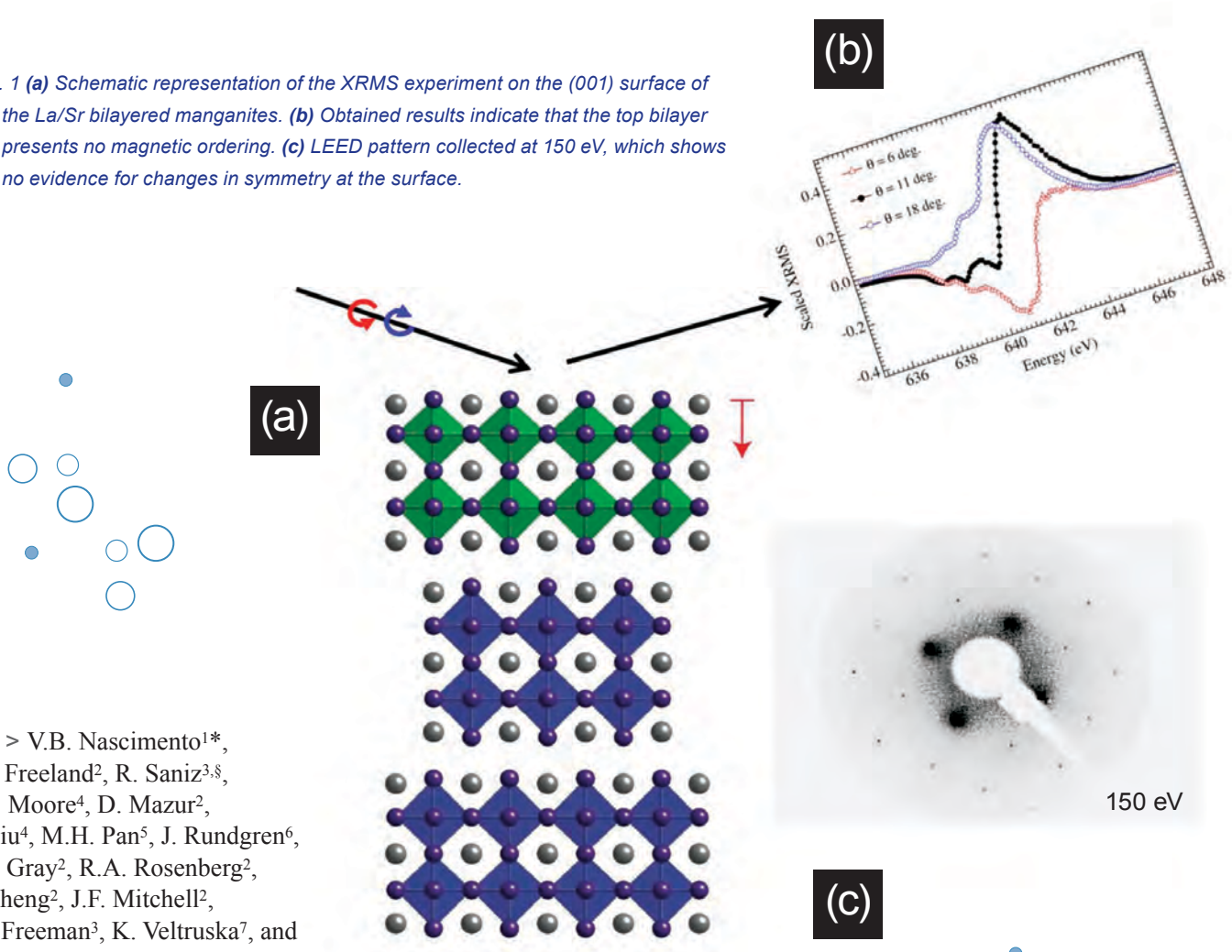

v *Fig. 1* ***(a)*** *Schematic representation of the XRMS experiment on the (001) surface of the La/Sr bilayered manganites.* ***(b)*** *Obtained results indicate that the top bilayer presents no magnetic ordering.* ***(c)*** *LEED pattern collected at 150 eV, which shows no evidence for changes in symmetry at the surface.*

See > V.B. Nascimento[1]*, J.W. Freeland[2], R. Saniz[3,§], R.G. Moore[4], D. Mazur[2], H. Liu[4], M.H. Pan[5], J. Rundgren[6], K.E. Gray[2], R.A. Rosenberg[2], H. Zheng[2], J.F. Mitchell[2], A.J. Freeman[3], K. Veltruska[7], and E.W. Plummer[1,4], "Surface-Stabilized Nonferromagnetic Ordering of a Layered Ferromagnetic Manganite," Phys. Rev. Lett. **103**, 227201 (27 November 2009). DOI: 10.1103/PhysRevLett.103.227201

Author affiliations >
[1]Louisiana State University,
[2]Argonne National Laboratory,
[3]Northwestern University,
[4]University of Tennessee,
[5]Oak Ridge National Laboratory,
[6]Royal Institute of Technology,
[7]Charles University [§]Present address Universiteit Antwerpen

Correspondence >
*vnascimento@lsu.edu

> Work at Argonne, including the Advanced Photon Source, was supported by the U.S. Department of Energy (DOE), Office of Science, Office of Basic Energy Sciences under Contract No. DE-AC02-06CH11357. Work at Northwestern University was supported by the DOE under Grant No. DE-FG02-88ER45372 and a grant of computer time at the National Energy Research Scientific Computing Center. V.B.N. acknowledges support from the Distinguished Scientist Program at UTK-ORNL (E.W.P.). The part of this work performed at the University of Tennessee and ORNL received support from the National Science Foundation and DOE (DMS&E) Grant No. NSF-DMR-0451163.

> 4-ID-C • XOR • Materials science, physics • Anomalous and resonant scattering (soft x-ray), magnetic circular dichroism (soft x-ray), magnetic x-ray scattering, x-ray photoemission electron microscopy, x-ray photoemission spectroscopy, x-ray magnetic linear dichroism • Circularly polarized undulator • Accepting general users

Stressing Out the Twins in Magnesium

IN SHORT > The way a material reacts under stress is a question of critical relevance, especially when considering that material's strength and versatility for various uses. Under stress, hexagonal-close-packed (HCP) metals are known to undergo crystallographic twinning, when parts of a grain abruptly flip and create mirror-image copies of themselves. Because twinning also results in new reoriented grain domains and shear patterns that can affect the mechanical qualities of a metal, a detailed understanding and precise characterization of such behavior is essential for the development and use of predictive models. Working at the XOR 1-ID beamline at the APS, a team of researchers has pioneered a method of using three-dimensional x-ray diffraction (3DXRD) to study the twinning process in low-symmetry materials and its evolution *in situ* on the level of individual grains, while also allowing the full stress tensor to be measured.

MORE > The experimenters—from the Los Alamos, Lawrence Livermore, and Argonne national laboratories—examined cylindrical samples of the magnesium alloy AZ31 on the 1-ID beamline, using 3DXRD with a 200-μm × 200-μm synchrotron x-ray beam at 80.7 keV. Compression stress at 20-MPa increments was applied perpendicular to the axis of the x-ray beam while the sample was rotated over 120° along the loading axis. Bragg reflections (diffraction spots) from various grains were picked up by an area detector in several crystallographic planes.

Data from the diffraction spots were analyzed by computer to identify grains in twinning orientations. Magnesium was chosen as an experimental material because its hexagonal structure allows twinning to be easily induced under stress.

Previous neutron diffraction studies of AZ31 clarified the need for obtaining data at a finer level of precision than is possible with that method. The researchers were looking for experimental input for some of their modeling efforts, to see how twinning influences deformation of materials in general. While neutron diffraction provides excellent statistical data, it cannot delineate the individual twinning process in single grains, unlike the 3DXRD technique used in the current work.

The researchers identified three grains that, because of their orientation, were good candidates for twinning, along with another grain in a completely different orientation for use as a control reference. They monitored these grains during the experimental runs as stress was applied. Because the team found that the overlapping of diffraction spots increased with stress, usable signal was no longer generated by two of the grains after a certain point, but the remaining grain displayed a good degree of twinning before it was also overlapped by diffraction spot signals at about 90 MPa.

When the orientation of the parent grain is known, it is possible to calculate the positions of the diffraction spots of the twins, and their subsequent appearance in the predicted locations indicates the presence of that particular twin variant. The grain displayed variants 2 and 5 of the 6 variants in the {1012}<1011> twinning system (as numbered clockwise around the *c* axis of the hexagonal unit cell), beginning at 40-MPa of compression. Although all six variants are possible, in general, only one is actually generated, and that is the one for which the resolved shear stress on the twin system is the highest. If two of them have a high value of the resolved shear stress, then you one have two. It all depends on the orientation of the parent grain.

The researchers were able to determine the three-dimensional stress tensors of the parent grain and its twin variants at every stage of evolution with greater precision than previously achieved with the 3DXRD technique (Fig. 1).

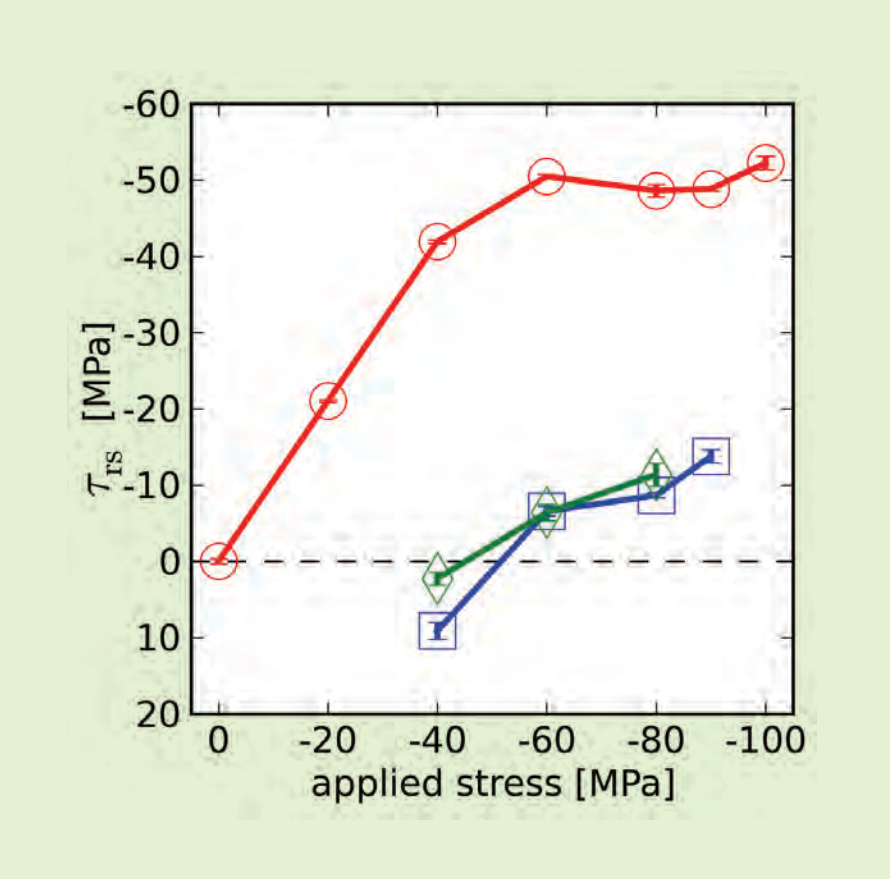

^ *Fig. 1 Resolved shear stress on the twin system as a function of applied stress; once the twinning occurs, the resolved shear stress in the parent saturates, and more importantly, the shear stress in the twin(s) is initially of the opposite sign than in the parent. This illustrates the significant stress relaxation associated with twinning.*

The team hopes to use the present data to refine their current models to predict how various low-symmetry materials will behave. A future question is how the surrounding grains affect the stresses on the twinning grain. Statistically, the grains around the parent grain that is twinning will also have some influence. In the future, the researchers would like to take into account all the actual grains around, because they are themselves anisotropic.

The models could also eventually be applicable to other hexagonal systems, including magnesium, zirconium, and titanium. The process of twinning is very similar to martensitic transformations, so the same techniques could be used for looking at domain switching in ferroelectrics and martensitic phase transformation in shape memory alloys.

— Mark Wolverton

See > C.C. Aydıner[1]*, J.V. Bernier[2], B. Clausen[1]**, U. Lienert[3], C.N. Tomé[1], and D.W. Brown[1], "Evolution of stress in individual grains and twins in a magnesium alloy aggregate," Phys. Rev. B **80**, 024113 (2009). DOI: 10.1103/PhysRevB.80.024113

Author affiliations > [1]Los Alamos National Laboratory, [2]Lawrence Livermore National Laboratory, [3]Argonne National Laboratory

Correspondence >
*can.aydiner@boun.edu.tr
**clausen@lanl.gov

> This work was supported by the U.S. Department of Energy Office of Basic Energy Science through Project No. FWP 06SCPE401. Use of the Advanced Photon Source was supported by the U.S. Department of Energy, Office of Science, Office of Basic Energy Sciences, under Contract No. DE-AC02-06CH11357.

> 1-ID • XOR • Materials science, physics, chemistry • High-energy x-ray diffraction • 3.3-cm Undulator A • Accepting general users

High-Pressure "Alchemy"

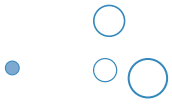

IN SHORT > The properties of magnetic materials continue to spark great scientific and practical interest. One of the most well-known magnetism-related phenomenon is the so-called Invar effect, in which Invar alloys maintain nearly constant size over a wide range of temperatures. This makes them ideal for use in watches, toasters, light bulbs, engine parts, satellites, lasers, scientific instruments, and even computer and television screens. While it has long been known that the chemical makeup of the alloys is responsible for Invar behavior by creating unusual electronic configurations that constrain lattice expansion, the Invar effect remains one of the oldest and most-studied unresolved problems in materials research. With the aid of a beamline at the APS, researchers have helped unify our understanding of Invar behavior.

MORE > Studies carried out by researchers from Caltech, The University of Chicago, and the Carnegie Institution of Washington show that Pd_3Fe, a ferromagnetic material that does not exhibit Invar behavior at ambient pressure, does show Invar characteristics when placed under great pressure, indicating the possibility of a kind of alchemy in which pressure makes electrons behave as if they were in a material of different chemical composition. The ability to use pressure to force a material's electrons into new states points to new directions in materials chemistry in which novel properties may be found, at least for magnetic materials.

Initial testing at the National Synchrotron Light Source (NSLS) at Brookhaven National Laboratory, using energy-dispersive x-ray diffraction at room temperature and pressures up to 33 GPa, showed that Pd_3Fe suffered a significant volume collapse between approximately 10 GPa and 15 GPa, and that the material stiffened by an unexpectedly large amount above 15 GPa.

To understand why, the scientists simulated the quantum mechanical behavior of the electrons in the alloy under pressure using density functional theory calculations. The simulations suggested that the electrons in the alloy shifted under pressure into the special electronic energy levels between strong and weak magnetism that are associated with normal Invar behavior. Up to this point, the researchers had been unaware that the material might be capable of the Invar effect.

To confirm the predicted change in electronic states, the researchers conducted a nuclear forward scattering (NFS) experiment on HP-CAT beamline 16-ID-D at the APS to gain a direct measure of the magnetic state of the material under pressure. NFS spectra from Pd_3Fe showed quantum beats at lower pressures, indicating that the material was magnetically ordered, but the beats decreased significantly in amplitude at 12.3 GPa and vanished altogether at higher pressures (Fig. 1). This result is consistent with a first-order phase transition in which pressure causes a shift from a high magnetization state to a low magnetization state. As a final check on the calculated result, the researchers heated a sample of Pd_3Fe under a pressure of 7 GPa and found negligible thermal expansion from 300K to 523K, demonstrating Invar behavior. These studies identified the necessary condition for Invar behavior as having an alloy at the edge of the transition from strong to weak ferromagnetism.

— Vic Comello

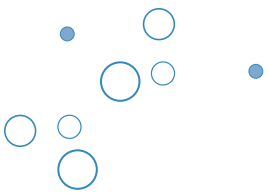

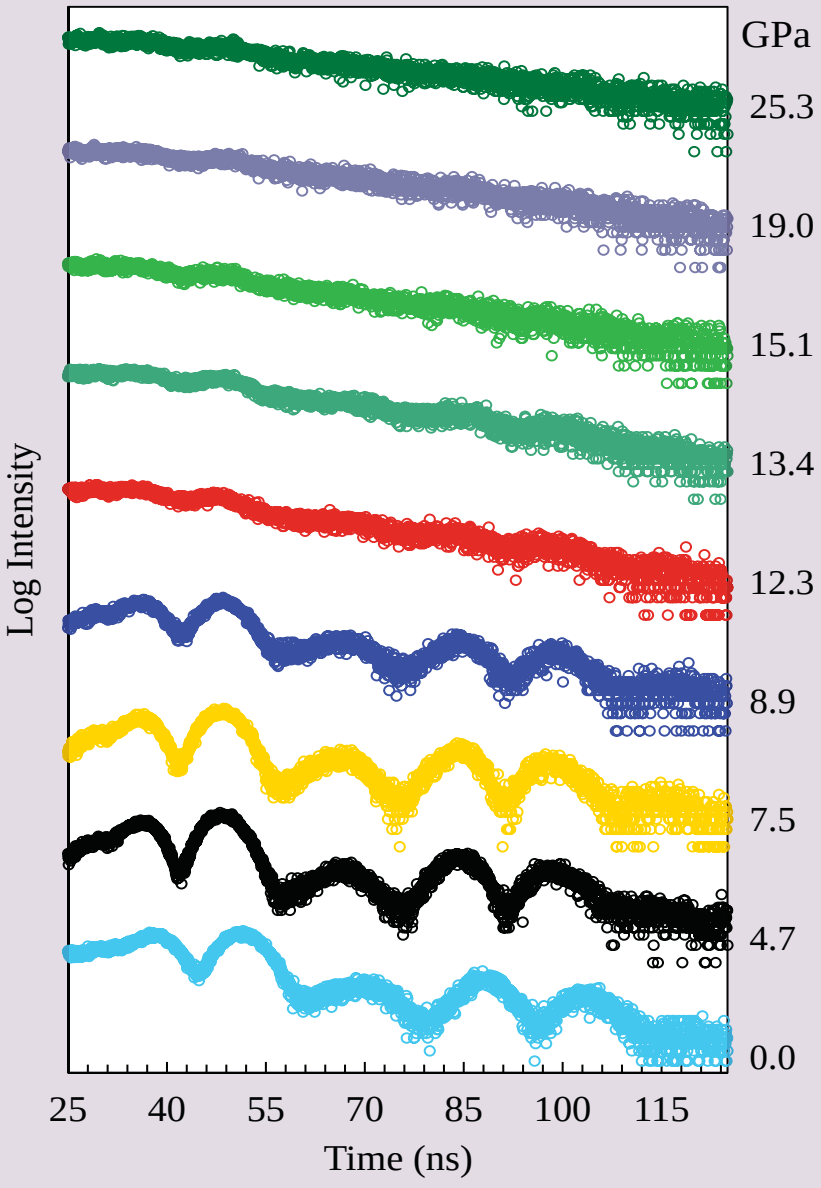

^ *Fig. 1 Nuclear forward scattering spectra from chemically ordered $Pd_3{}^{57}Fe$ showing a sudden decrease of the hyperfine magnetic fields in the material at around 12 GPa.*

See > Michael L. Winterrose[1], Matthew S. Lucas[1], Alan F. Yue[1], Itzhak Halevy[1], Lisa Mauger[1], Jorge A. Muñoz[1], Jingzhu Hu[2], Michael Lerche[3], and Brent Fultz[1]*, "Pressure-Induced Invar Behavior in Pd_3Fe," Phys. Rev. Lett. **102**, 237202 (12 June 2009). DOI:10.1103/PhysRevLett. 102.237202

Author affiliations >
[1]California Institute of Technology,
[2]The University of Chicago,
[3]Carnegie Institution of Washington

Correspondence >
*btf@caltech.edu

> This work was supported by the Carnegie-U.S. Department of Energy (DOE) Alliance Center and was funded by the DOE through the Stewardship Sciences Academic Alliance of the National Nuclear Security Administration (NNSA). HP-CAT was supported by DOE-Basic Energy Sciences (DOE-BES), DOE-National Nuclear Security Administration, the National Science Foundation (NSF), and the W. M. Keck Foundation. Use of the NSLS was supported by DOE-BES under Contract No. DE-AC02-98CH10886. Beamline X17C at NSLS was supported by the Consortium for Materials Properties Research in Earth Sciences (COMPRES) of the NSF. Use of the Advanced Photon Source at Argonne National Laboratory was supported by the U.S. Department of Energy, Office of Science, Office of Basic Energy Sciences, under Contract No. DE-AC0206CH11357.

> 16-ID-D • HP-CAT • Materials science, geoscience, physics • Nuclear resonant scattering, inelastic x-ray scattering, x-ray Raman scattering, x-ray emission spectroscopy • 3.3-cm Undulator A • Accepting general users

Revealing Degradation Mechanisms in Solid-Oxide Fuel Cells

IN SHORT > Technologists anticipate that solid-oxide fuel cells will play an important role in high-efficiency power plants and clean-coal technology, but these future energy devices are not without problems. Solid-oxide fuel cells, SOFCs, produce electricity by electro-chemically oxidizing a fuel, such as hydrogen or carbon monoxide, to water or CO_2. Like all fuel cells they have an ion-conducting electrolyte that divides two electrodes, anode and cathode, which are fed by fuel gas and air, respectively. The electric current starts to flow when the electrodes are connected with the external load while charged ions, produced electrochemically, are transported through electrolyte inside of the fuel cells. In a polymer electrolyte fuel cell, a polymer membrane carries hydrogen ions (protons) from the cell's anode to its cathode. In a SOFC, the membrane is replaced by a solid-oxide electrolyte that carries negative oxygen ions from the cathode to the anode. Experiments carried out by Argonne scientists using the XOR 1-ID beamline at the APS revealed important facets of the cells' construction and operation, and could lead to improved performance and longer lifetimes for these devices.

MORE > All types of fuel cell device have their own advantages and challenges. SOFCs typically operate at a temperature range of 600° C to 1000° C, producing power outputs from less than 100 W to better than megawatts with a putative efficiency of more than 60%. The high-temperature operation also makes it feasible to recover the waste heat produced from SOFCs to drive gas turbines for secondary power generation, therefore further boosting the total efficiency.

So-called planar SOFCs use inexpensive metallic interconnects made from ferritic stainless steels to draw the electric current produced at the electrodes. These materials are cheaper than the alternatives, but contain high levels of chromium (Cr). Under operating conditions, chromium forms various kinds of oxides, which segregate from the interconnects and accumulate on the cathode through diffusion, leading to degradation and failure of the SOFC—a phenomenon known as chromium poisoning.

Researchers have attempted to develop coatings to prevent chromium diffusion to the cathode, but a long-term solution is yet to be found, which threatens to stifle the development of SOFCs. Part of the problem is that researchers do not have a complete picture of the chromium migration process despite various studies using elemental analysis, surface x-ray scattering, scanning electron microscopy, and transmission electron microscopy. These conventional techniques have all failed so far to provide a comprehensive picture of the nature and distribution of the chromium contaminants, as well as changes in the cell's physical properties that they may induce.

The Argonne researchers turned to recently developed high energy microbeam synchrotron x-ray diffraction and radiographic techniques to investigate the layer composition and internal strain inside of SOFC layers with unprecedented spatial resolution (Fig. 1). They conducted the first accurate measurement of two-dimensional (2-D) Cr species distributions and revealed the presence of manganese-chromium spinel and chromium(III) oxide as the main contaminants in the chromium poisoned SOFCs. The accumulation of these two materials at the cathode catalyst and electrolyte interface prevents the normal flow of fuel gas, damages the cathode's structural integrity, and ultimately deactivates the SOFC.

An additional important point emerges from this study. Earlier work by others had suggested that chromium might be transported through gas diffusion to the cathode.

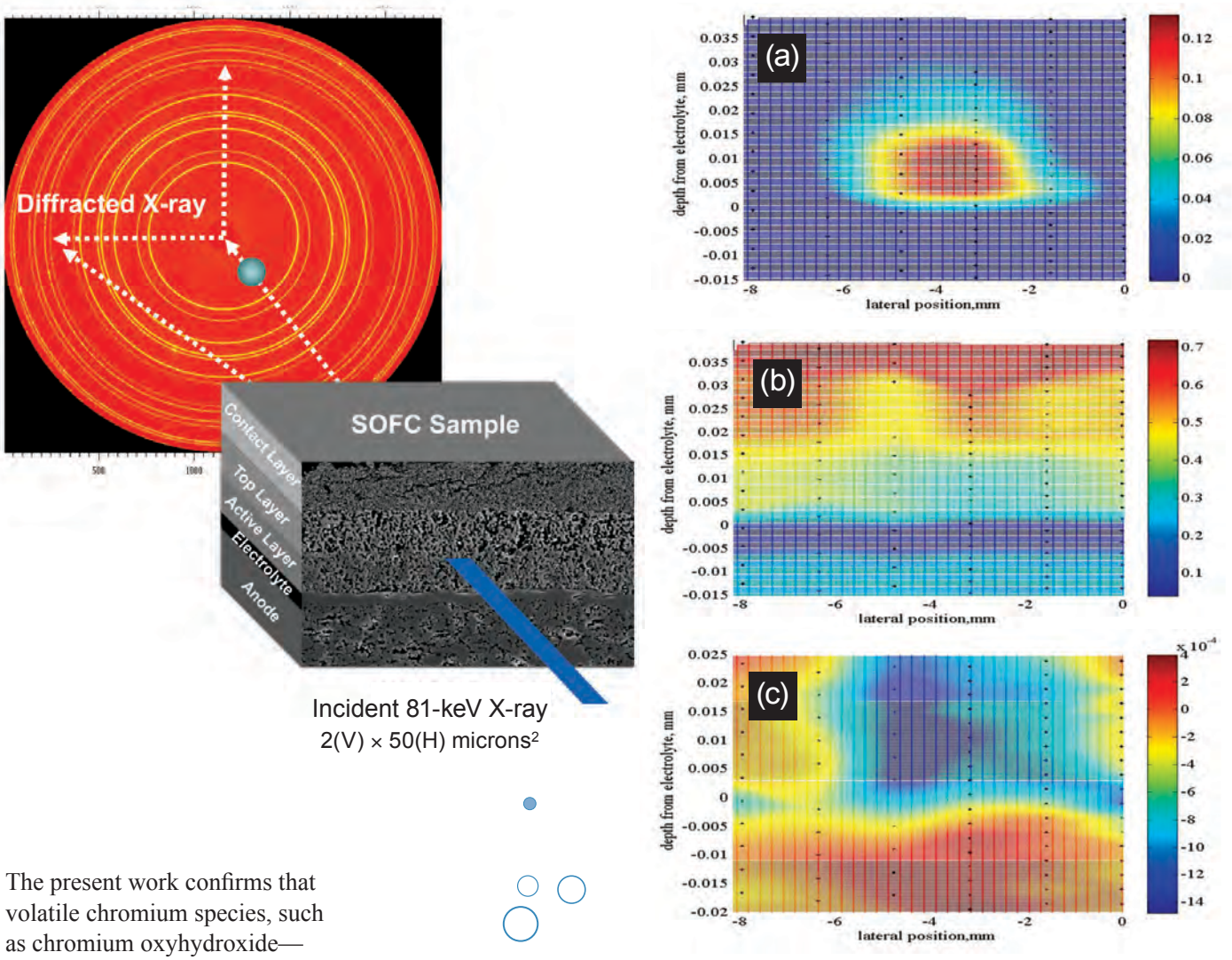

^ *Fig. 1 Schematic showing the high-energy microbeam synchrotron x-ray diffraction and radiographic technique with a typical diffraction pattern along with 2-D distributions of* ***(a)*** *Cr_2O_3 weight fraction,* ***(b)*** *porosity and* ***(c)*** *deviatoric strain in the YSZ phase.*

The present work confirms that volatile chromium species, such as chromium oxyhydroxide—$CrO_2(OH)_2$,—and chromium(VI) oxide—CrO_3,—are generated on the surface of the metallic interconnects and permeated through the porous layers of the cathode. As soon as these high-valance-state, volatile species come into contact with the electrolyte and catalyst, they are reduced to low-valance oxides and deposited inside the most active region of the cathode. The process continues until the SOFC fails.

The Argonne researchers add that it is the strong penetrating power of the APS high-energy x-rays and high spatial resolution of the technique that make up a powerful tool for investigating SOFCs and other layered electrochemical devices under actual operating conditions.

— David Bradley

See > Di-Jia Liu* and Jonathan Almer, "Phase and strain distributions associated with reactive contaminants inside of a solid oxide fuel cell," Appl. Phys. Lett. **94**, 224106 (2009). DOI: 10.1063/1.3148362

Author affiliation >
Argonne National Laboratory

Correspondence >
*djliu@anl.gov

> This study was supported by the U.S. Department of Energy offices of Basic Energy Sciences and Fossil Energy. Use of the Advanced Photon Source was supported by the Office of Science, Office of Basic Energy Science, under Contract No. DE-AC02-06CH11357.

> 1-ID • XOR • Materials science, physics, chemistry • High-energy x-ray diffraction • 3.3-cm Undulator A • Accepting general users

Ordering the "Nano" World

IN SHORT > A variety of novel technologies, including drug delivery systems, photovoltaic cells, and computer microprocessors, depend on the use of nanotechnology, which makes use of the submicroscopic particles called nanoparticles. The assembly of nanoparticles into uniformly-ordered materials is critical for the reliable functioning of nanotechnology. More than a decade ago, researchers at Northwestern University developed a process that used small strands of DNA attached to gold nanoparticles to direct nanoparticle assembly. DNA consists of building blocks called nucleotides that pair together in a predictable manner, and the process is used to assemble nanoparticles by programming specific nucleotide sequences. In 2008, the research team further expanded this method of assembly to create highly ordered, three-dimensional (3-D) nanoparticle architectures. In the current study, these researchers and colleagues from Argonne used two x-ray beamlines at the APS to characterize the way in which these 3-D crystal structures are formed as a path to creating ordered crystal structures that can be used to extend the useful applications of this technology.

MORE > Nanoparticles are typically about 100 nm or less in size, smaller than most cells, or about the size of a large virus. Nanomaterials often exhibit unique properties due to their extremely small size and large surface area-to-volume ratio. For example, a solution of gold nanoparticles, appears red in color, as opposed to the shiny yellow of bulk gold. Well-ordered 3-D structures are necessary for creating consistent physical properties in the materials used in nanotechnology. The researchers in this study used small angle x-ray scattering measurements carried out during the crystallization process at the DND-CAT 5-ID beamline and the XOR/BESSRC 12-ID beamline at the APS to characterize the three-phase process in which DNA-functionalized gold nanoparticles assemble into well-ordered crystal structures (Fig. 1).

They found that when the appropriate DNA linkers are added to a solution of DNA-functionalized nanoparticles, they first form small, disordered clusters consisting of just a few nanoparticles. In a second step, these clusters simultaneously reorganize into ordered crystals and aggregate to form larger cluster-cluster aggregates. In a third and final step, the cluster-cluster aggregates rearrange to form well-ordered, larger (micrometer-size) crystal structures.

The researchers also examined the effects of various environmental parameters on the assembly process. For example, higher temperatures are necessary to achieve the greatest extent of ordering among the structures, whereas at room temperature, no crystallinity is observed in the aggregates. In addition, DNA length has a significant impact on the timescale of the assembly process, with longer DNA linkers forming crystals at a slower rate. The group also determined that the assembly process affected the final structure of crystals obtained. Distinct crystal types were obtained depending on whether a single self-complementary strand of DNA (i.e., a one-component system) or a more complex (two-component) system was used. They also characterized the timing of the assembly depending on whether a one- or two-component system was used.

By understanding these processes and the manner in which DNA can be used to create ordered crystal structures, it is possible to design more effective and efficient methods and procedures for creating gold nanoparticle crystal systems used in nanotechnology, thereby extending the useful applications of this technology.

— Emma Hitt

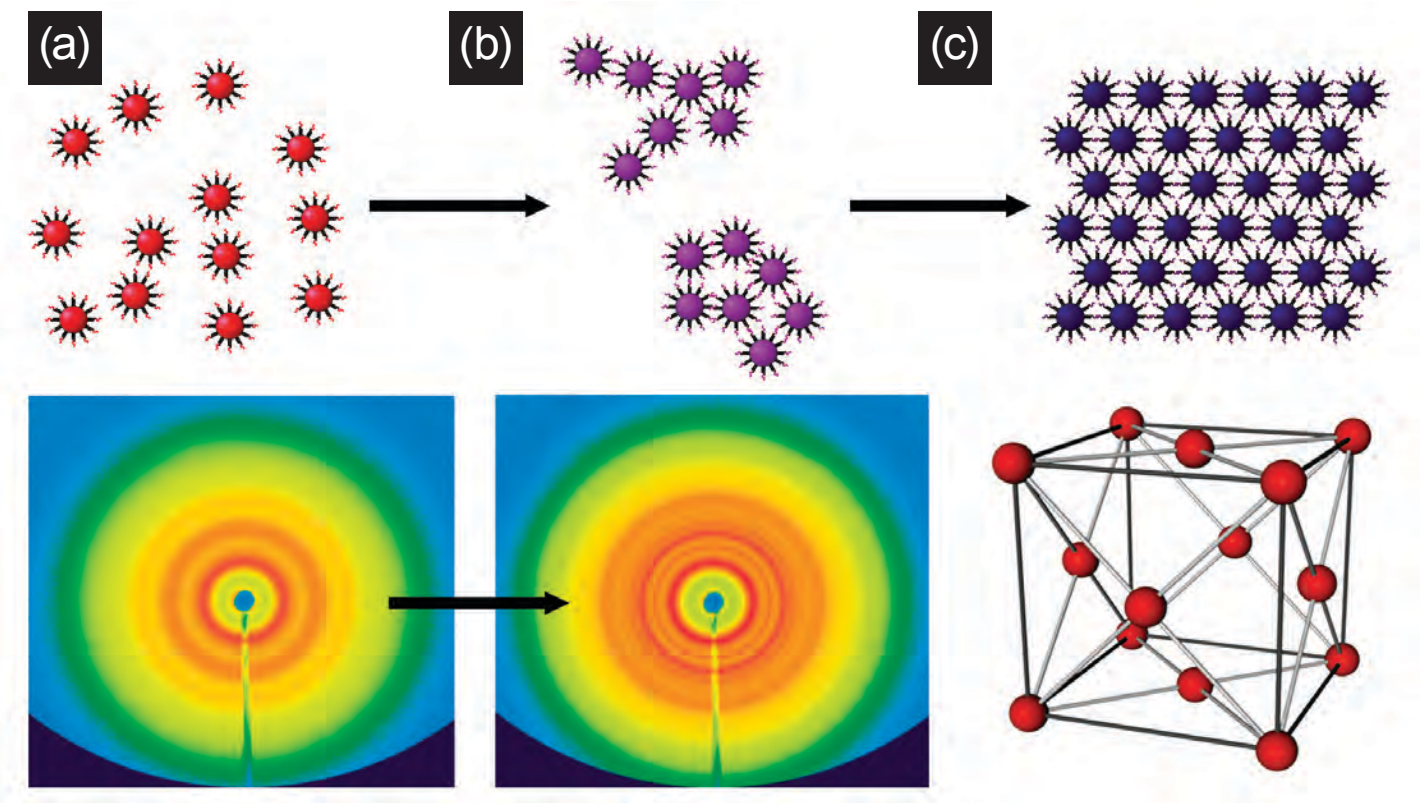

^ *Fig. 1* ***Top:*** *Programmable DNA interactions assemble nanoparticles into ordered 3-D structures via a process of a) small, disordered cluster formation, b) simultaneous cluster reorganization and cluster-cluster aggregation, and c) reorganization of cluster-cluster aggregates into ordered crystals.* ***Bottom left:*** *Small-angle x-ray scattering patterns demonstrating the transition from a disordered aggregate to an ordered crystal.* ***Bottom right:*** *A face-centered cubic unit cell, demonstrating the final arrangement of nanoparticles within the 3-D lattice.*

References > C.A. Mirkin, R.L Letsinger, R.C. Mucic, and J.J. Storhoff, "A DNA-Based Method for Rationally Assembling Nanoparticles into Macroscopic Materials," Nature **382(**6592**)**, 607 (1996). S.Y. Park et al., DNA-Programmable Nanoparticle Crystallization," Nature **451**(7178), 553 (2008).

See > Robert J. Macfarlane[1], Byeongdu Lee[2], Haley D. Hill[1], Andrew J. Senesi[1], Soenke Seifert[2], and Chad A. Mirkin[1]*, "Assembly and organization processes in DNA-directed colloidal crystallization," Proc. Nat. Acad. Sci. USA **106**(26), 10493 (2009). DOI:10.1073/pnas.0900630106

Author affiliations > [1]Northwestern University, [2]Argonne National Laboratory

Correspondence > *chadnano@northwestern.edu

> This work was supported by the National Science Foundation Nanoscience and Engineering Center, the Air Force Office of Scientific Research, the National Cancer Institute Center for Cancer Nanotechnology Excellence, and a National Institutes of Health Director's Pioneer Award (to C.A.M.); and a U.S. Department of Homeland Security Graduate Fellowship under the DHS Scholarship and Fellowship Program (to H.D.H.). The DND-CAT is supported by E. I. DuPont de Nemours & Co., The Dow Chemical Company, and the State of Illinois. Use of the Advanced Photon Source was supported by U.S. Department of Energy, Office of Science, Office of Basic Energy Sciences, under Contract DE-AC02-06CH11357.

> 5-ID • DND-CAT • Materials science, polymer science • Powder diffraction, small-angle x-ray scattering, surface diffraction, wide-angle x-ray scattering, x-ray optics development/techniques, x-ray reflectivity, x-ray standing waves • 3.3-cm Undulator A • Accepting general users

> 12-ID • XOR/BESSRC • Chemistry, materials science, physics • Grazing incidence small-angle scattering, small-angle x-ray scattering, surface diffraction, wide-angle x-ray scattering • 3.3-cm Undulator A • Accepting general users

Exploring the Constructs of Bird Feather Color

IN SHORT > Bird feathers are adorned with some of the richest, deepest colors in the animal kingdom. Many of these colors are formed not from pigment, but from the scattering of light by extremely small, ordered structures within the cells of the bird feathers. These "nanostructures," which cause light to scatter and make color, are made of beta-keratin (not to be confused with β-carotene, or vitamin A). Beta-keratin is a protein found in the feathers and skin of birds and reptiles that confers waterproofing and prevents desiccation. Bird feathers and their colors play an important role in social and sexual communication among birds, so the way in which the shape and form of these nanostructures translate into projecting various colors is of interest. To find out more about this process, researchers from Yale University used the XOR 8-ID-I beamline at the APS in their investigations into precisely how these nanostructures develop. Their findings may provide additional information about the way in which other photonic (i.e., light sensing, detecting, and emitting) nanostructures can be synthesized.

MORE > The field of photonics incorporates many applications, including laser manufacturing, biological and chemical sensing, medical diagnostics and therapy, and display technology. By understanding more about photonics, it may be possible to advance the understanding of the field and develop new and useful applications.

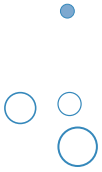

In their study, the Yale researchers sought to understand more about the function and evolution of the coloration of bird feathers and how photonic nanostructures form during bird development.

According to the researchers, colors vary according to differences in the size and shape of nanostructures. Given the role of colors and their appearance in bird social and sexual communication, it is important that the growth of these nanostructures is tightly controlled during development by "templates" that direct cellular growth. However, a contrasting way in which color can be created is through the undirected self-assembly of crystal-like particles. The Yale group hypothesized that photonic nanostructures in bird feathers self-assemble, and sought to elucidate the way in which this occurs.

Feathers consist almost entirely of beta-keratins that self-assemble into strands called filaments. Two types of these nanostructures have been identified based on their structure. One type is referred to as a "channel" type that has a twisted, string-like appearance. This channel type nanostructure is found in the blue back plumage of the Eastern Bluebird. The other type of nanostructure is referred to as "spherical" and is the type found in the vivid turquoise-blue plumage of the Plum-Throated Cotinga bird. It appears that channel and spherical types of nanostructures have evolved independently in birds.

The researchers compared the optical light scattering properties between the Eastern Bluebird and the Plum-Throated Cotinga using small-angle x-ray scattering. They found several differences between the optical properties of the feathers of these two birds. One difference was that the light emitted by the Plum-Throated Cotinga was about eight times that emitted by the feathers of the Eastern Bluebird.

On the basis of their observations, the researchers conclude that birds develop color-producing nanostructures by arresting structural formation during development. Structures vary due to the rate of beta-keratin expression;

v ***(a)*** *Photograph of crown feathers from* ***L. coronata****: the field of view is 1 cm.* ***(b)*** *TEM image of air spheres in beta-keratin from* ***L. coronata****: the field of view is 5.5 µm.*

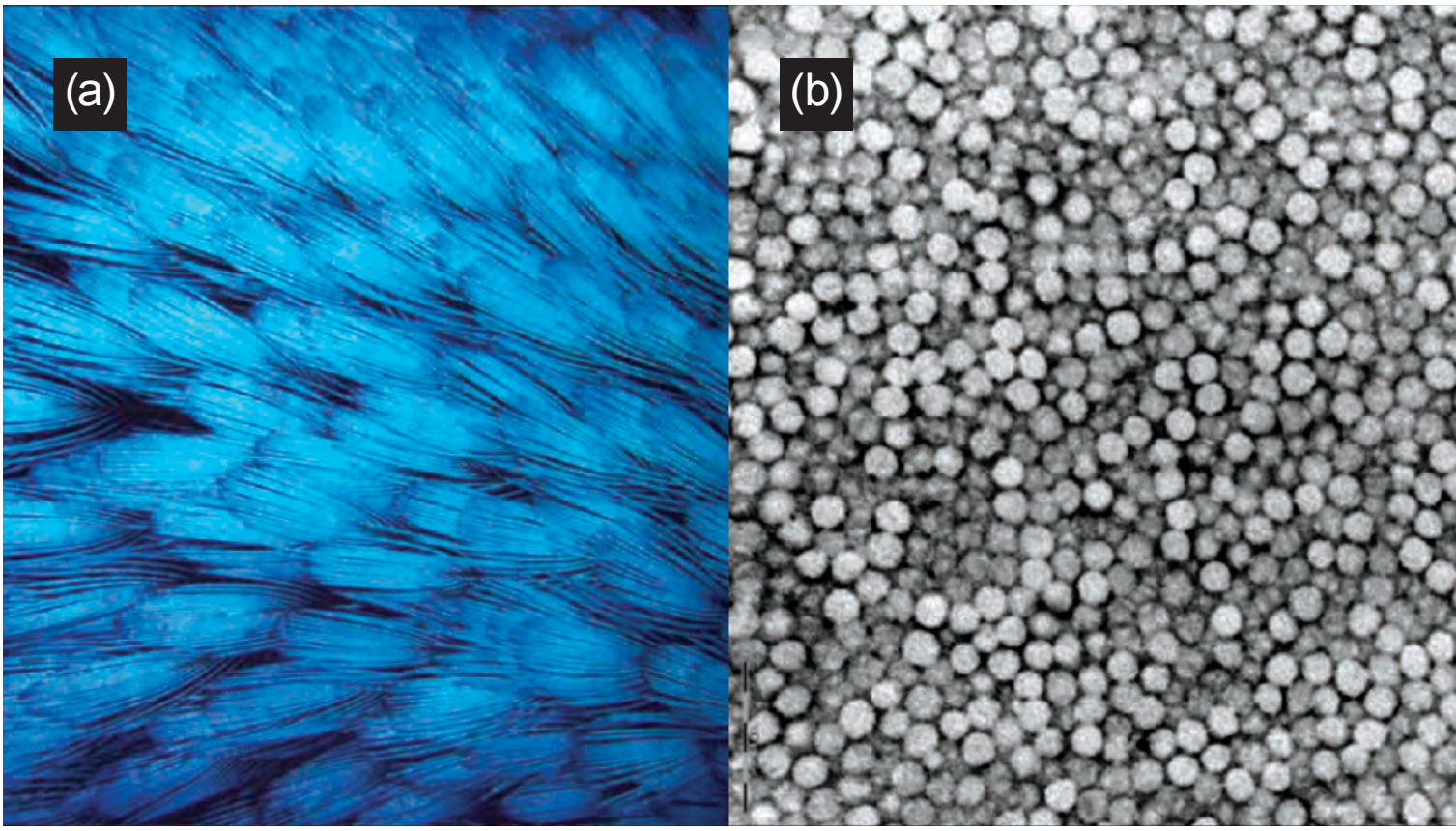

the rate of polymerization (i.e., joining together) of the beta-keratin subunits; and the rate of cross-linking of beta-keratin strands. In addition, the group also determined that beta-keratins appear to self-assemble during a process called phase-separation in which beta-keratins separate from other components within the cellular cytoplasm.

By mimicking this process with other biological substances, it may be possible to create new ways to develop photonic nanostructures.

— Emma Hitt

See > Eric R. Dufresne*, Heeso Noh, Vinodkumar Saranathan, Simon G.J. Mochrie, Hui Cao, and Richard O. Prum**, "Self-assembly of amorphous biophotonic nanostructures by phase separation," Soft Matter **5**(9), 1792 (2009). DOI:10.1039/b902775k

Author affiliation >
Yale University

Correspondence >
*eric.dufresne@yale.edu
**richard.prum@yale.edu

> This work was supported with seed funding from the Yale NSF-MRSEC (DMR-0520495) and National Science Foundation grants to E.R.D. (CBET), S.G.J.M. (DMR), H.C. (EECS), and R.O.P. (DBI). Use of the Advanced Photon Source at Argonne National Laboratory was supported by the U.S. Department of Energy, Office of Science, Office of Basic Energy Sciences, under Contract No. DE-AC02-06CH11357.

> 8-ID-I • XOR • Materials science, physics, polymer science • Intensity fluctuation spectroscopy, small-angle x-ray scattering, x-ray photon correlation spectroscopy • 3.3-cm Undulator A • Accepting general users

Two Ways of Laying Down the Lipids

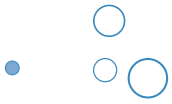

IN SHORT > Lipid monolayer and bilayer structures are interesting not only because they can be studied as a working model of cellular membranes, but also because the ability to better understand and create them could lead to the development of new medical applications and treatments. Generally, the extreme thinness and delicacy of these bilayers makes them notoriously difficult to examine in precise detail. A research team from the University of California, Davis; and Los Alamos National Laboratory employed the MU/XOR 6-ID-B,C beamline at the APS to carry out experiments comparing two different methods for artificially forming lipid bilayers, using x-ray reflectivity and grazing incidence diffraction (GIXD) to characterize and measure the formation and structure of lipid bilayers with unprecedented clarity.

MORE > The experimenters studied membranes formed from dipalmitoyl-phosphatidylcholine (DPPC). DPPC is one of the most common phospholipids, a class of molecules with "heads" that attract water (hydrophilia) and "tails" that repel it (hydrophobia), causing these molecules to spontaneously arrange themselves when in water into a two-molecule-thick bilayer with the hydrophilic heads facing out and the hydrophobic tails inward. For this study, bilayers were created on a solid quartz substrate either by vesicular fusion, the most popular bilayer preparation method, or via the Langmuir-Blodgett-Schaeffer (LBS) deposition technique. The team's goal was to determine which method yielded the most complete, well-packed, and easily reproducible membranes, among other questions. Monolayer observations were performed at HASYLAB's BW1 undulator beamline in Hamburg, Germany; the bilayer observations were done at the 6-ID-B,C beamline.

Aside from comparing the two bilayer preparation techniques, the team also sought to determine the role of the solid substrate on the membrane structure and the qualities of any ordered domains that might form within the layers. LBS DPPC bilayers were formed by the deposition of DPPC monolayers in a Langmuir trough, while vesicular fusion samples were prepared from unilamellar vesicles of about 500-Å diameter made with a tip probe sonicator. A very thin water cushion was present between the inner leaflet of the bilayers and the substrate support.

In comparing the samples prepared by vesicle fusion and LBS deposition (Fig. 1), the experimenters found that while both have highly similar structures, the bilayers formed by vesicular fusion show asymmetric electron density distribution between their two leaflets, with the inner leaflet showing a higher than expected electron density. This seems to be due to greater disorder in the inner leaflet caused by the vesicular fusion process. The bilayers formed by vesicular fusion are also in general about 5% thicker than bilayers prepared by LBS.

Scattering intensity, as shown by GIXD, displayed distorted hexagonal lattices similar to DPPC multilayers. Bragg rod analysis showed that despite being deposited independently of one another, the lipid tails in opposing leaflets quickly self-organized and coupled, and scattered accordingly as a single entity. Modeling using the intensity distribution bilayer Bragg data suggested the existence of orientational texture of the lipid tilt directions. The observed Bragg peaks also suggested that the substrate has no appreciable effect on the bilayer structure. The major difference between the LBS and the vesicular bilayers is the greater disorder within the inner leaflet of the bilayers formed by vesicular fusion.

The ability to measure and characterize in high resolution these relatively stable, supported bilayer molecular films opens up new avenues of research for even more precise characterization and perhaps even control of their formation. Aside from the obvious value of acquiring a greater understanding of lipid bilayers in living cells, these

> Fig. 1 Electron density profile, ρ(z), for DPPC bilayers deposited by LBS and vesicle fusion at the quartz-H^2O interface. The thick green curve demonstrates the bilayer structural variation for the LBS bilayer preparation over approximately a dozen measurements and four sample preparations. The dotted curves encompass the variation of vesicle fusion bilayers and show a larger variation in structure than the LBS bilayers. The largest differences between the two sample preparation methods occur in the inner leaflet, adjacent to the quartz substrate. The dark blue curve corresponds to a representative LBS DPPC bilayer. 0 Å denotes the center of the bilayer. A volume-constrained model for each lipid leaflet was constructed for the representative LBS bilayer; these are shown in dotted red. The solid red line is the lipid contribution to the total electron density. The light blue curves denote the contribution of water to the total electron density and gives a quantified amount of hydration between the bilayers and the quartz substrate.

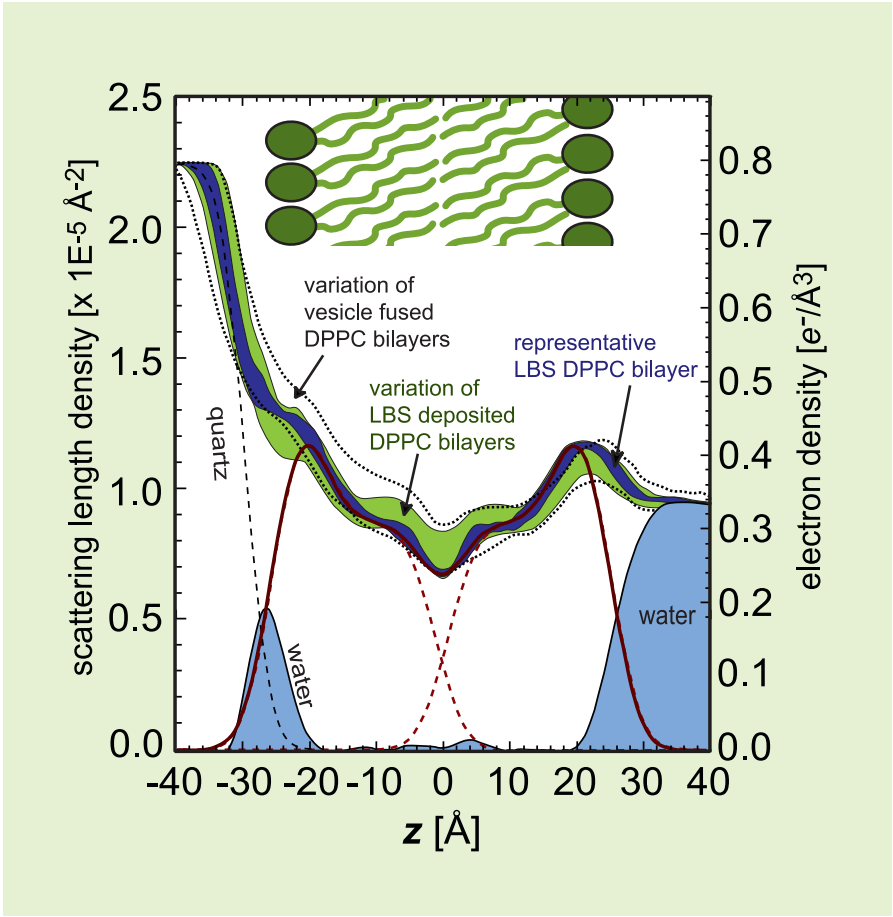

possibilities include the development of sophisticated biosensors and more advanced liposomes for targeted drug delivery within the body.

— Mark Wolverton

See > E.B. Watkins[1,2], C.E. Miller[2]*, D.J. Mulder[1], T.L. Kuhl[1], and J. Majewski[2], "Structure and Orientational Texture of Self-Organizing Lipid Bilayers," Phys. Rev. Lett. **102,** 238101 (12 June 2009). DOI: 10.1103/PhysRevLett.102.238101

Author affiliations >
[1]University of California, Davis;
[2]Los Alamos National Laboratory

Correspondence >
*chad.ed.miller@gmail.com

> This work was supported by the Department of Energy, Office of Science, Office of Basic Energy Sciences through Grant No. 46340 and Los Alamos National Laboratory under DOE Contract No. W7405-ENG-36. Use of the Advanced Photon Source is supported by the U.S. Department of Energy, Office of Science, Office of Basic Energy Sciences, under Contract No. DE-AC02-06CH11357.

> 6-ID-B,C • MU/XOR • Materials science, physics • Anomalous and resonant scattering (hard x-ray), general diffraction, grazing incidence diffraction, liquid scattering, magnetic x-ray scattering, surface diffraction (UHV) • 3.3-cm Undulator A • Accepting general users

Tracking Polymer Melt Dynamics at the Nanometer Scale

IN SHORT > Disordered, glassy materials are ubiquitous in nature. Often, the microscopic constituents of these materials can move exceedingly slowly, and one of the major challenges for materials scientists is to gain direct information about the nature of this motion at the relevant small length scales and long time intervals. By applying x-ray photon correlation spectroscopy (XPCS) to track the mobility of tiny gold nanoparticles suspended in polymer liquids as they are cooled into glass, a team of researchers has succeeded in elucidating the motion in the polymers at the nanometer scale (i.e., one billionth of a meter). A surprising observation in the experiments was the increasing prevalence of slow, heterogeneous flow in the polymers as they were cooled closer and closer to the glass state. The apparently universal nature of that complex, low-temperature flow indicates a generic origin that any microscopic theory for glassy materials will need to confront.

MORE > At higher temperature, where the liquids have a lower viscosity, the observed motion of the nanoparticles was diffusive; that is, the particles exhibited random walks as a consequence of their constant bombardment by surrounding polymer molecules. At lower temperature, however, this diffusion was superseded by a second process that suggested the particles became caught up in complicated flow that appeared in the polymer when it was cooled. The emergence of this flow bears strong resemblance to similar behavior seen in other disordered materials in which the microscopic constituents move slowly, such as gels.

To capture the behavior of the nanoparticles in isolation within the polymer, without undue influence from neighboring particles, the researchers—from Johns Hopkins University, McGill University,and the University of Ottawa—kept the concentration of gold very low (between 0.04% to 0.1% by volume) and the sizes of the gold nanoparticles quite small as well (diameters of either 2 nm or 3 nm). To prevent the particles from clumping, the researchers attached to the surfaces a dense layer of polymer molecules that were chemically identical to the surrounding material. In the XPCS experiments, carried out at XOR beamline 8-ID-I of the APS, a highly intense beam of monochromatic, coherent x-rays was aimed at the samples. The scattered x-rays produced a pattern of "speckles," which are variations in x-ray intensity from one spot to another within the scattering pattern that occur when coherent light impinges on a disordered material. Over time, the motion of the gold nanoparticles altered the pattern of speckles, and recording and analyzing this evolution enabled the researchers to determine a statistical average of the particle motion.

Among the key outputs of the XPCS measurement was a set of characteristic times that described the duration required for the particles to move on average different distances. More precisely, these times were measured at different scattering wave vectors (wave vectors represent waves in vector form; they find use in the characterization of groups of coherent waves moving in the same direction, such as from an x-ray beam derived from the APS). At temperatures well above the glass transition temperature T_g of the polymer, the characteristic times were observed to vary inversely with the square of the wave vector; i.e., when plotted against the wave vector on a log-log scale, the times followed a line with a slope of negative two, as shown in Fig.1. This behavior is a signature of diffusion, where the random-walk motions cover distances that on average increase as the square-root of the elapsed time. However, as the polymer's temperature approached the glass transition—at around

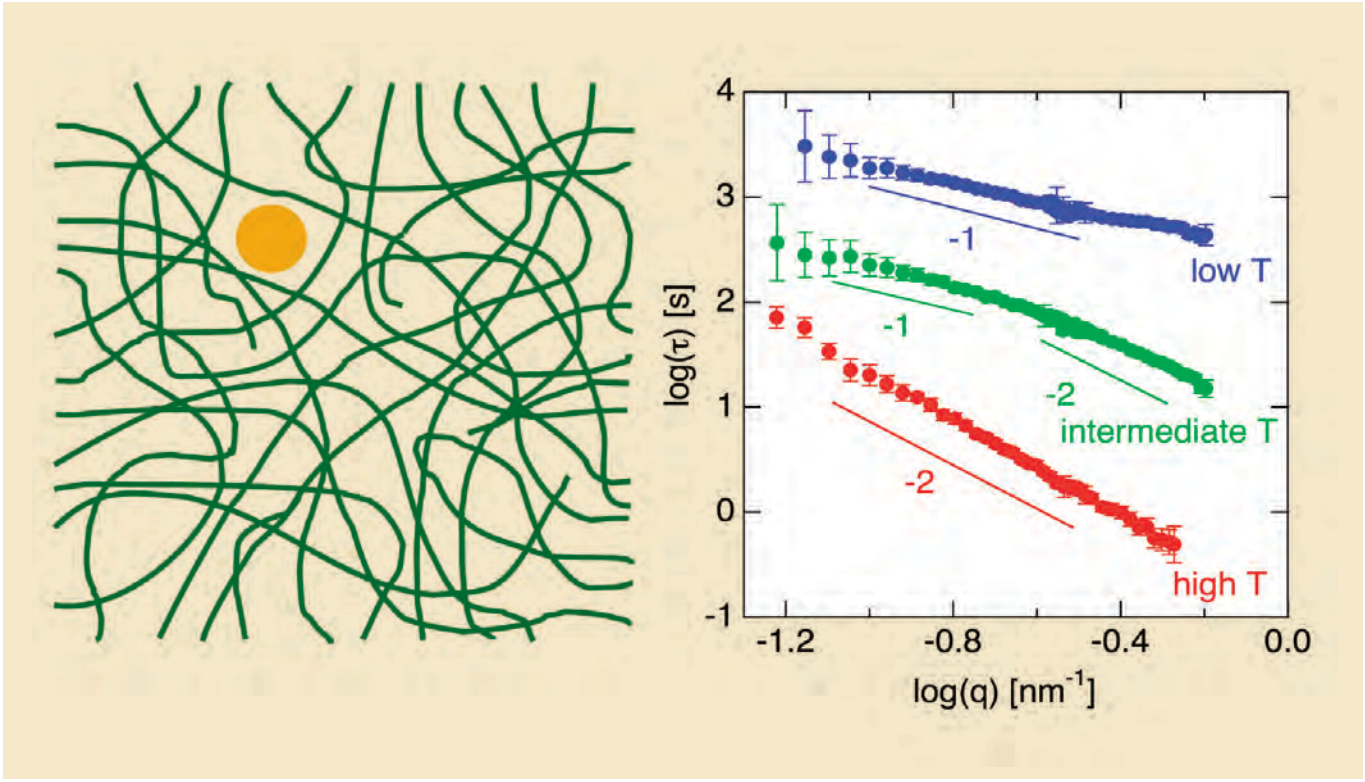

^ *Fig. 1* ***Left:*** *Schematic of a nanoparticle in a polymer melt.* ***Right:*** *Characteristic times vs wave vector measured by XPCS for nanoparticle motion in polymer melts.*

1.1T_g—the characteristic times adopted a different trend, varying inversely with a linear power of the wave vector. This linear relationship implied that the particles on average traveled a distance in direct proportion to the time elapsed, as if they had a characteristic velocity. The magnitude of these velocities was exceedingly small, less than a tenth of a nanometer per second, illustrating the power of XPCS to monitor small motions occurring over long durations; nevertheless, those seemingly minute velocities were still much faster than any diffusion that occurred within the highly viscous polymer at low temperatures. The researchers interpreted this motion as the velocity of slow, heterogeneous flow in the polymer that appears as a consequence of the deep cooling. The observation of this complex flow adds a new piece to the overall picture of the internal dynamics occurring within disordered, glassy materials, and presents a significant new challenge to materials scientists attempting to understand their properties.

— Philip Koth

See > Hongyu Guo[1], Gilles Bourret[2], Muriel K. Corbierre[2], Simona Rucareanu[2], R. Bruce Lennox[2], Khalid Laaziri[3], Luc Piche[2], Mark Sutton[2], James L. Harden[3], and Robert L. Leheny[1]*, "Nanoparticle Motion within Glassy Polymer Melts," Phys. Rev. Lett. **102**, 075702 (2009). DOI: 10.1103/PhysRevLett.102.075702

Author affiliations >
[1]Johns Hopkins University, [2]McGill University, [3]University of Ottawa

Correspondence >
*leheny@pha.jhu.edu

> Funding for this research was provided by the Petroleum Research Fund and the Natural Sciences and Engineering Research Council of Canada. Use of the Advanced Photon Source at Argonne National Laboratory was supported by the U.S. Department of Energy, Office of Science, Office of Basic Energy Sciences, under Contract No. DE-AC02-06CH11357.

> 8-ID-I • XOR • Materials science, physics, polymer science • Intensity fluctuation spectroscopy, small-angle x-ray scattering, x-ray photon correlation spectroscopy • 3.3-cm Undulator A • Accepting general users

Mixing and Matching Detergents for NMR Membrane Protein Structure Determinations

IN SHORT > Membrane proteins make up about 25% of the proteins in a cell and are crucial for transport and signaling across cell membranes. Yet these important proteins account for less than 1% of the known protein structures. One reason is the difficulty of selecting a detergent that mimics the native lipid bilayer comprising the cell membrane; suitable detergents must stabilize protein folding while solubilizing membrane proteins for structural and functional investigations. The problem is that detergents are unlike lipid bilayer sheets in that they form micelles that have different shapes and sizes depending on their chemical structure. Currently, detergents are selected by exhaustive screening because the effects of protein-detergent interactions on protein structure are poorly understood. Researchers addressed this problem by investigating how different detergents and detergent mixtures affect the structure and dynamics of the membrane protein TM0026, using small-angle x-ray scattering (SAXS) at the XOR/BESSRC 12-ID beamline at the APS in conjunction with nuclear magnetic resonance (NMR) and electron paramagnetic resonance (EPR) spectroscopy. The results suggest that matching micelle dimensions to the protein's hydrophobic surface combats the line broadening that reduces the completeness of NMR observations. The finding possibly provides a basis for the rational design of mixed micelles that may advance membrane protein structure determinations by NMR.

MORE > TM0026 was found to produce NMR spectra that were drastically different as assessed by ^{15}N, ^{1}H-TROSY (transverse relaxation-optimized spectroscopy) with respect to four different detergents: decyl maltoside (DM), dodecyl maltoside (DDM), decylphosphocholine (FC-10), and dodecylphosphocholine (FC-12). For the detergents DM and FC-12, 51 of 66 expected cross peaks were observed, while only 32 and 36 cross peaks were observed for the detergents FC-10 and DDM, respectively. The expected cross peaks were not observed in FC-10 and DDM because of extensive line broadening.

EPR was used to investigate the physical origin of the line broadening by studying the structure and dynamics of TM0026 under different detergent conditions. The data demonstrated that the structure of TM0026 was perturbed by FC-10 and DDM.

To understand how the detergents influence TM0026 structure, SAXS was used to investigate the sizes and shapes of the micelles formed by the different detergents. The researchers, from the University of Virginia, The Scripps Research Institute, and Stanford University found that the detergents for which poor NMR spectra were observed form micelles that were either smaller and thinner (FC-10), or larger and thicker (DDM) than the micelles formed by DM and FC-12 (Fig. 1). The researchers then investigated whether mixing detergents at different ratios might be a way to systematically change the size and shape of detergent micelles. Toward this end, SAXS data were obtained for a comprehensive set of mixed micelles.

The researchers found that the thickness of mixed micelles depends linearly on the mixing ratio for a significant range of detergent mixtures and that this thickness appears to correlate strongly with the quality of NMR observations. The generality of this result is difficult to assess; however, the observations are in qualitative agreement with previous findings. Future work will explore whether similar relationships can be observed for different

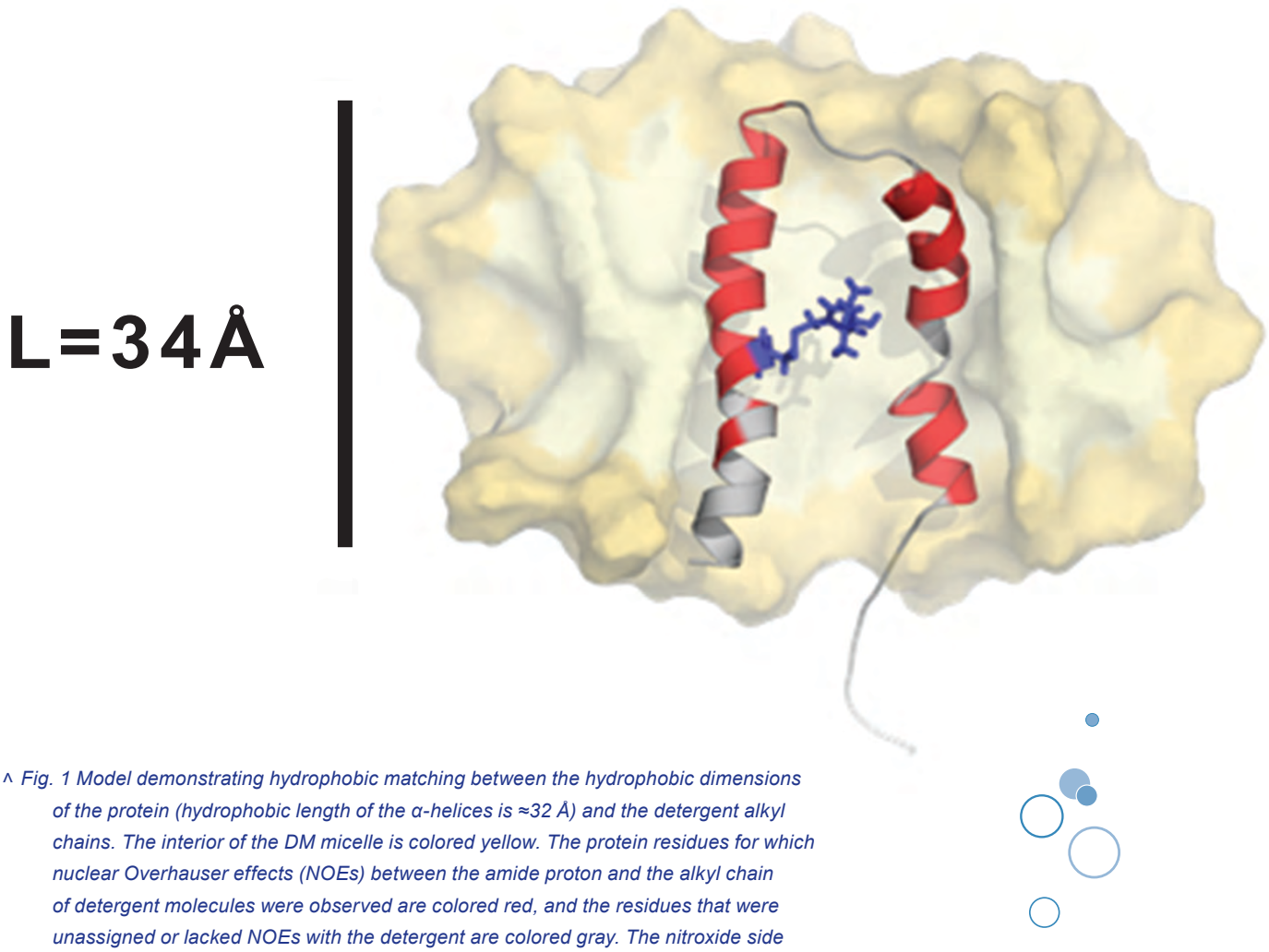

^ *Fig. 1 Model demonstrating hydrophobic matching between the hydrophobic dimensions of the protein (hydrophobic length of the α-helices is ≈32 Å) and the detergent alkyl chains. The interior of the DM micelle is colored yellow. The protein residues for which nuclear Overhauser effects (NOEs) between the amide proton and the alkyl chain of detergent molecules were observed are colored red, and the residues that were unassigned or lacked NOEs with the detergent are colored gray. The nitroxide side chain at residue 13 is rendered as blue sticks. The dominant head group separation (L) is labeled.*

membrane proteins varying in size, fold, and origin. Other micelle properties (such as the total micelle volume) will likely have to be taken into account to fully understand protein-detergent interactions. Nonetheless, the data suggest that, rather than exhaustively screening a multitude of detergents, it might be possible to rationally engineer appropriate mixed micelles for NMR structure determinations following simple principles and using a limited set of detergents.

— Vic Comello

See > Linda Columbus[1,2]*, Jan Lipfert[3], Kalyani Jambunathan[1], Daniel A. Fox[1], Adelene Y.L. Sim[3], Sebastian Doniach[3], and Scott A. Lesley[2], "Mixing and Matching Detergents for Membrane Protein NMR Structure Determination," J. Am. Chem. Soc. **131**, 7320 (2009). DOI:10.1021/ja808776j

Author affiliations >
[1]University of Virginia,
[2]Scripps Research Institute,
[3]Stanford University

Correspondence >
*Columbus@virginia.edu

> Support for this research was provided by National Institutes of Health Grants 1F32GM068286 and The Jeffress Memorial Trust (L.C.) PO1 GM0066275 (S.D.), and Protein Structure Initiative Grants P50 GM62411 and U54 GM074898 (S.L.). A.Y.L.S. is supported by A*STAR. Use of the Advanced Photon Source was supported by the U.S. Department of Energy, Office of Science, Office of Basic Energy Sciences, under Contract DE-AC02-06CH11357.

> 12-ID • XOR/BESSRC • Chemistry, physics, materials science • Small-angle x-ray scattering, wide-angle x-ray scattering, grazing incidence small-angle scattering, surface diffraction • 3.3-cm Undulator A • Accepting general users

Development of Icosahedral Short-Range Order Confirmed in Glass Transition

IN SHORT > Much remains to be discovered about how metallic glasses form from the liquid state upon cooling, which should not be surprising given that the glass transition in general is one of the most significant outstanding problems in condensed matter physics. While there is general agreement that the dynamics of the transition involve the development of local and perhaps intermediate-range order in the metastable liquid, the nature of this order has remained controversial. Icosahedral short-range order (ISRO) has been frequently argued to dominate the local structures of supercooled metallic liquids and glasses, but definitive experimental confirmation of a link between developing ISRO and the glass transition has been lacking, until now. Researchers from Washington University made the first quantitative measurements of the time-dependent nucleation rate in a metallic glass, studying the crystallization of a $Zr_{59}Ti_3Cu_{20}Ni_8Al_{10}$ bulk metallic glass to an icosahedral quasicrystal of the same chemical composition. The researchers then obtained direct measurements of the evolution of the local structure of the liquid in the deeply supercooled and amorphous states based on a reverse Monte Carlo (RMC) analysis of liquid diffraction data obtained at the APS. The results from the two very different experiments provide the strongest experimental demonstration to date that ISRO dominates the structures of both the liquid and the glass and strongly supports an ISRO-based frustration model for the glass transition in this and possibly other zirconium-based metallic glasses.

> *Fig. 1* ***(a)*** *The scaled number of quasicrystal grains as a function of scaled annealing time; N is the number per unit volume, I^s is the steady-state nucleation rate, and τ is the transient time.* ***(b)*** *Left, electrostatic levitation facility used for the x-ray diffraction studies; right, levitated liquid sample.* ***(c)*** *The pair correlation function computed from the experimental scattering data (circles) and Reverse Monte Carlo fits (solid lines); the data were sparsely plotted to show the quality of the fits.* ***(d)*** *The intensity of the 1551 Honeycutt-Andersen index (characteristic of icosahedral short-range order) as a function of liquid temperature. The dashed line is a polynomial fit; T_g indicates the glass transition temperature.*

MORE > According to classical nucleation theory, random fluctuations in a liquid produce an ensemble of small clusters having the structure of the ordered phase. However, only those clusters exceeding a critical size can nucleate and grow. The researchers first annealed ribbons of amorphous $Zr_{59}Ti_3Cu_{20}Ni_8Al_{10}$ at a range of nucleation temperatures and anneal times to produce populations of nuclei. Subsequent 2-min anneals at the higher temperature of 430° C allowed these nuclei to grow to observable size. X-ray diffraction and transmission electron microscopy (TEM) studies confirmed that only the icosahedral quasicrystal phase was formed during these anneals. The number of icosahedral quasicrystal phase grains produced after the nucleation and growth treatments were counted manually from TEM images. A detailed analysis of these data revealed an extremely small value for the interfacial free energy between the amorphous and icosahedral quasicrystal phase. Such a small interfacial free energy—almost an order of magnitude smaller than the values obtained between a supercooled liquid and a quasicrystal—implies very strong ISRO in the glass.

This conclusion was further supported by x-ray diffraction measurements made at the MU/XOR 6-ID-D beamline at the

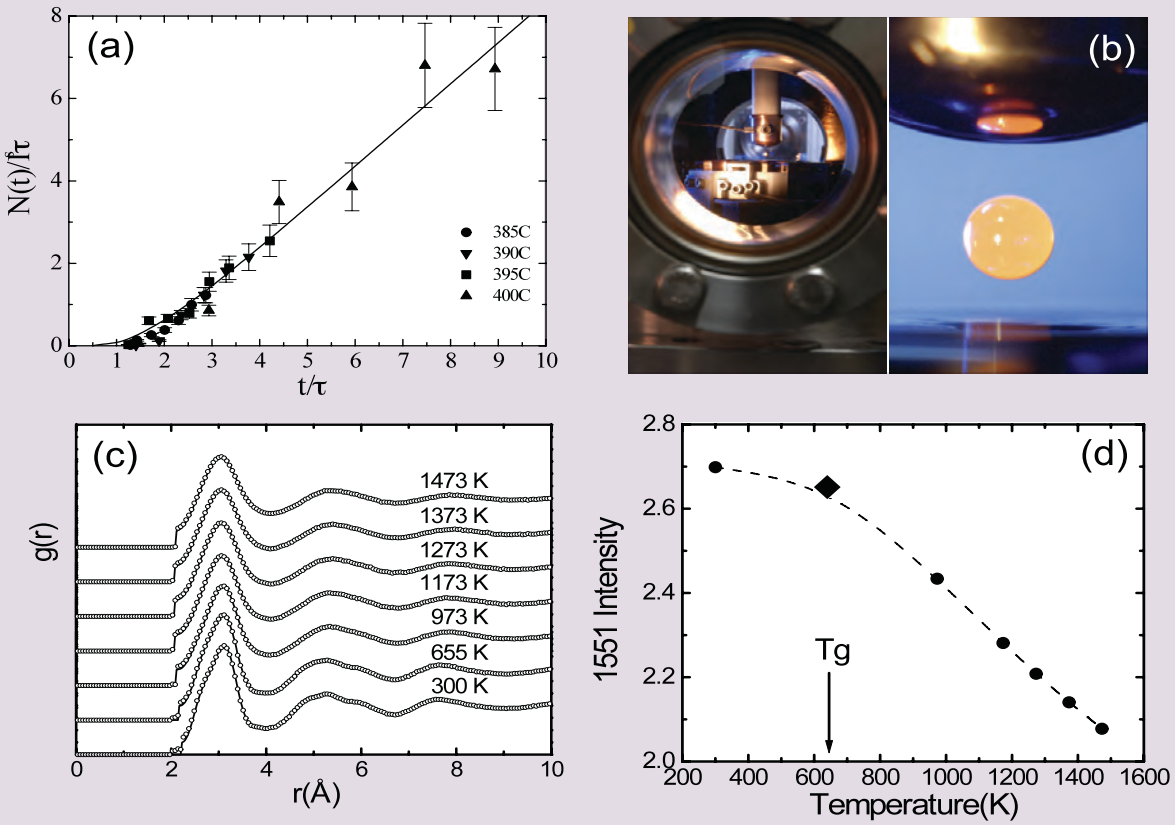

APS on electrostatically levitated, nearly spherical droplets of the supercooled liquid and glass on. Structural models for the liquids were obtained from RMC simulations, and the topologies of the RMC-generated structures were then analyzed. ISRO was found to increase dramatically with supercooling to the glass transition (Fig. 1). These two results provide the strongest experimental evidence to date of the connection between ISRO and the topological frustration underlying the glass transition in this and related glasses. Further, they indicate that ISRO can play a central role in glass formation in Zr-based bulk metallic glasses. The growth of ISRO in the supercooled liquid raises the nucleation barrier for the formation of crystal phases and increases the viscosity of the liquid, making it easier to form the glass.

— Vic Comello

See > Y.T. Shen, T.H. Kim, A.K. Gangopadhyay, and K.F. Kelton*, "Icosahedral Order, Frustration, and the Glass Transition: Evidence from Time-Dependent Nucleation and Supercooled Liquid Structure Studies," Phys. Rev. Lett. **102**, 057801. DOI:10.1103/PhysRevLett.102.057801

Author affiliation >
Washington University

Correspondence >
*kfk@wuphys.wustl.edu

> The work at Washington University was partially supported by the National Science Foundation under Grant No. DMR-0606065 and by NASA under Contract No. NNM04AA016. MU/XOR is supported by the U.S. Department of Energy, Office of Science, Office of Basic Energy Sciences. Use of the Advanced Photon Source is supported by the U.S. Department of Energy, Office of Science, Office of Basic Energy Sciences under Contract No. DE-AC02-06CH11357.

> 6-ID-D • MU/XOR • Materials science, physics • High-energy x-ray diffraction, magnetic x-ray scattering, pair distribution function, powder diffraction • 3.3-cm Undulator A • Accepting general users

Nano-Layered Organic/Inorganic Structures Make Better Photoconductors

IN SHORT > For reasons ranging from cheaper solar cells to reducing the use of toxic metals, researchers want to find materials for light harvesters that are different than the semiconductors used today. Although the photodetectors now in use are very efficient, they are based on the same single-crystal silicon used for computer chips (which is expensive) or compounds made with cadmium, lead, mercury, or arsenic (which are toxic). A less-expensive, less-hazardous photodetector that, ideally, can also be tuned to detect different wavelengths could enable new applications that need these properties as well as flexibility and light weight. Researchers from Northwestern University created a nano-engineered, self-assembling photodetecting material that they studied with a variety of methods, including x-ray absorption spectroscopy (XAS), at the DND-CAT 5-BM-D beamline at the APS. The researchers found this material to be very efficient compared to similar technologies, and they researchers hope that the new, environmentally-benign material could provide low-power, flexible light detectors.

MORE > Organic materials are less expensive than inorganics, and more flexible. By manipulating the molecular structure of these materials, organic dyes allow users to "tune" a photodetector to a specific wavelength, and the wide range of available molecules allows control over the lifetime of charge-trapping states. A major drawback of organic photodetectors, however, is that they degrade quickly, usually due to chemical changes that occur when electrical charges are trapped or the materials react with oxygen.

Another approach is to combine organic and inorganic materials in ways that use the strengths of each. Ideally, organic and inorganic materials would work together to trap photons, generate charge-carriers, and conduct the separated charges to the appropriate electrodes. Previous work by other researchers showed that fused nanoparticles could be very sensitive light detectors if the trap states at the edges of crystals didn't disrupt their conductivity. Adding organic dyes might improve conduction by reducing edge disruption. For the best performance, however, the organic and inorganic materials need to be intimately connected in an organized way.

The Northwestern group made a nano-ordered, self-assembled hybrid of inorganic semiconductor zinc oxide and thiophene, using electrodeposition to grow plate-like structures from solution on an electrode. The thiophene-based small molecules are electrically active conjugated surfactants. The parts of the molecules that share electrons control assembly and enhance long-range ordering. As grown, the inorganic layers didn't show a response to light, but after heating to 150° C, the conductivity increased dramatically.

To see what, exactly, they had made, the researchers used several imaging methods. Images of the material show tiny plates 1-nm thick made of crystalline zinc oxide layered on 2- or 3-nm thick layers of organic molecules. The XAS measurements carried out at beamline 5-BM-D determined the identity of the inorganic phase at specific temperatures. When they looked at the K absorption near-edge structure of the inorganic before annealing, the results looked like insulating $Zn(OH)_2$. After annealing, the structure suggested the material had changed to tetrahedral ZnO crystallites smaller than a nanometer in diameter. The nanocrystalline ZnO matrix conducts charges well.

The group used a variety of thiophene molecules, and found that by designing a surfactant that

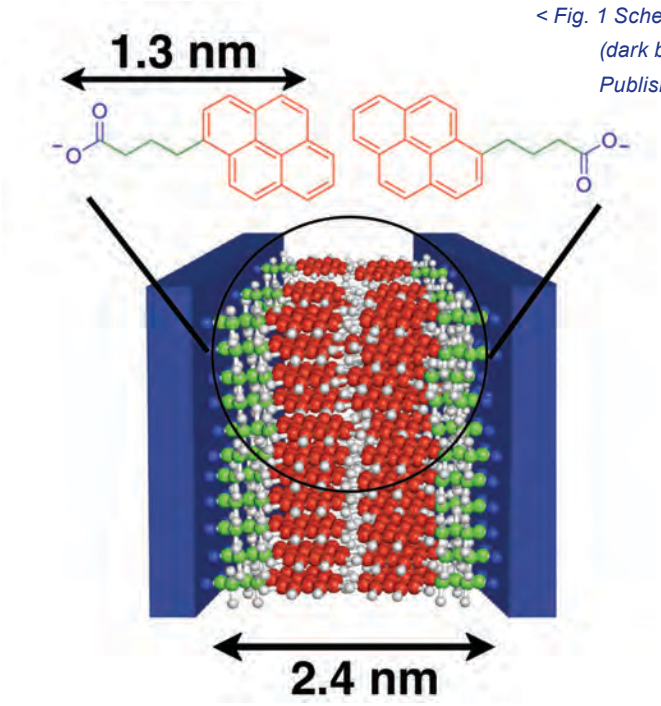

< *Fig. 1 Schematic diagram of lamellar ordering composed of inorganic Zn-rich regions (dark blue) and bilayers of 1-pyrenebutyric acid (PyBA). (Copyright © 2010 Nature Publishing Group, a division of Macmillan Publishers Limited.)*

absorbs light at energies below the ZnO bandgap (which created fiber-like, rather than plate-like structures, but retained the layering), they could engineer a system where light is absorbed by the organic, which then transfers electrons to the ZnO, which efficiently shepherds the charges to the electrode.

— *Yvonne Carts-Powell*

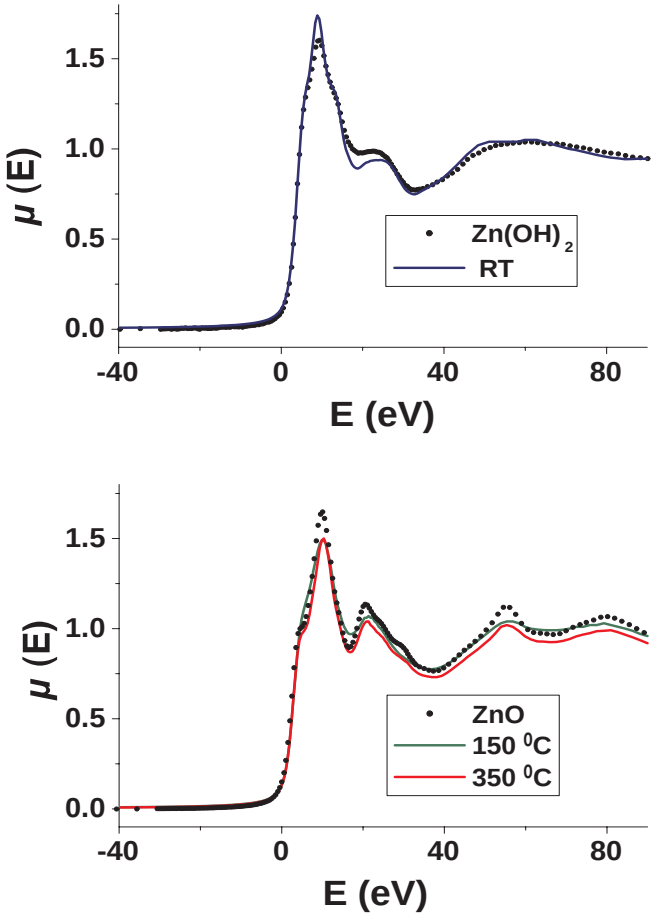

^ *Fig. 2 XANES (x-ray absorption near edge structure) spectra of hybrid films deposited with PyBA as a function of heat treatment (pre-anneal, 150° C and 350° C) and of $Zn(OH)_2$ and ZnO standards. XANES proved that the initial hybrid film had $Zn(OH)_2$ as the inorganic phase, which converted to ZnO upon annealing.*

See > Marina Sofos, Joshua Goldberger, David A. Stone, Jonathan E. Allen, Qing Ma, David J. Herman, Wei-Wen Tsai, Lincoln J. Lauhon, and Samuel I. Stupp*, "A synergistic assembly of nanoscale lamellar photoconductor hybrids," Nat. Mater. **8**, 68 (2009). DOI: 10.1038/NMAT2336

Author affiliation >
Northwestern University

Correspondence >
*s-stupp@northwestern.edu

> This work was supported by the U.S. Department of Energy under Award DE-FG02-00ER54810 and the National Science Foundation under award DMR 0605427. DND-CAT is supported by the E.I. DuPont de Nemours & Co., The Dow Chemical Company, the U.S. National Science Foundation through Grant DMR-9304725, and the State of Illinois through the Department of Commerce and Board of Higher Education Grant IBHE HECA NWU 96. Use of the Advanced Photon Source was supported by the U.S. Department of Energy, Office of Science, Office of Basic Energy Sciences, under Contract No. DE-AC02-06CH11357.

> 5-BM-D • DND-CAT • Materials science, polymer science • High-energy x-ray diffraction, x-ray absorption fine structure • Bending magnet • Accepting general users

Perfecting Catalytic Arrays

IN SHORT > Catalysts speed up chemical reactions and remain largely unchanged themselves at the end of the process. This apparently simple statement harbors a chemical secret: catalysts are much more complicated than that. Now, work carried out on beamline 11-ID-D at the APS, as well as at the Argonne Center for Nanoscale Materials (CNM) and Electron Microscopy Center for Materials Research (EMC), could improve our understanding of at least one class of industrially important catalyst: metal nanoparticle catalysts.

MORE > Chemists can disperse metal nanoparticles on high-surface-area support materials to produce an enormous area of catalyst to interact with the starting materials in a reaction mixture. This allows those materials to come together very readily, to then react and transformation into large quantities of product with little waste.

The added advantage of this type of catalyst is that it can reduce the need for energy-intensive pressurization or high temperatures. In other words, it can make a process that would be otherwise environmentally unfriendly into a greener way to manufacture a chemical product. The same principle applies whether that chemical is a pharmaceutical drug, a technological material, or an agrochemical, such as a pesticide or herbicide.

Researchers from Safarik University, Argonne, and the Paul Scherrer Institut investigated how metal nanoparticle catalysts might themselves be produced more consistently. They reasoned that various factors could further improve these catalysts For instance, if it were possible to constrain the sizes of the nanoparticles to a tighter range of diameters, then the catalytic process would be more consistent. It might also be possible to optimize the nanoparticle size and shape as well as the detailed nature of their surface structure to improve industrial catalytic reactions.

The researchers have used density functional theory (DFT) calculations to guide their studies on arrays of nanoparticles made from platinum. Their calculations allowed them to control the growth of identical platinum nanoparticles, which form arrays on a strontium titanate (STO) substrate, using electron beam lithography at the CNM. The team points out that they can produce three distinct shapes of nanoparticle. These can be produced selectively simply by changing the crystallographic surface features of the strontium titanate substrate on which they form and the physical conditions used to anneal, or fix, the nanoparticles to that surface.

In order to characterize the resulting nanoparticle arrays, the team turned to scanning electron microscopy at the EMC and synchrotron x-ray scattering at the APS (Fig. 1). They found that they could produce nanoparticles in a small size range from 30 nm to 40 nm by annealing at a temperature of 1450K under a flow of the relatively unreactive gas, nitrogen.

The team demonstrated that each array on the strontium titanate surface contains 75 million particles in a square lattice, with a spacing of 200 nm between the particles. The x-ray diffraction measurements suggest that the particles lock on to the crystal structure of the substrate and are shaped like a cuboctahedron cut in half.

The researchers once more used DFT calculations to explain how this particular shape arises during the process and suggest that it is due to the partial “wetting” of platinum on the strontium titanate during annealing. They add that wide-angle reflectivity scans showed that only a negligible few of the platinum nanoparticles are misoriented on the surface.

Having produced such perfect platinum nanoparticle arrays, the team then carried out some bulk tests of their catalytic prowess. Oxygen-reduction electrocatalytic activity was used to test each of the three arrays produced on different crystal forms of strontium titanate with good results. This catalytic test, the researchers say, is one of the most important ways of evaluating electrocatalytic activity.

Intriguingly, the crystallographic surface form of the nanoparticles displayed activity opposite to what is seen with conventional non-nanoscopic platinum catalysts traditionally modeled with single crystal extended surfaces. The one

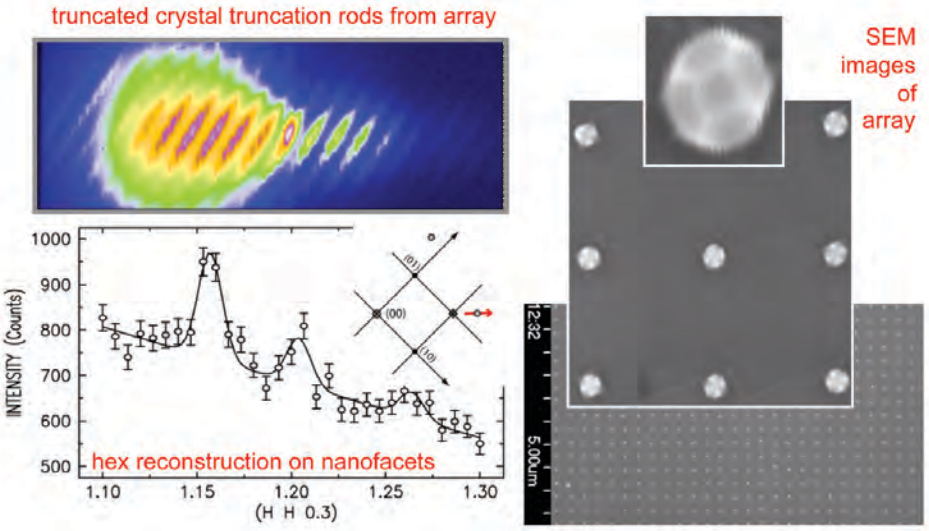

< Fig. 1 ***Left:*** *Truncated crystal truncation rods of (111) facets (top) and hex reconstruction peaks from (100) nanofacets (bottom).* ***Right:*** *Successively zoomed images of nanoparticles. The top image shows clearly a cuboctahedron; one (100) facet at the center and four adjacent (111) facets.*

that would conventionally be most reactive turned out to be the least catalytically active form, and vice versa. The researchers suggest that this is due to a "division of labor" effect arising through the close proximity of the facets of the divided cuboctahedrons, which allows oxygen to be adsorbed on to the conventionally less catalytic surface more effectively than it would otherwise be.

Such insights regarding the behavior of catalysts is allowing researchers to lay bare the simplistic notion that catalysts simply speed up reactions and so is helping them developing novel materials with a wide range of potential applications.

This work demonstrates, for the first time, full control over all possible variables connected with high surface area catalysts, such as size, shape, number, and even the orientation of particles. From the standpoint of x-ray scientists, control over spatial orientation of particles and their arrangement in a relatively perfect square lattice would allow single nanoparticle scattering experiments to be performed, but with millions of nanoparticles.

The team concedes that electron beam lithography, being a serial, or sequential, rather than parallel technique, limits how much surface can be covered with catalytic nanoparticles in a given time However, they also point out that parallel nanofabrication techniques are being developed and could soon overcome such a limitation, allowing the approach to be extended for the production of optimized metal catalysts for use in the chemical industry.

According to the team, the APS played a crucial role in the characterization of the arrays produced. Since the coverage of platinum catalyst on the STO substrate is relatively low, use of a high-brilliance x-ray source was necessary for confident characterization of epitaxial relation between the catalyst particles and the substrate and detection of misoriented particles.

— David Bradley

See > Vladimir Komanicky[1,2]*, Hakim Iddir[2], Kee-Chul Chang[2], Andreas Menzel[2,3], Goran Karapetrov[2], Daniel Hennessy[2], Peter Zapol[2], and Hoydoo You[2]**, "Shape-Dependent Activity of Platinum Array Catalyst," J. Am. Chem. Soc. **131**, 5732 (2009). DOI: 10.1021/ja900459w

Author affiliations > [1]Safarik University, [2]Argonne National Laboratory, [3]Paul Scherrer Institut

Correspondence >
*vladimir.komanicky@upjs.sk
**hyou@anl.gov

> This work and use of the Advanced Photon Source, the Center for Nanoscale Materials, and the Electron Microscopy Center for Materials Research were supported by the U.S. Department of Energy, Office of Science, Office of Basic Energy Sciences, under Contract No. DE-AC02-06CH11357.

> 11-ID-D • XOR/BESSRC • Chemistry, geoscience, materials science • General diffraction, time-resolved x-ray absorption fine structure, x-ray absorption fine structure • 3.3-cm Undulator A (US), 2.3-cm undulator (DS) • Accepting general users

Storing Hydrogen

IN SHORT > Researchers have been studying mesoporous materials for almost two decades with a view to using them as hosts for small molecules and scaffolds for molding organic compounds into new hybrid materials and nanoparticles. Their use as potential storage systems for large quantities of hydrogen has also been mooted. Such systems that might hold large quantities of hydrogen safely and in a very compact volume would have enormous potential for powering fuel cell vehicles, for instance. A sponge-like form of silicon dioxide, the stuff of sand particles and computer chips, can soak up and store other compounds including hydrogen. Studies carried out at the XOR/BESSRC 11-ID-B beamline at the APS have revealed that the nanoscopic properties of the hydrogen-rich compound ammonia borane help it store hydrogen more efficiently than usual. The material may have potential for addressing the storage issues associated with a future hydrogen economy.

> *Fig. 1 The phase diagram of bulk and nanophase ammonia borane. When heated, bulk ammonia borane undergoes an orthorhombic to tetragonal phase transition at 225K and becomes amorphous above 343K. However, confined nanophase ammonia borane does not undergo the phase transition at 225K. Instead, it remains in the tetragonal phase from 110K to 240K. Amorphization of nanophase ammonia borane occurs at a much lower temperature, 240K, than bulk ammonia borane.*

MORE > Researchers from Los Alamos National Laboratory, the Pacific Northwest National Laboratory, and Argonne carried out synchrotron x-ray powder diffraction experiments at the 11-ID-B beamline. The team sought to uncover the properties and structure of the nanophase of ammonia borane held within mesoporous silica, in which the pore diameters are 2 to 50 nm, which is midway between microporous (less than 2 nm) and macroporous (greater than 50 nm). Ammonia borane itself, with the formula NH_3BH_3, is loaded with hydrogen and has been the focus of hydrogen storage aspirations for some time. It forms stable molecular crystals that hook together via dihydrogen bonds. Packing it into mesoporous silica could have a synergetic effect on the storage properties.

The researchers obtained diffraction patterns for ammonia borane embedded in the mesoporous silica, MCM-41, across a temperature range from 80K to 300K. They then used an analytical technique known as atomic pair distribution function (PDF) to unravel the x-ray data.

The key finding from their research is that the nanophase ammonia borane held within the confined spaces of the mesoporous silica begin to lose their crystalline character at much lower temperatures, above 240K, and surprisingly do not undergo the expected structural phase change at 225K (Fig. 1). This transition is observed for bulk crystals of ammonia borane not confined in a porous structure. Instead, the molecular crystals retain their tetragonal phase over a wide temperature range of temperatures from 110K to 240K.

The data suggest that trapping ammonia borane in MCM-41 destabilizes the molecular crystal at temperatures above 240K and stabilizes its high-temperature disordered tetragonal phase even at much lower temperatures than would be expected. The PDF analyses of the data, coupled with previously available results of xenon-129 nuclear magnetic resonance spectroscopy, hints at how this might work to improve the hydrogen storage capacity of porous silica composite materials containing ammonia borane.

The research not only provides useful information about the nanophase of ammonia borane confined in mesoporous silica, but also demonstrates the prowess of PDF analysis of x-ray powder diffraction data for the determination of soft materials—compounds containing light elements—trapped

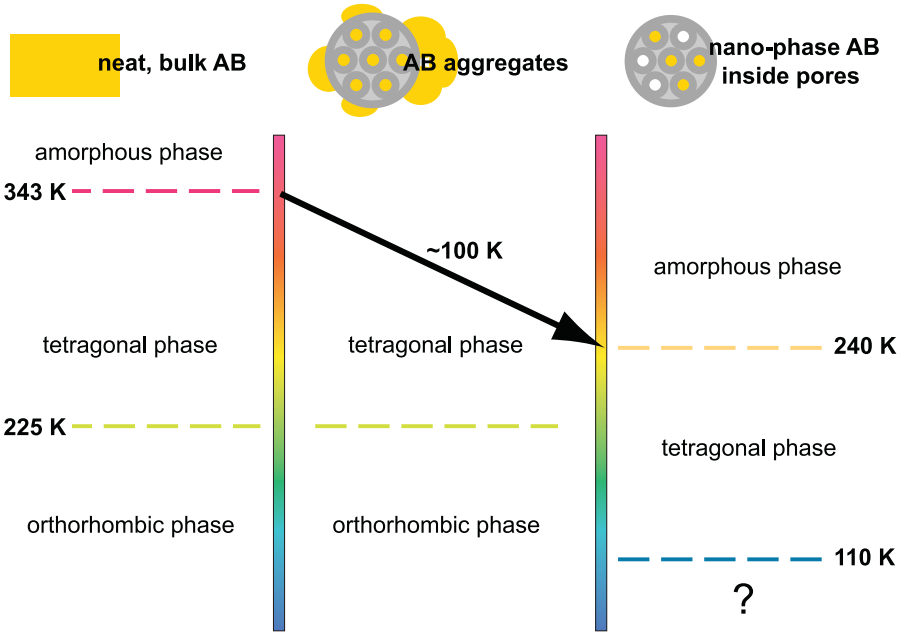

within heavy mesoporous materials. Conventional crystallographic diffraction techniques are insufficient to characterize such guest species with limited long-range order. Below 240K, nanophase ammonia borane inside MCM-41 pores has a tetragonal structure. However, the structural correlation only persists up to 40 Å because it is confined in 40-Å-diameter pores. Therefore, below 240K, nanophase ammonia borane has medium-range structural order, which usually does not give well defined, sharp Bragg peaks.

Currently available high-flux synchrotron x-ray sources, such as those offered by the APS, together with area-detector technology allow researchers to obtain data even from very small amounts of sample and in a relatively short time, which can then be analyzed using PDF, for instance, to differentiate between the light guest molecules and the heavy host material.

The team concludes that their analytical technique could be broadly applied to any number of encapsulated materials as well as to organic functional groups supported on mesoporous surfaces. This will allow researchers to study the chemical and physical properties of such systems in a way that was not previously possible.

— David Bradley

See > Hyunjeong Kim[1]*, Abhi Karkamkar[2], Tom Autrey[2]**, Peter Chupas[3], and Thomas Proffen[1], "Determination of Structure and Phase Transition of Light Element Nanocomposites in Mesoporous Silica: Case study of NH3BH3 in MCM-41," J. Am. Chem. Soc. **131**, 13749 (2009). DOI: 1021/ja904901d

Author affiliations > [1]Los Alamos National Laboratory, [2]Pacific Northwest National Laboratory, [3]Argonne National Laboratory

Correspondence >
*hjkim@lanl.gov
**tom.autrey@pnl.gov

> H.K. and T.P. acknowledge support from the Lujan Neutron Scattering Center, funded by the U.S. Department of Energy Office of Basic Energy Sciences. Los Alamos National Laboratory is operated by Los Alamos National Security LLC under Contract DE-AC52-06NA25396. T.A. and A.K. acknowledge support from the U.S. Department of Energy, Office of Basic Energy Sciences, Division of Chemical Sciences, Biosciences, and Geosciences. Pacific Northwest National Laboratory is operated by Battelle for the U.S. Department of Energy. Use of the Advanced Photon Source is supported by the U.S. Department of Energy, Office of Science, Office of Basic Energy Sciences, under Contract No. DE-AC02-6CH11357.

> 11-ID-B • XOR/BESSRC • Chemistry, environmental science, materials science • Pair distribution function • 2.3-cm undulator • Accepting general users

A Stable Open Framework with Wide Open Spaces

IN SHORT > Porous materials frameworks with open structures, containing substantial numbers of cavities and extended internal surfaces where smaller guest molecules can attach, are potentially useful for a wide range of applications, such as gas storage, catalysis, and drug delivery. One class of such open-framework materials is metal-organic frameworks (MOFs), with metal ions or clusters of ions fixed in a scaffold of organic linkers. The more porous these frameworks are, with bigger open spaces, the more fragile they tend to become. Now, researchers have made a MOF that is remarkably open but also stable through the incorporation of cavities that are larger than 20 Å (mesocavities) but with openings less than 20 Å (microwindows), a strategy demonstrated by x-ray diffraction studies at the ChemMatCARS beamline 15-ID at the APS. This new synthetic strategy may serve as a general approach toward stable MOFs with even higher surface areas, eventually leading to even greater practical applications.

MORE > A standard way to construct MOFs is to connect metal ions using organic linking molecules, or ligands. Solvothermal reactions, which are carried out in organic solvents under high temperature, are used to form bonds between the linkers and the metal ions. Increasing the size of the ligands will expose otherwise hidden edges of these molecules, leading to higher surface area. However, the frameworks tend to be "fragile," reducing their practical value.

Researchers at Texas A&M University and Shandong University in China chose as their building blocks copper-containing cuboctahedra, well-known structures that have 6 square faces and 8 triangular faces enclosing a cavity about 13 Å (1.3 nm) across. To incorporate the cuboctahedra within MOFs in a novel way, the researchers designed two new ligands, each one a planar molecule with three arms extending out at 120° from each other. The ligands are similar in molecular form, with one having slightly longer arms than the other.

Solvothermal reactions of the ligands with copper salts formed a three-dimensional arrangement of cuboctahedra, with a well-defined crystal structure, that the researchers call a porous coordinated network (PCN). Use of the smaller ligand produces a structure in which the cuboctahedra pack together leading to cavities of two distinct sizes arranged in a regular way. X-ray diffraction studies of this crystalline solid, dubbed PCN-61, reveals that the smaller of the two cavities (yellow in the accompanying diagram) are 15 Å across, while the larger are 23 Å. PCN-66, the metal-organic framework formed using the larger ligand has the same cuboctahedra packed similarly, leading to slightly larger cavities, measuring 16 Å and 26 Å, respectively.

X-ray diffraction measurements also show that the two PCN structures do not change when small molecules adsorbed in their interior cavities are removed. That is in contrast to some other large-pored metal-organic frameworks, whose cavities have been found to collapse when they are empty. The stability of the large mesoscale cavities in the PCN comes about because their surfaces are formed from the rigid ligands and the relatively small faces of the cuboctahedra, which control the size of the openings of the cavities and give stability to the overall structure.

The cuboctahedra faces act as "microwindows" opening to the interior of the mesocavities. The PCN structure is akin to a building that has many large rooms with small doors and narrow hallways connecting them. A large number of people could fit into the rooms, but

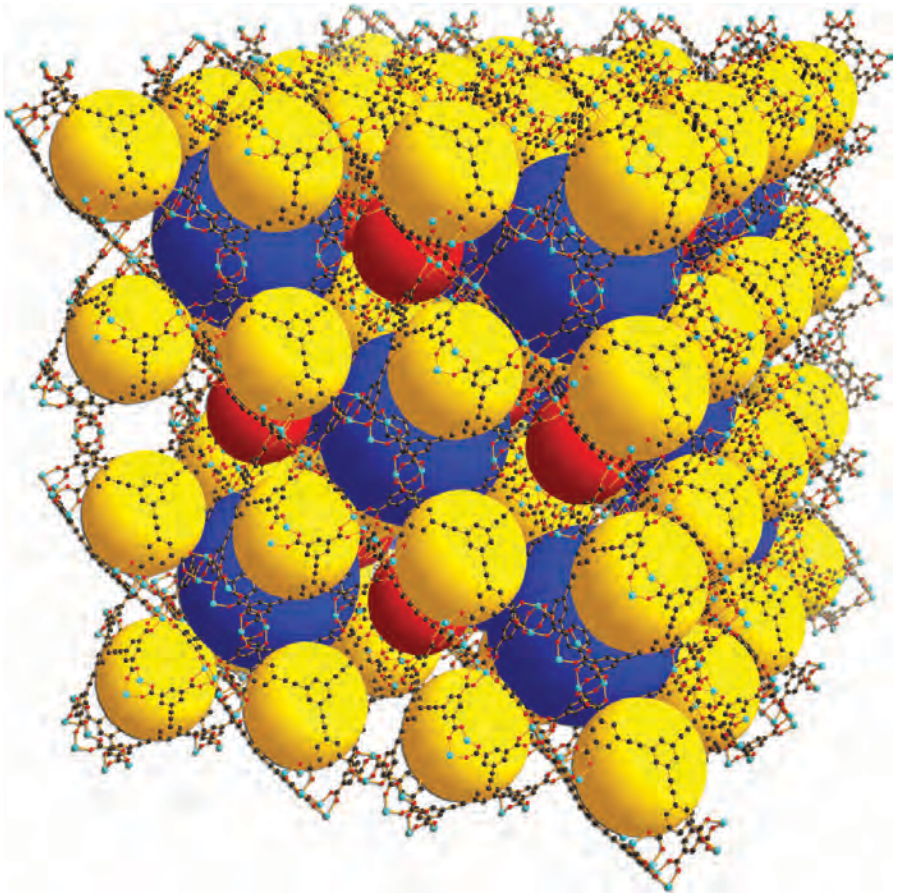

^ *Fig. 1 In this depiction of the structure of PCN-61, a metal-organic framework, copper atoms (blue) sit in "paddlewheel" structures with oxygen (red) and carbon (black) atoms. The paddlewheels link together to form cuboctahedra enclosing volumes about 13 Å across (large red spheres). Three-armed ligand molecules then connect the cuboctahedra into a larger structure enclosing cavities 15 Å (yellow spheres) and 23 Å (blue) across. (Credit: Zhou et al.)*

the small doors control how fast they could move in and out. Similarly, the PCNs can store large amounts of gas inside the cavities, but the rate of gas molecules going in and out is controlled by the microwindows.

These porous molecules have large internal surfaces on which smaller molecules may be adsorbed. For PCN-61, the surface area amounts to 3,000 to 3,500 m^2 per gram, depending on how it is estimated, while for PCN-66, constructed with the larger ligands, the surface area is from 4,000 to 4,600 m^2 per gram—among the highest values ever found for metal-organic frameworks. Zhou and his colleagues are now working to employ the techniques demonstrated with these two frameworks to build framework structures with still larger pores and surface areas.

— David Lindley

See > Dan Zhao[1], Daqiang Yuan[1], Daofeng Sun[2], and Hong-Cai Zhou[1]*, "Stabilization of Metal-Organic Frameworks with High Surface Areas by the Incorporation of Mesocavities with Microwindows," J. Am. Chem. Soc. **131**, 9186 (2009). DOI: 10.1021/ja901109t

Author affiliations >
[1]Texas A&M University,
[2]Shandong University

Correspondence >
*zhou@mail.chem.tamu.edu

> This work was supported by the U.S. Department of Energy (DE-FC36-07GO17033), the U.S. Defense Logistics Agency (N00164-07-P-1300), and the U.S. National Science Foundation (CHE-0449634). The microcrystal diffraction was carried out with the kind assistance of Yu-Sheng Chen at Argonne National Laboratory (CHE-0535644, DEAC02-06CH11357).

Use of the Advanced Photon Source at Argonne National Laboratory was supported by the U.S. Department of Energy, Office of Science, Office of Basic Energy Sciences (DOE-BES), under Contract No. DE-AC02-06CH11357.

> 15-ID • ChemMatCARS • Chemistry, materials science • Anomalous and resonant scattering (hard x-ray), liquid scattering, microdiffraction, single-crystal diffraction, small-angle x-ray scattering, surface diffraction, wide-angle x-ray scattering • 3.3-cm Undulator A • Accepting general users

Tracing Selenium with XFM

IN SHORT > Sometimes even a tiny amount of something can make a big difference. An example can be found within our own bodies, in which a number of trace elements, in spite of their small quantity, can play important roles in keeping the body healthy and functioning. Selenium (Se) is one of these, an essential element of various proteins needed for some cellular and developmental processes, such as the generation of sperm cells. But imaging selenium and other such trace elements within the body with enough resolution and sensitivity to map their distribution and activity has been a challenge, making it difficult to determine their precise role and functions. Using XFM (x-ray fluorescence microscopy) at the XOR beamline 2-ID-E at the APS, researchers have now managed for the first time to both identify and quantify Se at high resolution in its native environment within the body, in the process revealing fresh insight into the role of Se in spermatogenesis.

MORE > Scientists from Argonne, the University of Nebraska, and the National Cancer Institute focused on selenium in mammalian spermatogenesis, examining tissue and sperm samples from mice under XFM at the 2-ID-E beamline. Although it was known that Se generally took the form of selenocysteine (Sec) within proteins and is important in spermatogenesis, its exact distribution and functions within the body tissues have been mystery. Different selenoproteins have been identified, including GPx4 (glutathione peroxidase 4), present in most cell types in some form and, within the testes, especially predominant in mitochondrial (mGPx4) and nuclear (nGPx4) type. Other important selenoproteins known to be involved in spermatogenesis are SelP (Selenoprotein P) and TGR (thioredoxin-glutathione reductase).

The use of synchrotron XFM at a third-generation, high-brilliance x-ray facility such as the APS lends itself especially well to this type of work because of its ability to map trace elements at submicrometer resolution. For the first time, the team was able to identify and quantify the distribution of Se (and other trace elements), obtaining high-quality, high-resolution images within tissue slices from seminiferous tubules and dried sperm cells.

Under XFM, the mouse seminiferous tubule tissues displayed a marked increase in Se within spermatids, compared to spermatogenic cells at earlier developmental stages. Using immunostaining of testis tissue with GPx4 and TGR antibodies, the researchers confirmed that the later stage spermatids had a sharp increase in mGPx4 expression, indicating that this particular selenoprotein form is chiefly responsible for the increased Se distribution in these cells.

Examining tissue sections from knockout mice subjects with deficiencies in certain selenoproteins (Fig. 1), the researchers found that while a lack of nGPx4 had no effect on Se content in the testis, knockout of mGPx4 and SelP selenoproteins did result in a marked decrease in overall Se distribution. This confirms the crucial role of SelP, which is made in the liver and delivers Se to testes, and of mGPx4, the main Se user in spermatids, during the spermatogenesis process.

*> Fig. 1 XFM scan of a mouse seminiferous tubule. **(a)** A paraffin embedded testis section (5 μm) of a C57BL/6J wild-type mouse was mounted on a silicon nitride window and both light microscope and XFM images were obtained. The corresponding element and its maximum and minimum threshold values in ng/cm² are given above each image. The scan was obtained by using 12-keV incident energy with a dwell time of 1.3-s per pixel and 1-μm steps through the sample. The upper left panel shows a phase contrast image, with the red rectangle indicating the area of fine elemental scan. **(b)** Overlays of P, Se, and Zn maps.*

In addition, Se was observed to concentrate in the midpiece of mature sperm cells and to a lesser degree in sperm cell heads. The XFM technique also revealed the presence of significant trace amounts of zinc, phosphorus, iron, copper, and sulfur during spermatogenesis. The greatest amount of Se was associated with decreased phosphorus levels, while zinc levels showed no such correlation. However, Se co-localized with copper in the midpiece of sperm cells.

The research team's work marks the first time that Se has ever been imaged at cellular or subcellular levels at high spatial resolution, and visualized, localized, and quantified in sperm. Still, this demonstration of the power of XFM techniques to accurately measure and image Se in tissues and cells is only a first step. The experimenters envision the extension of these methods to studying the role of Se and other trace elements in other mammalian physiological functions, a great potential that will only be enhanced as XFM methods grow in sensitivity and sophistication.

— Mark Wolverton

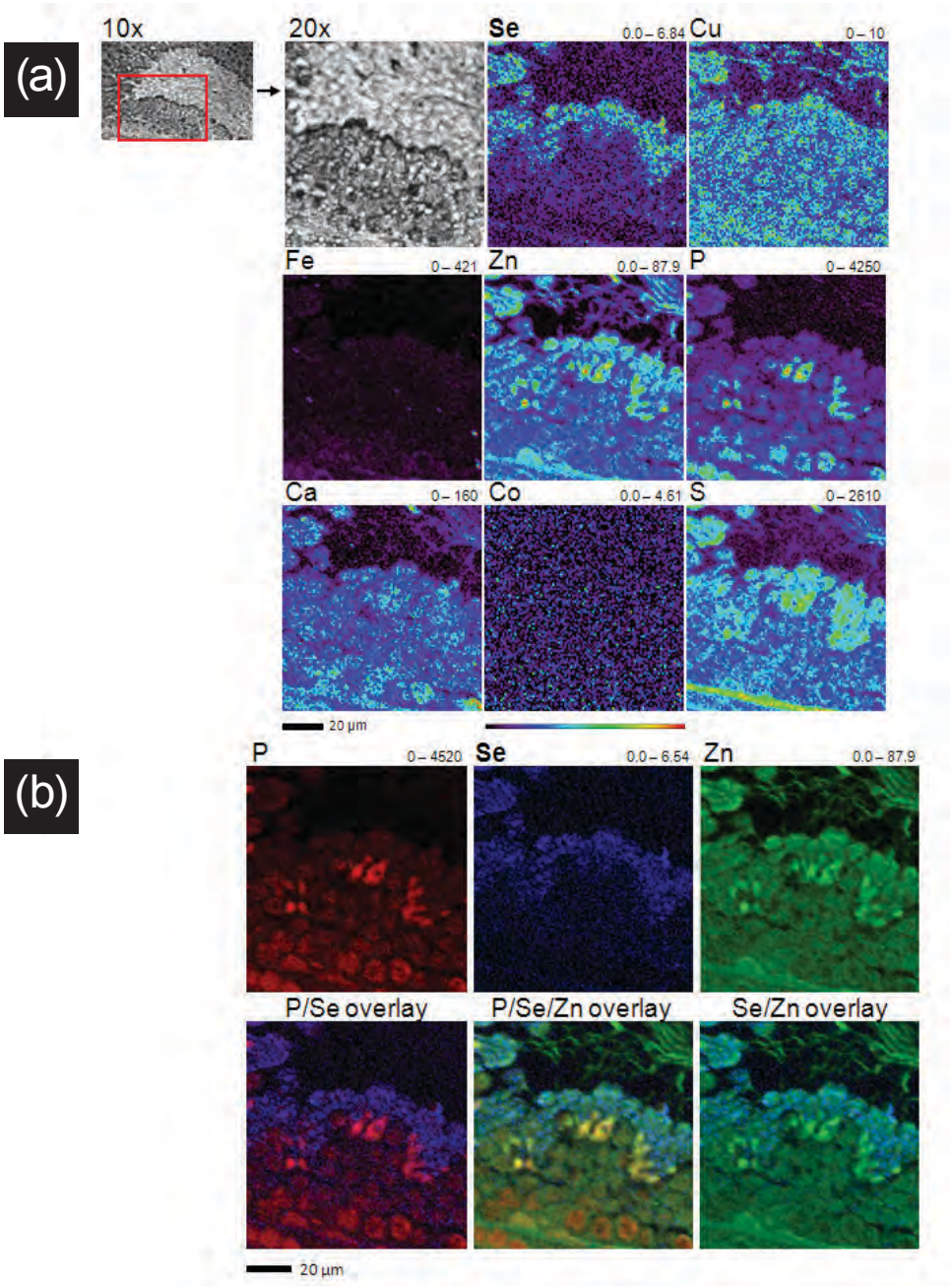

See > Sebastian Kehr[1], Mikalai Malinouski[1], Lydia Finney[2], Stefan Vogt[2], Vyacheslav M. Labunskyy[1], Marina V. Kasaikina[1], Bradley A. Carlson[3], You Zhou[1], Dolph L. Hatfield[3], and Vadim N. Gladyshev[1]*, "X-Ray Fluorescence Microscopy Reveals the Role of Selenium in Spermatogenesis," J. Mol. Biol. **389**, 808 (2009). DOI:10.1016/j.jmb.2009.04.024

Author affiliations >
[1]University of Nebraska-Lincoln,
[2]Argonne National Laboratory,
[3]National Cancer Institute

Correspondence >
*vgladyshev1@unl.edu

> This study was supported by National Institutes of Health Grant GM065204 (to V.N.G.) and the Intramural Research Program of the Center for Cancer Research, National Cancer Institute, National Institutes of Health (to D.L.H.). Use of the Advanced Photon Source was supported by the Department of Energy, Office of Science, Office of Basic Energy

> 2-ID-E • XOR • Life science, materials science, environmental science • Microfluorescence (hard x-ray • 3.3-cm Undulator A • Accepting general users

Frozen Fruit Flies

IN SHORT > The larvae of the common fruit fly, with which we share more than 70% of our genes, cannot survive freezing, whereas a distant cousin can do so. But an x-ray study carried out by researchers using the XOR 32-ID beamline at the APS suggests that there is little difference between how freezing takes place in both the survivors and those killed by the big chill. This work is the first to use phase-contrast synchrotron x-ray imaging to visualize ice formation in intact, freeze-surviving insects. Understanding the underlying process of ice formation in these insects, and the extent to which these processes differ among insects that do and do not survive freezing, plays an important role in understanding the freezing process. The work suggests that key adaptations taking place during the freezing process occur at the cellular, molecular, and biochemical levels and might eventually lead to frozen storage of fruit flies that are so widely used in important studies of genetics, development, evolution, and ageing.

MORE > Some insects can be frozen solid and survive at very low temperatures, while chilling others to a few degrees below freezing kills them. Scientists have known about biological antifreeze compounds in some species of insect for many years. However, even synchrotron x-ray studies could not spot the difference between the formation of ice crystals in insects during lethal and non-lethal freezing. Our limited understanding of insect freezing survival points to the existence of various protection mechanisms.

Carbohydrates, for instance, are thought to protect cell membranes and proteins as water in an insect's body expands and freezes and the cells undergo dehydration. There are also ice nucleators that control the freezing processes, while antifreeze proteins control the shape and structure of the ice as it forms. However, none of the protection mechanisms seems to be necessary or sufficient to allow an insect to survive the big freeze.

Other researchers have turned to light microscopy, thermal imaging, magnetic resonance imaging, x-ray spectroscopy, and other techniques in an effort to home in on the fundamentals of the ice protection racket. Particularly poignant is that larvae of the model organism *Drosophila melanogaster* do not survive freezing, whereas their Canadian cousins *Chymomyza amoena*, another type of fruit fly can survive ice.

Synchrotron x-ray phase-contrast imaging has emerged as a useful tool for studying internal processes in insects, including respiratory tracheal compression and internal fluid dynamics of digestion and circulation because the technique is just as amenable to observing the water-to-ice phase transition at high resolution.

The researchers in this study, from The University of Western Ontario, the University of Nevada-Las Vegas, Argonne, and Virginia Polytechnic Institute and State University, used a two-dimension synchrotron x-ray technique to observe ice forming, for the first time, within intact insect larvae of the two fruit fly species in real time (Fig. 1). The chamber containing the larvae was placed on a translation stage in the path of the x-ray at beamline 32-ID. The initial hypothesis was that there would be visible differences in the pattern of ice formation and its interaction with the insect's tissues between the larvae that do and do not survive freezing.

The team says that the prolonged exposure to x-rays caused a slight rise in temperature of all larvae studied and ultimately killed the insects. However, control experiments in which larvae of each species were frozen under similar conditions, but without the x-ray exposure, allowed the team to confirm which species survived and which didn't. Although *C. amoena* froze and survived down to −14° C, the freezing processes were remarkably similar to those in

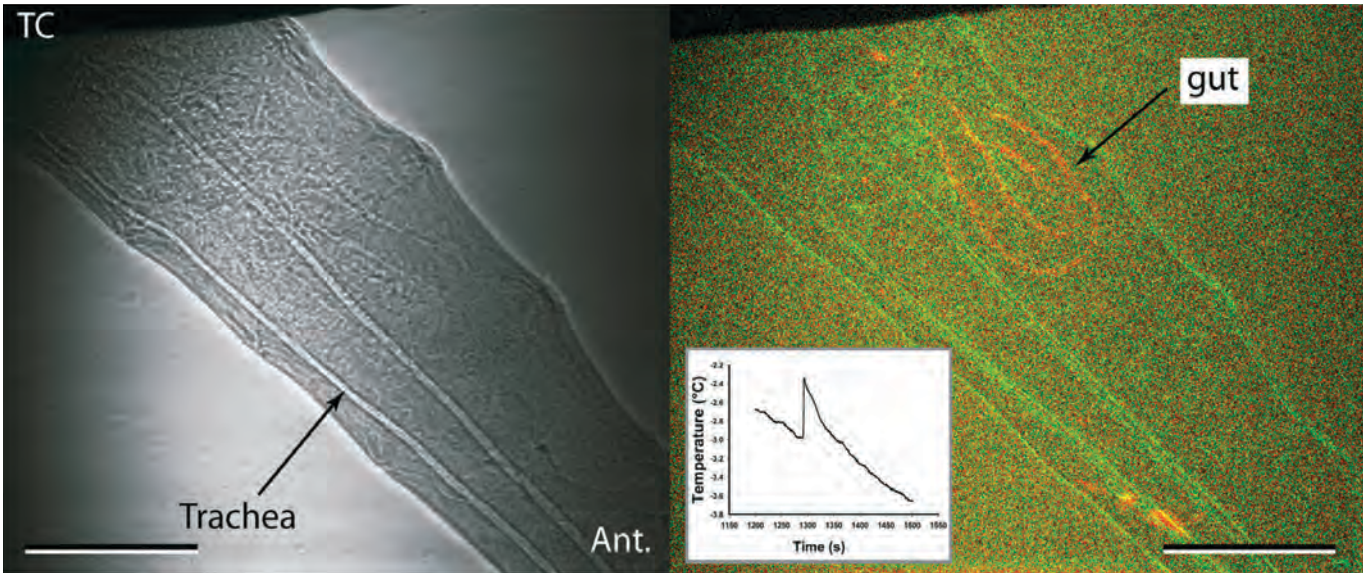

^ *Fig. 1 Ice formation in gut during freezing. Apparent gut freezing in a non-diapausing* ***C. amoena*** *larva.* ***Left image*** *is the x-ray image,* ***right*** *is a composite of subtraction images of the frames where the gut appeared to freeze (orange) and the initial freezing frame (green), which shows the locations of the cuticle and tracheal landmarks. The individual froze at −3.0° C, and the gut froze 67.6 s after the initiation of freezing; inset shows exotherm from this individual, note the lack of a double exotherm. "Ant.' indicates the anterior of the animal, TC indicates the thermocouple.*

D. melanogaster, which was killed by the low-temperature exposure. This, the team says, implies that the physical ice formation process itself does not differ between different larval species regardless of whether they survive freezing.

The team did notice that the body of the freeze-tolerant species wasn't stretched as much during ice formation as *D. melanogaster*, and that freezing seemed to happen at a more reliable temperature in *C. costata*. This suggests that insects that survive freezing have some control over ice formation, but the overall differences were not striking. The research suggests that studies might glean more about cryoprotection in fruit flies by focusing on differences at the cellular and biochemical level.

— David Bradley

See > Brent J. Sinclair[1]*, Allen G. Gibbs[2], Wah-Keat Lee[3], Arun Rajamohan[1§], Stephen P. Roberts[2§§], John J. Socha[4], "Synchrotron X-Ray Visualisation of Ice Formation in Insects during Lethal and Non-Lethal Freezing," PLoS ONE **4**(12), e8259 (December 2009).

Author affiliations >
[1]The University of Western Ontario, [2]University of Nevada-Las Vegas, [3]Argonne National Laboratory, [4]Virginia Polytechnic Institute and State University §Present address: North Dakota State University, §§Present address: Central Michigan University

Correspondence >
*bsincla7@uwo.ca

> This work was supported by grant number RR022885 from the National Center for Research Resources, a component of the National Institutes of Health; an NSERC Discovery Grant; and grants from the Canada Foundation for Innovation and the Ontario Research Fund to B.J.S. Use of the Advanced Photon Source at Argonne National Laboratory was supported by the U.S. Department of Energy, Office of Science, Office of Basic Energy Sciences, under Contract No. DE-AC02-06CH11357.

> 32-ID • XOR • Materials science, life science • Phase-contrast imaging, ultra-small-angle x-ray scattering, radiography • 3.3-cm Undulator A • Accepting general users

A New Way to Peer in a Grasshopper

IN SHORT > Until now, directly viewing the flow of blood in living, opaque insects—such as the grasshopper—has not been possible due to the lack of an effective imaging technique. Researchers using the XOR 32-ID beamline at the APS to study grasshoppers have produced the first images with certain details of insect blood flow, flow patterns within the heart, and the relationship between respiratory and circulatory systems. The ability to directly view basic functions of blood flow in living insects promises to advance our knowledge of circulation in small animals.

MORE > In studies of insect physiology, it is necessary to measure events that occur in less than 0.1 sec and to visualize structures smaller than 50 μm. Current imaging methods such as magnetic resonance imaging, ultrasound, and visible light probes are limited in their ability to view fine and moving structures in opaque insects and to elucidate some of the finer physiologic details. As a result, certain questions regarding small animal physiology—for example the precise movement of insect blood—remain poorly understood.

Although current non-imaging techniques can be used to indirectly infer movement of the heart and insect blood flow, these methods cannot reveal the finer details of the beating heart or blood flow patterns. Obstacles include a lack of contrast between blood vessels and the surrounding tissue, as well as resolution too low to observe most physiological processes. To overcome these hurdles, researchers from Virginia Polytechnic Institute and State University, and Argonne borrowed a trick from ultrasound imaging in order to enhance what could already be seen with real-time synchrotron x-ray phase-contrast imaging carried out at the 32-ID beamline.

The real-time synchrotron x-ray phase-contrast imaging technique has the necessary resolution to visualize small-insect physiology, but lacks the ability to distinguish blood from other soft tissue because the densities of blood and soft tissue are nearly the same. The researchers adapted this imaging technique to include microbubble injection, a procedure used in patients undergoing ultrasound imaging. When used to enhance ultrasound images, microbubbles are administered intravenously to the systemic circulation. By combining synchrotron x-ray phase-contrast imaging with microbubble injection, sufficient resolution—as well as the necessary image contrast—was achieved. It was possible to clearly visualize the respiratory structures of the air sacs and tracheae, and a main longitudinal tracheal trunk running alongside the heart (Fig. 1). The researchers were also able to visualize the contraction of the heart and ascertain details about blood flow within the heart.

> Fig. 1 A still x-ray image, taken from a video, shows a side view of the grasshopper heart (edges are outlined in red). The dashed blue line is the ventral diaphragm and the solid blue line near the top indicates the dorsal surface (back) of the grasshopper. Microbubbles can be seen on the upper edge of the heart tube. Two large side air sacs (outlined in green) can be seen. The field of view is about 1.3 mm horizontal by 0.9 mm vertical.

They concluded that insect blood transport may be more complicated than the simple peristaltic motion previously assumed to take place. In addition, they determined that the respiratory structures contracted in ways that were both synchronous and asynchronous to the local heartbeat, which was previously unknown. The researchers were also able to image individual microbubbles, which range in size from 10–150-μm in diameter, enabling them to quantify the speed of flow and to map complex details, which would not be possible using any other technique.

The application of this combined technique has produced the first measurements of blood-flow rates and patterns within an insect heart. Being able to directly view the basic physiological functions of blood flow in living insects will help

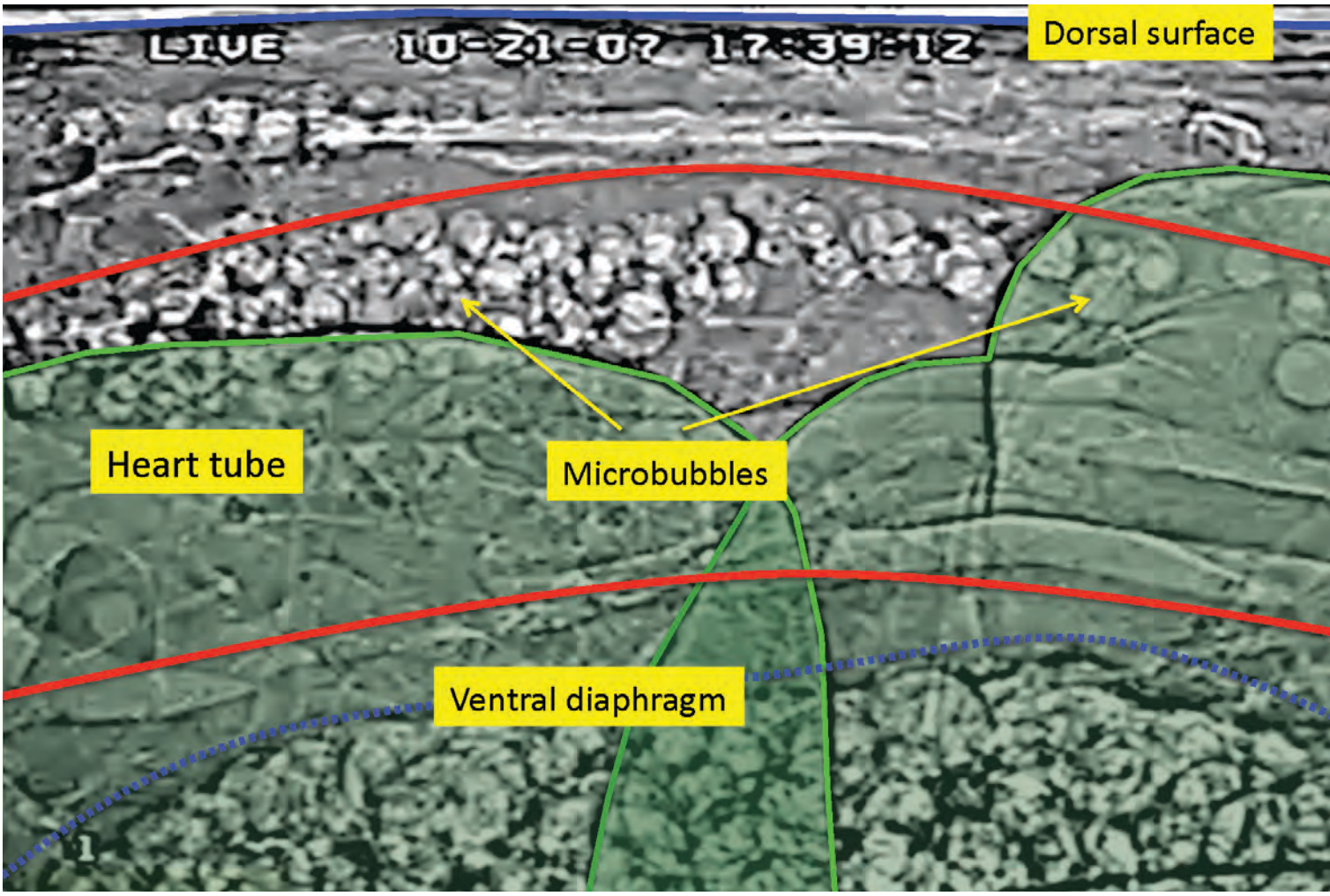

answer many long-standing questions about circulation, which extends to subjects such as insect retrograde heart flow and the development of blood flow in embryonic vertebrates.

— *Emma Hitt*

See > Wah-Keat Lee[1]* and John J. Socha[2]**, "Direct visualization of hemolymph flow in the heart of a grasshopper (*Schistocerca americana*)," BMC Physiology 2009, **9**:2. DOI: 10.1186/1472-6793-9-2

Author affiliations >
[1]Argonne National Laboratory,
[2]Virginia Polytechnic Institute and State University

Correspondence >
*wklee@aps.anl.gov
**jjsocha@vt.edu

> Use of the Advanced Photon Source at Argonne National Laboratory was supported by the U.S. Department of Energy, Office of Science, Office of Basic Energy Sciences, under Contract No. DE-AC02-06CH11357.

> 32-ID • XOR • Materials science, life science • Phase-contrast imaging, ultra-small-angle x-ray scattering, radiography • 3.3-cm Undulator A • Accepting general users

Protein Assembly and Disease

IN SHORT > For some time now, proteins known as amyloids have been implicated in the onset and advance of Alzheimer's and other diseases, such as type 2 diabetes. One of the curious aspects of linking these proteins to diseases is that it seems to be primarily unusual protein folding and assembly that leads to disease. This is especially so in the case of Alzheimer's and cerebral amyloid angiopathy, where mutations such as the Iowa mutant are associated with familial inheritance and early onset of the disease. Patients carrying the mutation develop neuritic plaques and large deposits of the mutant protein in cerebral blood vessels. Exactly how the protein does so much damage has been the subject of intense recent research, including these findings by researchers from The University of Chicago, the National Institutes of Health, and the Illinois Institute of Technology. With the help of the Bio-CAT 18-ID beamline at the APS, the team used x-ray diffraction, electron microscopy, and nuclear magnetic resonance (NMR) spectroscopy to show how the mutant and normal proteins differ with respect to folding and assembly. What the research group found goes a long way toward explaining how the mutant protein is able to create so much havoc in tissues and how β-amyloids relate to disease.

MORE > The researchers focused on the β-amyloid coded by the Iowa mutation, which differs from the normal protein by only one amino acid. They found that the mutant protein, known as D23N-Aβ40, forms fibrils much more rapidly than the normal protein and does so without first undergoing the lag phase observed for the normal protein. X-ray diffraction patterns from the mutant protein showed cross-β patterns and other attributes that differed from the normal protein. Observing the mutant protein using electron microscopy, the team found that it occurs in more than one morphotype (organisms that are classified together on the basis of similar physical features without knowledge of their genetic relationship).

Further investigations using NMR spectroscopy showed that only a minority of the mutant protein fibrils looked like the typical β-amyloid protein fibrils, which exhibit a parallel β-sheet structure. Thus, a majority of the mutant protein fibrils looked quite different from the normal fibrils. Further examination of the mutant fibrils indicated that they are put together differently and had a smaller average diameter when compared to the normal fibrils.

In perhaps the most exciting of the new findings presented by the investigators, a majority of the mutant fibrils exhibited a structure consistent with antiparallel β-sheets and are thus assembled quite differently from the parallel β-sheet of the normal protein. This clear difference in orientation between the mutant and normal molecules represents one of the first truly distinguishing characteristics of the mutant protein and will certainly lead to better ways of detecting and treating the resulting disease states.

Using these new data, the research team proposed a link between aberrant assembly and tissue pathology of the patients carrying the mutation for D23N-Aβ40 (Fig. 1). Further work is planned to answer questions about how exactly the mutant protein assembles to produce some molecules that look like the normal protein, even though most of them do not. Previous work by the research group showed that examining the mechanisms for bends or folds between sheets holds promise for explaining these differences and allowed them to construct a model consistent with their current results. Additional questions include how the substitution of a single amino acid in the mutant protein allows it to form the very different anti-parallel β-sheet structure. And the large protein deposits characteristic of the disease in patients carrying the Iowa mutation, as well as the frequency with which β-amyloid protein is transported into the

v *Fig. 1 Protein shape changes in wild type and mutant β-amyloids related to classic Alzheimer's disease and hemorrhagic stroke.*

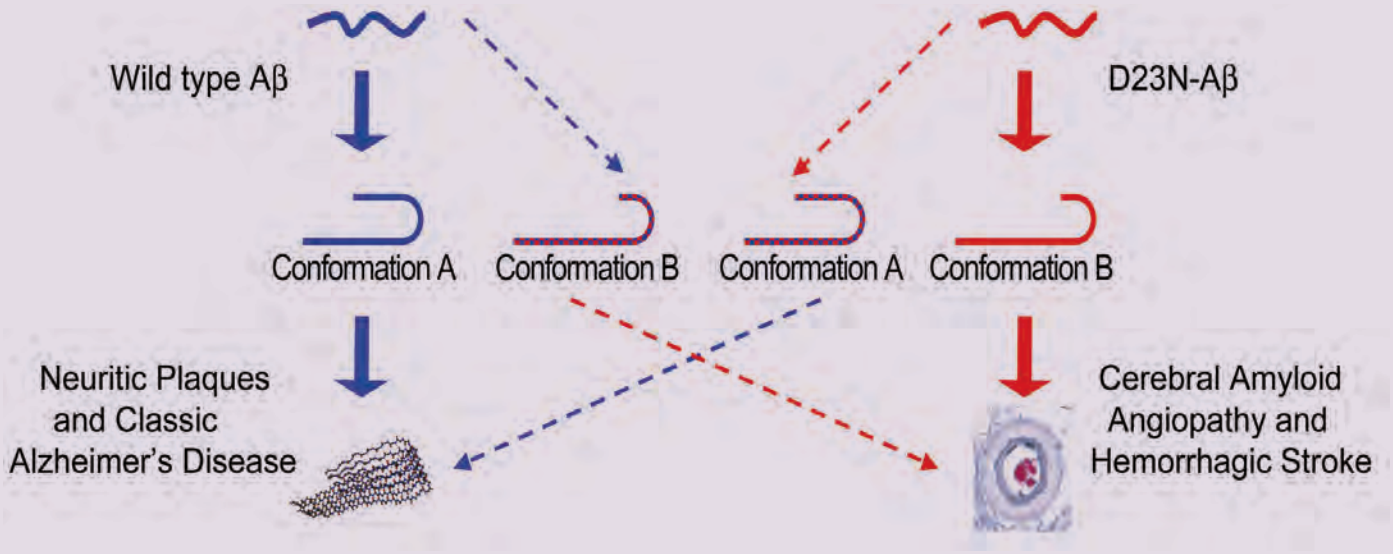

blood vessel wall, may also be related to how and when the fibrils are assembled.

The work reported by the research team points to two characteristics of proteins that can never be ignored: the amino acid sequence and how the protein is assembled. In the case of the β-amyloid proteins, changing one amino acid creates a mutant protein that can assemble quite differently and lead to diseases such as Alzheimer's, an understanding of which may lead to the development of new therapeutic options.

— *Mona Mort*

See > Robert Tycko[1], Kimberly L. Sciarretta[2], Joseph P.R.O. Orgel[3], and Stephen C. Meredith[2]*, "Evidence for Novel β-Sheet Structures in Iowa Mutant β-Amyloid Fibrils," Biochemistry-US **48**, 6072 (2009). DOI: 10.1021/bi9002666

Author affiliations >
[1]National Institutes of Health,
[2]The University of Chicago,
[3]Illinois Institute of Technology

Correspondence >
*scmeredi@uchicago.edu

> This work benefited from the support of the NSF Research Collaborative Network, "Fibernet" (MCB-0234001). Use of the Advanced Photon Source was supported by the U.S. Department of Energy, Office of Science, Office of Basic Energy Sciences, under Contract No. DE-AC02-06CH11357

> 18-ID • Bio-CAT • Life science • Fiber diffraction, microdiffraction, microfluorescence (hard x-ray), micro x-ray absorption fine structure, small-angle x-ray scattering, time-resolved x-ray scattering • 3.3-cm Undulator A • Accepting general users

The Power of Proteins: Prion Diseases Demystified

IN SHORT > It is hard to believe that a single protein can be responsible for the damage inflicted by diseases such as human Creutzfeldt-Jakob and bovine spongiform encephalopathy (Mad Cow Disease). Yet the implicated protein, known as a prion and only about 200 amino acids long, can initiate and propagate a disease cycle just by changing its shape. Studying the prion diseases has required patience because of the disorder and insolubility of the prion samples. Aided by beamlines at the APS, the Stanford Synchrotron Radiation Lightsource (SSRL), and the Advanced Light Source, a collaborative research team of scientists from Vanderbilt University and the University of California, San Francisco, have achieved a significant advance in our understanding of the infectious power of the prion protein.

*> Fig. 1 Diffraction from natural and recombinant prions: the observed x-ray diffraction pattern **(A)** from natural prions best fits the calculated pattern **(B)** from a 3-protofilament helical model **(C)**; the observed x-ray diffraction pattern **(D)** from recombinant prions best fits the calculated pattern **(E)** from a stacked β-sheet model **(F)**. (From H. Wille et al., Proc. Nat. Acad. Sci. USA **106**[40], 16990 [2009], (Copyright © 2009 National Academy of Sciences, U.S.A.)*

MORE > Prions are amyloids, which are misfolded proteins now implicated in numerous diseases. Prions and other misfolded proteins, such as those associated with Alzheimer's disease, represent both a fascinating problem in protein folding and an excellent application of fiber diffraction. Previous work had definitively shown that a particular conformation, or isoform, of the mammalian prion protein was responsible for causing the central nervous system (CNS) diseases now known as prion diseases: Creutzfeldt-Jakob, bovine spongiform encephalopathy, ovine scrapie, and other mammalian CNS disorders.

The research team used the BioCARS beamline 14-ID-B at the APS and an SSRL beamline to obtain diffraction patterns from infectious prions, compared them with diffraction patterns from genetically engineered prions, and discovered important differences, both in structure, as determined by diffraction studies, and in heterogeneity, as determined by electron microscopy (Fig. 1). Both types of samples exhibit cross-β diffraction, which is indicative of amyloid structure. The most prominent difference was equatorial intensity indicative of stacked β-sheets, which is present in the recombinant samples but missing from the brain-derived prions. Some of the patterns from infectious prions produced data consistent with a repeating unit of 4 β strands, which is consistent with the group's earlier model derived from electron crystallography.

Discovering that the structure was cross-β was not surprising. For many years, researchers had proposed that the prion structure was a cross-β structure, and the most convincing models from collaborators and other groups all incorporated this feature. However, it took many years to prove this, until this study. Recent work is showing that biologically significant amyloids come in a variety of structures, all cross-β, but with the β-strands connected in very different ways.

On an interesting side note, the research team found that the synthetic prions recovered from mice inoculated with recombinant prions were more like the naturally occurring prion proteins than the recombinant ones. The investigators put forth several hypotheses that would explain the observed structural differences, including the intriguing idea that only some of the recombinant prion proteins have a conformation that would make them infectious or that some difference in the recombinant protein is inhibiting its transformation to an infectious conformation.

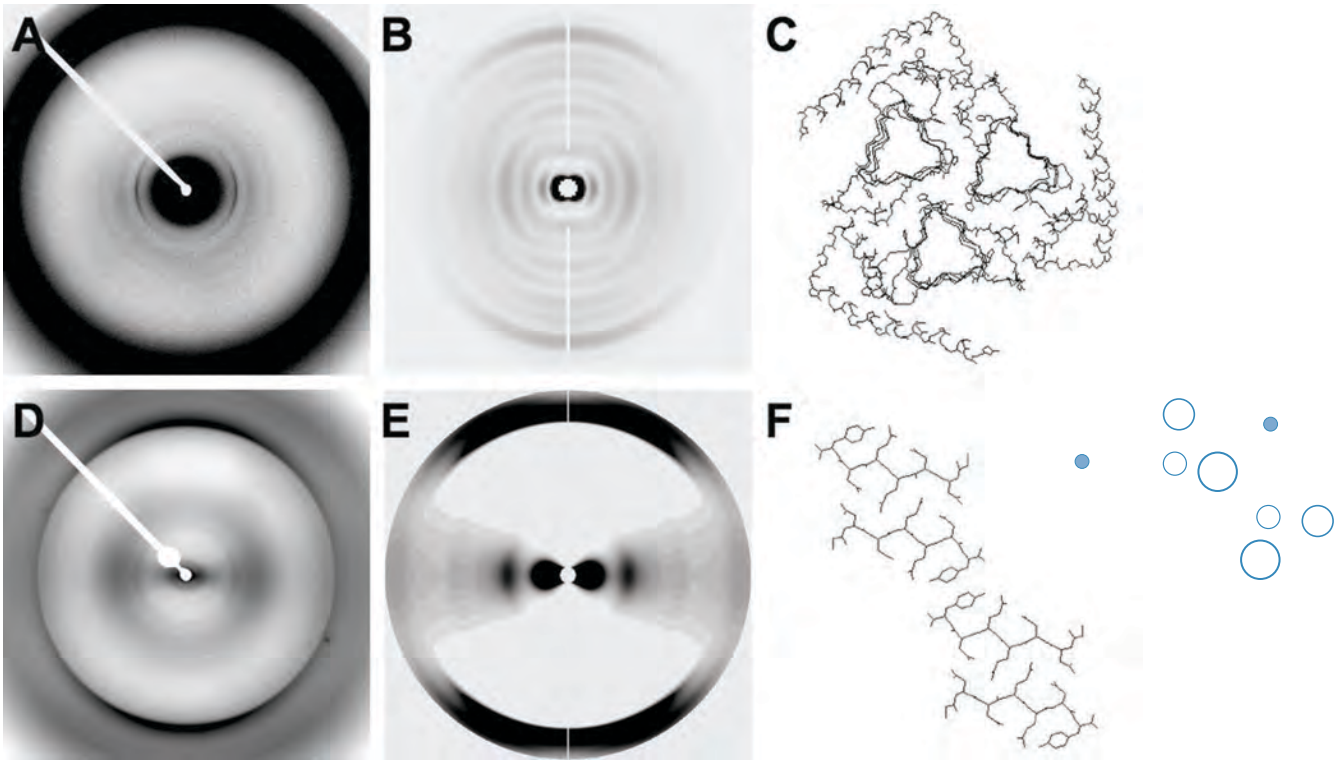

Though more work needs to be done to pinpoint the exact structural changes that make the prion infectious, the present work sets the stage for that next set of experiments. The team is particularly interested in looking at strains of prions in which the molecules are slightly differently folded, with significant consequences for infectivity, symptoms, and even in rare cases the ability to be transmitted from one species to another. Transmission across species is what makes the question of strain structure one of the most interesting in prion research at present.

By elucidating and underscoring the differences between the brain-derived infectious form and the recombinant forms of the prion proteins, the present work provides bright beacons on the path to understanding the infectious power of the prion protein.

— Mona Mort

See > Holger Wille,[1], Wen Bian[2], Michele McDonald[2], Amy Kendall[2], David W. Colby[1], Lillian Bloch[1], Julian Ollesch[1§], Alexander L. Borovinskiy[2§§], Fred E. Cohen[1], Stanley B. Prusiner[1], and Gerald Stubbs[2]*, "Natural and synthetic prion structure from X-ray fiber diffraction," Proc. Nat. Acad. Sci. USA **106**(40), 16990 (2009). DOI: 10.1073_pnas.0909006106

Author affiliations >
[1]University of California, San Francisco; [2]Vanderbilt University
[§]Present address: Max-Planck-Forschungsstelle für Enzymologie der Proteinfaltung, Martin-Luther Universität Halle-Wittenberg,
[§§]Present address: Genesys Telecommunications Laboratory

Correspondence >
*gerald.stubbs@vanderbilt.edu

> This work was supported by National Institutes of Health (NIH) grants NS064, AG010770, and AG02132; the Fairchild Foundation; the G. Harold and Leila Y. Mathers Foundation; and a Jane Coffin Childs postdoctoral fellowship (to D.W.C). Diffraction data were collected at BioCARS under the Bio-CAT/BioCARS collaborative agreement; preliminary data were collected at beamline 12.3.1 at the Advanced Light Source, Lawrence Berkeley National Laboratory. The SSRL and ALS are supported by the U.S. Department of Energy; beamlines 4-2, BioCAT, and BioCARS are also supported by the NIH National Center for Research Resources. Use of the Advanced Photon Source was supported by the U.S. Department of Energy, Office of Science, Office of Basic Energy Sciences, under Contract No. DE-AC02-06CH11357. The Stanford Synchrotron Radiation Lightsource is a national user facility operated by Stanford University on behalf of the U.S. Department of Energy, Office of Basic Energy Sciences.

> 14-ID-B • BioCARS • Life sciences • Anomalous diffraction (MAD/SAD), biohazards at the BSL2/3 level, Laue crystallography, macromolecular crystallography, time-resolved x-ray scattering • 2.7-cm undulator, 2.3-cm undulator • Accepting general users

Receptor Structure, Caffeine, and Preventing Disease

IN SHORT > Coffee drinkers tend to have a lower risk of developing Parkinson's disease. Since these data have come to the fore, much effort has been expended on finding the underlying mechanism for this effect. Once the exact mechanism is known, drugs and therapies can be designed that would help treat the disease. Earlier studies showed that caffeine interacts with an adenosine receptor that, in association with dopamine and glutamate receptors, controls locomotor behavior. If more selective compounds could be designed for interaction with the various adenosine receptor subtypes, the result would be better therapies not only for Parkinson's, but also for related neurological diseases, such as pain, Huntington's disease, asthma, and seizures. With an eye toward obtaining fine detail on adenosine receptor structure, and aided by the GM/CA-CAT beamline 23-ID-D at the APS, researchers determined the crystal structure of the human adenosine A_{2A} receptor. Their data provide, in exquisite detail, important structural information that can now be used in improving therapies for diseases in which adenosine receptors play an important role.

> Fig. 1 The three-dimensional structure of the human adenosine A_{2A} receptor (red) in a neuron.

MORE > The research team, from the Scripps Research Institute and the Leiden/Amsterdam Center for Drug Research, studied the adenosine A_{2A} receptor from a class of receptors known as GPCRs (G Protein-Coupled Receptors). The receptor family is the largest single protein family in the human genome and binds to G proteins (guanine nucleotide-binding proteins). Of the four adenosine-receptor subtypes (A_1, A_{2A}, A_{2B}, and A_3), the A_{2A} subtype is the one that is linked to caffeine and lowered risk of Parkinson's disease (Figs. 1 and 2). The adenosine A_{2A} receptor had already been shown to have its action blocked, or antagonized, by caffeine. The researchers characterized the crystal structure of the A_{2A} adenosine receptor, to a resolution of 2.6 Å, when the receptor was in complex with a high-affinity subtype-selective antagonist to treat Parkinson's disease known as ZM241385. By choosing to study the adenosine A_{2A} structure, in complex with an antagonist for which the receptor had high specificity, the research team was able to clearly focus on what particular structural changes occur when adenosine A_{2A} binds to an antagonist.

The researchers found that, when binding the antagonist, the adenosine A_{2A} receptor forms a pocket that is different than that found in previously determined GPCR structures. The pocket is formed by four disulfide bridges in the extracellular domain, along with a repacking of transmembrane helices relative to associated receptor structures. This arrangement, in addition to being previously undetected in GPCRs, is interesting because it allows the antagonist to bind in an extended conformation perpendicular to the membrane plane. The data also show that there is not really a conserved structure among pockets of the receptor subtypes. With a conserved structure, specificity could be achieved by varying only the side chains. Rather, the structure of the entire pocket varies significantly among the receptor subtypes, suggesting that specificity comes from varying the pocket's position and orientation. These last pieces of information will be especially important in future drug design.

Additional findings about the adenosine A_{2A} receptor-binding site suggest important roles for the extracellular loops and helical core in recognizing binding molecules and also point to telling details about binding and subsequent shape

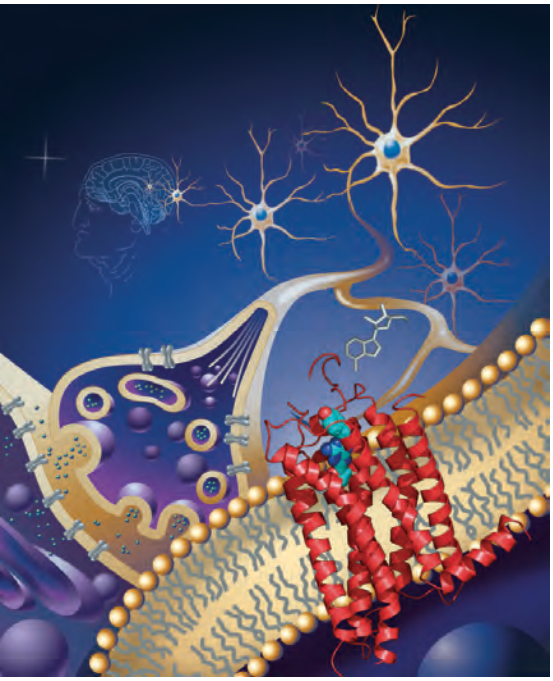

changes. All of these results were unexpected based on previously determined GPCR structures and highlighted in a community-wide assessment that was conducted to evaluate where the field is at in GPCR modeling and docking for drug discovery [1].

By diligently collecting details about ZM241385 and its specificity for the adenosine A_{2A} receptor, and combining these observations with previously reported mutagenesis data, the research team can now paint a very clear picture of how the adenosine A_{2A} receptor functions in binding an antagonist such as caffeine. And now that the research team has provided a structure for another human GPCR, structural differences can be analyzed for their relevance to pharmacology, ligand recognition, and receptor activation for other receptors.

— Mona Mort

^ *Fig. 2 The three-dimensional structure of the human adenosine A_{2A} receptor and caffeine molecules floating above a cup of coffee; the adenosine A_{2A} receptor is the molecule in the human body that recognizes the caffeine that we consume.*

Reference > [1] M. Michino; E. Abola; C.L. Brooks, 3rd; J.S. Dixon; J. Moult; and R.C. Stevens, "Community-wide assessment of GPCR structure modeling and ligand docking: GPCR Dock 2008," Nat. Rev. Drug Discov. **8**, 455 (June 2009). DOI:10.1038/nrd2877

See > V.P. Jaakola[1], M.T. Griffith[1], M.A. Hanson[1], V. Cherezov[1], E.Y. Chien[1], J.R. Lane[2], A.P. IJzerman[2], and R. C. Stevens[1]*, "The 2.6 Angstrom Crystal Structure of a Human A_{2A} Adenosine Receptor Bound to an Antagonist," Science **322**(5905), 1211 (21 November 2008). DOI: 10.1126/science.1164772

Author affiliations >
[1]The Scripps Research Institute, [2]Leiden/Amsterdam Center for Drug Research

Correspondence >
*stevens@scripps.edu

> This work was supported by the National Institutes of Health Roadmap Initiative grant P50 GM073197 for technology development, Protein Structure Initiative grant U54 GM074961 for target processing, and Pfizer (R.C.S.). A.P.IJ. and J.R.L. thank the Dutch Top Institute Pharma for financial support through the GPCR forum program (D1-105). The GM/CA-CAT beamline (23-ID) is supported by the National Cancer Institute (Y1-CO-1020) and the National Institute of General Medical Sciences (Y1-GM-1104). Use of the Advanced Photon Source at Argonne National Laboratory was supported by the U.S. Department of Energy, Office of Science, Office of Basic Energy Sciences, under Contract No. DE-AC02-06CH11357.

> 23-ID-D • GM/CA-CAT • Life science • Macromolecular crystallography, microbeam, microdiffraction, anomalous diffraction (MAD/SAD), subatomic (<0.85 Å) resolution • 3.0-cm undulator • Accepting general users

Molecular Mechanisms and Drug-Resistant Cancers

IN SHORT > When cells need a vacuum cleaner, it's good to have one that cleans up all sorts of molecules that are not wanted or are potentially toxic. The P-glycoprotein (P-gp) is a great candidate for this activity because it can tidy up cells by expelling many different kinds of toxins. Under normal circumstances, this substrate promiscuity would make P-gp the ideal vacuum cleaner. But in cancer treatment, P-gp activity can present a problem. If all of the drugs used are exported by P-gp before they can perform their therapeutic functions, the result is multidrug resistance (MDR). Because P-gp is implicated in MDR cancers, knowing how the protein structure results in binding so many types of drugs is critical to designing anticancer drugs and MDR inhibitors. With the goal of learning the underpinnings of polyspecific drug binding in the P-glycoprotein, a research team used two GM/CAT-CAT 23-ID beamlines at the APS, two beamlines at the Stanford Synchrotron Radiation Lightsource, and two beamlines at the Advanced Light Source to produce detailed structures of P-gp in both its free state and drug-bound. Their work provides new, important insight on how P-gp operates and advances the search for understanding of MDR cancers.

> Fig. 1 A surface model of the inward-facing conformation of the multidrug transporter P-gp. (Image created by Graham Johnson of www.grahamj.com and TSRI.)

MORE > The P-gp is the most prevalent of three molecular "pumps" that transport drugs out of cells. And P-gp appears to have the broadest range of compounds that it taps for export; the size range of the expelled compounds ranges from 330 to 4000 daltons. Because most of the compounds that P-gp binds are hydrophobic, and thus are found in the lipid bilayer of the cell membrane, P-gp has been called a "hydrophobic vacuum cleaner." P-gp removes molecules from the membrane and exports them, resulting in MDR. Previous work had yielded low-resolution structural data. Recognizing the clinical value of high-resolution structural data, the researchers, from the Scripps Research Institute and Texas Tech University, set out to produce an x-ray structure of P-gp. They used mouse P-gp, which has high (87%) sequence similarity to human P-gp and studied the glycoprotein both with and without bound drugs. By carefully choosing the bound compounds, the research team produced structures at a resolution of 3.8 Å, which then allowed them to model the molecular basis for P-gp's poly-specificity.

The researchers found an architecturally and biochemically interesting x-ray structure for P-gp (Fig. 1). The overall structure is inward facing and arranged as two symmetrical halves. An internal cavity of about 6000 Å, which is large enough to hold at least two molecules simultaneously, contains two nucleotide-binding domains separated by 30 Å. There are chemical differences between the upper and lower halves of the drug-binding pocket that would allow for spatial heterogeneity in terms of what types of molecules bind: the upper half contains more hydrophobic and aromatic residues while the lower half has more polar and charged residues. Both unbound and drug-bound P-gp structures have two portals that are open to the cytoplasm and to the inner lipid bilayer, allowing entry of hydrophobic molecules directly from the membrane.

Because the inward-facing structure would not allow molecules to enter from the outer cell membrane or from outside the cell, the researchers propose that this structure depicts P-gp in

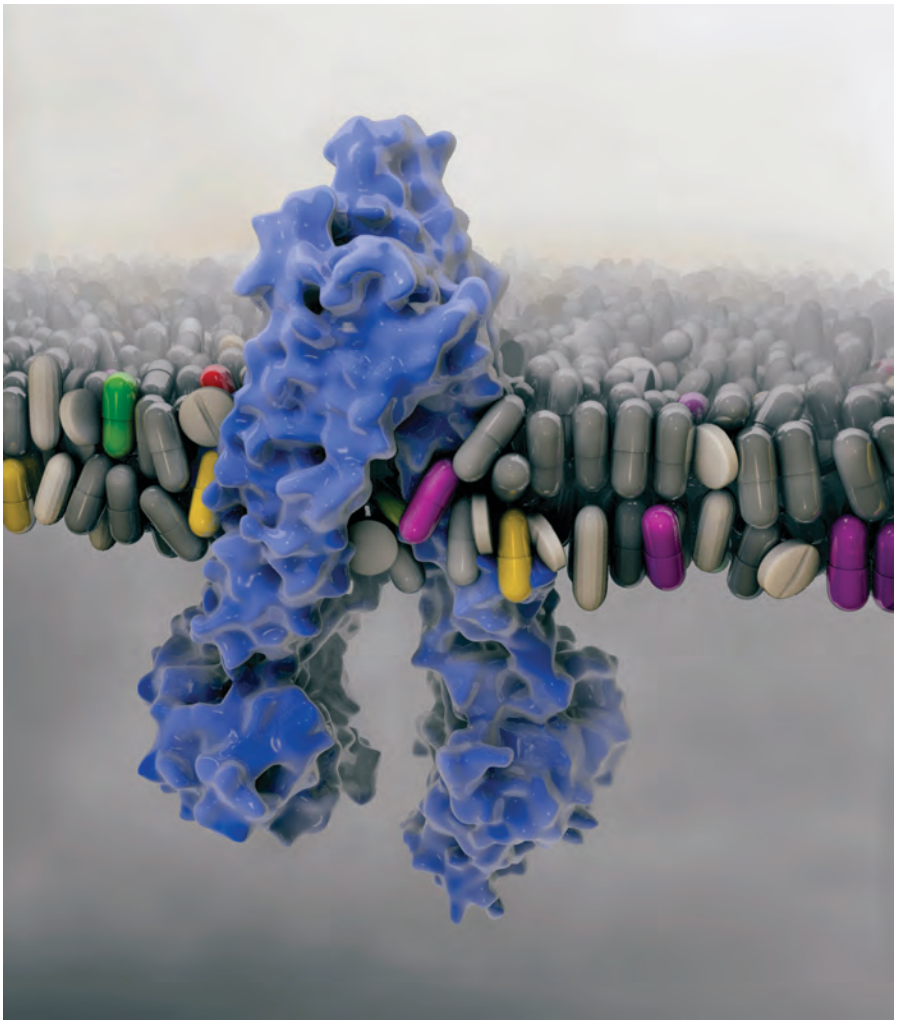

a pre-transport state, when it binds molecules inside the cell and readies them for eviction. Then, binding of ATP and the resulting catalytic cycle would change P-gp to its outward-facing conformation and allow it to escort molecules outside the cell. After the ATP is released, the P-gp molecule would return to its inward-facing structure, ready to bind the next molecule that is to be expelled from the cell.

— Mona Mort

See > Stephen G. Aller[1], Jodie Yu[1], Andrew Ward[1], Yue Weng[1,3], Srinivas Chittaboina[1], Rupeng Zhuo[2], Patina M. Harrell[2], Yenphuong T. Trinh[2], Qinghai Zhang[1], Ina L. Urbatsch[2], and Geoffrey Chang[1]*, "Structure of P-Glycoprotein Reveals a Molecular Basis for Poly-Specific Drug Binding," Science **323**, 1718 (27 March 2009). DOI: 10.1126/science.1168750

Author affiliations >
[1]The Scripps Research Institute, [2]Texas Tech University Health Sciences Center, [3]Wuhan University

Correspondence >
*gchang@scripps.edu

> This work was supported by grants from the U.S. Army (W81XWH-05-1-0316), National Institutes of Health (GM61905, GM078914, and GM073197), the Beckman Foundation, the Skaggs Chemical Biology Foundation, Jasper L. and Jack Denton Wilson Foundation, the Southwest Cancer and Treatment Center, and the Norton B. Gilula Fellowship. Use of the Advanced Photon Source at Argonne National Laboratory was supported by the U.S. Department of Energy, Office of Science, Office of Basic Energy Sciences, under Contract No. DE-AC02-06CH11357.

> 23-ID-B • GM/CA-CAT • Life science • Microbeam, macromolecular crystallography, microdiffraction, anomalous diffraction (MAD/SAD), subatomic (<0.85 Å) resolution • 3.3-cm Undulator A • Accepting general users

> 23-ID-D • GM/CA-CAT • Life science • Macromolecular crystallography, microbeam, microdiffraction, anomalous diffraction (MAD/SAD), subatomic (<0.85 Å) resolution • 3.0-cm undulator • Accepting general users

Getting to Know Cellulose

IN SHORT > As humans continue to deplete the Earth's supply of fossil fuels, finding new sources of energy becomes a priority. Biomass, such as cornhusks left after harvest, is one such alternative energy source. Before efficient use can be made of such materials, understanding how to break down cellulose—the fiber in human nutrition and the main component of much biomass waste—is crucial. With the help of the NE-CAT and Bio-CAT beamlines at the APS and the SPring-8 (Japan) beamline BL38B1, an international research team from Los Alamos National Laboratory, the University of Tokyo, and the University of Grenoble has identified important new features of cellulose structure. Their work provides important new details that could be used in designing more efficient treatments for cellulosic biomass.

MORE > Cellulose is a complicated macromolecule and only a few living things, including the microbes inhabiting the stomachs of cows and other ruminates, have figured out how to metabolize it. Yet biochemists and biophysicists have made significant progress in learning how cellulose is put together and how to break it apart. Among the most promising research in this area is the work done with compounds called amines, which are used in the processing of cellulose and cellulosic biomass. The amines swell the cellulose fibers and make them more susceptible to the cellulase enzymes used in converting biomass to biofuels. The researchers had already studied how amines affect the naturally occurring crystal forms of cellulose, called cellulose I. During the course of their studies, the team found that the amines turned the cellulose into intermediate crystalline amine-cellulose I complexes and then, when the amines were removed, into a form called cellulose III that happens to be in an activated state for hydrolysis by cellulases. This latter finding is good news if the goal is to make cellulose easier to turn into biofuels. The researchers were also able to find conditions under which they could turn the cellulose III back into cellulose I, important information for those who want to clearly understand the process and how to control it.

To add further intrigue to the story, cellulose I can also be irreversibly converted to a form called cellulose II, which has improved properties for use in textiles. It turns out that, like cellulose I, cellulose II can also be converted into cellulose III by treatment with amines. As the plot thickened, the research group focused more on visualizing the structure and ways of producing cellulose III, the form that would be most advantageous for biofuels production.

The investigators had previously reported the first high-resolution x-ray data for a crystalline form of cellulose III (III_{II}) that they produced by treating cellulose II with ammonia. The team now extended the emerging picture by using crystallography and spectroscopy to determine a new crystal structure for cellulose III_{II}. Their data reveal diffuse patterns in cellulose III that indicate a relatively high level of disorder when compared to naturally occurring cellulose chains (Fig. 1). Not only does the cellulose III show more disorder, it also is present in three different types of molecular conformation. The data also led the researchers to propose a new crystal structure for cellulose, a structure that would be consistent with an aggregated microdomain structure for cellulose III_{II}. Further work will help determine if modifying the amine treatment of cellulose II will result in a more ordered cellulose III, or whether statistical disorder is an inherent property of cellulose III.

— Mona Mort

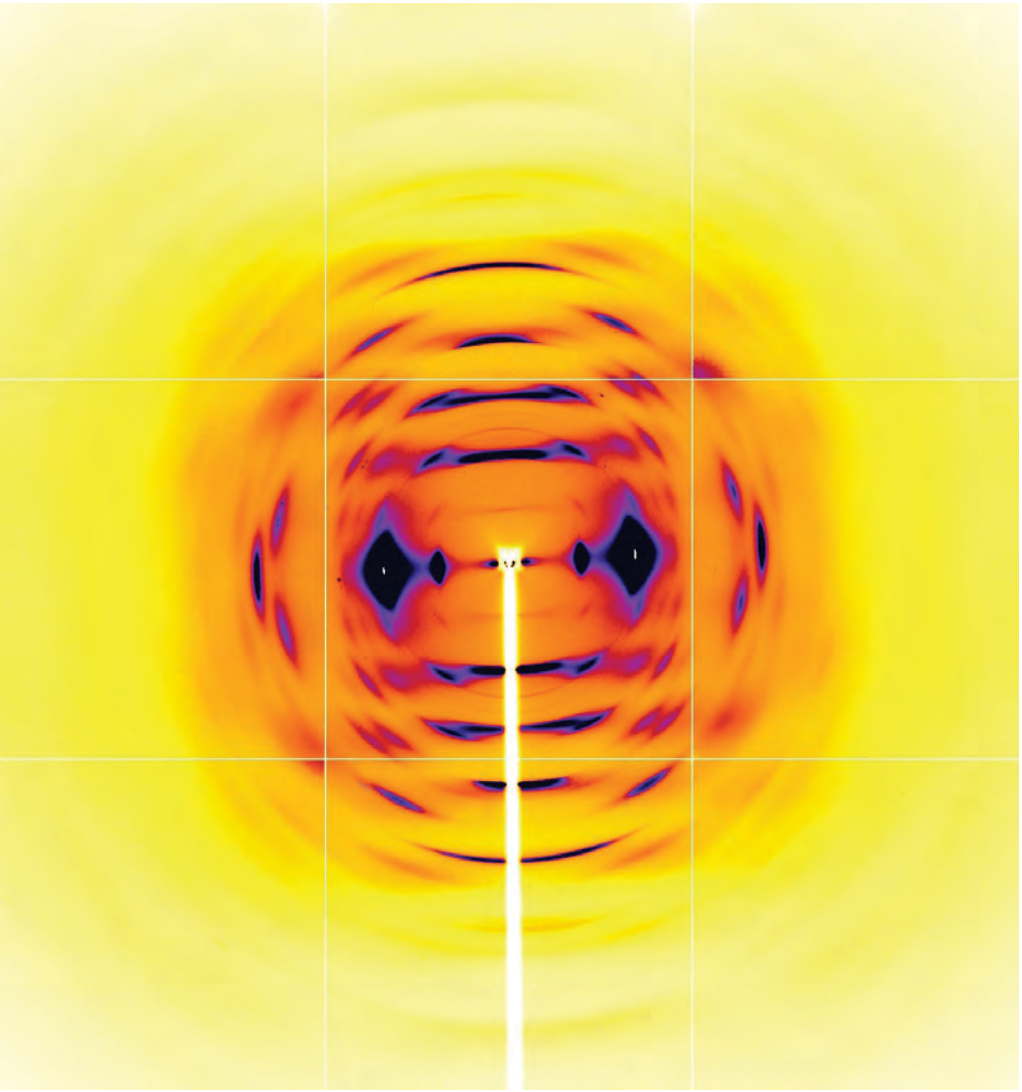

^ *Fig. 1 Color palette figure showing x-ray data collected at the NE-CAT beamline from fiber samples of cellulose that have been converted into cellulose III_{II}.*

See > Masahisa Wada[1], Laurent Heux[2], Yoshiharu Nishiyama[2], and Paul Langan[3]*, "X-ray Crystallographic, Scanning Microprobe X-ray Diffraction, and Cross-Polarized/Magic Angle Spinning 13C NMR Studies of the Structure of Cellulose III_{II}" Biomacromolecules **10**(2), 302 (2009). DOI: 10.1021/bm8010227

Author affiliations >
[1]The University of Tokyo, [2]CNRS, [3]Los Alamos National Laboratory

Correspondence >
*langan_paul@lanl.gov

> M.W. was supported by a Grant-in-Aid for Scientific Research (18780131). This study was partly funded by the French Agence Nationale de la Recherche. P.L. was supported in part by the Office of Biological and Environmental Research of the Department of Energy, a grant from the National Institute of Medical Sciences of the National Institutes of Health (1R01GM071939-01), and a Laboratory Directed Research and Development grant from Los Alamos National Laboratory (20080001DR).

Use of the Advanced Photon Source is supported by the U.S. Department of Energy, Office of Science, Office of Basic Energy Sciences, under Contract No. DE-AC02-06CH11357.

> 18-ID • Bio-CAT • Life science • Fiber diffraction, microdiffraction, microfluorescence (hard x-ray), micro x-ray absorption fine structure, small-angle x-ray scattering, time-resolved x-ray scattering • 3.3-cm Undulator A • Accepting general users

> 24-ID-E • NE-CAT • Life science • Macromolecular crystallography, microdiffraction, microbeam, single-crystal diffraction, single-wavelength anomalous dispersion • 3.3-cm Undulator A • Accepting general users

Visualizing an ATP-Gated Ion Channel

IN SHORT > It is almost always referred to as ATP, not by its complete name of adenosine triphosphate, and usually in the context of carrying cellular energy. But ATP has of late been popping up in other, seemingly unrelated contexts. One such case is that of extracellular signalling for sensory and vascular functions, where an ATP-gated receptor known as P2X has been identified. Though dysfunctional P2X receptors have been implicated in cancer and inflammatory, cardiovascular, and neuronal diseases, high-resolution structural data have not been available until now. With the help of the NE-CAT beamline 24-ID-E at the APS, and Advanced Light Source beamlines 5.0.2, 8.2.1, and 8.2.2 at Lawrence Berkeley National Laboratory, researchers have produced, in exquisite detail, crystal structures for an ATP-gated P2X ion channel in a closed, resting state. Their work shows how ATP could help in opening a closed channel and provides important new details about how a system malfunction could lead to disease.

MORE > The research team from the Vollum Institute and the Oregon Health and Science University started out in somewhat unknown territory: P2X receptors are not related to other ion channel proteins of known structure, so it was not possible to predict either structural details or possible mechanisms for opening and closing of the ion channel. Their studies focused on obtaining crystal structures for the zebrafish $P2X_4$ receptor in its closed, resting state. What they revealed is an architecturally beautiful structure that is shaped like a chalice and has three subunits. The ways in which the subunits are knit together is critical to proper functioning of the channel gates and receptor assembly. Extracellular regions of the receptor, with their multiple β-strands, provide acidic regions that are important to attracting the right ions to the gate. In the pore that crosses the cell membrane, a gate-like area is formed with a protein slab. And the fine level of detail at which the team was able to visualize the structure allowed them to identify three unusual ATP-binding sites between the receptor's subunits. The location of the ATP binding sites suggests that ATP is important in mediating the rearrangement necessary for opening the closed gate.

> Fig. 1 Architecture of the P2X receptors showing subunit folds and dolphin-like shape, grey bars indicate inner (in) and outer (out) leaflets of the membrane bilayer.

Further structural details showed an hourglass shape for the transmembrane region, which is made of six helices, two from each of the receptors subunits. Looking at how the subunits themselves are constructed, the research team found a dolphin-like shape, where the transmembrane helices would be the flukes and the extracellular region analogous to the upper body (Fig. 1). Attached to the body are the head region and three additional domains: the dorsal fin, left flipper, and right flipper. Extending the dolphin analogy, the team identified three major subunit interfaces: body-to-body, head-to-body, and left flipper-to-dorsal fin. These data led the researchers to postulate that the subunit interactions, especially head-to-body and left flipper-to-dorsal fin, are important in receptor function. Support for this hypothesis comes from experiments on another receptor ($P2X_3$), where a single mutation in the left flipper slowed the receptor desensitization rate.

Perhaps the most surprising aspect of the team's results lies in predicting an unusual binding mode and function for ATP. By binding where proposed—at three sites that would be look like an open jaw of the dolphin—ATP would play an important role in changing the molecular shape of the receptor and allowing the ion channel to change state. If the proposed model is correct, the ATP molecule would

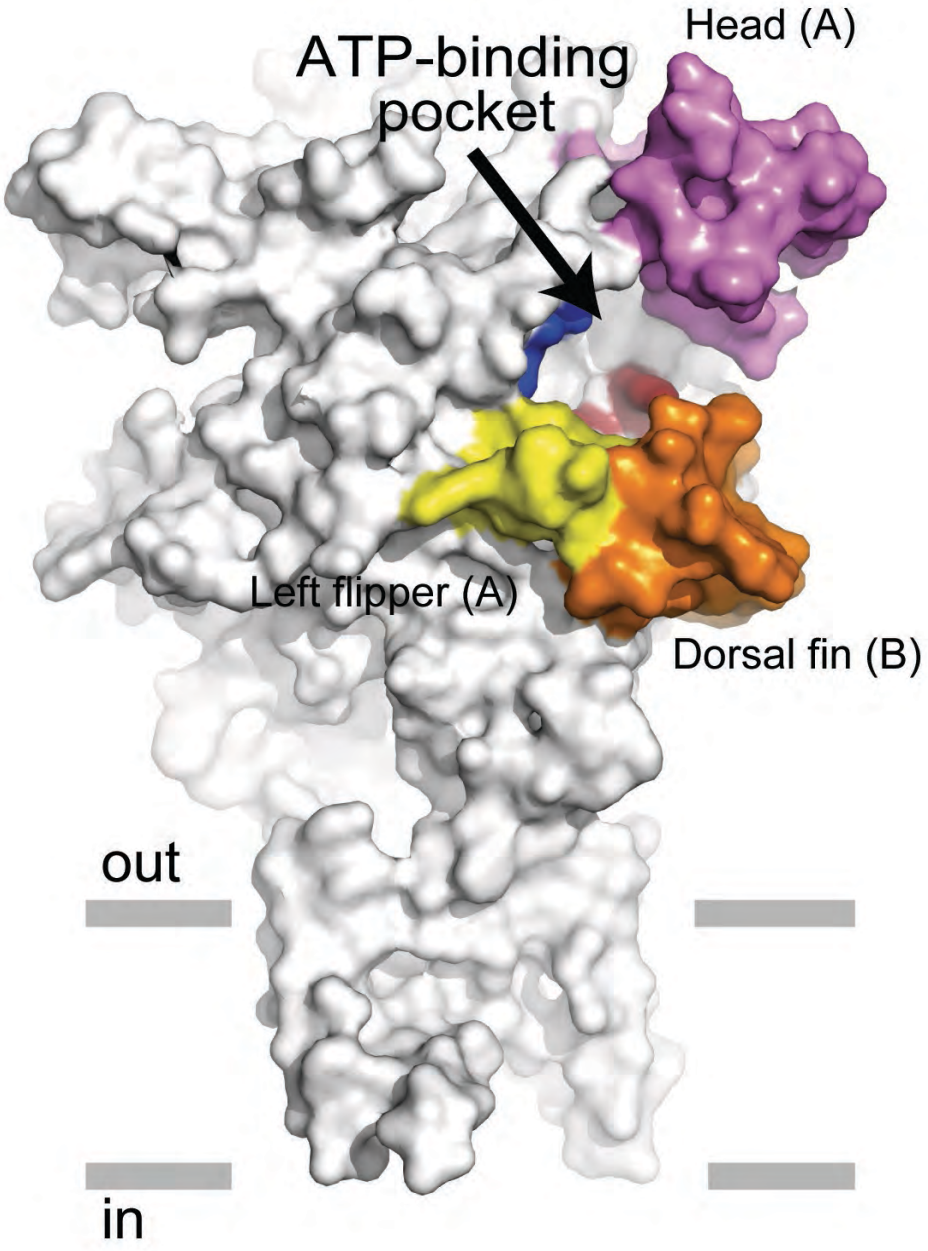

See > Toshimitsu Kawate[1,2], Jennifer Carlisle Michel[1,2], William T. Birdsong[1,2], and Eric Gouaux[1,2,3]*, "Crystal structure of the ATP-gated P2X4 ion channel in the closed state," Nature **460**, 592 (30 July 2009). DOI:10.1038/nature08198

Author affiliations >
[1]Vollum Institute, [2]Oregon Health and Science University, [3]Howard Hughes Medical Institute

Correspondence >
*gouauxe@ohsu.edu

See also > "Structural biology: Trimeric ion-channel design," by Shai D. Silberberg and Kenton J. Swartz, *Nature* News and Views, Nature **460**, 580 (30 July 2009). DOI:10.1038/460580a;

> This work was supported by the National Institutes of Health (NIH) and the American Asthma Foundation. E.G. is an investigator with the Howard Hughes Medical Institute. Use of the Advanced Photon Source at Argonne National Laboratory was supported by the U.S. Department of Energy, Office of Science, Office of Basic Energy Sciences, under Contract No. DE-AC02-06CH11357.

cause the head, right flipper, and dorsal fin to close the jaws, and by doing so, start the cascade of changes leading to the opening of the gate.

Along with a previously unknown structure for a P2X ion channel, the research team has provided intriguing details and a proposed model for how ATP, in an unusual role, can mediate opening the channel. Their work provides important foundations for continued studied, especially when considering the role of dysfunctional P2X receptors in disease.

— Mona Mort

> 24-ID-E • NE-CAT • Life science • Macromolecular crystallography, microdiffraction, microbeam, single-crystal diffraction, single-wavelength anomalous dispersion • 3.3-cm Undulator A • Accepting general users

Secrets of the Lacewing's Silk

IN SHORT > Green lacewings (*Chrysopidae*) are beneficial insects well known to naturalists and scientists for their many elegant solutions to life's problems, such as how to eat without being eaten. The larvae of many species adopt a wolf-in-sheep's-clothing strategy when feeding upon their major prey item, aphids. They cover themselves with either the tufted wax exudate or the spent carcasses of their prey in order to escape detection by honeydew-feeding ants, which normally attack intruders in their aphid herds. The adult female protects her eggs from detection and predation (especially by ants) by suspending each egg at the end of a fine strand of silk (top figure, next page). Utilizing the high-flux ChemMatCARS 15-ID beamline at the APS, researchers from Australia's Commonwealth Scientific and Industrial Research Organisation (CSIRO) recently completed studies that confirm the elegant and unique structure of the lacewing's silken egg stalk. The information they obtained suggests that lacewing silk may have potential value as a biomaterial.

MORE > Lacewing egg stalk silk is based on completely different design principles to the well-known silks of domesticated silkworms or spider webs. The lacewing silk evolved to function as a rigid support column, rather than a long flexible thread. Its protein sequence and structure are unique.

The scientists studied *Mallada signata*, a species of green lacewing native to Australia. A half-century earlier, classic protein structural studies had reported on the unusual cross-beta sheet structure of the silk of another green lacewing species, *Chrysopa flava*. The CSIRO researchers were able to apply the technological advances of recent decades to identifying the genes that encode the silk proteins and developing a more detailed model of the structure.

The researchers used wide-angle x-ray scattering at the ChemMatCARS facility to obtain detailed information about the protein structure of a single silk fiber. Since the tiny egg stalks are only 3-mm long and 15 μm in diameter, they couldn't have obtained clear data anywhere except at a high-flux third-generation synchrotron source.

Functional proteins with a cross-beta structure are rare in nature and appear to be limited to extruded products such as arthropod silks. Within a cellular environment, cross-beta structures occur as errors in protein folding. These misfolded proteins can aggregate to form the amyloid plaques that characterize neurodegenerative diseases such as Alzheimer's and Parkinson's. Accordingly, cross-beta structures are of great interest to researchers in diverse fields.

The CSIRO researchers identified and sequenced two silk genes, which they named *MalXB1* and *MalXB2*. These genes are expressed in adult female *M. signata* only, not in males or larvae, confirming that the silk of lacewing cocoons is composed of different proteins. Over 70% of each protein is composed of repeating 16-residue motifs, suggesting a high level of crystallinity. Based on their data, the CSIRO researchers propose that the cross-beta structure is made up of 8-residue crystallite strands stacked perpendicular to the direction of the fiber. As the lacewing female draws the liquid silk into a strand, a network of cysteine cross links are created that result in rapid hardening of the stalk.

The cross-beta structure accounts for the remarkable extensibility of the egg stalk silk, which can be stretched to nearly 500% of its length before breaking. Its bending rigidity, achieved by cysteine cross linking, is almost three times greater than that of silkworm fibers. These properties, along with reasonable tensile strength and the relative simplicity of its production, suggest lacewing silk may have potential value as a biomaterial.

— Carol Hart

See > Sarah Weisman[1], Shoko Okada[1], Stephen T. Mudie[2], Mickey G. Huson[2], Holly E. Trueman[1], Alagacone Sriskantha[1], Victoria S. Haritos[1], and Tara D. Sutherland[1]*, "Fifty Years Later: The Sequence, Structure and Function of Lacewing Cross-Beta Silk," J. Struct. Biol. **168**, 467 (2009). DOI: 10.1016/j.jsb.2009.07.002

Author affiliations >
[1]CSIRO Entomology, [2]CSIRO Material Science and Engineering

Correspondence >
*Tara.Sutherland@csiro.au

> This work was financially supported by the Grains Research and Development Corporation. Use of ChemMatCARS Sector 15 at the Advanced Photon Source was supported by the Australian Synchrotron Research Program, which is funded by the Commonwealth of Australia under the Major National Research Facilities Program. ChemMatCARS Sector 15 is principally supported by the National Science Foundation/Department of Energy under Grant No. CHE-0535644.

Use of the Advanced Photon Source is supported by the U.S. Department of Energy, Office of Science, Office of Basic Energy Sciences, under Contract No. DE-AC02-06CH11357.

^ *Fig. 1* ***Top:*** *In laying her eggs, the female green lacewing first secretes a drop of liquid silk onto a stem or leaf, then stretches the silk out into a fine strand as she lifts her abdomen from the substrate. A few seconds later, she deposits an egg on the tip of the stalk. Then she repositions herself to repeat the process for subsequent eggs. The eggs are effectively removed from the search paths of most likely predators. Moreover, the separation of the eggs reduces the risk of brood cannibalism, which can occur when eggs are deposited in clusters.* ***Bottom:*** *Lacewing* ***(Chrysopa perla)****. (Top image: the authors. Bottom image: Quartl, Wikimedia Commons, http://commons.wikimedia.org/wiki/File:Chrysopa_perla_Goldauge_seite.jpg)*

> 15-ID • ChemMatCARS • Chemistry, materials science • Anomalous and resonant scattering (hard x-ray), liquid scattering, microdiffraction, single-crystal diffraction, small-angle x-ray scattering, surface diffraction, wide-angle x-ray scattering • 3.3-cm Undulator A • Accepting general users

Visualizing the HIV Capsid

IN SHORT > In mature infective human immunodeficiency virus (HIV) particles, the capsid (CA) protein forms a shell that packages and organizes the virus replication complex. The capsid of HIV (and of retroviruses in general) is a self-assembling, highly variable lattice of hexagonal and pentagonal rings of CA protein. Previous work with electron cryomicroscopy had established the lattice architecture of the capsid to a resolution of about 9 Å. Using x-ray beamlines at two U.S. Department of Energy synchrotron light source facilities, researchers succeeded in visualizing the hexagonal units of the HIV capsid to the atomic level (2 Å). Their findings may advance work on capsid assembly inhibitors as a new class of antiretroviral agents to augment existing highly active antiretroviral therapy regimens for treating HIV.

MORE > The HIV capsid utilizes about 1,500 copies of CA protein to form a variably curved cone made up of six-sided rings (hexamers) with five-sided rings (pentamers) capping the two ends of the cone (Fig. 1). Each capsid has a variable number of hexameric units (approximately 250) and exactly 12 pentamers, 7 at the broad end, and 5 at the narrow end of the conical structure. The CA protein folds primarily into helices with two independent, flexibly linked domains: an N-terminal domain (NTD) and a C-terminal domain (CTD).

The flexible link between the two CA domains, coupled with the natural variability in the curvature of the capsids, made it challenging to grow stable crystals of a complete hexagonal array. Guided by a model of the hexameric CA lattice developed from their electron cryomicroscopy studies, the researchers in this study, from The Scripps Research Institute, the University of Utah School of Medicine, the Scripps Clinic, and University of Virginia Health System, engineered CA hexamers that were stable enough to grow crystals. X-ray crystallography at SER-CAT beamline 22-BM at the APS, and at the Stanford Synchrotron Radiation Lightsource beamline 7-1 revealed that the CA hexamer is composed of two concentric rings, with six NTDs forming a relatively rigid inner ring and with the CTDs arranged in a more mobile outer ring. The mobility of this outer ring permits the variable curvature needed for the capsid to assume its conical form.

The two CA domains maintain their independence in the assembled hexamer, interacting minimally within the individual protein but forming three distinct interfaces with the domains of adjacent proteins: the NTD-NTD interface that creates the symmetric hexameric rings, a CTD-CTD interface that links neighboring hexamers, and an intermolecular NTD-CTD interface that reinforces the hexamer.

The first three helices of CA make the symmetric 6-fold NTD-NTD interactions, which form a loose barrel at the center of the hexamer. Despite the presence of a small hydrophobic core, much of this interface is mediated by interactions with water molecules, with hydrogen bridge bonds between hydrophilic side chain and backbone atoms. Water interactions are also present in the NTD-CTD interface. Every helix in the NTD-CTD interface has a flexible side chain that extends to form a cap for a helix in the other domain. These caps may serve as pivot points for producing the varying degrees of surface curvature of the conical capsid. The water interactions at the NTD-NTD interface may facilitate alternate packing as pentamers rather than hexamers.

The atomic detail of their x-ray structures allowed the researchers to analyze the precise mechanisms and targets of two capsid assembly inhibitors currently in development, the small molecules CAP-1 and CA-I, both of which act at the NTD-CTD interface. Knowing the molecular structures of the hexameric interfaces will undoubtedly aid in the design of novel capsid assembly inhibitors, a new and potentially very valuable class of HIV therapeutics.

— Carol Hart

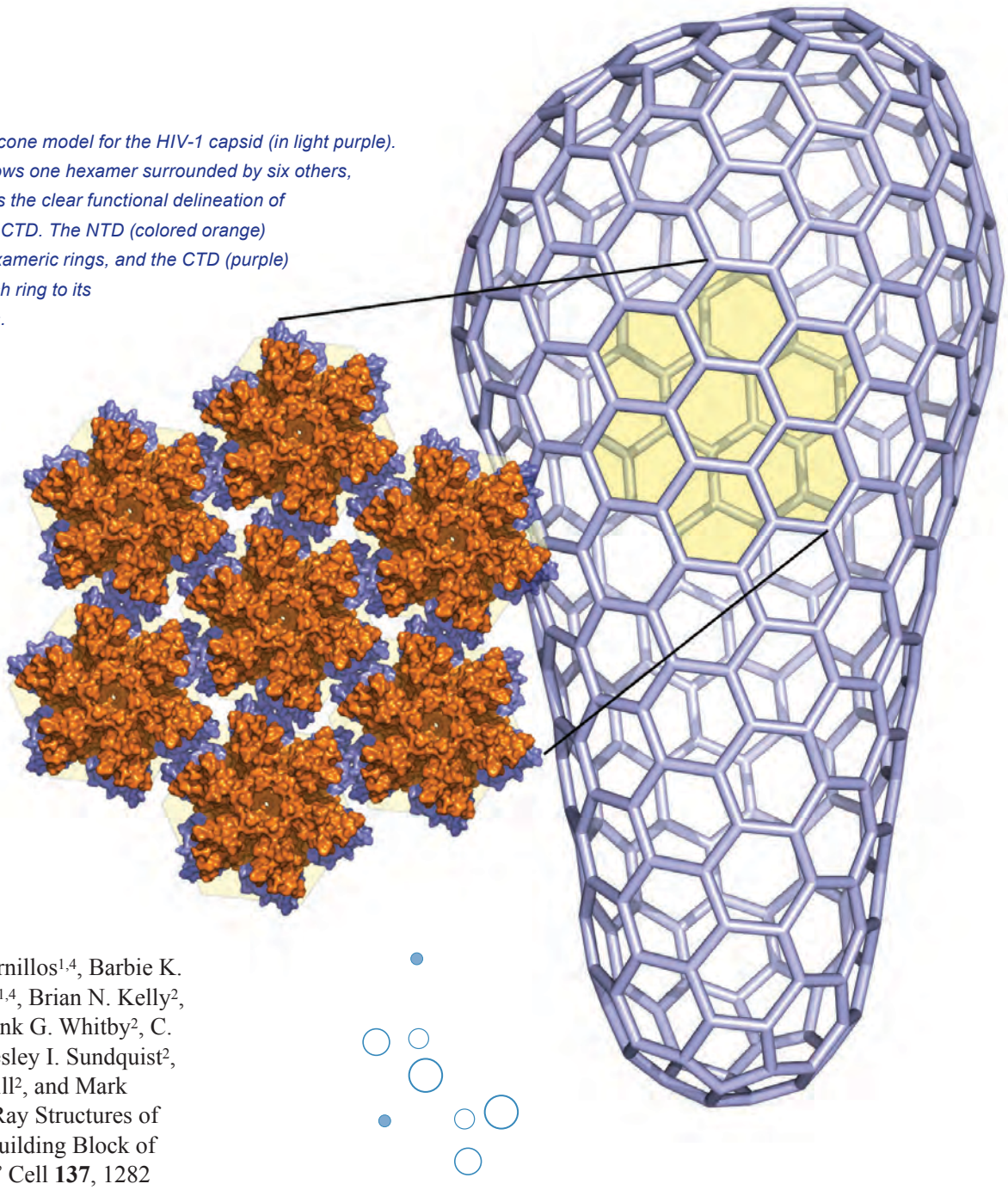

> Fig. 1 A fullerene cone model for the HIV-1 capsid (in light purple). The inset shows one hexamer surrounded by six others, and illustrates the clear functional delineation of the NTD and CTD. The NTD (colored orange) forms the hexameric rings, and the CTD (purple) connects each ring to its six neighbors.

See > Owen Pornillos[1,4], Barbie K. Ganser-Pornillos[1,4], Brian N. Kelly[2], Yuanzi Hua[1], Frank G. Whitby[2], C. David Stout[1], Wesley I. Sundquist[2], Christopher P. Hill[2], and Mark Yeager[1,3,4]*, "X-Ray Structures of the Hexameric Building Block of the HIV Capsid," Cell **137**, 1282 (June 26, 2009). DOI:10.1016/j.cell.2009.04.063

Author affiliations >
[1]The Scripps Research Institute, [2]University of Utah School of Medicine, [3]Scripps Clinic, [4]University of Virginia Health System

Correspondence >
*yeager@scripps.edu

> This study was funded by National Institute of Health grants R01-GM066087 (M.Y.) and P50-GM082545 (M.Y., C.P.H., and W.I.S.). B.G.-P. was supported by a postdoctoral fellowship from the George E. Hewitt Foundation for Medical Research. Use of the Advanced Photon Source at Argonne National Laboratory was supported by the U.S. Department of Energy, Office of Science, Office of Basic Energy Sciences, under Contract No. DE-AC02-06CH11357.

> 22-BM • SER-CAT • Life science • Macromolecular crystallography • Bending magnet • Accepting general users

A Potent Antibody against Influenza

IN SHORT > The initial shortage of vaccine against the 2009 pandemic H1N1 swine flu highlights the difficulty of forecasting and combating influenza outbreaks. In the last century, three influenza pandemics—the 1918 Spanish flu (H1N1), the 1957 Asian flu (H2N2), and the 1968 Hong Kong flu (H3N2)—were responsible for an estimated 50 to 100 million deaths worldwide. Because the influenza A virus readily mutates to escape immune system recognition, prevention has relied on inactivated or attenuated virus vaccines that must be reformulated annually based on surveillance to predict the seasonally prevalent subtypes. Now a team of researchers from the Scripps Research Institute and the Dutch biopharmaceutical company Crucell have discovered a neutralizing antibody with broad efficacy against multiple strains of influenza virus. Antibody-antigen crystals imaged at the GM/CA-CAT 23-ID-B beamline at the APS demonstrated that the antibody targets a highly conserved portion of the influenza A virus. This discovery will guide ongoing research to develop a long-lasting, cross-protective vaccine as well as new antibody-based therapies.

MORE > Influenza A virus evades immune system targeting by accumulating point mutations in its two integral membrane proteins, hemagglutinin (HA) and neuraminidase. There are at least 16 HA subtypes, designated H1 through H16. HA is responsible for host cell attachment and membrane fusion and is the primary target (antigen) of neutralizing antibodies. However, the variability of the protein means that new viral strains may not be recognized by antibodies to previous infections.

The CR6261 antibody was identified by using phage display technology to screen for antibodies capable of neutralizing recombinant H5 avian influenza virus. To determine the antibody's epitope (binding site) on HA, the researchers crystallized the fragment antigen–binding region (Fab) of the antibody in complex with HAs from the human 1918 H1N1 pandemic virus and from a highly pathogenic avian H5N1 virus. The crystals were imaged to 2.2-Å and 2.7-Å resolution, respectively.

Influenza HA has two subunits, HA1 and HA2, and is assembled as a trimer. The mature protein projects from the viral membrane in a spike-shaped structure, with the three helical HA2 subunits predominating in the stalk and the three globular HA1 subunits forming the spike head. The globular HA1 subunits are responsible for attaching to the host cell membrane. The fusion mechanism resides in the HA2 subunits, which each contain a large CD helix and a shorter A helix. Exposure to low pH following endocytosis triggers a conformational change in HA that results in fusion of the viral and cellular membranes.

Analysis of the crystals revealed three antibodies bound to each HA trimer. CR6261 binds primarily to the short A helix of the HA2 stalk, close to the viral membrane. Comparison of the two crystals confirmed that this site constitutes 70% of the epitope in both H1 and H5 HAs. Other binding contacts, including those to residues of the HA1 subunit, also play a role in virus neutralization.

Review of a large database of influenza HA sequences confirmed that the A helix is highly conserved in all influenza A viruses. The conservation of this epitope suggests it plays a critical role in membrane fusion. The researchers propose that epitope binding by CR6261 freezes HA in its prefusion conformation, thus preventing the pH-induced conformational changes in the endosomal compartments that allow the virus to infect the host cell.

Most neutralizing antibodies against influenza HA target the hypervariable regions of the HA1 globular domain that surround the receptor binding site. By targeting a crucial, conserved region associated with the HA2 fusion machinery, CR6261 is able to neutralize the viruses from about half of the 16 HA subtypes. Identification of the

v *Fig. 1 Structure of the broadly neutralizing antibody CR6261 bound to an H5 avian influenza hemagglutinin. A trimeric hemagglutinin spike is represented as a molecular surface, with one HA1 subunit highlighted in magenta and an HA2 subunit highlighted in cyan. As depicted, the surface of the virus would be located at the bottom edge of the hemagglutinin, while attachment to a target cell would occur at the top. Antibody CR6261 (ribbon representation, colored red and blue) recognizes a conserved epitope in the bottom half of the hemagglutinin molecule, near the viral membrane, preventing membrane fusion.*

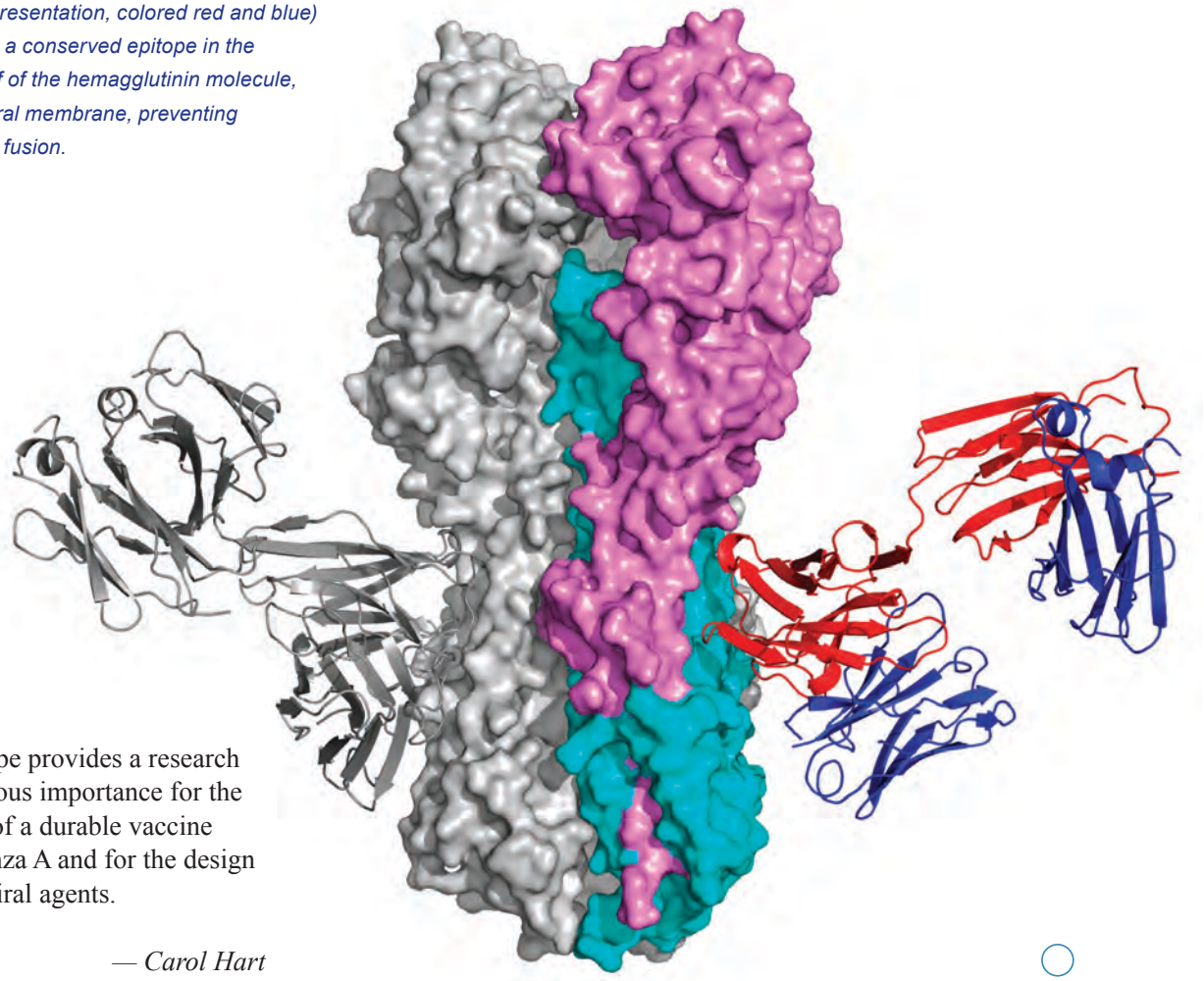

CR6261 epitope provides a research lead of enormous importance for the development of a durable vaccine against influenza A and for the design of better antiviral agents.

— *Carol Hart*

See > Damian C. Ekiert[1], Gira Bhabha[1], Marc-André Elsliger[1], Robert H.E. Friesen[2], Mandy Jongeneelen[2], Mark Throsby[2], Jaap Goudsmit[2], and Ian A. Wilson[1*], "Antibody Recognition of a Highly Conserved Influenza Virus Epitope," Science **324**, 246 (10 April 2009). DOI: 10.1126/science.1171491

Author affiliations >
[1]The Scripps Research Institute,
[2]Crucell Holland BV

Correspondence >
*wilson@scripps.edu

> This work was supported in part by National Institutes of Health grant AI-058113 (I.A.W.) and a predoctoral fellowship from the Achievement Rewards for College Scientists Foundation (D.C.E.) and the Skaggs Institute. The Joint Center for Structural Genomics (JCSG) is supported by NIH National Institute of General Medical Sciences (NIGMS) (U54GM074898). The GM/CA CAT 23-ID-B beamline is funded in whole or in part with federal funds from National Cancer Institute (Y1-CO-1020) and NIGMS (Y1-GM-1104). Use of the Advanced Photon Source at Argonne National Laboratory was supported by the U.S. Department of Energy, Office of Science, Office of Basic Energy Sciences, under Contract no. DE-AC02-06CH11357.

> 23-ID-B • GM/CA-CAT • Life science • Microbeam, macromolecular crystallography, microdiffraction, anomalous diffraction (MAD/SAD), subatomic (<0.85 Å) resolution • 3.3-cm Undulator A • Accepting general users

How Get3 Moves Tail-Anchored Proteins to Their Destination

IN SHORT > Within every cell, newly synthesized proteins must be sorted and directed to the correct cellular destination. Most membrane and secretory proteins are targeted to the endoplasmic reticulum (ER) early in the translation process by a cytosolic signal recognition particle (SRP) that binds to an identifying sequence near the N terminal of the protein as it emerges from the ribosome. But some membrane proteins cannot be directed to the ER by SRP because their recognition site is at the C terminal tail and does not emerge from the ribosome until translation is complete. These proteins are characterized by a single transmembrane domain (TMD) near the C terminal that anchors them in the membrane, with the functional N terminal end positioned in the cytosol, and are thereby known as tail-anchored (TA) membrane proteins. Important members of the TA protein class include the SNARE proteins, which traffic vesicles within the cell, and the Bcl-2 family of apoptosis regulators. The mechanism for targeting TA proteins is not as well understood as the SRP pathway, but it is known to be powered by hydrolysis of the nucleotide adenosine triphosphate (ATP). Recent studies identified TRC40/Get3, a highly conserved ATPase, as a central player in transporting TA proteins from the cytosol to the ER. Using the LS-CAT beamline 21-ID-G and GM/CA-CAT beamline 23-ID-D at the APS, a team of researchers have investigated crystal structures of this ATPase and proposed a coherent account of its function in TA protein recognition and transport.

MORE > Working with Get3, the yeast homologue of mammalian TRC40, the researchers, from The University of Chicago, the National Institutes of Health, the University of Wroclaw, and Jagiellonian University crystallized the protein in two configurations: open (nucleotide free) and closed (ADP x AlF_4- bound), with the latter simulating the ATP-bound state (Fig. 1). In both states, Get3 forms a symmetric homodimer in which the monomers consist of a core ATPase subdomain and an α-helical subdomain. But there are striking differences between the two configurations. In the closed state, Get3 displays an enormous hydrophobic groove (~30 × 15 × 15 Å), while in the open, unbound state, the groove's hydrophobic surfaces are buried. A single zinc ion within the interface acts as a hinge to stabilize the two conformations.

TA protein recognition is TMD dependent: all the targeting information is contained within the hydrophobic tail of these proteins. To enable efficient binding, the recognition site would need to be hydrophobic as well (i.e., non-polar or neutral). Both the crystallographic analysis and functional studies of site-directed mutants indicate that the hydrophobic groove that is exposed in the ATP-bound state of Get3 forms the TMD binding site. The non-polar character of the groove is retained in TRC40/Get3 homologues, as are two other key structures in the Get3 homodimer: 1) a 20-residue insertion in the α-helical subdomains that may function as a dynamic lid for shielding the binding site, and 2) a switching mechanism within the ATP binding site. This switch is thought to relay structural changes induced by ATP binding and its subsequent hydrolysis to the dimer interface and the TA binding site.

In the model developed by the researchers, ATP binding drivesGet3 toward the closed conformation, facilitating recognition of newly synthesized TA membrane proteins within the hydrophobic groove. The Get3-TA protein complex is then targeted to the ER by an interaction with other members of the Get

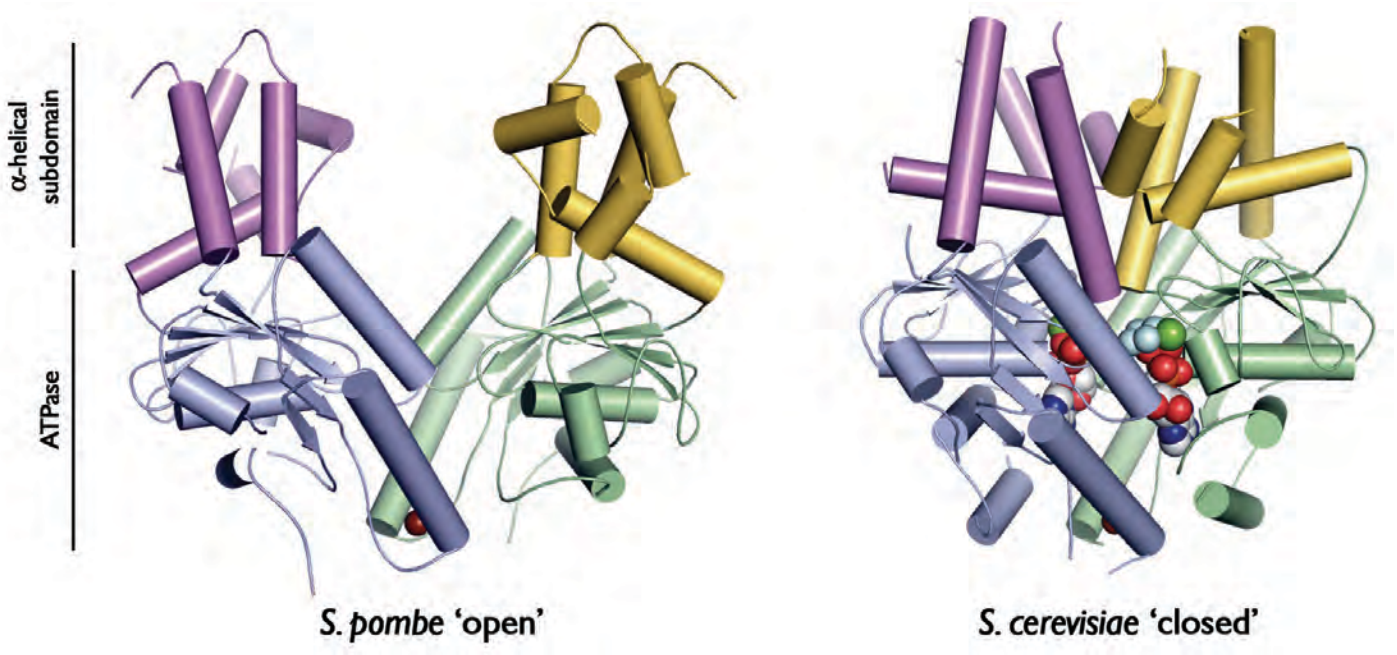

^ *Fig. 1 Structure of yeast Get3 in "open" **(left)** and "closed" (**right**; bound to ADP-AlF4-) dimer conformations. Each monomer comprises a core ATPase subdomain (blue, green) and an α-helical subdomain (magenta, yellow). Juxtaposition of the α-helical subdomains in the closed conformation **(right)** creates a large hydrophobic groove suitable for binding to a tail-anchored membrane protein substrate.*

family, the membrane-bound Get1/2. After ATP hydrolysis, conformational changes in the conserved switching mechanism destabilize the groove, releasing the TA protein for membrane insertion. Disruption of the closed dimer also releases Get3 from the membrane and switches it to the open configuration, whereupon it returns to the cytosol, ready for another round of TA protein targeting.

— Carol Hart

See > Agnieszka Mateja[1], Anna Szlachcic[1,3], Maureen E. Downing[1], Malgorzata Dobosz[1,4], Malaiyalam Mariappan[2], Ramanujan S. Hegde[2], and Robert J. Keenan[1]*, "The structural basis of tail-anchored membrane protein recognition by Get3," Nature **461**, 361 (17 September 2009). DOI:10.1038/nature08319

Author affiliations >
[1]The University of Chicago,
[2]National Institutes of Health,
[3]University of Wroclaw,
[4]Jagiellonian University

Correspondence >
*bkeenan@uchicago.edu

> This work was supported by a grant from the Edward Mallinckrodt, Jr. Foundation (to R.J.K.) and by the Intramural Research Program of the National Institutes of Health (to R.S.H.). Use of the Advanced Photon Source at Argonne National Laboratory was supported by the U.S. Department of Energy, Office of Science, Office of Basic Energy Sciences, under Contract No. DE-AC02-06CH11357.

> 21-ID-G • LS-CAT • Life science • Macromolecular crystallography, anomalous diffraction (MAD/SAD) • U33S undulator • Accepting general users

> 23-ID-D • GM/CA-CAT • Life science • Macromolecular crystallography, microbeam, microdiffraction, anomalous diffraction (MAD/SAD), subatomic (<0.85 Å) resolution • 3.0-cm undulator • Accepting general users

Closing in on a Common Cancer Mutation

IN SHORT > Phosphoinositide 3-kinases (PI3Ks) are a family of signal transduction enzymes that participate in regulating cellular proliferation and survival in all tissue types. Mutational activation of PI3Ks is implicated in many cancers, including those of the breast, colon, uterus, stomach, and ovary. The oncogene *PIK3CA*, which encodes the p110α subunit of PI3Kα, is one of the two most commonly mutated genes in human tumors. Using data collected at the LRL-CAT 31-ID beamline at the APS, researchers from The Johns Hopkins University have uncovered the atomic structure and probable mechanism of the most common oncogenic mutant of *PIK3CA*. Their research offers direction to ongoing research efforts to design targeted PI3K inhibitors for the treatment of cancer.

MORE > PI3Ks produce lipid secondary messengers that serve as membrane docking sites for effector proteins. They are heterodimers consisting of a p110 catalytic subunit bound to a p85 regulatory subunit. The mutation in p110α that was studied has an amino acid substitution in the kinase domain (an arginine for a histidine at residue 1047) that results in a twofold increase in lipid kinase activity. Of over 1,500 known cancer-related mutations in *PIK3CA*, the His1047Arg mutation is the most common.

The regulatory p85 subunit includes several modular domains that interact with other signaling proteins, including two SH2 domains, which typically bind phosphopeptides. The region between these two SH2 domains, called the inter-SH2 domain, interacts with the catalytic p110 subunit. The researchers compared the crystal structures of wild-type and mutant p110α in complex with the two interacting domains of p85α (the inter-SH2 and the N-terminal SH2), both free and bound to wortmannin, a nonspecific PI3K inhibitor.

Wortmannin binds the p110α kinase domain at the ATP binding site in a pocket that is largely conserved between p110α and another well-studied isoform, p110γ. Upon binding to wortmannin, the mutant p110α underwent a conformational shift in a kinase domain loop. This conformational shift has not been reported in studies of wortmannin binding to p110γ. Although wortmannin itself is both unstable and toxic, derivatives are currently being investigated as potential cancer therapeutics. The discovery of these distinct conformational changes may offer new leads for the development of more tolerable inhibitors that are specific to a PI3Kα isoform.

In the crystal structure of the p85α-p110α, the N-terminal SH2 domain of p85α serves as a broad scaffold for the enzyme complex, interacting with four distinct domains: the inter-SH2 domain of p85α, as well as three of p110α's five domains: the C2, helical, and kinase domains (Fig. 1). The N-terminal SH2 domain is thus well positioned to transmit signals from bound phosphopeptides to other domains within the complex. Analysis of the structure confirms the suspected oncogenic mechanism of two other hotspot *PIK3CA* mutations that occur in the helical domain; by interfering with N-terminal SH2 binding to p110α, these mutations release the catalytic subunit from regulatory inhibition by p85α.

Oncogenic mutations in other kinases typically increase activity by locking the kinase activation loop into an active conformation or by destabilizing the inactive conformation. However, the mutant Arg1047 is positioned further from the activation loop than the His1047 of the wild-type enzyme. Instead, Arg1047 points toward the cell membrane and causes two other loops to change their conformation, bringing them into contact with the membrane. The researchers therefore propose that the His1047Arg

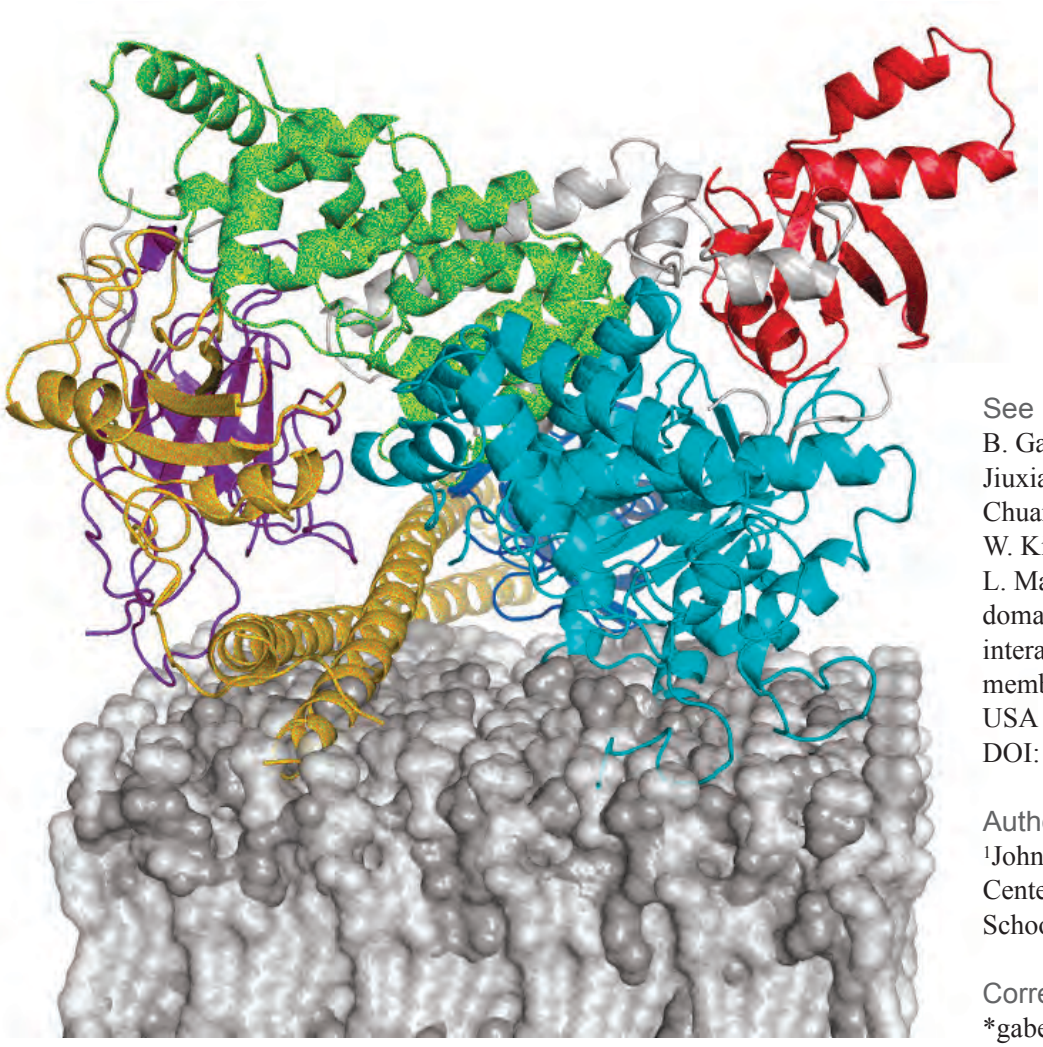

^ *Fig. 1 Effects of the oncogenic His1047Arg mutation on the structure of the PI3Kα. Ribbon diagram of the inter-SH2 domain (gold, coiled coil) and the N-terminal SH2 domain (gold, α plus β-fold) of the regulatory p85α subunit in complex with the five domains of p110α: the adaptor-binding domain (blue), the Ras-binding domain (red), the C2 domain (purple), the helical domain (green) and the catalytic kinase domain (cyan). The two loops of the kinase domain (residues 864-874 and 1050-1062) that change conformation in the mutant enzyme and contact the cell membrane are at the forefront.*

mutation changes the interaction with the cell membrane in such a way as to increase substrate access to the kinase binding site, thereby increasing the signaling along oncogenic pathways. This is a novel mechanism for mutational activation of a kinase that may well offer further direction for the development of targeted therapeutics.

— Carol Hart

See > Diana Mandelker[1], Sandra B. Gabelli[2]*, Oleg Schmidt-Kittler[1], Jiuxiang Zhu[1], Ian Cheong[1], Chuan-Hsiang Huang[2], Kenneth W. Kinzler[1], Bert Vogelstein[1], and L. Mario Amzel[2], "A frequent kinase domain mutation that changes the interaction between PI3Kα and the membrane," Proc. Nat. Acad. Sci. USA **106**, 16996 (October 6, 2009). DOI:10.1073_pnas.0908444106

Author affiliations >
[1]Johns Hopkins Kimmel Cancer Center, [2]Johns Hopkins University School of Medicine

Correspondence >
*gabelli@jhmi.edu

> Use of the LRL-CAT beamline was provided by Eli Lilly & Company, which operates the facility. Support for this research was provided by the Virginia and D.K. Ludwig Fund for Cancer Research and National Institutes of Health Grants CA43460, GM07309, and GM07184. Use of the Advanced Photon Source was supported by the U.S. Department of Energy, Office of Science, Office of Basic Energy Sciences, under Contract No. DE-AC02-06CH11357.

> 31-ID • LRL-CAT • Life science • Macromolecular crystallography, single-crystal diffraction, fiber diffraction, single-wavelength anomalous dispersion • 3.3-cm Undulator A • Accepting general users

Toxin-Spewing Bacteria Take a Page from Viruses

IN SHORT > New research performed at the APS confirms a suspected link between a virus that infects bacteria and a system many bacteria use to inject toxins into their host. Researchers solved the three-dimensional structure of a key protein in the type VI secretion system (T6SS) found in bacteria that cause cholera and other diseases. The finding confirms the suspicion that the protein shares the same needle-like structure as the tip complex of the virus T4, which uses the tip to puncture bacteria and infect them with its DNA.

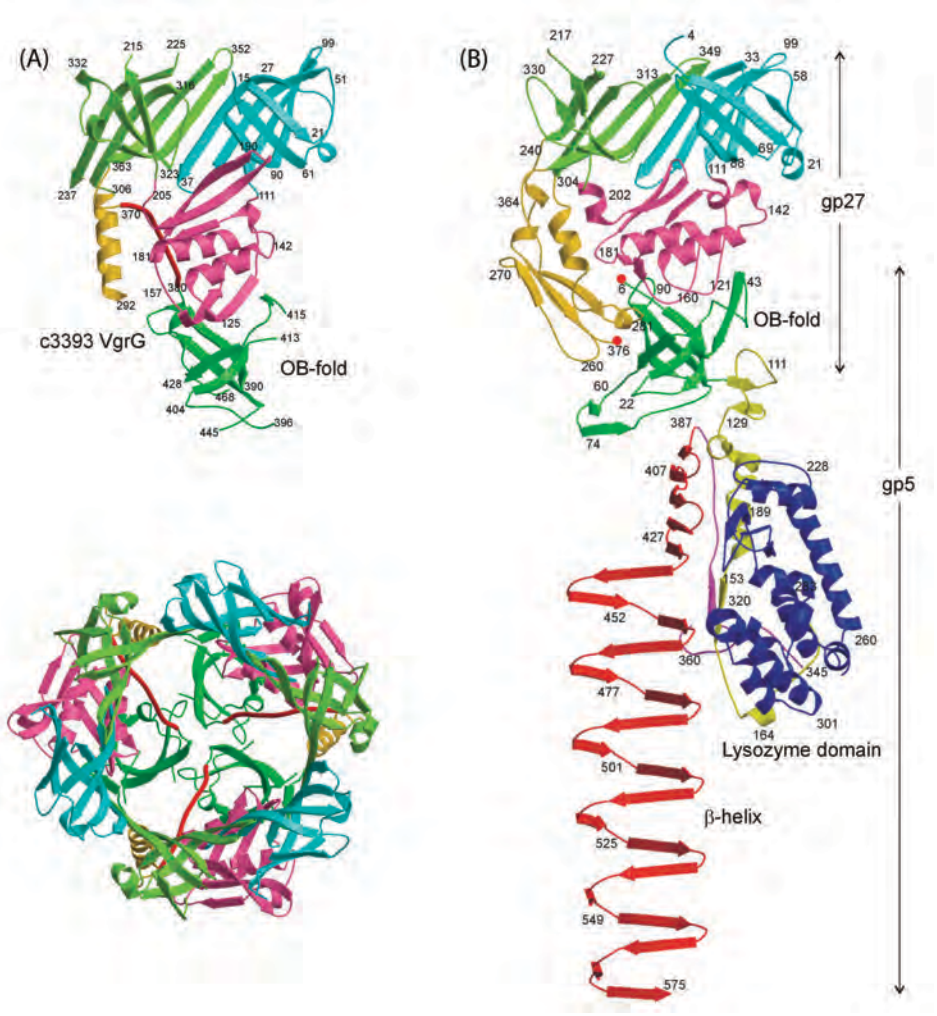

^ *Fig. 1 Schematic structure of the **E. coli** VgrG-1 protein **(left)**, part of a system for injecting toxin into host cells, next to the needle complex **(right)** of T4 bacteriophage, a virus that infects bacteria. The close match implies a common function: puncturing host cells.*

MORE > Many infectious bacteria cause disease by secreting toxic proteins into or around the cells of their host. Before 2006, biologists knew of five bacterial systems for secreting proteins. That year, researchers working in the lab of John Mekalanos, a microbiologist and molecular geneticist at Harvard Medical School, discovered a sixth mechanism—the type six secretion system (T6SS)—in a strain of Vibrio cholerae. The team identified 15 to 20 protein-coding genes responsible for the T6SS and found corresponding genes in a full one-quarter of a group of pathogenic bacteria that includes *Salmonella*, *E. coli*, and *Pseudomonas aeruginosa*, which infects people with cystic fibrosis.

An analysis of the amino acid sequence of one of those proteins, VgrG-1, immediately suggested a mechanism by which T6SS might inject toxin into host cells. The sequence was similar to that of a protein complex found in bacteriophage T4, a virus that infects *E. coli*. At the base of T4's cylindrical body is a spike made of two proteins, gp5 and gp27, which the virus uses to

pierce the outer membrane of a host cell and inject its DNA through an opening in the needle tip. Similarly, a bacterium wielding the T6SS might extend a spike into a host cell and inject toxin inside.

To find out if the protein structures matched, the researchers from Purdue University, the Harvard Medical School, the Albert Einstein College of Medicine, the University of Alberta, and SGX Pharmaceuticals, Inc., isolated VgrG-1 from an *E. coli* strain that infects the urinary tract. Then they crystallized it and measured its x-ray diffraction pattern using the LRL-CAT facility at APS sector 31-ID. As predicted, the structure of VgrG-1 is nearly identical to that of the T4 gp5-gp27 complex (Fig. 1).

In previous work, the group solved the structure of a second T6SS protein called Hcp, isolated from *P. aeruginosa*. The protein formed a donut shape containing a hole big enough around for a stretched-out protein to pass through. In the new study, the researchers took a second look at the structure and found that it corresponds to a part of T4 that attaches to the needle-tip (Fig. 2), suggesting that Hcp binds to VgrG-1.

The researchers found that when Hcp proteins are concentrated in solution, they appear to stack together into elongated tubes. They propose that the T6SS pumps Hcp and VgrG proteins into the space between a bacterium's two outer envelopes, where Hcp proteins stack together into a tube with a VgrG needle at the tip. This sharp tube would project through the outer membrane of the bacterium and into the host, perhaps driven by the force of Hcp donuts assembling together. The needle tip might be toxic itself, or the tube might serve as a conduit for other toxins.

The T6SS is not the first bacterial secretion system to have seemingly been plucked from another organism. *Yersinia pestis*, the bacterium that causes bubonic plague, injects toxin into host cells using protein machinery derived from the flagellum, the whip-like structure some bacteria use to propel themselves. The existence of the T6SS suggests that bacteria might have picked up tricks from viruses, too.

— JR Minkel

See > Petr G. Leiman[1,§], Marek Basler[2], Udupi A. Ramagopa[3], Jeffrey B. Bonanno[3], J. Michael Sauder[4], Stefan Pukatzki[5], Stephen K. Burley[4], Steven C. Almo[3], and John J. Mekalanos[2,*], "Type VI secretion apparatus and phagetail-associated protein complexes share a common evolutionary origin," Proc. Nat. Acad. Sci. USA **106**(11), 4154 (March 17, 2009). DOI:10.1073/pnas.0813360106

Author affiliations >
[1]Purdue University; [2]Harvard Medical School; [3]Albert Einstein College of Medicine; [4]SGX Pharmaceuticals, Inc.; [5]University of Alberta
§Present address: École Polytechnique Fédérale de Lausanne

Correspondence >
*john_mekalanos@hms.harvard.edu

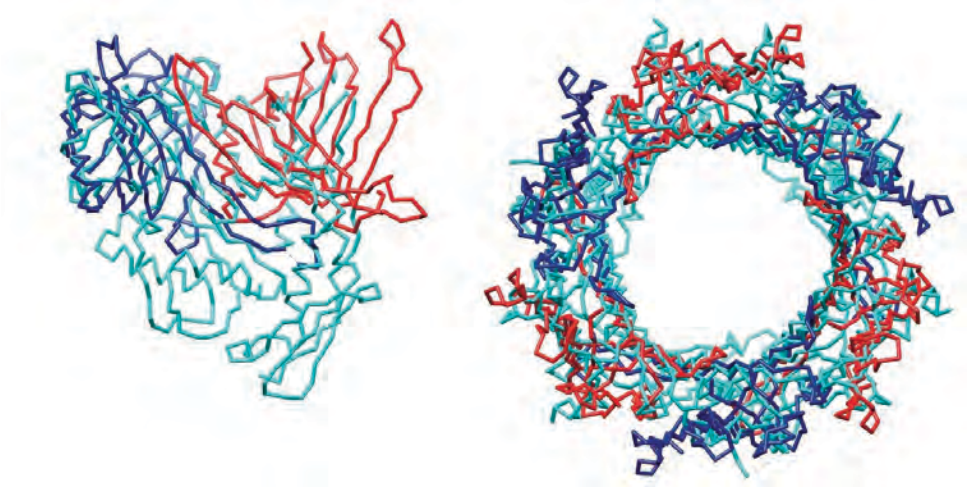

^ *Fig. 2 Structure of the toxin secretion protein Hcp1 (red and blue) superimposed on the gp27 protein (light blue) of T4 virus. Hcp1 corresponds to the so-called tube-like domain of gp27, which is structurally similar to a second T4 protein that composes the virus's tube, suggesting that Hcp1 has the potential to form tubes.*

> Work in J.J.M.'s laboratory on Type VI secretion has been supported by Grant AI-18045 and AI-26289 from the National Institutes of Allergy and Infectious Disease. P.G.L.'s work in Michael Rossmann's laboratory is supported by the National Science Foundation grant MCB-0443899. M.B. was supported by EMBO fellowship ALTF 350-2008. Use of the Advanced Photon Source at Argonne National Laboratory was supported by the U.S. Department of Energy, Office of Science, Office of Basic Energy Sciences, under Contract No. DE-AC02-06CH11357.

> 31-ID • LRL-CAT • Life science • Macromolecular crystallography, single-crystal diffraction, fiber diffraction, single-wavelength anomalous dispersion • 3.3-cm Undulator A • Accepting general users

How a Gate, Latch, and Lock Activate a Plant Hormone

IN SHORT > Researchers have figured out the structure of a protein that allows a key plant hormone to regulate growth and development. The hormone, called abscisic acid (ABA), triggers a cascade of chemical reactions that allows plants to adapt to conditions of drought, cold, and high salt. Less clear were the molecular details that allow ABA to exert its effects. In a study derived from work on two LS-CAT beamlines at the APS, researchers reported the first three-dimensional structure of ABA bound to a so-called "receptor molecule." The structures show a "gate-and-latch" mechanism, by which the receptor protein encloses itself around the hormone, and which appears to be widespread in the plant kingdom.

The hormone is useless without a receptor to recognize it and transfer its message to the rest of the cell. The importance of this process is such that, of 14 ABA receptors isolated from the same species of plant, all of them share certain amino acids, which implies they all work in the same way in a highly redundant manner. In the study, based on research at the LS-CAT 21-ID-D and 21-ID-F beamlines, the researchers from the Van Andel Research Institute; the National University of Singapore; the University of California, Riverside; the Medical College of Wisconsin; King Abdullah University of Science and Technology; and the National Center for Plant Gene Research (China) purified a receptor called PYL2 from the lab plant *Arabidopsis* that was amenable to crystallization, and therefore x-ray crystallography, to determine the plant's atomic structure.

The researchers first prepared two samples of PYL2, one by itself and one bound to ABA. Much like before and after photos, the researchers used these two structures to determine what happens after the receptor binds to its hormone. According to the group's report, the receptor forms a pocket shaped such that ABA can enter inside. When that happens, a pair of protein wings flanking the entrance close together like a gate and latch (Fig. 1). These wings are made of nearly identical amino acids in other receptors, which suggest they all work the same way.

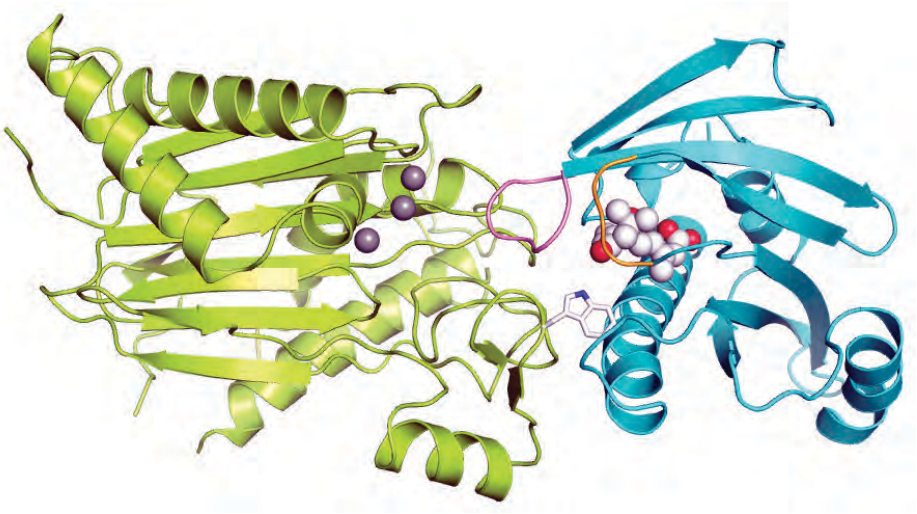

v Fig. 1 Image of the receptor PYL2 (turquoise) bound to abscisic acid (white and red) and to the enzyme HAB1 (yellow-green). The gate loop (pink) and latch loop (gold) regions of PYL2 enclose abscisic acid and present a face to which HAB1 can bind. (Purple spheres represent magnesium ions.) HAB1 extends part of the amino acid tryptophan (white and blue) into the gate and latch mechanism of PYL2.

MORE > Like any organism, when a plant is faced with a stressful environment, it activates counter-measures to minimize the stress, starting with abscisic acid.

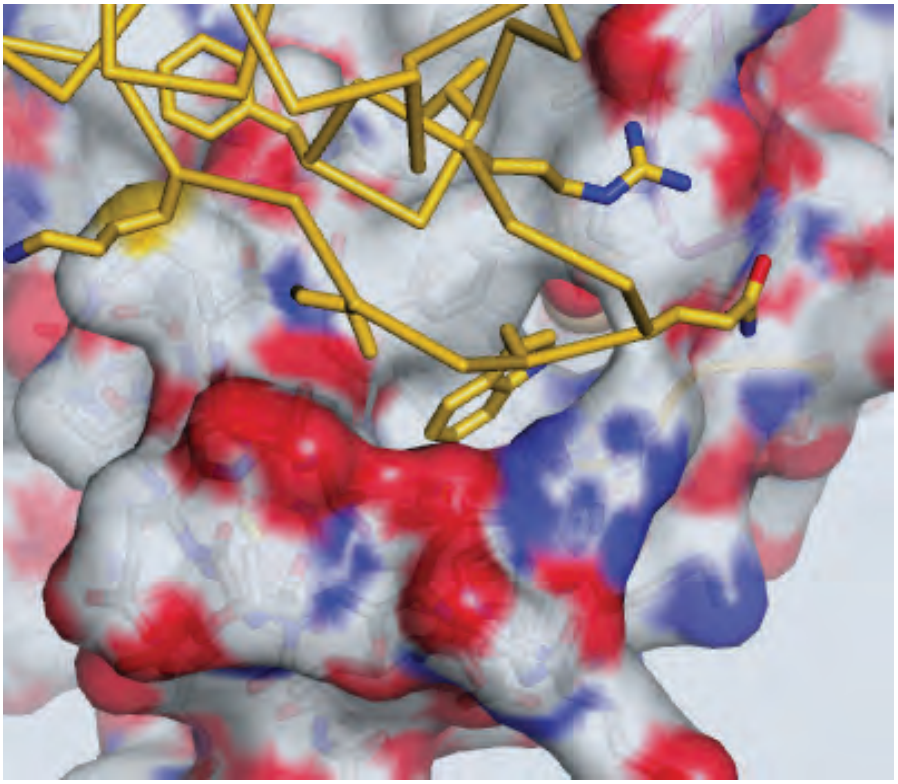

> Fig. 2 Close-up of the interface between absisic acid-bound PYL2 (shown as surface) and the HAB1 phosphatase (gold). The amino acid tryptophan inserts into the PYL2 cavity between the gate and latch regions.

The team next prepared a complex of ABA, PYL2, and HAB1, a so-called phosphatase, which maintains calm in the cell by removing bulky phosphate groups (phosphorous and oxygen) from other proteins in the cell. Together the ABA and its receptor form a new molecular surface capable of binding to HAB1 and inhibiting it, which activates genes that help the plant cope with stress. The team found that HAB1 inserts an amino acid into the gate and latch of PYL2 (Fig. 2), which would stabilize the structure so that it doesn't easily come apart. In other words, HAB1 locks the receptor and hormone together like a key inserted in a lock.

As confirmation of the importance of these structural details, the researchers conducted experiments to change key amino acids in the gate, latch, and lock areas to see what effect it had on the phosphatase. As would be predicted if the amino acids were keeping the structure together, changing them led to a reduction in inhibition of the phosphatase enzyme. The researchers also introduced a second protein to see if it would compete for the space on the phosphatase where the receptor and ABA bind. The other protein caused an increase in phosphatase activity, suggesting that the ABA receptor competes for space on the phosphatase but doesn't bind to it irreversibly.

Together, these results indicate the gate-latch-lock mechanism is widespread in the plant kingdom.

— JR Minkel

See > Karsten Melcher[1], Ley-Moy Ng[1,2], X. Edward Zhou[1], Fen-Fen Soon[1,2], Yong Xu[1], Kelly M. Suino-Powell[1], Sang-Youl Park[3], Joshua J. Weiner[4], Hiroaki Fujii[3,5], Viswanathan Chinnusamy[3,5], Amanda Kovach[1], Jun Li[1,2], Yonghong Wang[6], Jiayang Li[6], Francis C. Peterson[4], Davin R. Jensen[4], Eu-Leong Yong[2], Brian F. Volkman[4], Sean R. Cutler[3], Jian-Kang Zhu[3,5], and H. Eric Xu[1]*, "Agate–latch–lock mechanism for hormone signalling by abscisic acid receptors," Nature **462**, 602 (3 December 2009). DOI:10.1038/nature08613

Author affiliations > [1]Van Andel Research Institute; [2]National University of Singapore; [3]University of California, Riverside; [4]Medical College of Wisconsin; [5]King Abdullah University of Science and Technology; [6]National Center for Plant Gene Research

Correspondence > *eric.xu@vai.org

> This work was supported by the Jay and Betty Van Andel Foundation (H.E.X.), the National Institutes of Health (H.E.X., B.F.V., and J-K. Z.), and the National Science Foundation (S.R.C.). L.-M.N. and F.-F.S. were supported by an overseas Ph.D. scholarship from the NUS Graduate School for Integrative Sciences & Engineering (NGS). LS-CAT is in part funded by the Michigan Economic Development Corporation and the Michigan Technology Tri-Corridor. Use of the Advanced Photon Source at Argonne National Laboratory was supported by the U.S. Department of Energy, Office of Science, Office of Basic Energy Sciences, under Contract No. DE-AC02-06CH11357.

> 21-ID-D • LS-CAT • Life science • Macromolecular crystallography, anomalous diffraction (MAD/SAD) • U33S undulator • Accepting general users

> 21-ID-F • LS-CAT • Life science • Anomalous diffraction (MAD/SAD), macromolecular crystallography • 3.0-cm undulator • Accepting general users

Breaking a Carbon-Carbon Bond

IN SHORT > Researchers have figured out how a simple bacterium is able to perform a chemical reaction that has never before been seen in the living world. The group, from the University of Illinois at Urbana-Champaign, used the LS-CAT beamlines 21-ID-D and 21-ID-F at the APS to solve the three-dimensional structure of a bacterial enzyme that breaks apart chemical bonds between two carbon atoms. Unlike other known reactions in enzymes, the bond between the carbon atoms has no preexisting activation to get the reaction started. The results might help in the design of new antibiotics.

> Fig. 1 Structure of the HEPD enzyme, which uses an iron atom to break carbon-carbon bonds. The iron atom in this structure has been replaced with cadmium (red).

MORE > Many of today's antibiotics were originally discovered in bacteria. The microorganisms have special enzymes for making these antibiotics out of raw materials. In this new study, the researchers were interested in a reaction that occurs in two bacterial species of the group *Streptomyces*. Prior research had found that when the bacteria made the antibiotic phosphinothricin, one of the chemical reactions involved splitting apart two carbon atoms in an unprecedented way.

In a chemical bond, two atoms share a pair (or more) of electrons. If one of the atoms is more electrically charged than the other, it may hog the electrons, making it easy for the bond to break apart. In the chemical reaction during the biosynthesis of phosphinothricin, the two carbon atoms being broken up shared two electrons equally. In this reaction, an enzyme called HEPD chews up a two-carbon molecule and spits out a pair of one-carbon molecules.

The researchers performed x-ray crystallography on the HEPD enzyme to get clues to how it worked. (Fig. 1) The enzyme requires iron atoms to carry out the reaction on the starting material, a molecule called HEP. Based on the structure of the enzyme, derived from work on the LS-CAT beamlines, the group came up with a specific sequence of events to explain the reaction. An iron atom latches on to a phosphonate group (phosphorous and oxygen atoms) in the two-carbon HEP molecule. After oxygen reacts with the iron, electrons in the carbon-carbon bond spontaneously jump to make bonds with other atoms in the molecule.

To confirm the details of the reaction, the team used a common technique of placing an atom of deuterium, a heavier isotope of hydrogen, on each of the two carbons that would be split apart. After the reaction, the group used mass spectrometry, a tool for analyzing the structure of a molecule by breaking it into smaller pieces. They saw two molecules containing deuterium, corresponding to the two single-carbon molecules generated by the HEPD enzyme.

The researchers say the ability to break carbon-carbon bonds may prove useful in making new antibiotics. Researchers could engineer other bacteria to express the HEPD enzyme, changing the structures of carbon molecules in new ways.

— JR Minkel

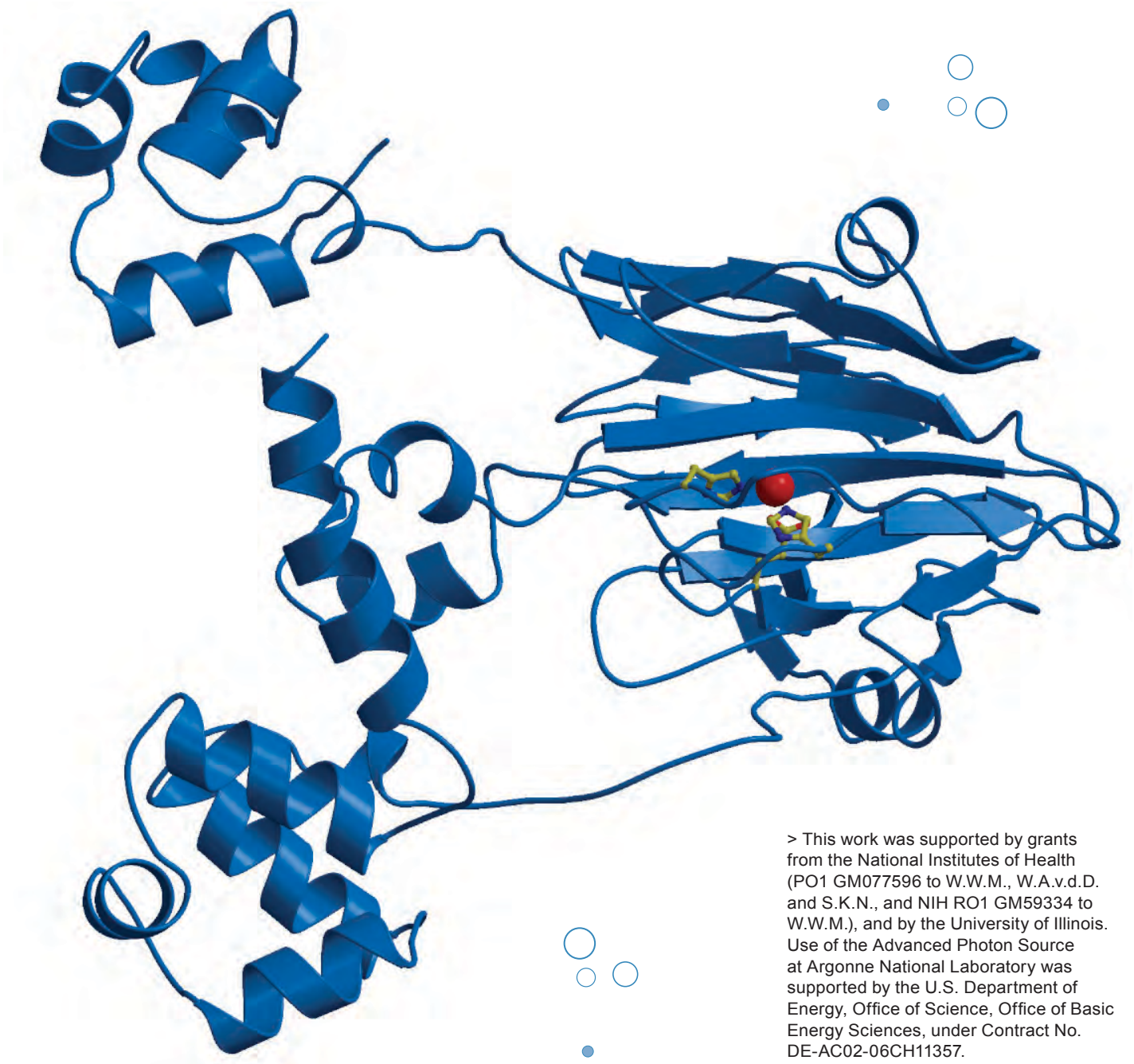

> This work was supported by grants from the National Institutes of Health (PO1 GM077596 to W.W.M., W.A.v.d.D. and S.K.N., and NIH RO1 GM59334 to W.W.M.), and by the University of Illinois. Use of the Advanced Photon Source at Argonne National Laboratory was supported by the U.S. Department of Energy, Office of Science, Office of Basic Energy Sciences, under Contract No. DE-AC02-06CH11357.

See > Robert M. Cicchillo, Houjin Zhang, Joshua A.V. Blodgett, John T. Whitteck, Gongyong Li, Satish K. Nair*, Wilfred A. van der Donk**, and William W. Metcalf***, "An unusual carbon–carbon bond cleavage reaction during phosphinothricin biosynthesis," Nature **459**, 871 (11 June 2009). DOI:10.1038/nature07972

Author affiliation >
University of Illinois at Urbana-Champaign

Correspondence >
*s-nair@life.uiuc.edu
**vddonk@illinois.edu
***metcalf@illinois.edu

> 21-ID-D • LS-CAT • Life science • Macromolecular crystallography, anomalous diffraction (MAD/SAD) • U33S undulator • Accepting general users

> 21-ID-F • LS-CAT • Life science • Anomalous diffraction (MAD/SAD), macromolecular crystallography • 3.0-cm undulator A • Accepting general users

Holding Steady to Form the First Peptide Bond

IN SHORT > Researchers using U.S. Department of Energy synchrotron light sources at Argonne and at Brookhaven National Laboratory are putting the finishing touches on a 30-year scientific story that garnered three biologists the 2009 Nobel Prize in Chemistry, awarded for uncovering the atomic structure of the ribosome, the molecular factory that synthesizes the thousands of proteins that make up every living cell. A study carried out by researchers from Yale University using two U.S. Department of Energy synchrotron light sources reported the three-dimensional structure of a bacterial ribosome bound to a helper protein called elongation factor P (EF-P). The structural details make it clearer how the ribosome takes the first step in protein synthesis; the fusing of two amino acids into a single molecule.

MORE > Since the 1960s, researchers have known that the job of the ribosome is to fuse together amino acids in a specific order under the direction of a molecule called messenger RNA, which carries an edited version of information encoded in DNA. What took decades to figure out was how the structure of the ribosome allows it to carry out the chemical steps required to form a chemical bond between two amino acids, called a peptide bond. In 2000, three researchers—Steitz; Venkatraman Ramakrishnan of the M.R.C. Laboratory of Molecular Biology in Cambridge, England; and Ada E. Yonath of the Weizmann Institute of Science in Rehovot, Israel—simultaneously published the first atomically detailed structures of the ribosome's two halves, paving the way for their shared Nobel Prize nine years later.

One of the mysteries Steitz's lab has been working on since then is how a specially modified version of the amino acid methionine triggers the start of protein synthesis in bacteria. Like other amino acids, this initiator methionine comes to the ribosome attached to an L-shaped molecule called transfer RNA. The first peptide bond is ready to be formed as soon as this so-called "initiator transfer RNA" becomes lodged in a pocket on the ribosome called the "P site." The ribosome then draws in a second amino acid and fuses methionine to it. The EF-P protein speeds up the formation of the initial peptide bond by making contact with the ribosome.

In their 2009 study, Steitz and his colleagues discovered how EF-P, the ribosome, and the initiator transfer RNA fit together. Using x-ray data obtained on NE-CAT beamline 24-ID-C at the APS, and National Synchrotron Light Source beamline X29, they reconstructed the atomic structure of a bacterial ribosome in complex with EF-P and initiator transfer RNA (Fig. 1). Their findings indicate that EF-P works by steadying the transfer RNA so that it doesn't wiggle and dislodge itself from the P site before the ribosome can transfer methionine to the next amino acid.

The structure shows EF-P pressed against the transfer RNA on one side and a mobile, finger-like projection of the ribosome, called the L1 stalk, on the other. The surface of EF-P exposed to the L1 stalk is negatively charged, which fits nicely into a positively charged pocket on L1. EF-P also touches a separate piece of RNA contained in the ribosome that is thought to help hold the transfer RNA in the correct position for peptide bond formation.

In non-bacterial cells, a protein called eIF5A takes the place of EF-P. Using the new structure to model that of eIF5A, the researchers find that the two proteins might make a similar but slightly different fit with the ribosome and transfer RNA, for the same end result: two amino acids become one molecule.

— JR Minkel

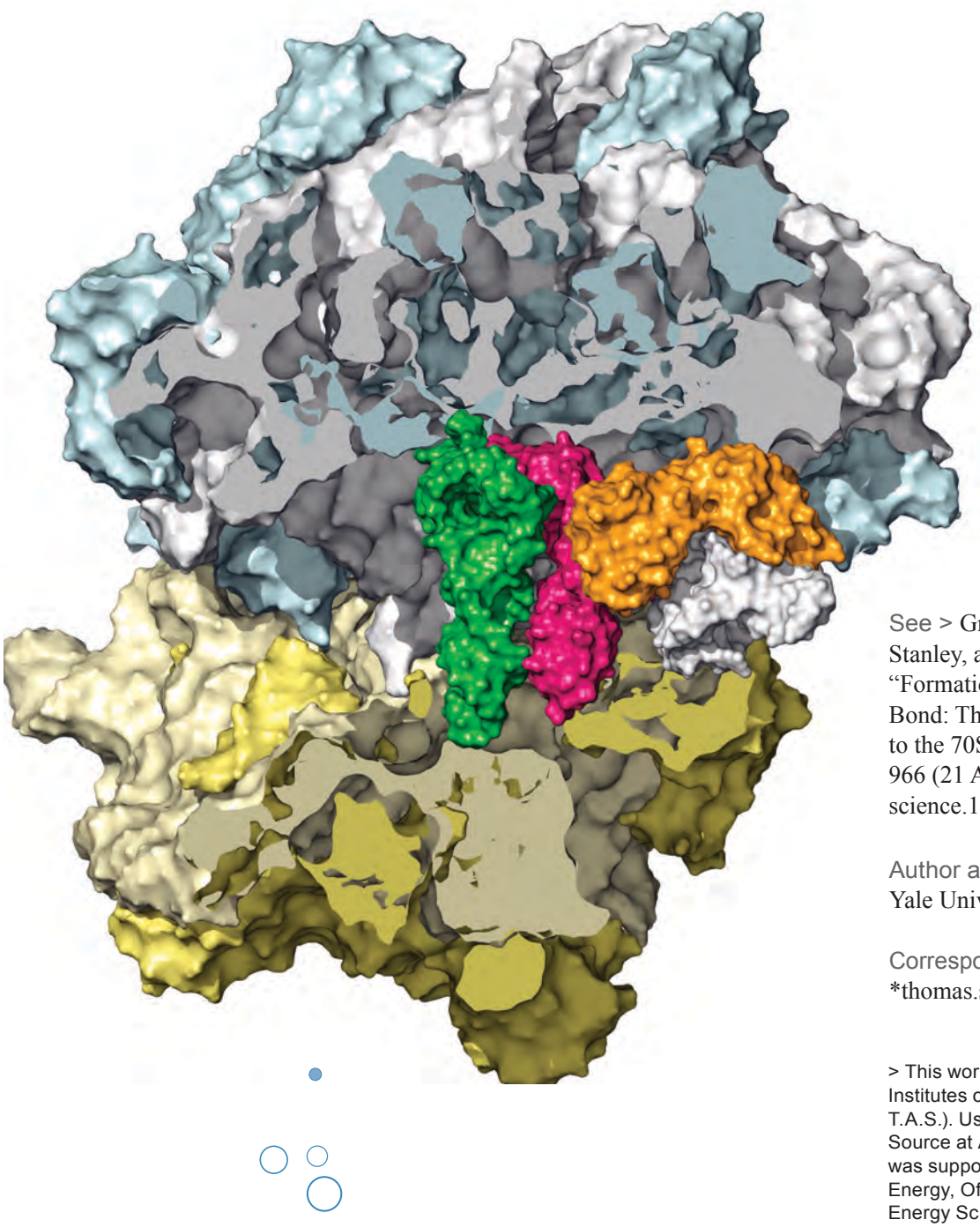

^ *Fig. 1 In this structure, the ribosome of **Thermus thermophilus**, a bacterium that thrives in high temperatures, is poised to take the first step of protein synthesis. Researchers believe the EF-P protein (pink) serves to maintain the proper orientation of initiator transfer RNA (green), which delivers the first amino acid to the ribosome. Helping to hold EF-P in place is a flexible part of the ribosome called the L1 stalk (gold).*

See > Gregor Blaha, Robin E. Stanley, and Thomas A. Steitz*, "Formation of the First Peptide Bond: The Structure of EF-P Bound to the 70S Ribosome," Science **325**, 966 (21 August 2009). DOI:10.1126/science.1175800

Author affiliation >
Yale University

Correspondence >
*thomas.steitz@yale.edu

> This work was supported by National Institutes of Health grant GM22778 (to T.A.S.). Use of the Advanced Photon Source at Argonne National Laboratory was supported by the U.S. Department of Energy, Office of Science, Office of Basic Energy Sciences, under Contract No. DE-AC02-06CH11357.

> 24-ID-C • NE-CAT • Life science • Anomalous diffraction (MAD/SAD), MAD phasing, macromolecular crystallography, microdiffraction, microbeam, single-crystal diffraction, single-wavelength anomalous dispersion • 3.3-cm Undulator A • Accepting general users

Some Self-Assembly Required

IN SHORT > Acting like microscopic lunar landers, bacteriophages, the viruses that infect bacteria, recognize and bind to specific molecules on the surface of their bacterial hosts. In an infection cycle very similar to that of the viruses that infect humans, once they are bound to the surface of the bacterial cell, bacteriophages break through the bacterial cell wall, inject their genomes, and proceed to take over the internal machinery of the cell. Within a short time, bacterial molecules have been hijacked to manufacture the proteins encoded by the viral genome. Once the viral proteins are made, the viruses go through a complex process of self-assembly, becoming particles that are ready to leave the cell to find new victims to infect. A deeper understanding of these complex infection processes is vital to designing treatments against viral infections in people.

> *Fig. 1 Model of bacteriophage ϕ29 structures approaching their bacterial host, **Bacillus subtilis**. Shown are fully assembled particles, in white and purple, and multicolored particles showing bacteriophage with tail spike assemblies, showing the autochaperone structure before and after autocatalytic processing.*

MORE > Structural studies of the tailed bacteriophage, ϕ29, have shed light on two steps in this infection cycle. The work, performed at the BioCARS 14-ID, SER-CAT 22-ID, and GM/CA-CAT 23-ID-D beamlines at the APS, has revealed the mechanism by which the tail spike of this bacteriophage is assembled in the host cell and provided clues to how it binds its host. Bacteriophage ϕ29 uses a 12-appendage tail spike to recognize glycopolymers on the cell wall of its bacterial host, *Bacillus subtilis*. Each of the 12 appendages consists of three copies of a protein called gp12 that assemble to form a trimeric coil containing the recognition sites for the *B. subtilis* cell wall. This complex structure is assembled inside the bacterium during infection and incorporated into new viral particles that are released from the cell. Elucidation of the structure of one of the trimeric appendages of the tail spike showed that the ϕ29 tail spike is assembled by a process involving a special autochaperone "base" region at the C-terminal end of the protein sequence that aids in formation of the gp12 trimer. Then, once its work is done, it neatly removes itself in an autocatalytic step that involves ATP hydrolysis.

The researchers in this study, from Purdue University and the University of Minnesota, first generated crystals of the gp12 protein before and after the autochaperone region had been removed, and then solved the structure of the protein using single anomalous dispersion phasing to a resolution of 2.0 Å (Fig. 1). The full-length structure reveals a coiled-coil trimeric domain with a globular trimeric base at one end. During assembly within the host cell, this base portion of the molecule is crucial for guiding the formation of the trimer by shielding certain water-insoluble amino acids (that will reside within the interior of the structure) from the watery milieu of the bacterial cytosol. If the base portion of the molecule is deleted, for example, the trimeric structure does not coil properly and results in an improperly folded, non-functional protein. Once self-assembly has completed, the chaperone base moves neatly over a portion of the coiled domain onto a putative proteolytic site, where it is cleaved and then released with the hydrolysis of a molecule of ATP. The researchers were able to identify and test possible amino acids in the structure to confirm that both the removal of the base portion by autocatalytic cleavage and the ATP hydrolysis could be accounted for by elements of the viral protein structure rather than external elements. This fascinating self-assembly and processing sequence appears to be conserved among other viruses that contain bacterial tail spikes similar to that of ϕ29 and may provide insight into how self-assembly of viruses could be blocked.

The structure also revealed information about the ability of

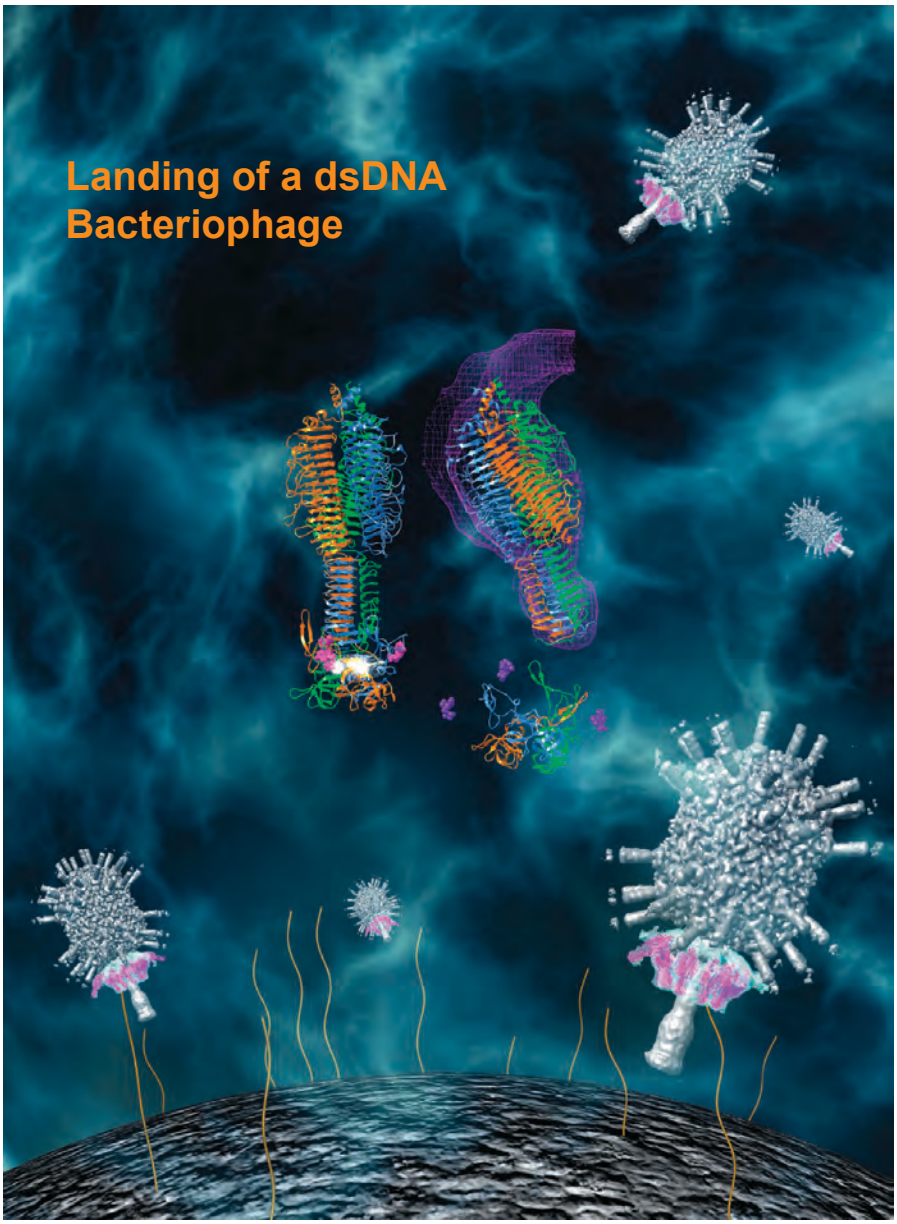

the ϕ29 tail spike to recognize host cell-wall molecules. In experiments where bacterial cell-wall analogs were bound to the gp12 trimeric structure, the researchers were able to show which specific regions of gp12 bind to the host, and that this interaction is dependent on metal ions in the viral protein structure. Their hypothesis, that each of the 12 appendages binds the host cell wall in succession to drive the virus through the bacterial cell wall, will be the subject of future investigations.

— Sandy Field

See > Ye Xiang[1], Petr G. Leiman[1,§], Long Li[1], Shelley Grimes[2], Dwight L. Anderson[2], and Michael G. Rossmann[1]*, "Crystallographic Insights into the Autocatalytic Assembly Mechanism of a Bacteriophage Tail Spike," Mol. Cell **34**, 375 (May 15, 2009). DOI:10.1016/j.molceI.2009.04.009

Author affiliations >
[1]Purdue University, [2]University of Minnesota [§]Present address: École Polytechnique Fédérale de Lausanne

Correspondence >
*mr@purdue.edu

> This work was supported by National Science Foundation Grant MCB-0443899 to M.G.R. and National Institutes of Health Grant DE003606 to D.LA, S.G., and M.G.R. Use of the Advanced Photon Source at Argonne National Laboratory was supported by the U.S. Department of Energy, Office of Science, Office of Basic Energy Sciences, under Contract No. DE-AC02-06CH11357.

> 14-ID • BioCARS • Life sciences • Anomalous diffraction (MAD/SAD), biohazards at the BSL2/3 level, Laue crystallography, macromolecular crystallography, time-resolved x-ray scattering • 2.7 undulator, 2.3 Undulator • Accepting general users

> 22-ID • SER-CAT • Life science • Macromolecular crystallography, multiwavelength anomalous dispersion • 3.3-cm Undulator A • Accepting general users

> 23-ID-D • GM/CA-CAT • Life science • Macromolecular crystallography, microbeam, microdiffraction, anomalous diffraction (MAD/SAD), subatomic (<0.85 Å) resolution • 3.0-cm undulator • Accepting general users

Inhibiting Estrogen-Dependent Breast Cancer at the Source

IN SHORT > Recent developments in breast cancer research have revealed that there are a number of different mechanisms by which this cancer may form. One of these is through inappropriate activation of cancer cell growth by naturally occurring estrogen in a woman's body. This knowledge has provided two possible targets for treatment: through inhibition of the binding of estrogen to the estrogen receptor or through inhibition of natural estrogen synthesis in the patient. Research at the SBC-CAT beamline 19-ID at the APS solved the structure of the enzyme aromatase to 2.9-Å resolution. This work provides important insights into the mechanism of action of aromatase, the specificity of its androgen binding cleft, and its membrane localization that will enable researchers to improve the existing inhibitors of this unique cytochrome P450-family enzyme.

> Fig. 1 A view of the human placental aromatase active site showing the bound androgen molecule within its unbiased electron density surface contoured at 4.5 times the standard deviation. Amino acid side chains, the heme group, and bound water molecules that snugly enclose the bound substrate are shown. Element colors are: C: gray, N: blue, O: red, S: yellow, Fe: firebrick, and H: orange. The C atoms of androgen are colored in light blue.

MORE > Estrogens are synthesized in the body by an enzyme called aromatase cytochrome P450 from their cellular precursors, androgens. Inhibition of this enzyme, therefore, has provided a target for small molecules that might inhibit its synthetic activity. Three of these aromatase inhibitors have been approved by the Food and Drug Administration for treatment of estrogen-dependent breast cancer. However, these molecules have all been developed without specific structural knowledge of the aromatase enzyme's androgen binding site or catalytic mechanism of action. Aromatase belongs to a large family of membrane-bound cytochrome P450 enzymes that play important roles in cellular metabolism. Research has shown that aromatase has a unique specificity among these enzymes and that the current inhibitors cross-react with other cytochrome P450 family members causing side effects.

Now, with solution of the crystal structure by researchers from the Hauptman-Woodward Medical Research Institute and the Roswell Park Cancer Institute, the molecular basis for the specificity of aromatase has been revealed (Fig.1). Within the binding cleft for androgen, there is a unique amino acid, proline 308, which changes the structure of the pocket to accommodate androgen perfectly. This confirms earlier studies showing that proline 308 plays a crucial role in aromatase activity and that it is unique among cytochrome P450 enzymes when one lines up their amino acid sequences.

The next step toward understanding how to design a better aromatase inhibitor was to create a model of the structure of aromatase with one of the inhibitors bound to the active site of the enzyme. By using the information they had gained from the structure and proposed catalytic mechanism of aromatase bound to androgen, the research team was able to model an aromatase inhibitor, exemestane, into the active site of aromatase. Analysis of the differences between the way androgens bind aromatase and the way the inhibitor binds showed that exemestane can bind to the active site but does not have the chemical group available for catalysis and therefore remains tightly bound, blocking any further androgen access to the catalytic cleft. The researchers are continuing to work on the structure of aromatase bound to the other inhibitors and have already made important strides towards the design of more specific aromatase inhibitors.

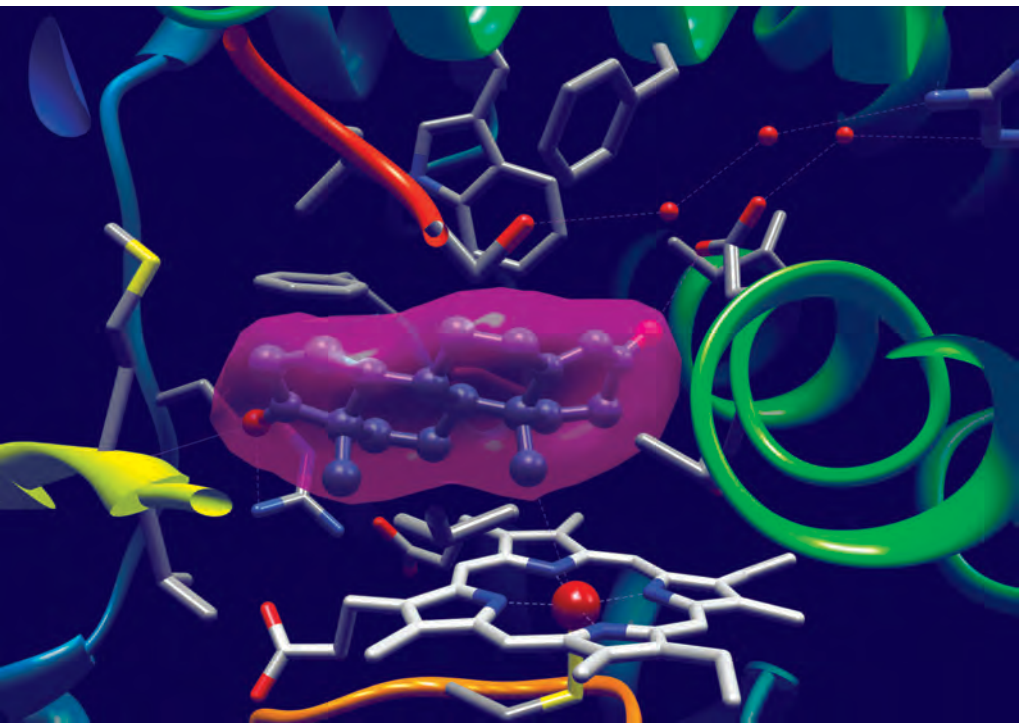

Another important aspect of cytochrome P450 enzymes is that they are bound to cellular membranes and catalyze reactions involving molecules that prefer a lipid environment to the watery environment of the cytosol. Analysis of the membrane-binding portions of aromatase allowed the researchers to hypothesize about how the orientation of the enzyme in the cellular membrane affects its interaction with its lipid-loving steroidal substrates. The analysis showed that the membrane binding portions of the enzyme bring the active site cleft of the enzyme into close proximity to the membrane, providing a channel for androgens and estrogens to get in and out of the enzyme through the lipid bilayer. This fascinating discovery provides a clue to the reason for the crucial membrane integration requirement of aromatase and other cytochrome P450 enzymes.

For the future, the researchers plan to focus on the design of more specific inhibitors for aromatase and to gain a more complete understanding of the mechanism of aromatase's unique catalytic chemistry.

— Sandy Field

See > Debashis Ghosh[1,2]*, Jennifer Griswold[1], Mary Erman[1], and Walter Pangborn[1], "Structural basis for androgen specificity and oestrogen synthesis in human aromatase," Nature **457**, 219 (8 January 2009). DOI:10.1038/nature07614.

Author affiliations >
[1]Hauptman-Woodward Medical Research Institute,
[2]Roswell Park Cancer Institute

Correspondence >
*ghosh@hwi.buffalo.edu

See also > "Structural biology: Anticancer drug target pictured," by Michael R. Waterman, *Nature* News and Views, Nature **457**, 159 (8 January 2009). DOI:10.1038/457159a

> This research is supported in part by grants GM62794 and GM59450 (to D.G.) from the National Institutes of Health. Use of the Advanced Photon Source at Argonne National Laboratory was supported by the U.S. Department of Energy, Office of Science, Office of Basic Energy Sciences, under Contract No. DE-AC02-06CH11357.

> 19-ID • SBC-CAT • Life science • Anomalous diffraction (MAD/SAD), subatomic (<0.85 Å) resolution, ultra-low-temperature (15K) • 3.3-cm Undulator A • Accepting general users

Ensuring that Proteins Reach Their Proper Destinations

IN SHORT > In eukaryotes (organisms with a cell nucleus), proteins are made by transcribing DNA into messenger RNA (mRNA), which is then translated to build proteins from amino acids. DNA is in the nucleus, and protein synthesis occurs outside the nucleus in the cytoplasm. However, many newly made proteins "work" in the nucleus and have to be transported there after they are made. The details of this transportation process are a mystery investigated by researchers from the University of Texas Southwestern Medical Center at Dallas, using the SBC-CAT 19-ID beamline at the APS.

MORE > Separation of nuclear activities from cytoplasmic activities is tightly regulated, so a complex but efficient system of moving cellular components into and out of the nucleus has evolved. This transport process involves a postal-like system wherein proteins contain an amino acid sequence that "tags" them for import into or export out of the nucleus. Special transporters recognize these nuclear localization signals (NLS) or leucine-rich nuclear export signals (NES), and guide them through pores in the nuclear membrane to their destinations. One of these transporter proteins is called CRM1 (exportin-1) and it is responsible for the transport of hundreds of proteins out of the nucleus. One of the CRM1 cargo proteins is called snurportin (SNUPN), which moves ribonucleoproteins into the nucleus and then must be recycled back out. Although amino acid sequence "tags" have been identified for many proteins that are imported into and out of the nucleus, many other proteins with similar sequences are, in fact, not transported. This suggests that these signals are not the only determinant for this process. This study has provided some answers to this mystery: The structure of CRM1 in complex with SNUPN at 2.9-Å resolution, solved by multiwave-length anomalous dispersion at the 19-ID beamline, has shown how CRM1 recognizes the SNUPN leucine-rich NES and an additional binding surface between these proteins, and has revealed how the drug Leptomycin B inhibits nuclear export by CRM1.

The first mystery solved by elucidation of the structure was the location of the leucine-rich NES on SNUPN. Investigators had previously reported that SNUPN didn't have a leucine-rich NES, but is an atypical cargo that bound CRM1 using a 300-amino acid domain. However, when the researchers in this study looked at the structure, they observed that a sequence in the N-terminus of SNUPN responsible for CRM1 recognition did actually contain the consensus for a leucine-rich NES. The leucine-rich NES nestles into a groove between two α-helices in ring-shaped CRM1 that provides a hydrophobic environment for the interaction (Fig. 1). Alteration of hydrophobic amino acids in the leucine-rich NES or the hydrophobic NES-binding groove of CRM1 interrupted the binding of CRM1 to SNUPN, proving that the N-terminus of SNUPN is a true NES and its binding site on CRM1 is the bona fide NES-binding site.

Leucine-rich NESs are known to be short stretches of hydrophobic amino acids interspersed with other amino acids. The interactions mediated by these regions are usually weak and these sequences are often found in proteins that are not exported from the nucleus. This led to the notion that there must be other factors involved in the specificity of nuclear export recognition. As predicted, the CRM1/ SNUPN structure shows that SNUPN contains a basic region that interacts with a complementary acidic surface on CRM1 adjacent to where it binds the SNUPN leucine-rich NES (Fig. 1). This interaction stabilizes the interaction with SNUPN and is likely to be present in other CRM1 cargoes. Interestingly, this model of bipartite binding of nuclear export receptor to its cargo is similar to one observed earlier for nuclear import processes and

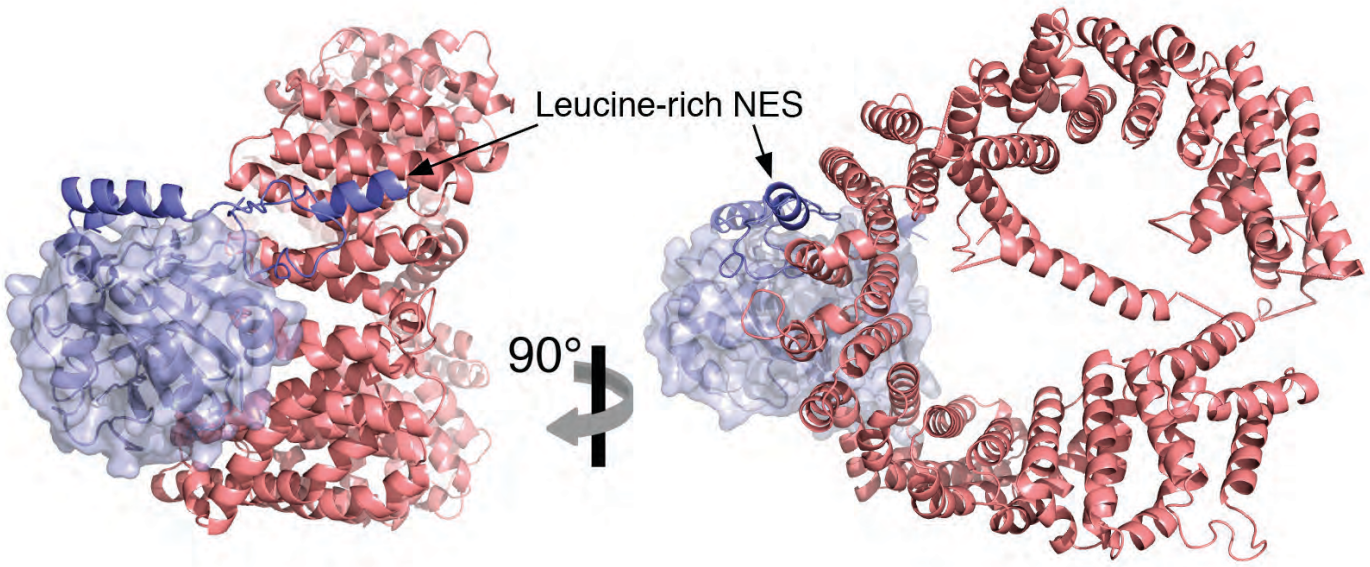

^ *Fig. 1 Overall structure of the CRM1–SNUPN complex. CRM1 is shown in pink and SNUPN is shown in blue. SNUPN binds CRM1 through its leucine-rich NES (labeled) and its basic nucleotide binding domain (shown as surface representation).*

suggests that these two processes are more similar than previously appreciated.

Finally, the CRM1/SNUPN structure was used to answer another outstanding question. Leptomycin B is an anti-fungal anti-bacterial agent that is known to inhibit nuclear export by binding to cysteine 528 of CRM1. In the structure, cysteine 528 sits in the binding groove for the SNUPN leucine-rich NES, showing clearly why Leptomycin B inhibits nuclear export by CRM1. This is important information because Leptomycin B, in addition to its uses as an anti-fungal and anti-bacterial agent, has shown promise as an anti-cancer agent. Knowledge of its mode of action could inform drug design efforts aimed at improving the efficacy of CRM1 inhibitors in medicine.

— Sandy Field

See > Xiuhua Dong, Anindita Biswas, Katherine E. Süel, Laurie K. Jackson, Rita Martinez, Hongmei Gu, and Yuh Min Chook*, "Structural basis for leucine-rich nuclear export signal recognition by CRM1," Nature **458**, 1136 (30 April 2009). DOI:10.1038/nature07975

Author affiliation >
University of Texas Southwestern Medical Center at Dallas

Correspondence >
*yuhmin.chook@utsouthwestern.edu

> This work is funded by National Institutes of Health grants R01GM069909, R01GM069909-03S1, and 5-T32-GM008297; Welch Foundation grant I-1532; and the UT Southwestern Endowed Scholars Program. Use of the SBC-CAT beamline was supported by the U.S. Department of Energy (DOE) Office of Biological and Environmental Research under Contract No. DE-AC02-06CH11357. Use of the Advanced Photon Source was supported by the DOE Office of Science, Office of Basic Energy Sciences, under Contract No. DE-AC02-06CH11357.

> 19-ID • SBC-CAT • Life science • Anomalous diffraction (MAD/SAD), subatomic (<0.85 Å) resolution, ultra-low-temperature (15K) • 3.3-cm Undulator A • Accepting general users

RNA Finds a Groove in ERA to Act as a GAP

IN SHORT > Making new proteins is one of the most fundamental functions of any cell, from bacteria to humans. All living things use DNA to create messenger RNA (mRNA) that contains the code for making the proteins of life from their component amino acids. Ribosomes are complexes of protein and RNA and are responsible for using the mRNA code to assemble proteins. Bacterial ribosomes consist of a complex of proteins and RNA that form two particles, the large 50S particle and the smaller 30S particle. The 30S particle contains 21 ribosomal proteins and a 1,540-nucleotide ribosomal RNA (16S rRNA). Before proteins can be made, this complex must be assembled, a process that is regulated by about 20 protein cofactors. Some of these cofactors, named GTPases, use the energy of hydrolysis of the GTP nucleotide as a molecular switch to check that each step occurs in the proper order before moving on to the next. One of these GTPases, ERA, is an essential protein in bacteria that is required for the final processing of the 16S rRNA and assembly of the 30S ribosomal subunit. Structural studies performed at two U.S. Department of Energy synchrotron x-ray light sources, including the SER-CAT 22-BM beamline at the APS, have now shown how the interaction of ERA with 16S rRNA affects its GTPase activity and function as a key regulator of protein translation.

> Fig. 1 The functional cycle of ERA is composed of four states, including apo-ERA, ERA-GTP, ERA-GTP-RNA and ERA-GDP. The GTPase domain (in yellow) and KH domain (in orange) of ERA and the 3′ end of 16S rRNA (12 nucleotides, in green) are shown as molecular surfaces, while the GTP (in blue) and GDP (in cyan) molecules are represented as atomic spheres.

MORE > Bacterial ERA contains an N-terminal GTPase domain connected by a 17 amino acid linker to a KH domain that binds to RNA. It has been shown to bind to both the 16S rRNA and to components of the 30s ribosomal subunit. However, the interaction of the two domains with each other and with RNA was unknown. In this work, carried out at the SER-CAT beamline and the X9B beamline of the National Synchrotron Light Source at Brookhaven National Laboratory, researchers from the National Cancer Institute of the National Institutes of Health solved two structures, one of ERA bound to GDP and the other of ERA bound to a GTP analog, GNP, plus the 3′ end of the 16S rRNA, $_{1531}$AUCACCUCCUUA$_{1542}$, which is thought to be the binding site of ERA. The AUCA of this RNA sequence is conserved among bacteria, archaea, and eukaryotes. The CCUCC is conserved among prokaryotes and is known as the anti-Shine-Delgarno sequence essential for translation start site recognition.

The GDP-bound form of ERA adopted the same conformation as a previously solved structure for ERA with no nucleotide, called apo-ERA. The ERA-GNP-RNA complex adopted a different conformation that was the same as the conformation previously shown for ERA-GNP without RNA and showed that RNA binding to ERA does not affect the structure of the protein. However, GTP binding does appear to have a large effect on the structure of the protein and also makes a big difference to the way RNA can bind. In the ERA-GNP-RNA structure, RNA lies within a positively-charged groove of the KH domain making contact through the first 9 nucleotides of the RNA. In the ligand-free and GDP-bound structures, this groove is occluded by the movement of a negatively charged helix, effectively

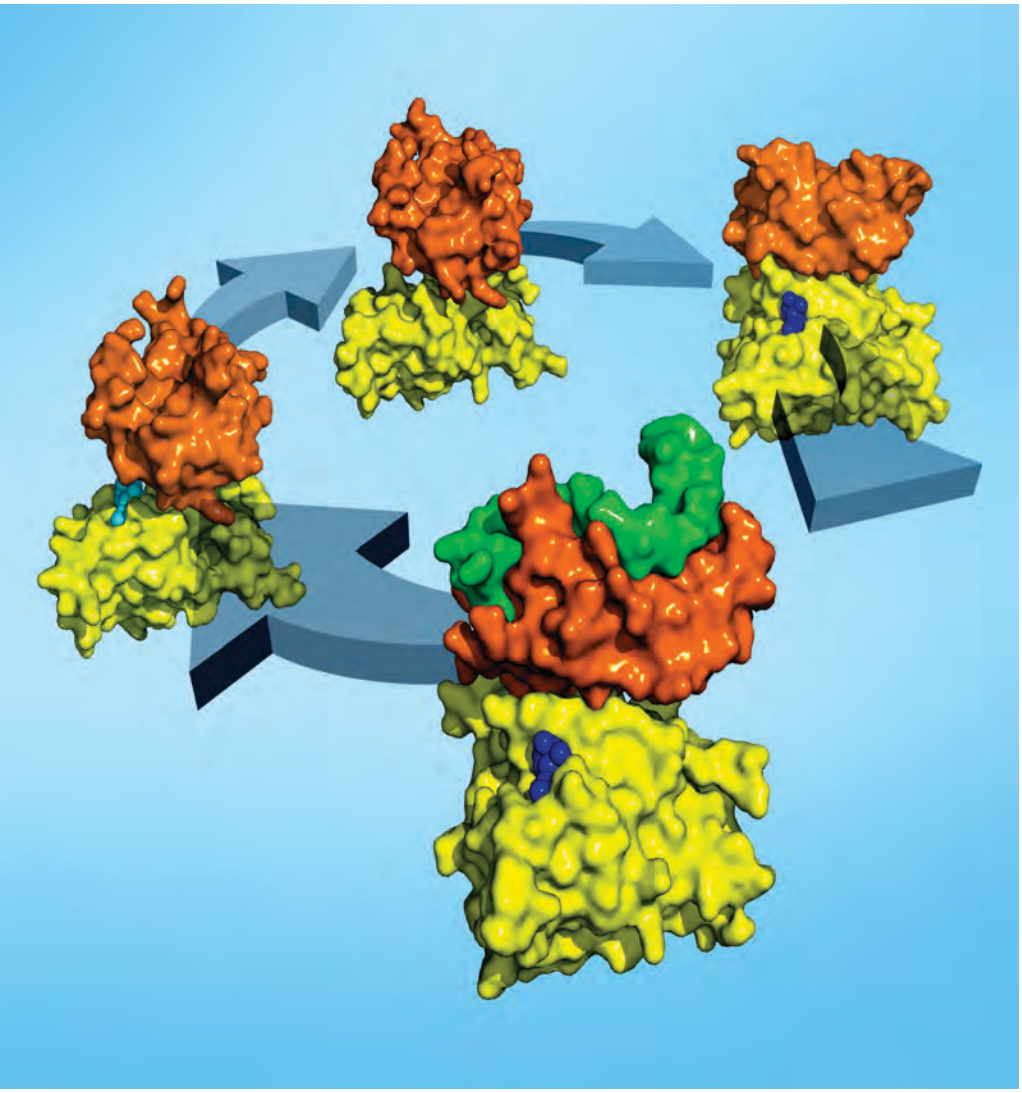

See > Chao Tu, Xiaomei Zhou, Joseph E. Tropea, Brian P. Austin, David S. Waugh, Donald L. Court, and Xinhua Ji*, "Structure of ERA in complex with the 3′ end of 16S rRNA: Implications for ribosome biogenesis," Proc. Nat. Acad. Sci. USA **106**(35), 14843 (September 1, 2009). DOI:10.1073/pnas.0904032106

Author affiliation >
National Cancer Institute,
National Institutes of Health

Correspondence >
*jix@ncifcrf.gov

blocking the binding of negatively charged RNA.

RNA binding does not affect the structure of ERA but it does affect the function. The team showed that RNA binding affects the rate of GTP hydrolysis of ERA by speeding it up, acting as a GTPase-activating protein or GAP. Further investigation showed that both the AUCA and the CCUCC were required for this GAP activity. However, the effect on GTPase activity was modest, only about a 6-fold increase, compared to 10^5 in other GTPases, leaving open the possibility that ERA's GTPase activity might be affected by other ribosomal proteins as well.

Based on their discoveries, these researchers propose a functional cycle for ERA activity including its GTP hydrolysis cycle and RNA binding (Fig. 1). Now, to fill in the gaps, the team will focus on identifying the impact of each nucleotide in the RNA on ERA binding and activity and on learning more about its function by studying the mouse and human forms of ERA.

— Sandy Field

> This work was supported by the Intramural Research Program of the National Institutes of Health, National Cancer Institute, Center for Cancer Research. Use of the Advanced Photon Source at Argonne National Laboratory was supported by the U.S. Department of Energy, Office of Science, Office of Basic Energy Sciences, under Contract No. DE-AC02-06CH11357.

> 22-BM • SER-CAT • Life science • Macromolecular crystallography • Bending magnet • Accepting general users

A Surprise in Old Water Pipes

IN SHORT > Although vanadium, a moderately abundant element in the Earth's crust, isn't known to cause significant human health problems, the U.S. Environmental Protection Agency (USEPA) lists it as a "contaminant candidate" in drinking water, meaning that regulatory action could follow if data emerge showing that the metal poses a health risk and is sufficiently widespread in occurrence. Meanwhile, surprisingly large amounts of the metal sometimes show up in scale deposits on the inner surfaces of old lead water pipes. Scientists from the USEPA used several x-ray techniques at the APS to probe the chemical make-up and structure of these deposits. The results illuminate how vanadium-containing minerals could have built up inside the pipes, even though the metal's concentration in water is low, and hint at ways in which changes in water treatment might release the trapped vanadium into the water supply.

MORE > While vanadium is not routinely tracked by the USEPA, in a 2008 study of scale taken from lead pipes that had been part of municipal drinking water systems for 70 years or more, the amount of vanadium in the mineralized deposits varied enormously, from as little as 13 ppm to as much as 22,500 ppm. Researchers from the USEPA and the University of Cincinnati decided to dig deeper into the origin of these vanadium deposits and to assess the dangers they might present.

The researchers collected 34 scale samples from 15 lead pipes representing 8 water systems in the northeast and midwestern U.S. (Fig 1). Analysis of these samples by x-ray powder diffraction failed to identify specific vanadium compounds, most likely because they were in an amorphous form or, if in a crystalline form, at very low concentration. Turning to the XOR/PNC 20-BM beamline at the APS, the team tested 19 powdered samples using the bulk x-ray absorption near edge spectroscopy (XANES) technique. Because vanadium can exist in several oxidation states, spectral signatures can arise from a confusing variety of compounds. The XANES technique was key in confirming that the oxidizing environment of the drinking waters produced vanadium compounds in the V^{5+} oxidation state. In 14 of the 19 samples, XANES identified the presence of the lead-vanadium mineral vanadinite, $Pb_5(VO_4)_3Cl$, along with a smaller fraction of vanadium oxide in some samples.

To pin down where in the pipe deposits the vanadinite resided, the researchers then used the micro-focused x-ray beam at beamline XOR/PNC 20-ID to analyze cross-sections cut through two scale samples (Fig. 2). Mapping by μ-x-ray fluorescence tests revealed vanadium mainly in the surface layers of the scales that would have had immediate contact with water. Subsequent μ-XANES spectra taken of spots highlighted in the fluorescence map again confirmed the presence of vanadinite.

One of the scale samples that included significant amounts of vanadinite came from a water supply system that used chloramine for disinfection and orthophosphate

> Fig. 1 Inner surface of old lead water pipes.

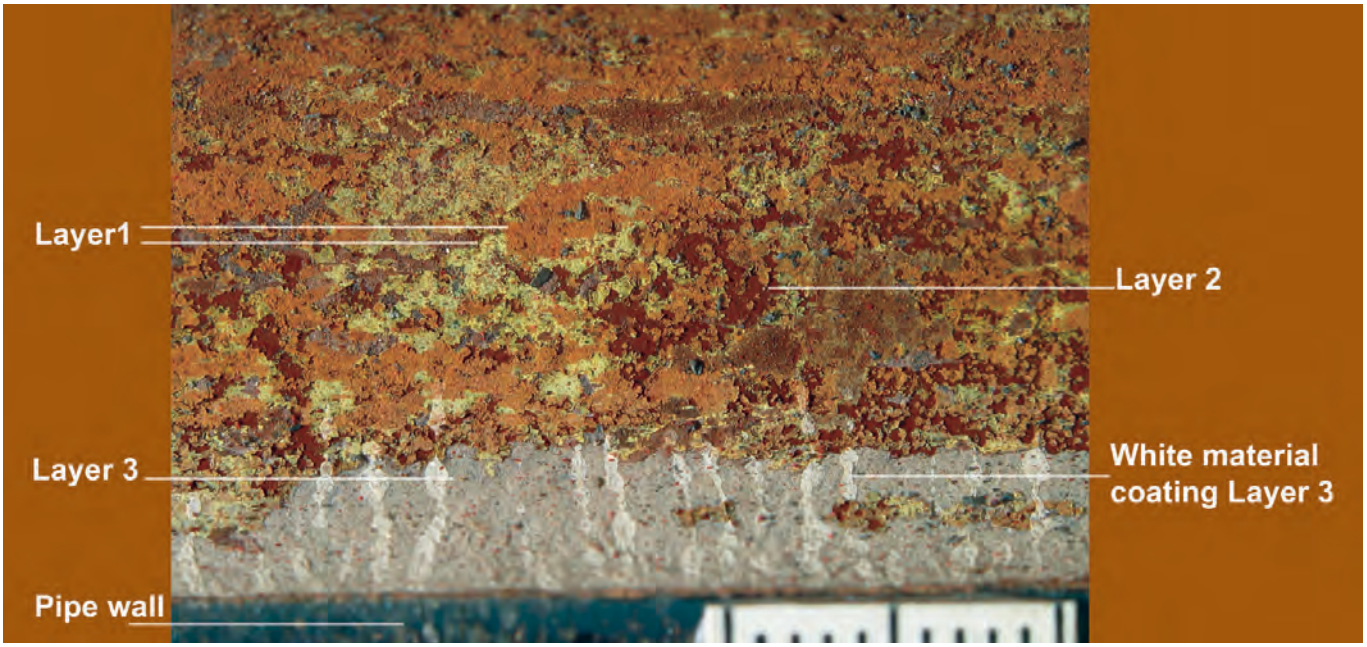

^ *Fig. 2 Scale deposits taken from a variety of locations on the inner surface the pipes in Fig. 1 turn out to have unexpectedly high concentrations of the vanadium-containing mineral vanadinite. (Photos courtesy of Michael K. DeSantis, Pegasus Technical Services [contractor for USEPA])*

to control corrosion of the pipes. Modeling these chemical conditions, the researchers concluded that dissolved V^{5+} ions in the water can react with lead(II) compounds in the surface layers of the pipe to form vanadinite, which is highly insoluble. In this way, the surface scale layers can accumulate high concentrations of vanadium from low concentrations in the water itself. The researchers also used these results to provide an estimate of an upper limit to the solubility of vanadinite, a very useful datum for environmental and geochemists.

These findings raise the possibility that changes in the chemicals used for water treatment could reverse the reactions by which vanadium is mineralized in the pipe surface, possibly leading to the release of large amounts of the metal into the water supply, the researchers caution. They also suggest that similar studies are needed of pipes made of other metals, notably iron, to see if vanadium deposits can build up in the same way, or if the accumulation mechanism (and hence, mobility) differs.

— David Lindley

See > Tammie L. Gerke[1], Kirk G. Scheckel [2] and Michael R. Schock[2]*, "Identification and Distribution of Vanadinite ($Pb_5(V^{5+}O_4)_3Cl$) in Lead Pipe Corrosion By-Products," Enviro. Sci. Tech. **43**, 4412 (2009). DOI:10.1021/es900501t

Author affiliations > [1]University of Cincinnati; [2]U.S. Environmental Protection Agency, Cincinnati

Correspondence > *Schock.Michael@epa.gov

> The XOR/PNC facilities at the Advanced Photon Source, and research at these facilities, are supported by the U.S. Department of Energy-Basic Energy Sciences, a major facilities access grant from NSERC, the University of Washington, Simon Fraser University, and the Advanced Photon Source. Use of the Advanced Photon Source is supported by the U.S. Department of Energy, Office of Science, Office of Basic Energy Sciences, under Contract DE-AC02-06CH11357. All ICP analyses were conducted by the United States Geological Survey's Mineral Resource Surveys Program under Interagency Agreement DWI4999901 under the direction of Dr. Stephen A. Wilson.

> 20-BM • XOR/PNC • Chemistry, environmental science, geoscience, materials science • Microfluorescence (hard x-ray), micro x-ray absorption fine structure, x-ray absorption fine structure • Bending magnet • Accepting general users

Rice's Reliability as a Source of Selenium

IN SHORT > Selenium is good for you—in tiny quantities, anyway. We need from 55 to 200 μg of the element per day in our food to avoid muscle and cartilage problems, reproductive impairment, and other disorders. Insufficient dietary selenium affects perhaps 1 billion people worldwide; for many of these people, rice provides a significant portion of their essential minerals. As part of a program to assess the selenium content of rice from different parts of the world, an international team of researchers used XOR/PNC beamline 20-ID at the APS to distinguish between organic and inorganic selenium-containing molecules, and to determine where in the rice grain the element is most likely to accumulate. Their findings provide guidance on how rice supplies can be mixed and managed to ensure adequate selenium content.

MORE > Scientists from the Chinese Academy of Sciences, the University of Aberdeen, the University of Copenhagen, the U.S. Environmental Protection Agency, and the University of Ghana collected 1,092 samples of polished or white rice from 11 countries that collectively produce about two-thirds of the world's rice. Chemical analyses of total selenium content revealed large variations both within and among countries, resulting from differences in soil chemistry as well as agricultural management techniques that influence water quality. Egyptian rice had the least selenium, averaging less than 10 ppt by weight of selenium, while rice from India and the United States had the most, averaging 157 ppt and 180 ppt, respectively, with some samples going as high as 400 ppt. Assuming an average rice consumption of 300 g per day, the researchers found that three quarters of the samples they tested could not provide even 70% of the minimum daily requirement.

Selenium's dietary value depends on whether it resides in inorganic or organic molecules, the latter being more useful. But it's difficult to identify chemical species and locate their distribution in rice grains when the concentration of the element is so low, so the researchers obtained an additional sample of rice, from Jianshi county in south-central China, where natural conditions produce extraordinarily high selenium concentrations—almost 10 parts ppm in brown and polished rice, and 17 ppm in rice bran. Residents of this area who subsist largely on local rice can suffer from selenium toxicity, leading to hair loss, liver enlargement and other disorders. For the research team, however, these high concentrations allowed detailed investigation of the chemical form and location of selenium in the rice, using x-ray fluorescence (XRF) and XANES (x-ray absorption near-edge structure) methods.

Bulk XANES analysis of powdered samples of Jianshi rice showed that selenium was about equally distributed between organic and inorganic forms in the husk and bran, but was about 95% organic in the endosperm (the starchy central part of the grain). To further pin down the location of selenium, the team cut individual rice grains to make transverse and longitudinal sections that they studied using μ-XRF and μ-XANES (Fig. 1). Fluorescence maps showed selenium mostly in the outer layers of the grain, infiltrating the endosperm through structures that carry nutrients into the growing grain. Micro-XANES analysis of a few 5-μm-wide spots in the cross sections indicated that most of the selenium was in the form of methyl-selenocysteine, an organic molecule thought to have anticarcinogenic properties.

The team's results provide a previously absent quantitative perspective on the problem of selenium deficiency around the world. About two-thirds of the rice from India, the world's second biggest producer and biggest exporter of the grain, already has adequate selenium content, whereas rice from Thailand, the second biggest exporter, is much poorer in the essential element. Rice like that from Jianshi, with selenium content hundreds of times higher than the global average, could be used as a simple food additive, the researchers say. They warn, though, that rice bran should probably not

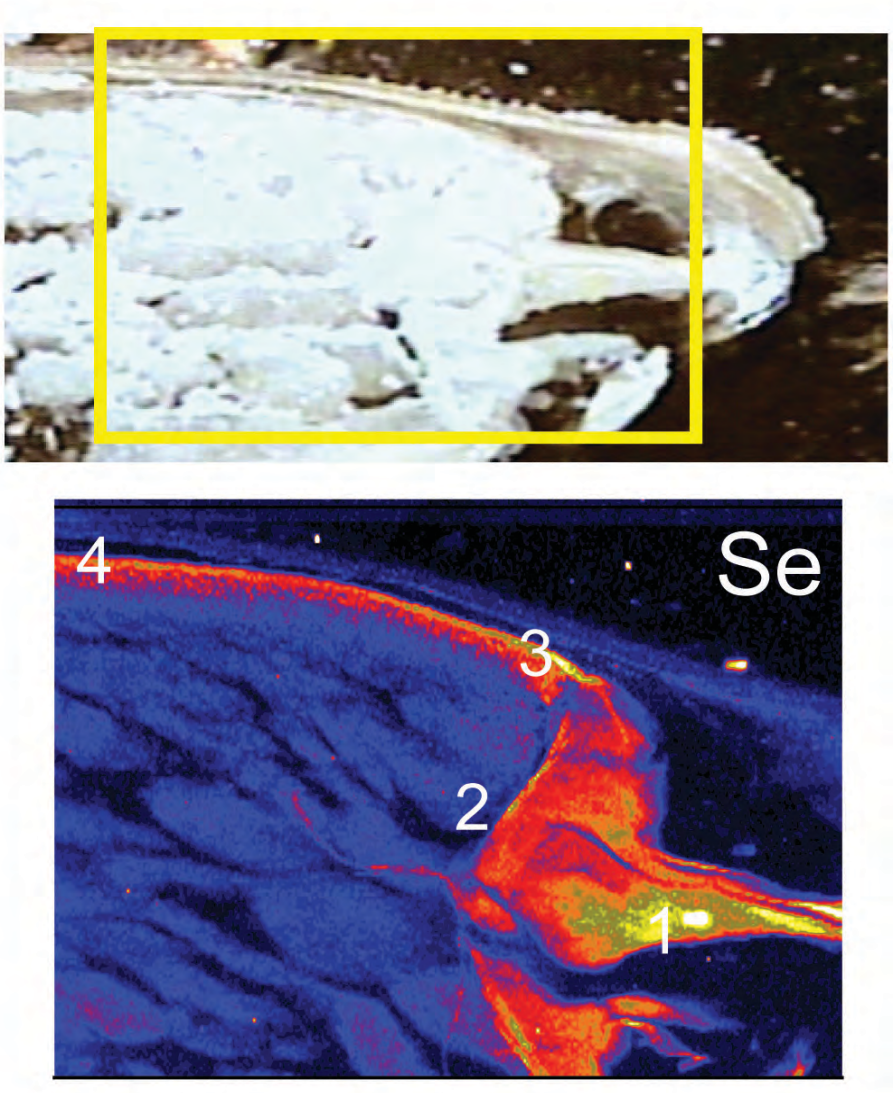

> *Fig. 1 Selenium content of a grain of Chinese rice **(top)** shows up in a image produced by x-ray fluorescence mapping **(below)**. XANES spectra of the numbered locations revealed the chemical form in which selenium accumulated in the grain, particularly the relative amounts of organic and inorganic species.*

be used as an additive, even though it holds most of the selenium in the rice grain, because toxic elements such as arsenic and lead also tend to accumulate there.

— David Lindley

See > Paul N. Williams[1,2], Enzo Lombi[3,4], Gui-Xin Sun[1], Kirk Scheckel[5], Yong-Guan Zhu[1]*, Xinbin Feng[1], Jianming Zhue[1], Anne-Marie Carey[2], Eureka Adomako[2,6], Youseff Lawgali[2], Claire Deacon[2], and Andrew A. Meharg[2]**, "Selenium Characterization in the Global Rice Supply Chain," Enviro. Sci. Tech. **43**, 6024 (2009). DOI:10.1021/es900671m

Author affiliations >
[1]Chinese Academy of Sciences;
[2]University of Aberdeen;
[3]University of Copenhagen;
[4]University of South Australia;
[5]U.S. Environmental Protection Agency, Cincinnati;
[6]University of Ghana

Correspondence >
*ygzhu@rcees.ac.cn
**a.meharg@abdn.ac.uk

> This research was supported by the Natural Science Foundation of China (20720102042), Chinese Academy of Sciences (KZCX1-YW-06-03), the CAS Research Fellowship for International Young Researchers, and the Royal Society of Edinburgh's International Exchange Programme. XOR/PNC facilities at the Advanced Photon Source and research at these facilities are supported by the U.S. Department of Energy, Office of Basic Energy Sciences, a major facilities access grant from NSERC, the University of Washington, Simon Fraser University, and the Advanced Photon Source. Use of the Advanced Photon Source is supported by the U.S. Department of Energy, Office of Science, Office of Basic Energy Sciences, under Contract DEAC02-06CH11357. The U.S EPA, through its Office of Research and Development, funded and managed a portion of the research. It has not been subject to Agency review and, therefore, does not necessarily reflect the views of the Agency.

> 20-ID • XOR/PNC • Materials science, environmental science, chemistry, geoscience • Microfluorescence (hard x-ray), x-ray absorption fine structure, surface diffraction, micro x-ray absorption fine structure, x-ray Raman scattering, time-resolved x-ray absorption fine structure, x-ray emission spectroscopy • 3.3-cm Undulator A • Accepting general users

Geology's "Insect in Amber"

IN SHORT > Tiny droplets of fluid trapped for millennia inside crystals within ancient rocks can reveal important clues about Earth's geological history. A detailed analysis of so-called "inclusions"—samples of a geological fluid or melt that were trapped in a crystal as it grew (a little like an insect in amber)—can provide useful information about how a rock or ore deposit formed. Over the last 15 years, researchers have published several thousand papers reporting such analyses. These inclusions are unique in that they essentially "lock in" the physical and chemical conditions present in a fluid or melt at the time the host rock crystallised. An international team used the GSECARS 13-ID beamline of the APS to study samples of a Russian granite. Their work revealed, for the first time, the type of copper molecules that are present in fluids that may form ore deposits. This research has implications for understanding fundamental geochemistry as well as in the hunt for valuable mineral ores.

MORE > Granite from the industrial region known as the Omsukchan trough in Russia is a particularly rich vein of geochemical information. Aqueous, or hydrothermal, fluids that de-gas from a magma are particularly important in geochemistry and forming ores. The researchers in this study published results on melt inclusions in *Nature*, **455**, 960 (2008,), which were featured in the article "Heat in the Archaean Mantle" in *APS Science 2008*, pg. 110. For the current study, the researchers, from Imperial College London, the University of Tasmania, and The University of Chicago, recorded copper K-edge x-ray absorption spectra from natural samples of Omsukchan granite (Fig. 1). More specifically, they recorded the spectra for polyphase brine fluid inclusions found in the miarolitic quartz component of this granite. They tracked the spectra up to 700° C for two different types of fluids that had been trapped as inclusions. One contained 0.02% by weight of copper and the other 0.94 wt.%. In both cases the copper distributed evenly throughout the inclusion above the salt dissolution temperature at 350° C to 550° C. This indicated that the copper was present in solution and not as a crystal.

The team studied the x-ray absorption near edge structure (XANES) spectra of the solution phase for the inclusions containing the low copper concentration. These displayed an intense edge feature at an energy close to 8983 eV. Extended x-ray absorption fine structure (EXAFS) spectra at 550° C point to a chlorine-copper bond length of 2.11(2) Å. The XANES and EXAFS data are consistent with a $[CuCl_2]^-$ ion. This species is apparent in the spectrum at all temperatures from 200° C to 700° C and was present in all 15 of the inclusions tested. The team also recorded XANES spectra for the copper-rich inclusions, which are similar to those of the low-copper samples, but shifted to higher energy. This characteristic was seen at 350° C to 700° C from all three of the copper-rich inclusions studied. The subsequent EXAFS study at 700° C seemed to show that a copper-containing ion with a different bond length—2.19(1) Å—was present, suggesting that chlorine may not be the partner atom in this case.

This is the first time that copper speciation has been determined at these temperatures and provides an example of how inclusions can be used as sample cells for the spectroscopic study of fluids at extreme conditions.

The team now plans to investigate iron, manganese, and zinc in the same inclusions. This will allow them to explore the geochemistry of these ore metals at much higher temperatures than have been studied before. The ultimate aim will be to understand how different metals speciate from magmatic to depositional temperatures and so help clarify the chemical and physical conditions that give rise to different types of ore deposits.

— David Bradley

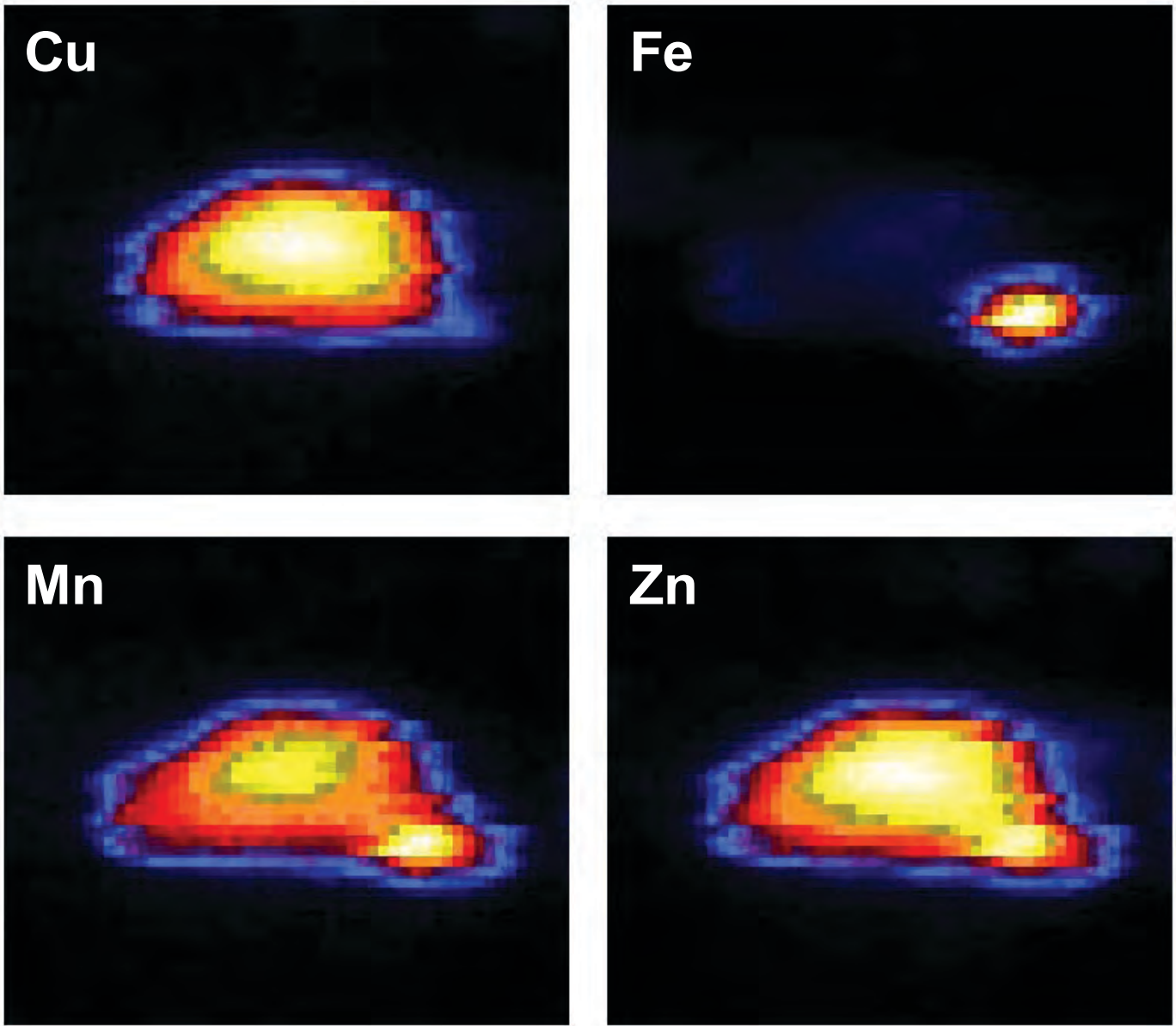

^ *Fig. 1 Kα x-ray fluorescence maps of a fluid inclusion at 500° C. The copper is homogeneously distributed in the fluid, as is most of the manganese and zinc. Iron is present as a crystal in the bottom-right corner. The inclusion is approximately 60 μm across.*

See > Andrew J. Berry[1]*, Anthony C. Harris[2], Vadim S. Kamenetsky[2], Matthew Newville[3], Stephen R. Sutton[3], "The speciation of copper in natural fluid inclusions at temperatures up to 700° C," Chem. Geol. **259**, 2 (2009). DOI:10.1016/j.chemgeo.2008.10.018

Author affiliations >
[1]Imperial College London,
[2]University of Tasmania,
[3]The University of Chicago

Correspondence >
*a.berry@imperial.ac.uk

> A.C.H. visited GSECARS with support from the Access to Major Research Facilities Program funded by the Commonwealth of Australia. GSECARS is supported by the U.S. National Science Foundation (EAR-0622171) and the U.S. Department of Energy (DEFG02-94ER14466). Use of the Advanced Photon Source was supported by the U.S. Department of Energy, Office of Science, Office of Basic Energy Sciences, under Contract No. DE-AC02-06CH11357.

13-ID • GSECARS • Geoscience, environmental science • Microfluorescence (hard x-ray), microdiffraction, x-ray absorption fine structure, micro x-ray absorption fine structure, high-pressure diamond anvil cell, high-pressure multianvil press, inelastic x-ray scattering • 3.3-cm Undulator A • Accepting general users

Airing the Laundry: What Happens to Silver Nanoparticles in the Wash?

IN SHORT > The number of commercial applications of nanotechnology is burgeoning. Products containing nanoparticles are entering the marketplace, and the environment, at a rapidly increasing rate, and well before their safety has been definitively determined. Among the products on store shelves today are socks that contain silver (Ag) nanoparticles with antibacterial and fungicidal properties. Laboratory experiments using zebrafish, the lab rat of the aquatic environment, have demonstrated serious developmental defects and mortality of fish exposed to ionic Ag nanoparticles in purified water. But the fate and toxicity of Ag nanoparticles in aquatic systems outside the lab remains uncertain, so gaining a better understanding of the chemical transformations that nanoparticles experience under a variety of real-world conditions is vital in assessing any potential health risks from this new technology. A research team from the U.S. Environmental Protection Agency (EPA) utilized the APS to explore the ways in which sock fabric impregnated with Ag nanoparticles reacts to simulations of an ordinary laundry process, using bleach, detergent, and tap water, and uncovered some enlightening transformations.

> Fig. 1 X-ray absorption near-edge structure spectra for Ag reference materials, sock samples, and elemental Ag nanoparticles in chloride and hypochlorite/detergent solutions. When the elemental Ag is exposed to chloride ion alone, there is no evidence for the formation of AgCl. The XANES spectra show that the edge energy shift in the hypochlorite solution is similar to that of the AgCl reference material. (Copyright © 2009 by the American Society of Agronomy, Crop Science Society of America, and Soil Science Society of America. All rights reserved.)

MORE > X-ray absorption near edge structure (XANES) spectroscopy was carried out at the MR-CAT beamline 10-ID to compare unwashed sock material with fabric that went through the washing process. The team also gathered XANES spectra from an Ag chloride reference material and elemental nanopowder in a chloride solution (NaCl). The researchers exposed samples of fabric to a mixture using products in common use around the house: bleach and detergent. The solution was agitated for two minutes and left to soak for 10 minutes, and this cycle was repeated once. Using tap water from Argonne, they then rinsed the fabric, wrung it out three times, and mounted the 10-cm^2 samples for XANES analysis.

The researchers found that ionic Ag nanoparticles react with chloride present in the hypochlorite bleach/detergent mixture, resulting in an inert and more stable compound, Ag chloride (AgCl). In the one wash and rinse operation, about 50% of the nanoparticles were converted to the chloride form. The EPA scientists suggest that repeated laundering of the sock material may convert additional Ag nanoparticles to AgCl, thus reducing or eliminating the odor-eating and antibacterial properties of the relatively expensive apparel.

The elemental Ag nanopowder immersed in an ionic saline (NaCl) solution, however, remained in its elemental, and potentially more toxic, state. It appears that the hypochlorite bleach/detergent solution used to wash the sock fabric provides an oxidation step necessary to transform ionic nanosilver into a stable, non-reactive compound. This is indicated by a distinct shift in the edge energy that is similar for the washed fabric and the reference material AgCl (Fig. 1). The scientists caution that

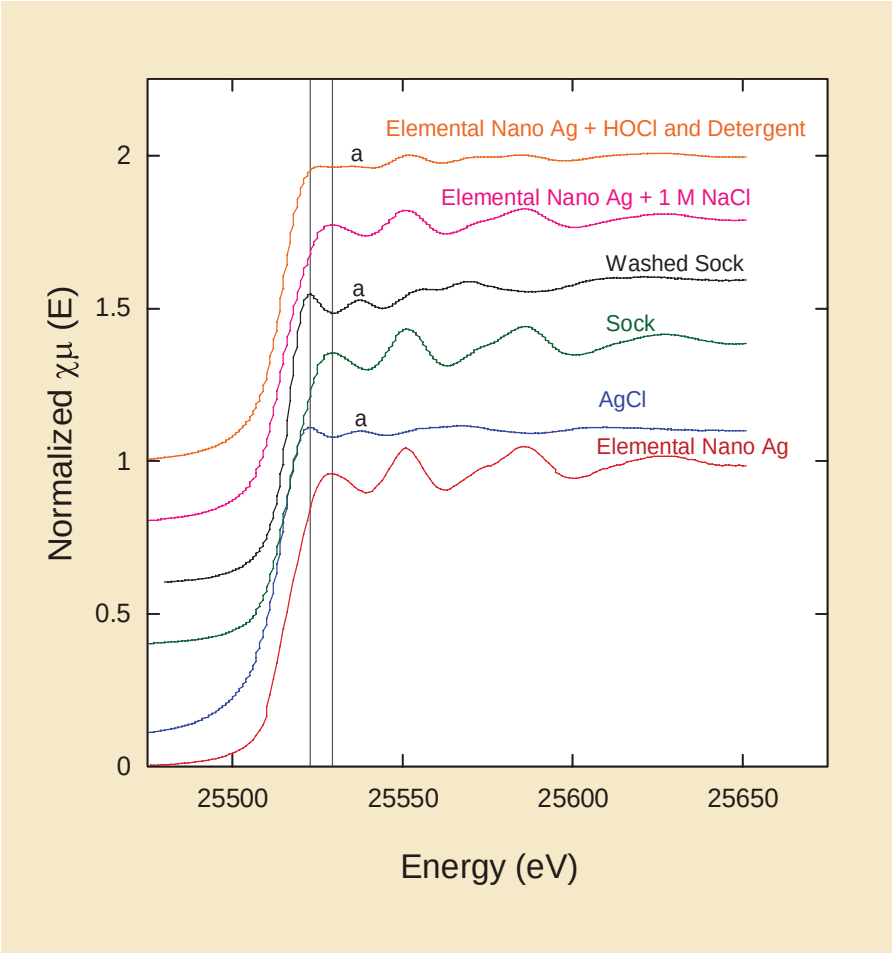

the solution used in this experiment may not be typical of an ordinary laundry process. Further studies with laundry detergent in ordinary washing machines may further clarify whether Ag nanoparticles are consistently converted to an inert form. Furthermore, the team proposes that as Ag nanoparticles enter public sewer systems and finally wastewater treatment plants, very little if any ionic Ag will remain because chloride is so common. Should Ag impregnated socks wind up in landfills, it is also likely that repeated washing in a chloride solution will have converted most of the Ag to the less reactive form.

Silver has been used since ancient times as a disinfectant. But only in the modern era have there been calls for its use to be regulated, whether by the U.S. Food and Drug Administration or the EPA. Some groups have petitioned the EPA to regulate ionic Ag nanoparticles as a pesticide. It is only by examining the properties of Ag species in real world conditions that regulators can ascertain whether Ag nanoparticles pose any real threat to aquatic resources or human health.

— Elise LeQuire

See > Christopher A. Impellitteri, Thabet M. Tolaymat*, and Kirk G. Scheckel, "The Speciation of Silver Nanoparticles in Antimicrobial Fabric Before and After Exposure to a Hypochlorite/Detergent Solution," J. Environ. Qual. **39**, 1528 (July-August 2009). DOI:10.2134/jeq2008.0390

Author affiliation >
U.S. Environmental Protection Agency, Cincinnati

Correspondence >
*tolaymat.thabet@epa.gov

 MR-CAT operations are supported by the Department of Energy and the MR-CAT member institutions. Use of the Advanced Photon Source is supported by the U.S. Department of Energy, Office of Science, Office of Basic Energy Sciences, under Contract No. DE-AC02-06CH11357.

> 10-ID • MR-CAT • Materials science, environmental science, chemistry • Microfluorescence (hard x-ray), x-ray absorption fine structure, diffraction anomalous fine structure, micro x-ray absorption fine structure • 3.3-cm Undulator A • Accepting general users

Electronic and Magnetic Structures of Hematite Post-Perovskite under Deep Planetary Conditions

IN SHORT > Iron compounds found on the surfaces of Earth and other terrestrial planets provide a paleomagnetic record that yields important clues to the history of the inner planets. Paleomagnetism was instrumental in uncovering seafloor spreading as the mechanism for tectonic plate movements on Earth, and iron compounds afford insight into magnetism deep in planetary interiors. Hematite (Fe_2O_3), for example, is proxy for iron in alloys in the core and silicates and oxides in the mantle. Using synchrotron Mössbauer spectroscopy (SMS) and x-ray diffraction (XRD) at two APS beamlines, researchers measured the electromagnetic properties of pure hematite (Fe_2O_3) at high pressure. It has been known that Fe_2O_3 undergoes a sequence of phase transitions at high pressure: from hematite to Rh2O3-II type (RhII), and then to post-perovskite (PPv). For iron, magnetic ordering is destroyed and then reconstructed, and electronic configuration changes from high-spin to low-spin and then about half converting back to high-spin. These results have implications for paleomagnetic studies at meteorite impact sites and geophysical applications for high-iron regions in deep planetary interiors.

MORE > To investigate the properties of the hematite at high pressures, the research team from the Massachusetts Institute of Technology, the University of Wisconsin, the University of Chicago, and Argonne exposed pure Fe_2O_3 to experimental pressures in a diamond-anvil cell. Analysis of the samples at the XOR 3-ID beamline and the GSECARS 13-ID beamline by synchrotron Mössbauer spectroscopy and x-ray diffraction was followed by theoretical first-principles calculations of Fe spin and magnetic states. The results show that Fe_2O_3 undergoes a structural transition from hematite to Rh2O3-II type (RhII) at 50 GPa and 300K. At this transition, magnetization is erased and the electron spin state collapses from high-spin (HS) to low-spin (LS). Laser heating at 73 GPa initiated the transition of RhII into postperovskite (PPv), which revived the magnetic ordering and reversed the spin from LS to HS of at least half of the Fe^{3+} ions. The Fe_2O_3 alters from a semiconductor to a metal (Fig. 1).

The behavior of Fe_2O_3 at high pressures can explain important geophysical observations. The weak magnetic field of Martian impact craters has been related to the demagnetization by the shocks of many impacts over time. However, this study reveals that, at least for hematite, the high temperatures and pressures generated by the impacts would trigger a sequence of changes in magnetic ordering rather than a monotonic decrease in magnetism.

In iron silicate and oxide phases at temperatures and pressures found in deep planetary interiors, recent studies revealed that the Fe transitions from HS to LS. However, this study demonstrated that the degree of spin pairing in the mantle may not increase monotonically with pressure and different environments for Fe in perovskite (PV) and PPv may result in a complicated pattern of spin state. The spin state change is particularly important because iron spin state affects physical properties such as density, optical properties, electrical conductivity, and element partitioning.

The evidence suggests that Fe_2O_3-PPv under lowermost mantle P-T conditions behaves as a metal. At the D″ layer, in the lowermost 200 to 400 km of Earth's mantle at the core-mantle boundary, the PPv has high electrical conductivity, which is important for the electromagnetic coupling between the mantle and core. The slight irregular motion of the planet, known as nutation, may be due to the metal-like electrical conductivity of the D″ layer.

— Dana Desonie

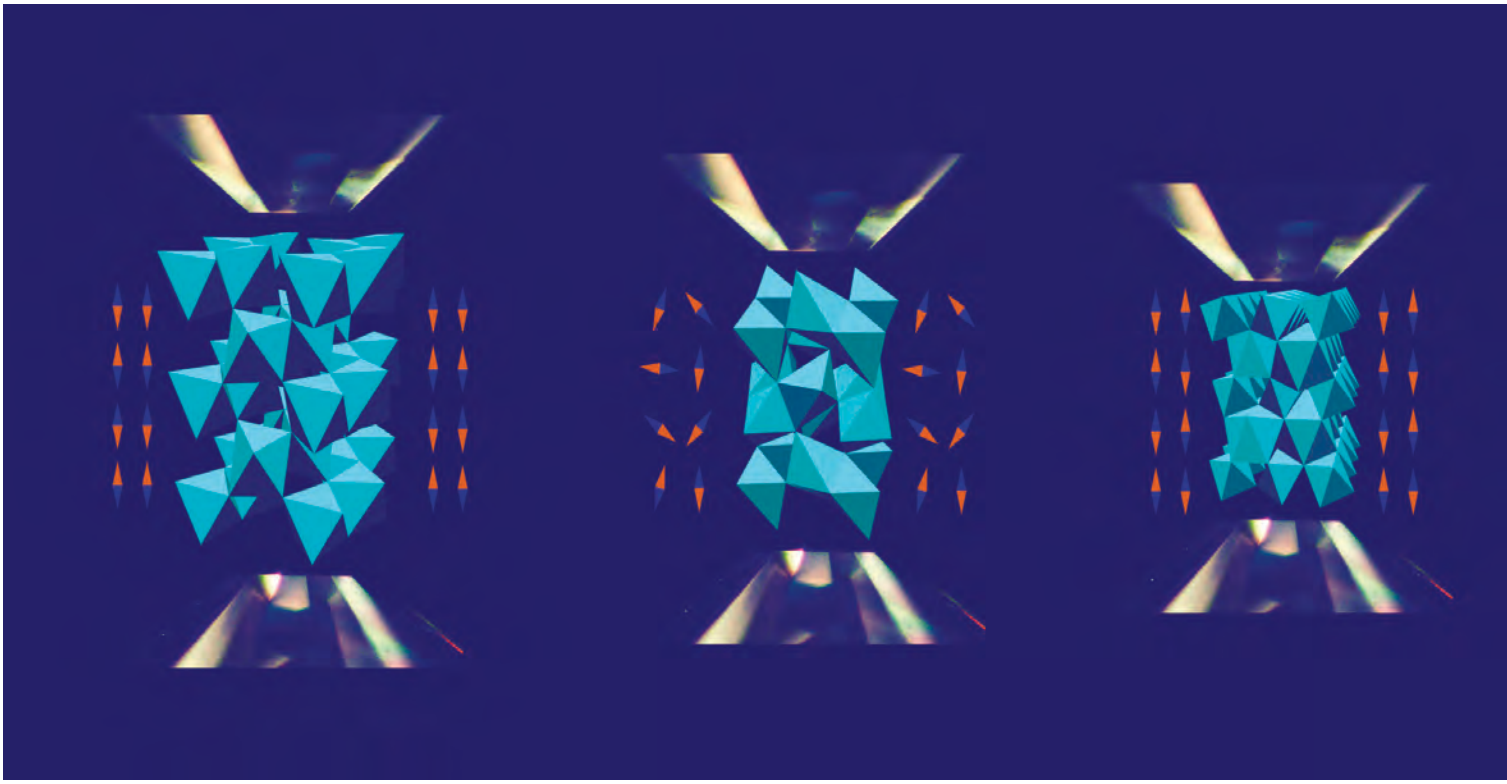

^ *Fig. 1* ***Left:*** *Hematite phase stable at 0-50 GPa.* ***Middle:*** *Rh2O3-II type phase stable at 50-70 and high temperature.* ***Right:*** *Post-perovskite phase stable at pressures above 70 GPa and high temperature.*

See > Sang-Heon Shim[1]*, Amelia Bengtson[2], Dane Morgan[2], Wolfgang Sturhahn[3], Krystle Catalli[1], Jiyong Zhao[3], Michael Lerche[3,4], and Vitali Prakapenka[5], "Electronic and magnetic structures of the postperovskite-type Fe_2O_3 and implications for planetary magnetic records and deep interiors," Proc. Natl. Acad. Sci. USA **106**(4), 5508 (April 7, 2009). DOI: 10.1073/pnas.0808549106

Author affiliations >
[1]Massachusetts Institute of Technology,
[2]University of Wisconsin,
[3]Argonne National Laboratory,
[4]Carnegie Institution of Washington,
[5]The University of Chicago

Correspondence >
*sangshim@mit.edu

> This work was supported by the National Science Foundation (NSF) Grants EAR0738655 (to S.H.S.) and EAR0738886 (to D.M.), respectively. K.C. is supported by a Department of Energy (DOE) National Nuclear Security Administration Stewardship Science Graduate Fellowship. GSECARS is supported by the NSF and DOE. Use of XOR 3-ID was supported in part by the Consortium for Materials Properties Research in Earth Sciences under NSF Cooperative Agreement EAR 06-49658. Use of the Advanced Photon Source was supported by the U.S. Department of Energy, Office of Science, Office of Basic Energy Sciences, under Contract No. DE-AC02-06CH11357.

> 3-ID • XOR • Physics, geoscience, life science, chemistry, materials science • Nuclear resonant scattering, high-pressure diamond anvil cell, inelastic x-ray scattering • 2.7-cm undulator (US), 2.7-cm undulator (DS) • Accepting general users

> 13-ID • GSECARS • Geoscience, environmental science • Microfluorescence (hard x-ray), microdiffraction, x-ray absorption fine structure, micro x-ray absorption fine structure, high-pressure diamond anvil cell, high-pressure multianvil press, inelastic x-ray scattering • 3.3-cm Undulator A • Accepting general users

Calcium and Heavy Metal Distribution in Fly Ash and Geopolymers

IN SHORT > Using fly ash to produce geopolymer concrete in place of limestone-derived Portland cement valorizes an abundant waste product and releases 80% less CO_2 into the atmosphere. To ensure safety when using waste materials to make concretes, and to better understand the formation of fly ash geopolymers, scientists mapped nanoscale elemental distributions in the ash by utilizing synchrotron x-ray fluorescence at the hard x-ray nanoprobe instrument on CNM/XOR beamline 26-ID at the APS. They found that the calcium distribution depends markedly on the pH of the geopolymer-forming system; chromium is bound to iron and is unlikely to problematically enter the environment.

MORE > To slow climate change, greenhouse gas emissions must be reduced in many different ways. Portland cement manufacturing currently produces 5% to 8% of anthropogenic greenhouse gas emissions worldwide, an amount that will expand as developing nations improve their infrastructures. Since nearly all of the Portland cement-derived CO_2 is due to the use of limestone in cement manufacture, researchers are seeking a replacement binder material that is widely available, inexpensive, durable, and environmentally sound. The need for such a binder is likely to explode as governments adopt climate change legislation.

Each year about 700 million tons of fly ash waste are produced from coal-fired electricity generation, and fly ash disposal is a large problem. Fly ash reacting with alkaline solutions creates a geopolymer that can be used as the binder in concrete. The resulting material is fire and acid resistant and does not have a high reaction heat. Most importantly, fly ash geopolymer cement emits around 80% less greenhouse gases than Portland cement.

While replacing a highly used commodity with a product that emits less climate-altering pollution and is made from abundant waste materials is obviously desirable, this is only true if the replacement product is safe to use. To look for any possible hazards from the use of fly ash and fly ash-derived geopolymers, researchers from the University of Melbourne, Universidad del Valle, and Argonne analyzed samples using the Hard X-ray Nanoprobe at 26-ID. Their research revealed the nanoscale elemental disposition in fly ash and in geopolymers activated with potassium silicate or hydroxide solutions, as determined by x-ray fluorescence mapping with nominal 30-nm spatial resolution.

v *Precast geopolymer concrete panels in use in residential construction in Melbourne, Australia. (Photographs courtesy of Zeobond Pty Ltd.)*

The hydroxide-activated fly ash contained regions a few tens of nanometers in size that were highly enriched in calcium, providing the first direct confirmation of the nucleation of $Ca(OH)_2$ precipitates in the solution. Calcium in the fly ash-potassium silicate geopolymer was more dispersed and was likely released in preference to iron from fly ash particles rich in both. These results have important implications for understanding the calcium chemistry within aluminosilicate geopolymer gel phases, which is key to controlling geopolymer permeability and durability.

Some fly ashes also contain measurable levels of heavy metals. Because leaching studies show that the most likely problems are due to species that form oxyanions, the researchers were particularly interested in chromium, which is highly mobile and toxic in its hexavalent form (CrO_4^{2-}), and can sometimes be present in fly ash. However, the x-ray fluorescence mapping shows that chromium in the fly ash appears to be bound as essentially immobile Cr^{3+} in ferrite spinel phases, which are relatively resistant to alkali attack during geopolymer synthesis. The use of a silicate activator can also minimize Cr extraction from the spinel phases. The researchers concluded that the likelihood of Cr being released problematically into the environment from the geopolymer is low, and potentially even lower than the possibility of it being released from the fly ash in a landfill.

— Dana Desonie

See > John L. Provis[1]*, Volker Rose[2], Susan A. Bernal[1,3], and Jannie S.J. van Deventer[1], "High-Resolution Nanoprobe X-ray Fluorescence Characterization of Heterogeneous Calcium and Heavy Metal Distributions in Alkali-Activated Fly Ash," Langmuir **25**(19), 11897 (2009). DOI: 10.1021/la901560h

Author affiliations >
[1]University of Melbourne,
[2]Argonne National Laboratory,
[3]Universidad del Valle

Correspondence >
jprovis@unimelb.edu.au

> This work was funded by the Australian Research Council (ARC), including partial funding from the Particulate Fluids Processing Centre, a Special Research Centre of the ARC, and through Discovery Project grants. The work of S.A.B. was supported by travelling scholarships from Colciencias and from the Walter Mangold Trust. Travel funding for J.L.P. was supplied by the Australian Synchrotron Research Program. Use of the Center for Nanoscale Materials and the Advanced Photon Source at Argonne National Laboratory was supported by the U.S. Department of Energy, Office of Science, Office of Basic Energy Sciences, under Contract No. DE-AC02-06CH11357.

> 26-ID • CNM/XOR • Materials science, physics • Microdiffraction, microfluorescence (hard x-ray), tomography • 3.3-cm Undulator A (US), 3.3-cm Undulator A (DS) • Operational

Pumping through the Middle Crust

IN SHORT > The movement and behavior of fluid—generally water, sometimes other types—is a prime factor in geological processes including earthquake nucleation, mantle degassing, and the formation of mineral deposits. The workings of fluid transfer in Earth's middle crust have been controversial and not well understood, although it has been clear that they are associated with shear zones where rock deforms viscously. When it comes to fluid migration, the middle crust is different from other crustal regions because it is generally thought to be both too hot and too viscous to allow fluid to pass through fractures. A team of geologists and geophysicists using the XOR 2-BM and 32-ID beamlines at the APS has shed light on a fluid transfer in the middle continental crust, a phenomenon that was formerly poorly understood. Their work could lead to a fuller understanding of fluid migration through rock, with possible wide application in deciphering important geological processes including earthquakes.

MORE > Researchers from the University of Western Australia, CSIRO Exploration & Mining, and Argonne have confirmed that a phenomenon called "creep cavitation" is instrumental in the deformation of rock and the creation of porosity that allows fluid to permeate into these mid-crustal shear zones, ultimately leading to large-scale structural weaknesses that can cause fault slippage, and even slow earthquakes. The team has developed a model for a granular fluid pump driven by stress gradients and chemical potentials on the grain scale that can move fluid through rocks deforming at mid-crustal conditions.

The research team used synchrotron x-ray microtomography at the 2-BM beamline to study a characteristic rock sample collected from the Redbank midcrustal shear zone in Central Australia (Fig. 1). Examining 55-mm-sized rock cubes culled from various points of a rock hand specimen, the team was able to visualize the structure of all pores larger than 1.3-μm in diameter. They could thus obtain a detailed picture of the porosity architecture of the entire rock sample.

The rock sample covered a strain gradient, allowing study and comparison of the evolution of porosity from the low- to high-strain regions. This strain gradient was traced by the microstructural transformation of the rock from a gneiss to a mylonite: low-strain regions are largely characterized by grains of K-feldspar and plagioclase minerals (hundreds of microns in diameter) interlayered with quartz bands, while towards the more deformed areas, this microfabric of the rock gives way to a finer-grained (>10 μm) homogenized mylonite pattern. The reduction in grain size in the high-strain areas of the sample shows that this rock was progressively softened as it deformed, and the gradual disappearance of K-feldspar and plagioclase indicates that they were dissolved and their chemical components redistributed through the rock by a fluid at the same time.

For the researchers, this realization pointed the way to their "granular fluid pump" model. Micron-scale grains in the high-strain regions of the rock slide past each other under stress, in a process called viscous grain-boundary sliding (VGBS). As this happens, pores open up while others close in the rock structure, to accommodate incompatibilities that arise between neighboring grains. This mechanism is called creep cavitation, and has been observed in some ceramic and metallic materials. In the middle crust, fluid moves from the closing to the opening pores as the fluid pressure changes from pore to pore during creep cavitation. This mechanism is supported by chemical reactions between the fluid and the minerals forming the rock; as minerals get dissolved in, or precipitated from the fluid, the fluid pressure changes locally. The resulting granular fluid pump is self-sustaining and steady as long as grains slide past each other, and creep cavitation occurs. The experimenters speculate that aside from affecting rock deformation on the small scale, the same combination of processes—creep cavitation and the granular fluid

^ *Fig. 1 The rock outcrop west of Alice Springs, central Australia, where the hand specimen was collected. The outcrop is characterized by a shear zone (from bottom left to upper right corner of the image) that formed in about 15-km depth in the middle continental crust. The rock specimen, which can be seen in the centre of the image still in-situ, covers the low-strain margin and high-strain centre of the shear zone.*

pump could—on a greater scale, influence phenomena such as fault slippage and slow earthquakes.

The work represents the first time that x-ray synchrotron tomography has been used to visualize porosity in a mid-crustal shear zone rock at such small scale. The x-ray tomography allowed the researchers to clearly follow the evolution of the porosity of the sample during rock deformation and quantify it with great precision, making synchrotron tomography the perfect technique for investigating porosity in crystalline rocks.

Using this technique, the researchers have managed to shed light on a phenomenon that was formerly poorly understood and to develop a model with possible wide application. The team believes that their granular fluid pump applies to many tectonic settings and explains fluid transfer in specific rock types quite well, and is, as such quite significant.

Fusseis and his team plan to expand upon the work by examining further mid-crustal shear zone samples at even finer resolutions of approximately 35 nm at the XOR 32-ID beamline. Along with the collection of this more detailed data, and comparison and study of different samples from other parts of the world, the researchers hope to use the micro- and nanotomography capabilities of the APS to observe porosity formation in real-time controlled experiments. This multipronged approach will lead to a better understanding of the highly complex and sometimes mysterious workings of the Earth's middle crustal zones.

— Mark Wolverton

See > F. Fusseis[1,3]*, K. Regenauer-Lieb[1,2,3], J. Liu[2], R.M. Hough[2], and F. De Carlo[3], "Creep cavitation can establish a dynamic granular fluid pump in ductile shear zones," Nature **459**, 975 (18 June, 2009). DOI: 10.1038/nature08051

Author affiliations >
[1]The University of Western Australia,
[2]CSIRO Exploration & Mining,
[3]Argonne National Laboratory

Correspondence >
*fusseis@cyllene.uwa.edu.au

> This work was supported by the Australian Synchrotron Research Program, which is funded by the Commonwealth of Australia under the Major National Research Facilities Program; the Western Australian Premier's Research Fellowship program and the University of Western Australia through a research grant; iVEC through the use of visualization resources and expertise provided by the WASP and ARRC facilities; and the Centre for Microscopy, Characterization and Analysis at the University of Western Australia for the use of its FESEM. Use of the Advanced Photon Source at Argonne National Laboratory was supported by the U.S. Department of Energy, Office of Science, Office of Basic Energy Sciences, under contract number DE-AC02-06CH11357.

> 2-BM • XOR • Physics, life science • Phase-contrast imaging, tomography, microdiffraction, general diffraction • Bending magnet • Accepting general users

> 32-ID • XOR • Materials science, life science • Phase-contrast imaging, ultra-small-angle x-ray scattering, radiography • 3.3-cm Undulator A • Accepting general users

Number of Walls, not Diameter, Determines Plasmon Behavior in Carbon Nanotubes

IN SHORT > The existence of carbon nanotubes was posited as early as the 1950s, but it has taken several generations of imaging advances to begin to understand the structure and properties of these nanomaterials, which exhibit extraordinary strength—several times that of steel—and a wide range of conductivity from metallic to semiconducting. They show great promise for use in solar cells, fuel cells, and medical delivery systems. A team of researchers has solved one question about plasmon behavior in carbon nanotubes that may be key in controlling the electronic length scale of these materials. Using two powerful and complementary instruments, electron energy loss spectroscopy (EELS) and inelastic x-ray scattering (IXS), the researchers teased out from three physical parameters—diameter, number of walls, and chirality—the single factor that may allow tailoring the properties of carbon nanotubes for useful optical applications.

MORE > Single-walled carbon nanotubes (SWCNT) are formed when a thin sheet of graphite with hexagonal lattice structure somewhat like chicken wire is rolled into a cylinder. Multi-walled carbon nanotubes (MWCNT) consist of two or more SWCNTs nestled one inside the other, and have been compared to Russian dolls. Previous probes of plasmon behavior using EELS seemed to suggest that shifts in the $\pi + \sigma$ plasmon energies occurred as the number of walls and the diameter of the nanotubes increased, but until now no one has shown whether the shift is related to the diameter or the number of walls. This study did not directly address the effect of chirality, but ruled it out as a factor because nanotubes with different diameters had identical plasmon energies and the chiral angle, or degree of twist of the cylinder, is extremely unlikely to be the same in different nanotubes.

The researchers in this study—from Argonne, the University of Illinois, Brookhaven National Laboratory, and Oak Ridge National Laboratory—measured EELS spectra from individual, double-walled CNTs measuring 14-nm, 7.2-nm, and 3.6-nm in diameter. A distinct shift of the $\pi + \sigma$ plasmon energies relative to graphite occurred at around 18 eV, a shift that was identical no matter the diameter of the tubes. Therefore,the research team ruled out diameter as a factor affecting plasmon energy, at the relatively large size scale in this study. These results apply only to nanotubes of a sufficiently large diameter.

The team then measured EELS spectra at Brookhaven National Laboratory (BNL), to individual nanotubes with two, three, five, and six walls, and samples of bulk graphite, and compared the plasmon peak energies as the number of walls varied. By observing the shift in the plasmon energy with the number of walls, changes in the strength of the screening (and, hence, the effective interactions at interatomic distances) can be determined.

While EELS is a powerful tool to examine individual CNTs, IXS is superior in measuring the momentum dependence of an array of nanotubes, though because of its low signal rates it cannot be used to probe individual nanotubes. To determine the momentum dependence of the plasmon shift, the team turned to IXS performed at XOR/CMC beamline 9-ID at the APS. The research team used few-walled (FW) and multi-walled (MW) CNT arrays grown on a silicon substrate and aligned in one orientation. Because the tubes were loosely packed, and therefore not prone to strong interactions, their behavior can be interpreted as that of single nanotubes (Fig. 1).

IXS verified the EELS findings that momentum of $\pi + \sigma$ plasmon energies differs in nanotubes with just two to three walls from those with 5 to 14 walls, with higher

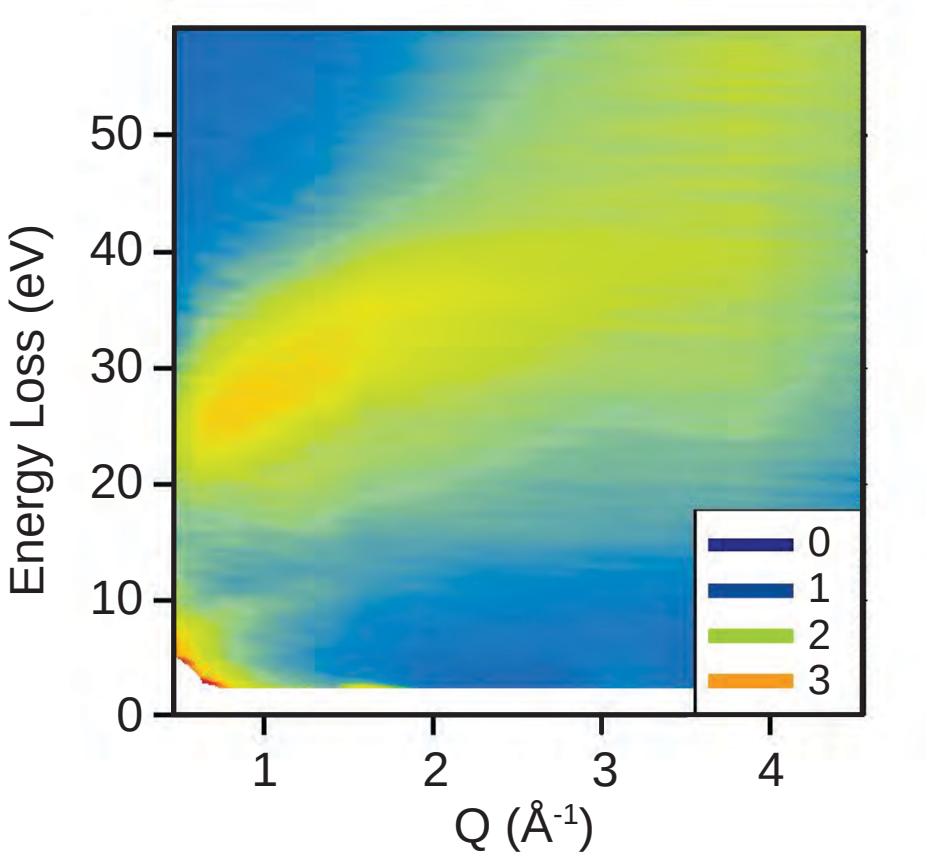

^ *Fig. 1 Inelastic x-ray scattering spectra from the few-walled carbon nanotube sample, as a contour plot.*

energies for the π + σ in graphite, lower energies in MWCNT, and lowest energies in FWCNT; that is, the fewer the walls, the lower the plasmon energies.

By chemically manipulating the number of walls, we may be one step closer to harnessing the energy of the sun via solar cells here on Earth.

— Elise LeQuire

See > M.H. Upton[1]*, R.F. Klie[2], J.P Hill[3], T. Gog[1], D. Casa[1], W. Ku[3], Y. Zhu[3], M.Y. Sfeir[3], J. Misewich[3], G. Eres[4], D. Lowndes[4], "Effect of number of walls on plasmon behavior in carbon nanotubes," Carbon **47**, 162 (2009). DOI: 10.1016/j.carbon.2008.09.044

Author affiliations >
[1]Argonne National Laboratory,
[2]University of Illinois,
[3]Brookhaven National Laboratory,
[4]Oak Ridge National Laboratory

Correspondence >
*mhupton@aps.anl.gov

> Work performed at BNL was supported by the U.S. Department of Energy, Division of Materials Science and Engineering, under Contract No. DE-AC02-98CH10886 and partially by DOE-CMSN. The contribution by GE and DHL was supported by the Division of Materials Sciences and Engineering, Basic Energy Sciences, U.S. Department of Energy, under Contract No. DE-AC05-00OR22725. The contribution by G.E. and D.H.L. was supported by the DMSE, under Contract No. DE-AC05-00OR22725. Use of the Advanced Photon Source at Argonne National Laboratory was supported by the U.S. Department of Energy, Office of Science, Office of Basic Energy Sciences, under Contract No. DE-AC02-06CH11357.

> 9-ID • XOR/CMC • Physics, materials science • Liquid scattering, inelastic x-ray scattering, resonant inelastic x-ray scattering • 3.3-cm Undulator A • Accepting general users

Tailoring Catalytic Systems: Platinum Nanoparticles on a Metallic Oxide Nanocubes

IN SHORT > The noble metal platinum (Pt) is widely recognized for its utility in achieving the high catalytic performance and reduction of toxic emissions desired in fuel cells, environmental remediation technologies, and production of liquid fuels. Like other noble metals, however, Pt is rare and expensive. For catalytic systems to become more efficient and economically viable, the amount of Pt needs to be minimized and a clearer understanding of the surface morphology and catalytic efficiencies of those systems must emerge. Using a suite of tools available at the APS—scanning electron microscopy (SEM), small- and wide- angle x-ray scattering (SAXS and WAXS), near-edge spectroscopy (XANES), and extended x-ray absorption fine structure (EXAFS)—a team of researchers from Northwestern University and Argonne has explored the dispersion, size, shape, chemical state, and local atomic coordination of Pt nanoparticles on nanocubes of the metal oxide strontium titanate ($SrTiO_3$: STO), adding to our understanding of catalytic systems.

MORE > In the synthetic manufacture of this heterogeneous catalytic system, organometallic vapors of Pt are deposited over a number of cycles, layer by layer, on metal oxide substrates through a process called atomic layer deposition (ALD). After hundreds of cycles of ALD, a thin, continuous film coats the support structure, but the initial phases, from 1 to 5 cycles of ALD, have remained unexplored. This early stage of ALD is optimal for catalyst synthesis with efficient platinum loading.

In this study, uncoated, nonporous STO nanocubes with an edge length of 60 nm and a high surface-area-to-volume-ratio were subjected to 1 through 5 cycles of ALD of Pt. SEM images following three cycles of ALD revealed Pt nanoparticles 2 to 3 nm in size uniformly dispersed on all exposed surfaces of the cubes approximately 4 to 8 nm apart (Fig. 1).

With each successive cycle of ALD, the Pt nanoparticles began to coalesce, and the center-to-center spacing between them increased, as revealed by the SAXS data, resulting in a linear dispersion ranging from 3.5 to 6.3 nm apart. Following 2 to 5 cycles of ALD, WAXS probes showed that the nanoparticles grew larger in a linear fashion, from 1.0 to 2.7 nm. Particle size with one cycle of ALD was extrapolated to be about 0.7 nm, though the size could, in fact, be smaller.
In addition, the chemical state of the Pt particles changed, as revealed by XANES data, shifting from an oxidated state with one and twocycles, to a bulk metallic state with further ALD cycles as the Pt-O bond weakened and the relative numbers of Pt-Pt bonded particles increased. The data were collected at the DND-CAT 5-BM-D and 5-ID beamlines, and the XOR/BESSRC 12-ID beamline.

Of particular interest was the observation that Pt loading—the amount of material adhering to the STO nanocubes—was unexpectedly low. An earlier study estimated that for Pt nanocatalysts used in the production of direct methanol fuel cells to become economically feasible in the market place, the loading must be on the order of 1 mg cm^{-2}. Pt loading in this study was 1.1×10^{-3} mg cm^{-2} after five ALD cycles, which was consistent with earlier observations of efficient Pt loading on high-surface-volume carbon aerogel substrates.

Controlling the growth of noble-metal nanoparticles on oxide substrates is crucial to improving the efficiency, and lowering production cost, of heterogeneous catalytic

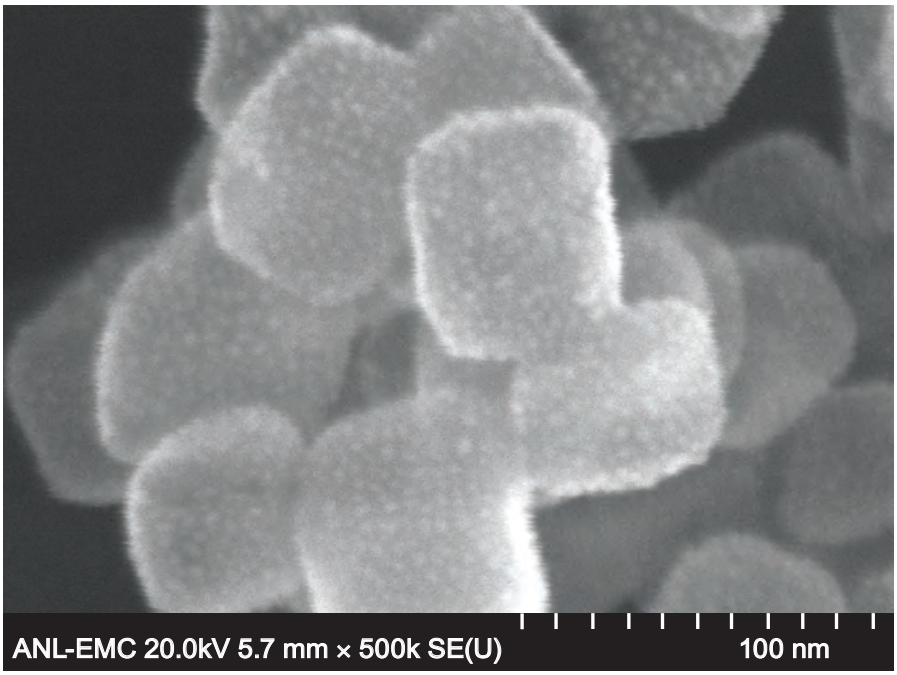

^ *Fig. 1 The scanning electron micrograph shows 2-nm platinum clusters grown by atomic layer deposition on strontium titanate nanocubes that measure 60 nm on an edge.*

process with applications in energy conservation and environmental remediation. X-ray probes at the nanoscale bring us one step closer to understanding the surface morphology and chemical properties of these systems.

— Elise LeQuire

See > Steven T. Christensen[1], Jeffrey W. Elam[2], Federico A. Rabuffetti[1], Qing Ma[1], Steven J. Weigand[1], Byeongu Lee[2], Soenke Seifert[2], Peter C. Stair[1], Kenneth R. Poeppelmeier[1], Mark C. Hersam[1], and Michael J. Bedzyk[1]*, "Controlled Growth of Platinum Nanoparticles on Strontium Titanate Nanocubes by Atomic Layer Deposition" Small **5**(6), 750 (2009).

Author affiliations >
[1]Northwestern University,
[2]Argonne National Laboratory

Correspondence >
*bedzyk@northwestern.edu

> This work was supported by the Institute for Catalysis in Energy Processes, Northwestern University (NU) (U.S. Department of Energy Grant DE-FG02-03ER15457) and by facilities support from the NU Materials Research Center (National Science Foundation MRSEC Grant DMR-0520513).DND-CAT is supported in part by: E. I. DuPont de Nemours & Co., Dow Chemical Co., and the State of Illinois. Electron microscopy was performed at ANL's Electron Microscopy Center for Materials Research. Use of the Advanced Photon Source was supported by the U.S. Department of Energy, Office of Science, Office of Basic Energy Sciences, under Contract No. DE-AC02-06CH11357.

> 5-BM-D • DND-CAT • Materials science, polymer science • High-energy x-ray diffraction • x-ray absorption fine structure • Bending magnet • Accepting general users

> 5-ID • DND-CAT • Materials science, polymer science • Powder diffraction, small-angle x-ray scattering, surface diffraction, wide-angle x-ray scattering, x-ray optics development/techniques, x-ray reflectivity, x-ray standing waves • 3.3-cm Undulator A • Accepting general users

> 12-ID • XOR/BESSRC • Chemistry, physics, materials science • Small-angle x-ray scattering, wide-angle x-ray scattering, grazing incidence small-angle scattering, surface diffraction • 3.3-cm Undulator A • Accepting general users

Self-Assembling, Polymer-Grafted Nanoparticles Lead to Unique Nanocomposites

IN SHORT > Nanocomposites typically consist of nanoparticles embedded within a matrix material, such as a polymer. Nanocomposites have elicited considerable interest because of their potential to synergistically combine the properties of both their organic and inorganic constituents, with favorable consequences for applications—for instance, using polymers in the creation of biomimetic materials that mimic those found in nature. To achieve these potential property gains from such nanocomposites, scientists must have the ability to control the spatial distribution of nanoparticles in a desired matrix. To date, there has been little progress in this field. Researchers using the XOR 32-ID beamline at the APS have derived results that address this significant challenge and present a novel strategy to achieve control over the nanoparticle spatial distribution.

MORE > The investigators chose spherical silica nanoparticles with a nominal diameter of 14 nm. Earlier research had shown that when such nanoparticles are dispersed within a liquid polymer they tend to clump together. It had been suggested that such clumping could be prevented if polystyrene chains were attached to the silica nanoparticles, thus shielding the hydrophilic particle core from the hydrophobic matrix. Instead, these researchers found that the resulting hybrid particles—consisting of molecular polystyrene chains grafted onto silica nanoparticles—exhibited amphiphile-like (or soap-like) behavior. The grafted nanoparticles assembled into a variety of nanostructures that reflected the relative ratio of the hydrophilic to hydrophobic domains. Notably, the polystyrene-grafted silica particles were, like the core silica particles themselves, spherical in shape; yet the grafted silica particles could spontaneously assemble into anisotropic (i.e., nonspherical) structures when mixed into the polymer matrix.

Ultra-small-angle x-ray scattering (USAXS) and transmission electron microscopy (TEM) were the two principal methods employed for determining the resulting nanoparticle superstructures (Fig. 1). The USAXS measurements, carried out at the 32-ID beamline of the APS, extended the TEM results spatially since the x-ray technique has a larger field of view, and hence can image larger structures than can the TEM device. Taken together, the USAXS and TEM measurements determined that the nanocomposite samples contained one of four distinct types of self-assembled microscopic structures: compact objects with spherical or "platelet-like" shapes; sheets and interconnected objects; short strings; and isolated particles.

The various structures observed by the USAXS and TEM techniques resulted from the way in which the nanocomposite was prepared. In the nanocomposite samples, some parameters were fixed, while others were varied. For example, in one set of experimental trials the molecular mass of the polystyrene matrix, as well as the total annealing time (five days), were both held constant, while the numbers and molecular weights of the grafted polystyrene chains were varied. Using such techniques, researchers observed the range of nanocomposite structures described above, including spherical clusters of nanoparticles, nanoparticle sheets (both thin and thick), and string-like structures.

Another important finding was that most of the nanocomposite samples demonstrated time-dependent structures, meaning that continued exposure to annealing and high-vacuum conditions changed the sizes of the various nanoparticle structures. It was also determined that mechanical stressing changed the characteristics of some of the nanocomposite samples.

The researchers demonstrated that the nanocomposite structure can be controlled by varying a number of parameters, including annealing time, mechanical processing,

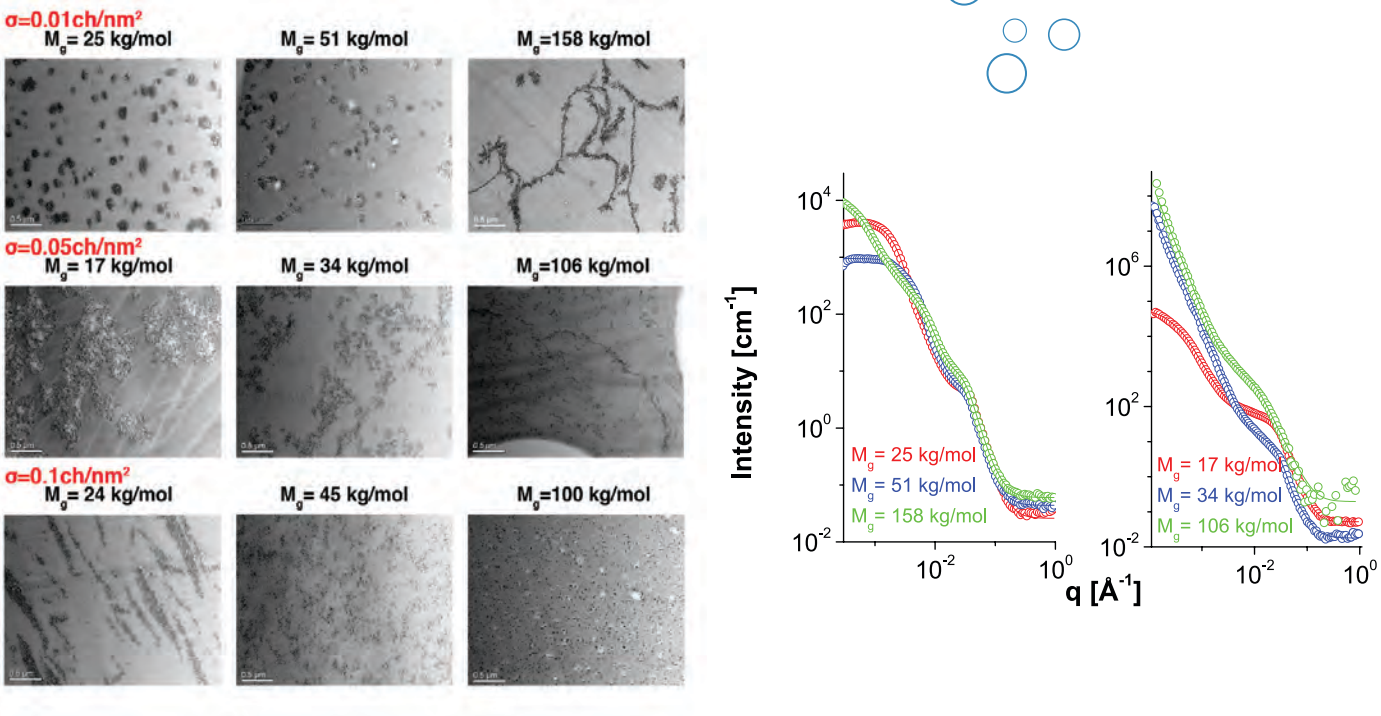

^ *Fig. 1* ***Left:*** *TEM-determined morphologies for several nanocomposites, where the polystyrene matrix molecular weight is fixed at 142 kg/mol. The polystyrene graft chain length (Mg) and grafting density (Greek sigma) are the variables. The samples were cast at room temperature and then annealed for five days at 150° C before sampling.* ***Right:*** *The USAXS data are for the samples represented in the top two rows of the TEM images, and corroborate the TEM results.*

grafting-chain density and chain molecular mass, and the molecular mass of the polymer matrix. Hence, it can be expected that a variety of useful properties can be fine-tuned when producing these unique and promising types of self-assembling nanocomposites.

— Philip Koth

See > Pinar Akcora[1], Hongjun Liu[1], Sanat K. Kumar[1]*, Joseph Moll[1], Yu Li[2], Brian C. Benicewicz[2], Linda S. Schadler[3], Devrim Acehan[4], Athanassios Z. Panagiotopoulos[5], Victor Pryamitsyn[6], Venkat Ganesan[6], Jan Ilavsky[7], Pappanan Thiyagarajan[7], Ralph H. Colby[8] and Jack F. Douglas[9] "Anisotropic self-assembly of spherical polymer-grafted nanoparticles," Nat. Mater. **8**, 354 (April 2009). DOI: 10.1038/nmat2404

Author affiliations >
[1]Columbia University, [2]University of South Carolina, [3]Rensselaer Polytechnic Institute, [4]New York University School of Medicine, [5]Princeton University, [6]University of Texas, [7]Argonne National Laboratory, [8]Pennsylvania State University, [9]National Institutes of Standards and Technology

Correspondence >
*sk2794@columbia.edu.

> This work was supported by the National Science Foundation (NSF) through the Division of Materials Research, DMR-0804647 (S.K.K.), a Nanoscale Science and Engineering Center, NSF Award Number DMR-0642573 (P.A., S.K.K., Y.L., B.C.B., and L.S.S.), and a Materials Research Science and Engineering at Princeton (A.Z.P.). D.A. is a member of the New York Structural Biology Center, which is a STAR Center supported by the New York State Office of Science, Technology, and Academic Research. V.G. and V.P. acknowledge partial support from the Welch Foundation, the U.S. Army Research Office under Grant No. W911NF-07-1-0268, and funds made available through the CONTACT program from AFOSR. Use of the Advanced Photon Source was supported by the U.S. Department of Energy, Office of Science, Office of Basic Energy Sciences, under Contract No. DE-AC02-06CH11357.

> 32-ID • XOR • Materials science, life science • Phase-contrast imaging, ultra-small-angle x-ray scattering, radiography • 3.3-cm Undulator A • Accepting general users

Growing Nanowires from Supercooled Liquid Nanodroplets

IN SHORT > The creation of nanowires constitutes a highly active area of research within the field of nanotechnology. Better techniques for producing nanowires could lead to improvements in a variety of devices including batteries, photovoltaic cells, gas sensors, and photonic crystals. Currently, several popular techniques used to make nanowires require a catalyst in order to synthesize the nanowires onto a substrate. The researchers in this study used relatively simple techniques to produce nanowires without a catalyst. Moreover, the researchers created their nanowires in a variety of sizes and from different metal oxides. In order to obtain real-time data detailing their nanowires' formation under varying conditions, the researchers utilized the grazing incidence small-angle x-ray scattering (GISAXS) technique at the XOR/BESSRC 12-ID beamline at the APS. The GISAXS data (Fig. 1) revealed real-time formation of nanowires from supercooled liquid nanodroplets formed by the condensation of metal oxide vapor.

MORE > As a first step, the researchers, from the University of California, Santa Barbara; Argonne; and Yale University heated metal oxide powder in a specially-made oven. Though nanowires were ultimately created using several different kinds of metal oxides, vanadium oxide was the sole material chosen for the GISAXS imaging. The oven contained an internal heater and a pair of ports to allow passage of synchrotron x-rays. In a series of experiments, vanadium oxide powder was heated to between 550 and 650˚C. The vaporized vanadium oxide subsequently condensed inside the oven on a thin film of silicon dioxide (SiO_2) overlaying a substrate of silicon (Si). In all cases either a reducing gas (helium) or oxidizing gas (oxygen) was blown over the heated metal oxide powder. A reducing environment (helium) within the furnace resulted in VO_2 crystallites (including nanowires), while oxidizing conditions lead to V_2O_5 nanowire formation.

In the GISAXS experiments carried out at the 12-ID beamline, an intense 8-keV x-ray beam impinged upon the SiO_2/Si substrate at a shallow angle of 0.15˚, which is just above the critical angle for total external reflection. The incident x-ray beam was both reflected and scattered from the sample material, and subsequently attenuated via a rod-shaped beam stop. The diffuse x-ray scattering from the sample was recorded using a two-dimensional charge-coupled device camera.

By quantitatively analyzing both horizontal and vertical cuts of the resulting GISAXS patterns, the sizes and shapes of the evolving nanostructures could be characterized over time. The GISAXS data revealed a process of nanowire formation in which vaporized metal oxide settled upon the SiO_2/Si substrate, forming nanodroplets of varying sizes. The liquid nanodroplets were supercooled because they existed at temperatures below the bulk melting point for vanadium oxide. The nanowires that formed and grew on the substrate did so largely by absorbing material from the supercooled liquid nanodroplets either through coalescence (merging), or through a process known as Ostwald ripening. Named for German chemist Wilhelm Ostwald who first described the phenomenon in 1896, Ostwald ripening involves the accretion of material into larger precipitates at the expense of smaller ones, which shrink. Real-time GISAXS imaging showed that nanostructure growth occurred more rapidly, and was much more complex, at a growth temperature of 600˚C versus those grown at 550˚C.

After a maximum of 30 min., the samples were quickly cooled. The solidified nanostructures were examined using scanning electron microscopy (SEM), and in some cases other techniques. The SEM images reinforced the GISAXS results indicating Ostwald ripening of both nanowires and nanodroplets.

The SEM micrographs also strongly linked nanostructure growth to the properties of their substrates. For instance, in a few experiments, sapphire was used as a substrate; post-cooling SEM images showed preferential nanowire growth along a line defect at the sapphire surface.

Experiments with oxides of molybdenum and ruthenium were also performed by the researchers, but without the real-time data provided by GISAXS. Instead, post-cooling analysis used SEM and other methods to confirm the existence of nanowires similar to those made of vanadium oxide produced in the GISAXS experiments.

This research demonstrated several straight-forward techniques for producing a variety of crystalline metal oxide nanowires from supercooled liquid nanodroplets without the need for catalysts. Real-time GISAXS data, corroborated by SEM images, revealed that the phenomenon of Ostwald ripening was a major factor contributing to growth of both nanodroplets and nanowires. SEM images also indicated a strong correlation between nanowire growth and the properties of its substrate. The researchers have confidence that their ability to synthesize a variety of metal oxide nanowire systems clearly demonstrates both the simplicity and generality of the new techniques.

— Philip Koth

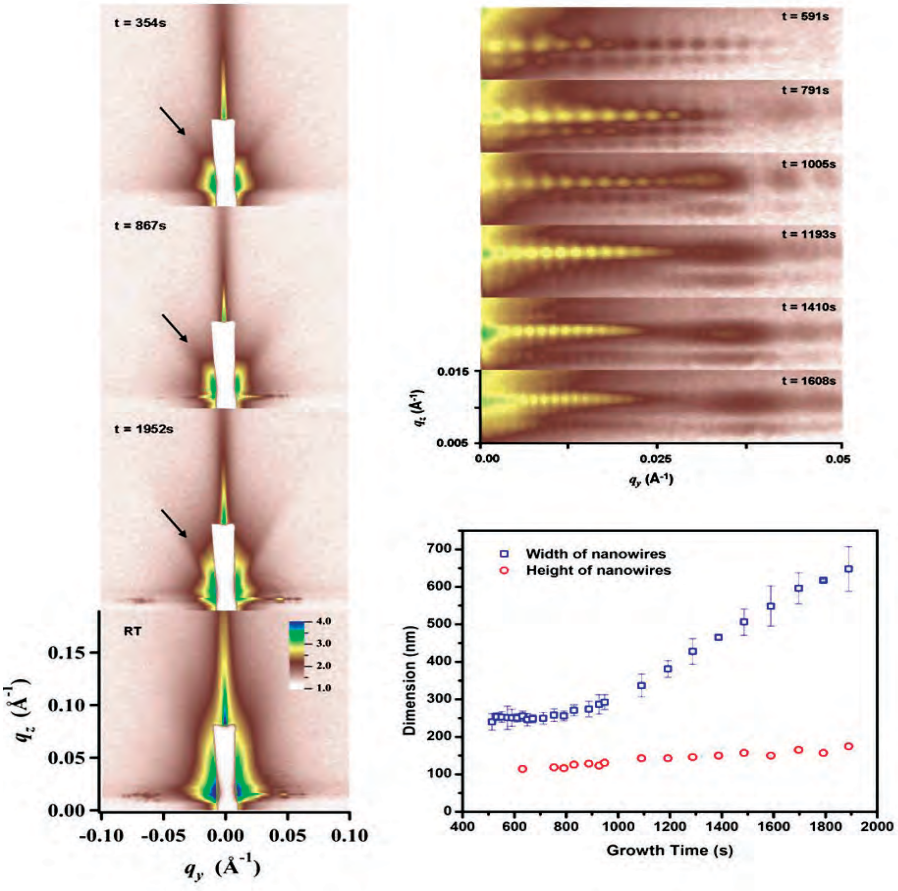

^ *Fig. 1 Real-time snapshot dynamics of the VO_2 nanowire growth at 600° C. (a) A series of GISAXS images of VO_2 nanowire growth acquired at various times during* ***in situ*** *experiments at 600° C under atmospheric pressure. Arrows represent the Bragg-rod scatterings originating from nanodroplets. (b)* ***In situ*** *GISAXS fringe patterns of the nanowire growth measured at different growth times for 600° C, showing that the spacing is gradually narrower with growth time. (c) The growth time dependence of the average width and height for nanowires extracted from the analysis of fringe patterns for 600° C. (Copyright © 2009 American Chemical Society)*

See > Myung Hwa Kim[1], Byeongdu Lee[2], Sungsik Lee[2], Christopher Larson[1], Jeong Min Baik[1], Cafer T. Yavuz[1], Sönke Seifert[2], Stefan Vajda[2,3], Randall E. Winans[2], Martin Moskovits[1], Galen D. Stucky[1,*], and Alec M. Wodtke[1,**], "Growth of Metal Oxide Nanowires from Supercooled Liquid Nanodroplets," Nano Lett. **9**(12), 4138 (2009). DOI: 10.1021/nl902357q

Author affiliations >
[1]University of California, Santa Barbara; [2]Argonne National Laboratory; [3]Yale University

Correspondence >
*stucky@chem.ucsb.edu
**wodtke@chem.ucsb.edu

> This work was supported by the Partnership for International Research and Education – for Electronic Chemistry and Catalysis at Interfaces – National Science Foundation Grant No. OISE-0530268. The work at the APS was supported by the U.S. Department of Energy, BES-Chemical Sciences, and BES Scientific User Facilities under Contract No. DE-AC-02-06CH11357.

> 12-ID • XOR/BESSRC • Chemistry, physics, materials science • Small-angle x-ray scattering, wide-angle x-ray scattering, grazing incidence small-angle scattering, surface diffraction • 3.3-cm Undulator A • Accepting general users

Structure of Quantum Dots Revealed

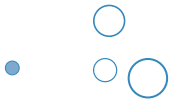

IN SHORT > Tiny semiconductor crystals 10 to 50 atoms across called quantum dots (QDs) promise to enable quantum computing and revolutionize photovoltaic cells, light-emitting devices, and many other applications because it should prove possible to tune their optoelectronic properties with unprecedented precision by carefully controlling their size, shape, composition, and strain characteristics. The day when scientists will actually be able to accomplish all this just got much closer, thanks to a breakthrough by researchers aided by the XOR/UNI 33-ID beamline at the APS. The group demonstrated the ability to construct three-dimensional (3-D) atomic-scale maps of these tiny bits of next to nothing that detail their structural and chemical compositions quantitatively. The new atomic-scale maps will let scientists measure the locations and chemical makeup of individual components of quantum dots at a resolution of 100th of a nanometer, thereby clearing the path to more rapid progress in the field of quantum-dot directed assembly.

MORE > The researchers, from the University of Michigan, Soreq NRC, and Hebrew University, studied QDs crystallized from indium (In) droplets exposed to antimony (Sb) as the QDs were deposited on a gallium arsenide (GaAs) (100) substrate. Measurements of the QD structures were performed in Bragg rod geometry on the 33-ID undulator beamline, which provides a highly intense, tunable beam of x-rays. The Bragg rod data were analyzed using coherent Bragg rod analysis (COBRA)—an x-ray phase retrieval method specific to epitaxial systems. The method consists of measuring diffraction intensities along the substrate-defined Bragg rods, analyzing the results to determine the diffraction phases, and then performing Fourier transformations of the resulting complex scattering factors to map the full 3-D electron density map, from which one can obtain key parameters such as chemical composition, stacking, strain, and dot shape. The method is generally applicable to any epitaxial QD system.

The researchers found that the QDs form coherently and extend a few unit cells below the GaAs surface. Their most interesting observation was that the GaAs content is qualitatively similar deep in the substrate and in the dots. This shows that the dots are not simply composed of In and Sb; their cores are practically pure GaAs. Also evident from the energy dependence of the x-ray scattering cross sections was a high concentration of InAs at the substrate–dot interface. The researchers were able to tell that the interfacial InAs was associated with the top unit cell of the substrate and not with the dots themselves. Similarly, the x-ray energy dependence of the cross sections provided a quantitative determination of the Sb content, which the researchers associated with an outer GaSb shell.

Much of this can be seen from Fig. 1, which depicts electron density profiles measured normal to the substrate surface through lines of Group III (top) and Group V (bottom) sites in the zinc-blende structure. The peaks to the left represent atoms in the substrate; those to the right correspond to the QD. The profiles are shown at the Ga-edge (red line) and As-edge (blue line) x-ray photon energies, in units of effective atomic number.

This work provides the first atomic-scale mapping of the interface between epitaxial QDs and a substrate, and establishes the usefulness of x-ray phasing techniques for this and similar systems. The ability to quantify structural and chemical distributions in QD systems at the atomic level could resolve long-standing puzzles relating, for example, to the inverted electron–hole alignment observed in some QD systems. The power of COBRA for detailed mapping of chemical, strain, and structural aspects of a broad range of epitaxial QD systems provides a new capability that should have a significant impact on nanotechnology as QD systems continue to be refined and controlled for many applications.

— Vic Comello

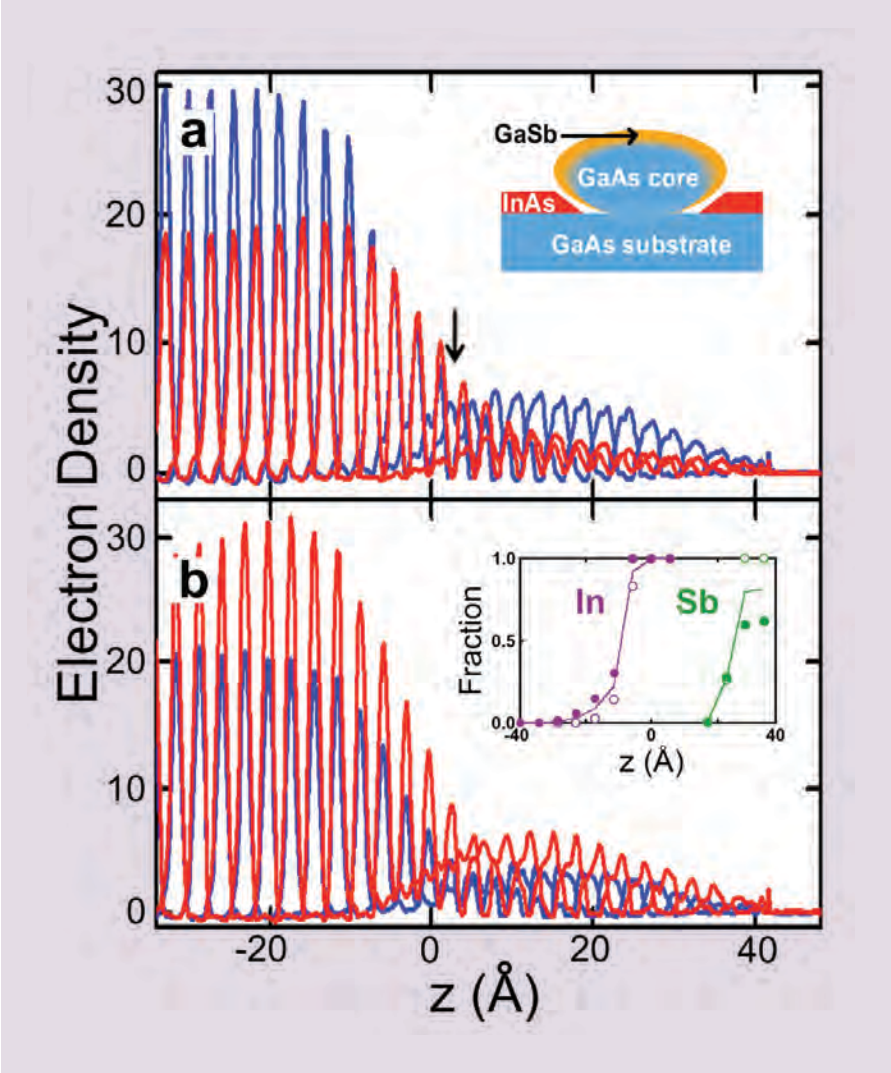

^ *Fig. 1 (a) The almost identical Group III peak heights at two energies in the range –6 Å ≤ z ≤0 indicate a high concentration of InAs at the substrate surface; (b) split Group V dot peaks for 6 Å ≤ z ≤ 40 Å indicate a GaSb-like shell. The black arrow indicates the stacking sequence shift between the substrate and the dot.* ***Top inset:*** *schematic of the core-shell structure of the droplet QDs, illustrating the penetration of the dot through the InAs surface layer into the GaAs substrate.* ***Bottom inset:*** *occupancy fraction of In and Sb as a function of height, z, above the nominal dot–substrate interface.*

See > Divine P. Kumah[1], Sergey Shusterman[2], Yossi Paltiel[3], Yizhak Yacoby[3], and Roy Clarke[1,*], "Atomic-Scale Mapping of Quantum Dots Formed by Droplet Epitaxy," Nat. Nano. **4**, 835 (27 September 2009). DOI: 10.1038/NNANO.2009.271

Author affiliations >
[1]University of Michigan,
[2]Soreq NRC,
[3]Hebrew University

Correspondence >
*royc@umich.edu

> The work was supported by the U.S. National Science Foundation under Grant DMR-0606048. Use of the Advanced Photon Source was supported by the U.S. Department of Energy, Office of Science, Office of Basic Energy Sciences, under Contract No. DE-AC02-06CH11357.

> 33-ID • XOR/UNI • Chemistry, materials science, physics • Anomalous and resonant scattering (hard x-ray), diffuse x-ray scattering, general diffraction, surface diffraction, x-ray reflectivity, x-ray standing waves • 3.3-cm Undulator A • Accepting general users

Seeing Strain Inside a Nanocrystal

IN SHORT > The electronic, optical, and magnetic properties of nanocrystals and other nanostructures can dramatically depend on fine details of these materials' atomic structures, such as departures from ideal crystal geometry. Such variations arise almost inevitably during the growth of nanocrystals on substrates, from the influence of neighboring nanocrystals, or from the presence of dopant atoms in the crystal lattice. Using the XOR/UNI 34-ID beamline at the APS, researchers for the first time measured x-ray diffraction patterns from a single nanocrystal in six different orientations, obtaining enough information to construct a full three-dimensional (3-D) map of the distortion of the crystal lattice from its ideal form. The technique allows researchers to study closely how a nanocrystal's properties relate to its structure, in principle enabling those properties to be fine-tuned for a desired application.

MORE > X-ray diffraction measurements can reveal the distortion or strain in a single crystal, provided the x-rays are coherent in phase throughout the crystal's volume. If x-rays hit an ideal crystal at certain angles, reflections from the atoms will maintain a coherent phase relationship and produce a strong signal. Any of the atoms that are displaced from their ideal positions will reflect x-rays out of phase, creating an interference pattern. Until now, however, the inability to adjust precisely a nanocrystal's alignment has meant that researchers have only been able to measure coherent x-ray diffraction from a single orientation, from which limited information about strain on the lattice can be deduced.

To get a fuller picture, researchers from University College London, Argonne, and the Diamond Light Source devised a mounting system that allowed them to move a nanocrystal through a series of chosen orientations. They first grew ZnO crystals in the form of hexagonal prisms measuring 2-4 μm long and 1- 2 μm across. They then selected a single nanocrystal and stood it end up on a small sheet of silicon. Heating the assembly in pure oxygen formed a thin SiO layer that secured the nanocrystal in place.

Placing the nanocrystal on its mounting sheet positioned in the path of the x-ray beam, the researchers tweaked its orientation until they found the first strong reflection. With that orientation identified, they could then move the nanocrystal into other alignments where the angle of the x-ray beam with respect to the lattice also produced strong reflections. At each of six positions, they recorded a series of 2-dimensional slices of the diffraction pattern, from which they could reconstruct the full 3-D pattern (Fig. 1).

Determining the strain on the nanocrystal from these measurements required inferring the phase shifts in the x-ray reflections from the diffraction patterns, then inferring the distortion of the crystal lattice from the phase shifts. The researchers did this through an iterative procedure, first modeling the lattice to predict diffraction patterns, then comparing the predictions against the experimental results in order to adjust the model. In principle, diffraction data from three crystal orientations are enough to obtain a 3-D map of the strain. With data from six orientations, over-determining the problem, the researchers employed a statistical technique to obtain a best-fit solution.

The resolution of the measurements is about 40 nm, an order or magnitude greater than the typical distances between atoms. On this scale, the ZnO nanocrystal showed a pattern of alternating compression and tension along its length, which the researchers suggest results from the absorption of oxygen atoms into the base of the crystal as it was being secured to the silicon mounting sheet.

Measurements at higher resolution, which would require

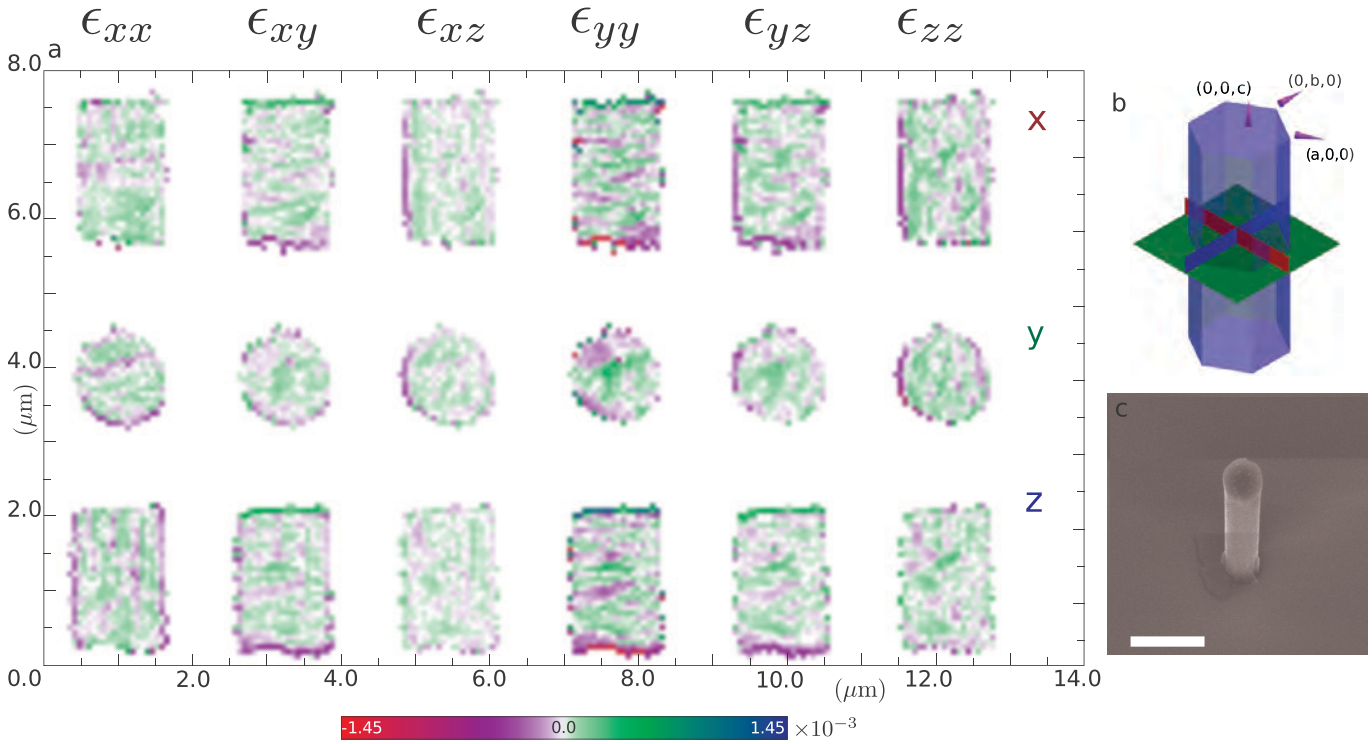

^ *Fig. 1* ***(a)*** *Two-dimensional slices showing the six independent components of the strain tensor for a ZnO nanocrystal, describing the distortion of its crystal lattice from ideal form. The orientations of the slices correspond to the three axes depicted in* ***(b)****. Purple and red indicate compression of the lattice, green and blue expansion. Scanning electron micrograph* ***(c)*** *shows the ZnO rod secured to a silicon sheet. (Scale bar: 2 µm)*

improvements to both the x-ray beam quality and the instrumentation, could measure the distortion introduced into a lattice by the presence of individual dopant atoms, or allow engineering of semiconductors to improve their electrical properties. Performed with femtosecond x-ray pulses from free-electron lasers, the technique could even capture snapshots of the dynamic distortion of a crystal structure.

— David Lindley

See > Marcus C. Newton[1]*[§], Steven J. Leake[1], Ross Harder[2], and Ian K. Robinson[1,3], "Three-dimensional imaging of strain a single ZnO nanorod," Nat.Mater., **9**, 120 (2010).

Author affiliations >
[1]University College London,
[2]Argonne National Laboratory,
[3]Diamond Light Source
[§]Present address: University of Surrey, U.K.

Correspondence >
*m.newton@surrey.ac.uk

> This work was supported by EPSRC Grant EP/D052939/1 and an ERC FP7 "advanced grant." Beamline 34-ID was built with funds from the U.S. National Science Foundation under Grant DMR-9724294 and operated by the U.S. Department of Energy, Office of Science, Office of Basic Energy Sciences, under Contract DE-AC02-06CH11357.

> 34-ID • XOR/UNI • Materials science, physics • Coherent x-ray scattering, microdiffraction • 3.3-cm Undulator A • Accepting general users

Atomic Structure of the Epitaxial BaO/Si Interface Revealed

IN SHORT > The semiconductor industry has relied on silica (SiO_2) as the gate dielectric in field effect transistors for nearly 50 years. Over this period, chipmakers have continued to boost electronic performance mainly through scaling—that is, by shrinking the conductors and the spaces between them in electronic devices to shorten the distance traveled by electrons. But with SiO_2 thicknesses currently in the regime below 50 Å, the scaling approach to achieving increased performance is nearing its limit, as further decreases in thickness could lead to excessive tunneling currents. In recent years, crystalline oxides have emerged as a promising alternative to amorphous SiO_2 because they could fundamentally change the scaling laws for silicon-based transistor technology by virtue of their high dielectric constants, so science is intent on experimentally proving theory in regard to these potentially important materials. Researchers using an APS beamline have determined the structure and composition of one such crystalline oxide, lighting the way to closing the theory-experiment gap.

MORE > Barium oxide (BaO) is the simplest crystalline oxide that can be grown on silicon (Si). Nevertheless, the structure of the BaO/Si interface is complex because of abrupt transitions in chemistry, bonding, and crystal structure. Several competing theoretical proposals as to the structure of this interface have been developed, which differ fundamentally on issues as basic as its elemental composition. Deciding among them experimentally has proven challenging because of the inherently complex chemistry involved and the nanoscale depth of the interface. Transmission electron microscopy and x-ray diffraction (XRD), for example, have failed to provide conclusive results on interface structure because of a lack of either resolution or sensitivity.

Despite all this, researchers from Yale University and Argonne were able to fully determine the structure and composition of the BaO/Si interface by using the existence of an epitaxial strain-induced 2 × 1 reconstruction at the interface to transform XRD into an interface-specific technique that permits detailed comparisons with the diffraction expected from first principles density functional theory (DFT) relaxed ground states. This approach offers advantages over structural refinement using only XRD data because the DFT relaxed ground state structures are sensitive to the position and composition of interface elements including those that scatter x-rays weakly, such as oxygen and Si, thus making little direct contribution to the diffracted intensities.

> Fig. 1 Comparison of measured x-ray scattering and DFT structure predictions. The measured scattering in the graphs is taken from CCD images of diffraction with 2 × 1 symmetry as shown in panel c. The open circles in the graphs are the data, and the solid black line is predicted from the DFT-derived structure in panel b. The sensitivity of the scattering to structural details is shown by the dashed red line, which is the predicted scattering from a DFT-derived structure that differs from the best-fit model by only 1 monolayer of oxygen at the interface.

Epitaxial BaO was grown on Si using molecular beam epitaxy in a layer-by-layer approach with barium being deposited in the presence of oxygen. The researchers then performed XRD measurements at the XOR/UNI 33-ID beamline, focusing on diffracted intensities related to the 2 × 1 unit cell reconstruction. This type of scattering occurs only in the interface region, since bulk Si and BaO do not have this in-plane periodicity. By homing in on this diffraction, the researchers were able to address questions concerning

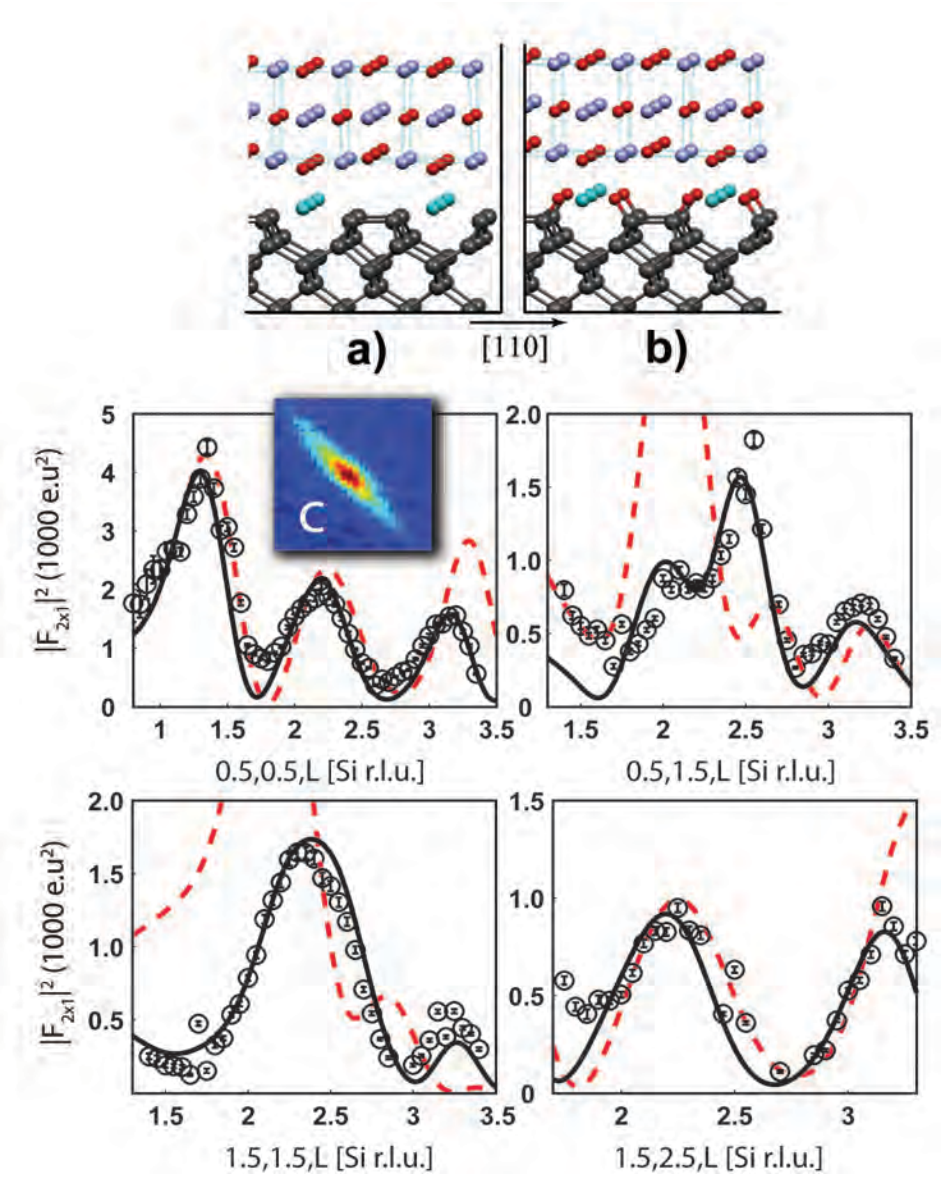

interface structure and composition far more precisely than would be possible with diffraction data from the entire structure. The diffraction data revealed a sub-angstrom rumpling of the BaO and Si layers adjacent to the interface.

DFT calculations for the relaxed ground states of several proposed interface structures revealed that only one was consistent with the observed XRD data (Fig. 1). The XRD intensities from this theoretical structure matched all of the features observed in the experimental XRD results with the use of only three adjustable parameters. The researchers concluded that the observed BaO/Si 2 × 1 interfacial reconstruction was driven by the bonding configuration of the first monolayer of oxygen in the BaO and that an additional monolayer of oxygen was bonded to the surface Si atoms. Two BaO layers and four Si layers adjacent to the interface were found to be significantly rumpled by epitaxial strain.

— Vic Comello

See > Yaron Segal[1], Jim W. Reiner[1], Alexie Kolpak[1], Zhan Zhang[2], Sohrab Ismail-Beigi[1], Charles Ahn[1], and Fred Walker[1]*, "Atomic Structure of the Epitaxial BaO/Si(001) Interface," Phys. Rev. Lett. **102**, 116101 (20 March 2009). DOI:10.1103/PhysRevLett.102.116101

Author affiliations >
[1]Yale University,
[2]Argonne National Laboratory

Correspondence >
*fred.walker@yale.edu

> Support for this work was provided by the National Science Foundation, under MRSEC DMR 0520495 and DMR 0705799, and SRC. Use of the Advanced Photon Source was supported by the U.S. Department of Energy, Office of Science, Office of Basic Energy Sciences, under Contract No. DE-AC02-06CH11357.

> 33-ID • XOR/UNI • Chemistry, materials science, physics • Anomalous and resonant scattering (hard x-ray), diffuse x-ray scattering, general diffraction, surface diffraction, x-ray reflectivity, x-ray standing waves • 3.3-cm Undulator A • Accepting general users

High Pressure Extinguishes Chromium's Magnetism

IN SHORT > The metallic element chromium possesses an unusual form of magnetism that comes about because of cooperative behavior among conduction electrons. Researchers working at XOR beamline 4-ID-D at the APS have shown that when the metal is squeezed by pressures approaching 10 Gpa—about 100,000 atmospheres—chromium's magnetism unexpectedly disappears. The transition is driven, the researchers argue, by quantum fluctuations that allow conduction electrons to hop out of their orderly state. Because pure chromium is such a "clean" system, it can serve as a model for understanding similar transitions in more chemically complex materials.

MORE > Chromium displays a property known as itinerant antiferromagnetism. In a typical antiferromagnet, magnetically polarized atoms line up alternately in opposite directions, so that the material as a whole has no magnetic moment. This orderly arrangement only exists when the material's temperature is below the critical value of the Néel temperature. In chromium, however, antiferromagnetism arises through the behavior of conduction electrons that can move freely through the metal's atomic lattice structure—hence the label "itinerant," as in itinerant ferromagnetism. Below the Néel temperature, these electrons do not move independently but maintain a fixed phase relationship throughout the lattice, forming so-called spin density waves with antiferromagnetic alignment. The theory of these spin density waves is analogous to the Bardeen-Cooper-Schrieffer (BCS) theory of superconductivity, which describes how electrons pair up in the superconducting state. One implication of the theory is that increasing the pressure on chromium should cause its antiferromagnetism to vary in a predictable way.

To test this prediction, a team of researchers from The University of Chicago, Argonne, the University of Cambridge, and the Massachusetts Institute of Technology made use of the fact that the wavelength of the spin density waves is slightly different from chromium's lattice constant, which defines the size of the unit cube in the metal's body-centered cubic structure. Placing a tiny crystal of chromium, mounted in a diamond anvil cell, in the 4-ID-D beamline, the team obtained diffraction patterns due to charge density waves that accompany the spin density waves (Fig. 1). An intense x-ray beam was needed because the diffraction peak from the electrons was only one ten billionth as strong as the diffraction signals from the crystal structure itself.

The scientists first established that the lattice constant of chromium shrinks in a smooth manner from ambient pressures all the way up to about 15 GPa at low temperature, meaning that no structural change in the lattice occurs. However, the characteristic length-scale of the spin density wave behaved quite

*> Fig. 1 Black dots show the measured intensity, relative to diffraction from the lattice, of the x-ray diffraction line from charge density waves (which are harmonically related to spin density waves) that characterize the antiferromagnetism in chromium. The Néel temperature, above which the spin and charge density waves cannot exist, can be inferred from the diffraction intensity. At the highest pressures, the intensity falls off sharply compared to theoretical expectation (blue dashed line), indicating the onset of quantum criticality. Cartoons are proposed representation of the density wavefronts. At low temperature and pressure, the waves are strong and well-defined **(bottom left)**, diminishing at higher temperature **(upper left)**; as the pressure grows to about 10 GPa, the waves weaken and lose their coherence **(bottom right)**.*

differently. Expressed as a ratio of the lattice constant, it decreased for pressures up to a few GPa, then reached a relative minimum at about 6 GPa, after which it began to increase. Similarly, the strength of the diffraction signal from the charge density wave exhibited different behavior in these two pressure ranges. Below 6 GPa it decreased exponentially with increasing pressure, as predicted by the BCS theory. Above 7 GPa, however, it began to fall off more sharply, and disappeared in a continuous way at a pressure somewhat less than 10 GPa.

The implication of these findings, the researchers say, is that the BCS-like spin density wave state disappears because electrons jump into other states that classically they should not be able to reach. These quantum fluctuations destroy chromium's antiferromagnetism, although it remains unclear what new states—disordered, or ordered in some novel way—the electrons jump into.

A similar transition has been known for decades to occur at zero pressure in alloys of chromium and vanadium as the proportion of vanadium steadily increases. In that case, though, the transition involves chemical changes and disorder, making the mechanism hard to figure out. The pressure-driven transition in pure chromium represents what the scientists call a "naked quantum singularity," in which there are no other obscuring phenomena. In contrast, a quantum transition from one kind of electronic order to another is suspected to drive the formation of Cooper pairs in high-temperature superconducting copper oxides, but the underlying physics is complicated by chemical disorder and is obscured by the superconducting phase itself. Although the quantum transition in chromium is technically demanding to study, the researchers believe its freedom from interfering causes makes it the ideal experimental example of this subtle form of quantum behavior.

— David Lindley

See > R. Jaramillo[1,§], Yejun Feng[1,2], J.C. Lang[2], Z. Islam[2], G. Srajer[2], P.B. Littlewood[3], D.B. McWhan[4], and T.F. Rosenbaum[1]*, "Breakdown of the Bardeen–Cooper–Schrieffer ground state at a quantum phase transition," Nature **459**, 405 (2009). DOI:10.1038/nature08008

Author affiliations >
[1]The University of Chicago,
[2]Argonne National Laboratory,
[3]University of Cambridge,
[4]Massachusetts Institute of Technology
[§]Present address: Harvard University

Correspondence >
*tfr@uchicago.edu

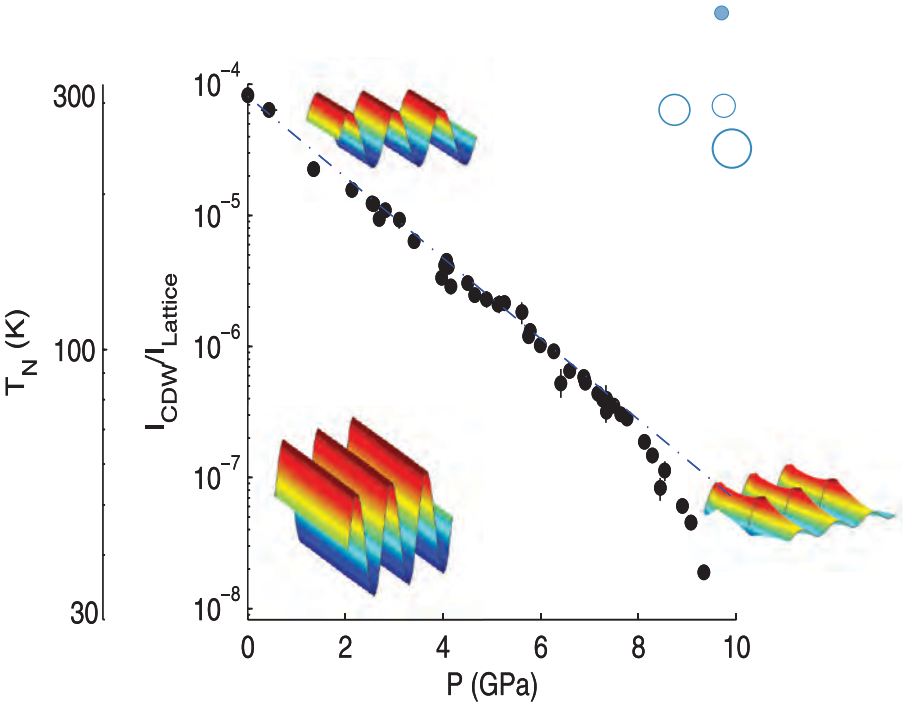

> The work at The University of Chicago was supported by the U.S. National Science Foundation (NSF) Division of Materials Research. Use of the Advanced Photon Source at Argonne National Laboratory was supported by the U.S. Department of Energy, Office of Science, Office of Basic Energy Sciences, under Contract No. DE-AC02-06CH11357.

> 4-ID-D • XOR • Physics, materials science • Anomalous and resonant scattering (hard x-ray), magnetic x-ray scattering, magnetic circular dichroism (hard x-ray) • 3.5-cm undulator • Accepting general users

Thin Films in the Thick of It

IN SHORT > Agglomeration is a phenomenon that can be seen on any rainy day, as water beads on the hood of a freshly-waxed car. On a much smaller scale, however, it is important in microelectronics. The breakup of a conducting film on a microchip can lead to broken electrical connections, data loss, and device malfunctions. But if properly controlled, the process can also be used to create conducting arrays. Experimenters using XOR/UNI beamline 34-ID employed GISAXS (grazing incidence small-angle x-ray scattering) to characterize the agglomeration process in thin metal films, showing for the first time how it happens in real time and *in situ*. The work provides another interesting example of how nanometer-sized systems can behave quite differently from bulk materials, and raises the possibility that similar agglomeration behaviors may emerge with nanofilms of different compositions.

MORE > The researchers—from the University of Genoa, the European Synchrotron Radiation Facility, and University College London —studied the evolution of Ni films as they were deposited onto a SiO_2 substrate. The team chose the 34-ID beamline because it allows the x-ray beam to strike the experimental film surface directly without an intervening beryllium window at the exit point. This was an important consideration in this case because the diffuse scattering from a Be window might make it difficult to measure the extremely small scattering signal generated by the nanoclusters that would form under agglomeration. The GISAXS technique was chosen for its facility in revealing fine surface morphology (Fig. 1).

After measuring the x-ray reflectivity of the silicon substrate, the experimenters carefully deposited an Ni film on each sample using an e-beam evaporator while carefully monitoring and maintaining the film thickness. Samples were prepared with different Ni film thicknesses of approximately 2 to 10 nm. The thickness and density of the Ni film on each sample was confirmed, and then the annealing process was begun under GISAXS monitoring as the silicon dioxide substrate temperature was raised in steps up to a maximum of about 700K. After the annealing procedure was completed, atomic force microscopy was employed to study the surface morphology of each sample film *ex situ*.

The researchers found that two different regimes emerged under the annealing process, depending on the initial thickness of the Ni films. The first regime (under 5-nm thickness) shows the formation of small clusters of Ni on a residual Ni layer, with no exposure of the Si substrate film. In films of more than 5-nm initial thickness, however, the Ni breaks up completely into large clusters, well-separated from each other, with a clean Si substrate fully exposed between the clusters. The process seems to be more time-dependent in the thicker films (greater than 5 nm), with little or no further development after about 7000 s at 625K, while in films that are thinner than 5 nm, a change in temperature results in a marked change in the evolution of the regime.

> *Fig. 1 Stages of evolution of GISAXS from an evaporated Ni film, as a function of time, held at a temperature that leads to the agglomeration process.*

To explain this behavior, the experimenters propose that in the thicker films, the film roughness increases with temperature until, at about 625K, grooves begin to form in the film surface. As these grooves grow and become deeper, the silicon substrate is eventually exposed, and then the enlarging grooves finally begin to merge and the film breaks up into large islands of Ni, separated by fully exposed substrate. In films thinner than 5 nm the overall energy of the system is insufficient to allow the grooves to deepen to the substrate, so the film cannot break up into large separated grains.

Although previous experiments have been done on agglomeration in thin films, the present work represents one of the few attempts

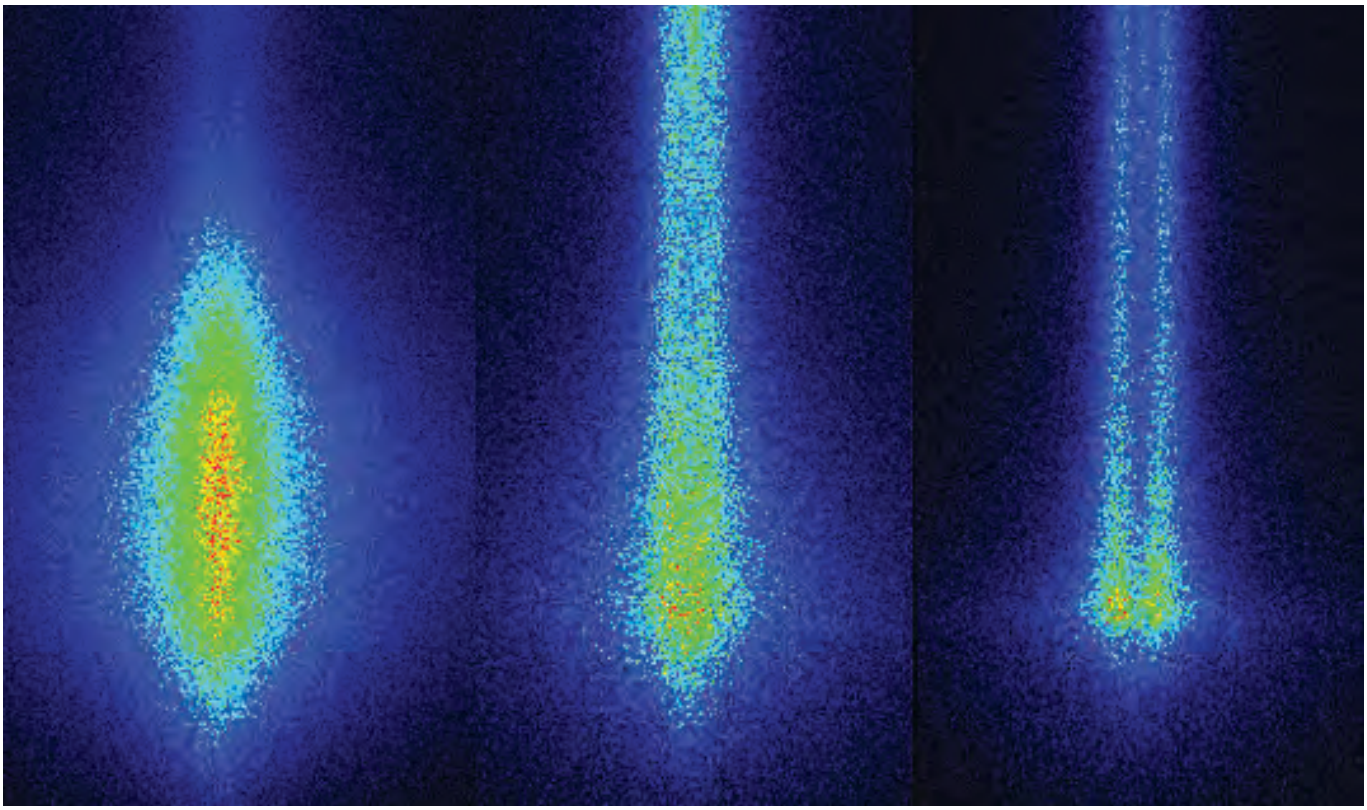

to study the process under real-time *in situ* conditions and in such detail. While the researchers allow that their experimental parameters do not rule out the possibility that agglomeration might still occur in thin films under different time and temperature conditions, they emphasize that their crucial finding is the development of separate thickness-dependent regimes.

The work provides another interesting example of how nanometer-sized systems can behave quite differently from bulk materials, and raises the possibility that similar agglomeration behaviors may emerge with nanofilms of different compositions. The important practical and commercial microelectronic implications of that question will welcome further investigation and study.

— *Mark Wolverton*

See > C. Boragno[1], F. Buatier de Mongeot[1], R. Felici[2], and I.K. Robinson[3]*, "Critical thickness for the agglomeration of thin metal films," Phys. Rev. B **79**, 155443 (2009). DOI: 10.1103/PhysRevB.79.155443

Author affiliations >
[1]Università di Genova, [2]European Synchrotron Radiation Facility, [3]University College London

Correspondence >
*i.robinson@ucl.ac.uk

> Use of the Advanced Photon Source was supported by the U.S. Department of Energy, Office of Science, Office of Basic Energy Sciences, under Contract No. DE-AC02-06CH11357.

> 34-ID • XOR/UNI • Materials science, physics • Coherent x-ray scattering, microdiffraction • 3.3-cm Undulator A • Accepting general users

Making Things Fit in a New Ce-Al Alloy

IN SHORT > Ever since the Bronze Age, humans have known the advantages of alloys. By combining atoms of different metals, it is possible to create a new material featuring not only the best qualities of both, but entirely new and highly useful properties. In general, alloys are formed by substituting the atoms of one material into the crystalline structure of another. But nature has imposed some strict limitations on which particular elements can be combined in this way. Those limits, called Hume-Rothery (HR) rules, dictate that metals can be combined only within certain limits of atomic size and valence. As is the case with many rules, there is some wiggle room, under the proper conditions. Working at two different APS beamlines, an international team of researchers stretched those rules a little and created a new alloy from Ce and Al, two elements that usually can't be put together in such a way according to the HR limits. This work provides insights about the ways two dissimilar materials can join together to form something completely new and different, with properties that could be employed in a wide range of applications.

MORE > The rare-earth metal cerium (Ce) and the common alloy ingredient aluminum (Al) are two elements that generally combine only in stoichiometric compounds or highly disordered metallic glasses within the framework of the Hume-Rothery rules. The experimenters sought to discover if high pressure might overcome the atomic size differences between Ce and Al atoms and allow the creation of a true substitutional face-centered cubic (fcc) structure in an alloy that could exist at room temperature and ambient pressures.

They first created a Ce_3Al metallic glass by rapid cooling of melt, examining the structure with XRD (x-ray diffraction) at the HP-CAT 16-ID-B beamline at the APS under various hydrostatic pressures (Fig. 1). Up to 24.4 GPa, the observed x-ray diffraction patterns were typical of the disordered amorphous glass state, as expected. But at 25.0 GPa, sharp diffraction features indicative of full crystallization in an fcc structure abruptly appeared. The crystallization persisted even as the pressure was reduced to the ambient level.

Next, the researchers subjected a Ce_3Al stoichiometric compound to hydrostatic pressure, again using XRD to detect changes in the compound's normal hexagonal crystalline structure. Beginning at 15 GPa, an fcc phase began to appear, replacing more and more of the hexagonal Ce_3Al as pressure was increased. Again, the new phase remained even as pressure was reduced. When the sample was heated with an Nd:YLF laser to temperatures of up to approximately 900K, the experimenters saw reversible transitions between the hexagonal and fcc phases in the range of 5 to 6 GPa.

Using Ce L_3-edge x-ray absorption spectroscopy at the XOR/PNC 20-BM beamline and *ab initio* calculation, the team determined that delocalization of the *4f* electron in Ce, along with Kondo volume collapse, are the major factors allowing the new fcc alloy to form under the HR limitations. After pressure was reduced to ambient levels, the *4f* electron in Ce returned to its normal state and the Kondo volume collapse reversed, but the new fcc alloy structure remained.

The work opens up some intriguing possibilities both for the creation of new and novel Ce-Al alloys and for the development of other Ce and *f*-electron alloys, all of which will provide further insight into the ways in which two dissimilar materials can join together to form something altogether different. New alloys also hold the promise of different and valuable properties that can be employed in a variety of materials to fit a wide range of applications. But the research team's work also serves to demonstrate that while nature's rules can sometimes seem impossible to overcome, they nevertheless allow human ingenuity to find new ways to work within those rules.

— Mark Wolverton

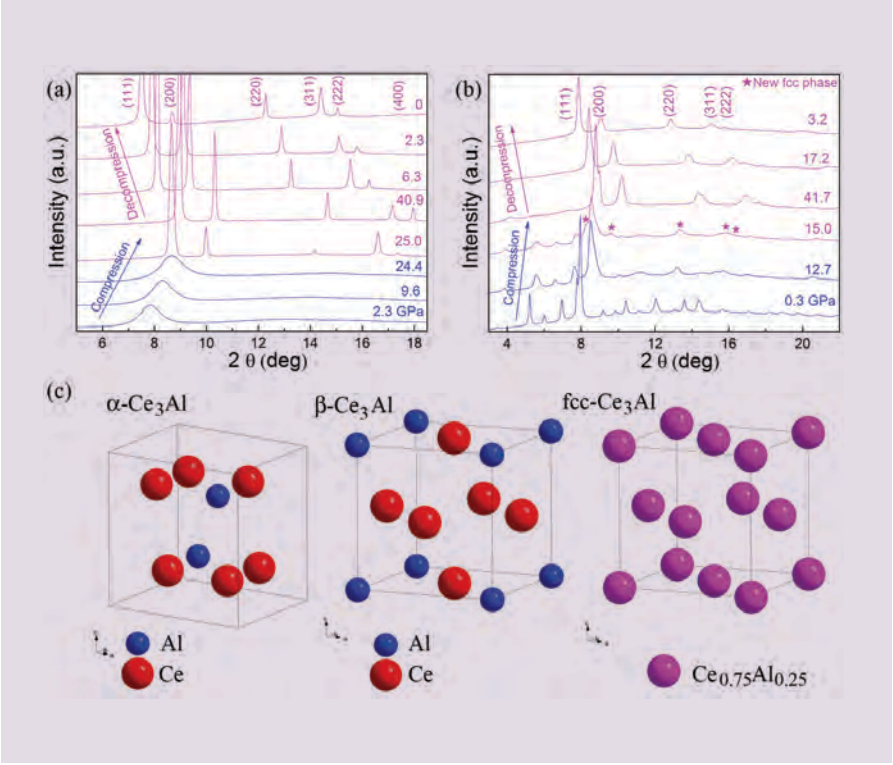

*< Fig. 1 **In situ** high-pressure synchrotron x-ray diffraction patterns of Ce_3Al at 298K using x-ray wavelength λ = 0.3681(1) Å and atomic structures of Ce_3Al phases. **(a)** Starting with a metallic glass, the transition occurs at 25 GPa. Intensity mismatch to the fcc structure is due to the growth of large crystals in the sample. **(b)** Starting with hexagonal α-Ce_3Al, the transition occurs at 15 GPa. **(c)** Crystal structures of the two ordered compounds α-Ce_3Al and β-Ce_3Al, and the new disordered fcc-Ce_3Al alloy.*

See > Qiao-Shi Zeng[1,2], Yang Ding[2], Wendy L. Mao[3,4], Wei Luo[5,6], Andreas Blomqvist[5], Rajeev Ahuja[5,6], Wenge Yang[2], Jinfu Shu[2], Stas V. Sinogeikin[2], Yue Meng[2], Dale L. Brewe[7], Jian-Zhong Jiang[1]*, and Ho-kwang Mao[1,2]**, "Substitutional alloy of Ce and Al," Proc. Natl. Acad. Sci. USA **106**(8), 2515 (February 24, 2009). DOI: 10.1073_pnas.0813328106

Author affiliations > [1]Zhejiang University, [2]Carnegie Institution of Washington, [3]Stanford University, [4]SLAC National Accelerator Laboratory, [5]Uppsala University, [6]Royal Institute of Technology, [7]Argonne National Laboratory

Correspondence >
*jiangjz@zju.edu.cn
**hmao@gl.ciw.edu

> This work was supported by the Balzan Foundation; National Natural Science Foundation of China Grants 50425102, 50601021, 50701038, 60776014, 60876002, and 10804096; the Zhejiang University–Helmholtz Cooperation Fund;the Ministry of Education of China (Program for Changjiang Scholars, the Research Fund for the Doctoral Program of Higher Education from China Scholarship Council); the Department of Science and Technology of Zhejiang Province; and Zhejiang University. W.L., A.B., and R.A. are grateful to the Swedish Research Council for providing financial support, the Swedish National Infrastructure for Computing, and the Uppsala Multidisciplinary Center for Advanced Computational Science for providing computational resources. Use of the High Pressure Collaborative Access Team facility was supported by the Department of Energy, Office of Basic Energy Sciences; Department of Energy, National Nuclear Security Administration (Carnegie/Department of Energy Alliance Center); the National Science Foundation; Department of Defense, Tank-Automotive and Armaments Command; and the W. M. Keck Foundation. XOR/PNC facilities at the Advanced Photon Source, and research at these facilities, are supported by the U.S. Department of Energy, Office of Basic Energy Sciences, a major facilities access grant from Natural Sciences and Engineering Research Council of Canada, the University of Washington, Simon Fraser University, and the Advanced Photon Source.

Use of the Advanced Photon Source was supported by the U.S. Department of Energy, Office of Science, Office of Basic Energy Sciences, under Contract No. DE-AC02-06CH11357.

> 16-ID-B • HP-CAT • Materials science, geoscience • Microdiffraction, powder diffraction, single-crystal diffraction • 3.3-cm Undulator A • Accepting general users

> 20-BM • XOR/PNC • Chemistry, environmental science, geoscience, materials science • Microfluorescence (hard x-ray), micro x-ray absorption fine structure, x-ray absorption fine structure • Bending magnet • Accepting general users

Seeing Microstates through the Speckles

IN SHORT > It is easy to miss the forest for the trees, but sometimes it is necessary to pay attention to both at the same time, as in the study of surfaces where interesting structural changes can occur. Using different techniques, scientists can look with high resolution at small areas of atoms (the trees) or at the average properties of the larger surface (the forest) during an experiment. It can also be important to observe changes on the atomic scale and over a very large area at the same time, such as when the average surface properties of a sample appear constant but the surface itself is dynamically evolving through different configurations. These microstates are important to catalytic processes and other interactions, but often difficult to study. Many techniques, such as standard x-ray scattering, average out information about the entire structure so that data on the very limited and transient microstates is lost. Working at the XOR 8-ID-E beamline at the APS, researchers used a new coherent x-ray scattering technique to capture microstate surface dynamics in a monolayer of gold atoms with unprecedented clarity in real time. Their work points to new possibilities for a greater and more detailed understanding of surface phase transitions and how various crystalline solids interact with other solids, liquids, and gases.

MORE > The researchers from Argonne, Safarik University, and HASYLAB collected speckled scattering patterns from the surface reconstruction of Au(001) (Fig. 1). Because each speckle pattern acts like a detailed picture of the microstate—a fingerprint of the system—observing changes in those patterns allowed the experimenters to see the temperature-dependent dynamics of this surface for the first time, even when the average properties of the system appeared static.

The surface reconstruction of Au(001) is a quasihexagonal (hex) arrangement of atoms, known to occur in two different orientations. The properties of the surface are also dependent on temperature, with the reconstruction vanishing at high temperature, leaving a disordered (1 × 1) surface. Although the general kinetics of the process has been observed in previous studies, the use of coherent scattering in the current work allowed the dynamics of the reconstructions to be directly observed in real time.

Speckle patterns obtained from the coherent x-ray scattering show that at room temperature, the surface dynamics of the Au(001) monolayer are fairly quiescent, but begin to change quickly as the temperature is increased. This is due to the movement of the boundaries of the hex domains and the rearrangement of a uniaxial corrugation within each domain. The increasingly rapid evolution of the microdomains is demonstrated by fluctuations in the speckle patterns at different temperatures. Speckle patterns were shown to be relatively stable at 1105K with only very slow changes in intensity and configuration. However, at higher temperatures such as 1120K and 1130K, the speckle evolved rapidly, indicating that the surface microstates were undergoing significant changes, even when the temperature was held constant and the overall intensity and width of the peak did not change.

By measuring how fast the speckle changed, the research team was able to obtain quantitative data on the surface dynamics, which revealed two definite temperature regimes separated by a transition point at ~1070K. Below this transition temperature, speckle patterns changed at a slow rate, but the rate of change sharply increased above the transition point. Above the transition temperature, the fast surface dynamics were governed mainly by hex domains changing to

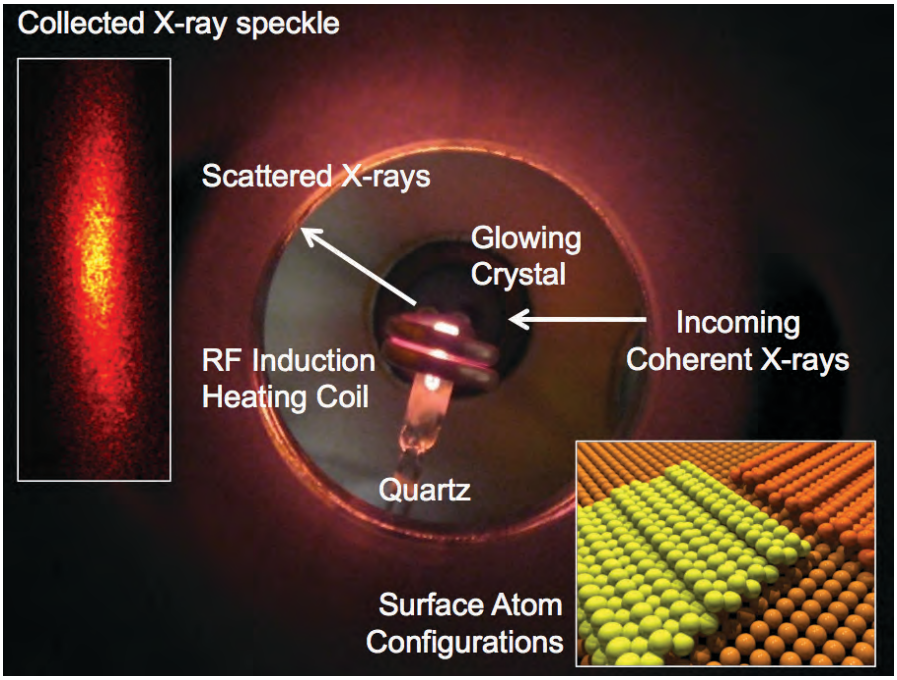

^ *Fig. 1 Highly coherent x-rays scatter from the gold surface at a position that maximizes the available signal from the surface atoms. The main view shows the inside of the sample chamber during the experiment. Because of the large degree of coherence of the x-rays, the scattering patterns are highly speckled and contain information about the configuration and profile of the surface. The sample is being held at a constant temperature of 1200K and the glow from the sample illuminates the inside of the chamber.* ***Top Left Inset****: An example of a speckle pattern collected. If the surface is unchanging then the speckle will stay in the same configuration. If the surface is changing, the speckle with change too.* ***Bottom Right Inset****: A cartoon picture of the two orientations of the quasi-hexagonal surface atom reconstruction over the (1 x 1) bulk. The height variation is exaggerated.*

(1 × 1) areas and by (1 × 1) areas reconstructing back to hex domains. The experimenters conclude that this is due to the increasing activation of the (1 × 1) domains, resulting from a steadily decreasing difference in free energy between the hex and (1 × 1) regions. Below the transition temperature, however, the slow dynamics consisted mostly of changes between the two hex phases.

Through this work, the experimenters have both demonstrated coherent x-ray surface scattering from a mono-atomic thick surface layer as a viable technique and used it to observe the microstate dynamics of the Au(001) surface layer phases with enhanced clarity in real time. The work opens new experimental possibilities for achieving a greater and more detailed understanding of surface phase transitions and how various crystalline solids interact with other solids, liquids, and gases.

— Mark Wolverton

See > M.S. Pierce[1]*, K.C. Chang[1], D. Hennessy[1], V. Komanicky[1,2], M. Sprung[1,3], A. Sandy[1], and H. You[1], "Surface X-Ray Speckles: Coherent Surface Diffraction from Au(001)," Phys. Rev. Lett. **103**, 165501 (16 October 2009). DOI: 10.1103/PhysRevLett.103.165501

Author affiliations >
[1]Argonne National Laboratory,
[2]Safarik University,
[3]Deutsches Elektronen-Synchrotron

Correspondence >
*mpierce@anl.gov

> This work and use of the Advanced Photon Source were supported by the U.S. Department of Energy, Office of Science, Office of Basic Energy Sciences, under Contract No. DE-AC02-06CH11357.

> 8-ID-E • XSD • Materials science, physics, polymer science • Grazing incidence small-angle scattering, intensity fluctuation spectroscopy, x-ray reflectivity, x-ray photon correlation spectroscopy • 3.3-cm Undulator A • Accepting general users

A Synchrotron as a Lens to Observe Condensed Matter under Extreme Shockwave Compression

IN SHORT > The behavior of materials under extreme conditions is of great scientific interest. The effects of planar shock waves—such as those generated by laser drivers, flyer plate impacts, or high explosives—can lead to large compressions and uniaxial strain in the material, but studies of these phenomena have been largely restricted to continuum measurements and analysis. The ability to perform real-time measurements of the changes taking place in the crystal structure and the lattice deformation at pico- to nanosecond time scales is crucial in order to better understand the physical and chemical properties of condensed matter under extreme conditions. Experiments carried out at the HP-CAT 16-ID-D beamline at the APS have yielded for the first time real-time, microstructural data on the lattice compression that occurs as a lithium fluoride crystal (LiF) plate is subjected to shock wave compression. More importantly, this research effort successfully demonstrated that a synchrotron, in tandem with an appropriate impact or shock wave facility, is a feasible approach to permit high resolution, real-time x-ray diffraction measurements in shock wave or plate impact experiments.

MORE > Previous work has shown that shocked single crystals are unable to sustain the large stress deviators associated with elastic compression, and this gives rise to plastic deformations at nanosecond or perhaps even shorter time scales. However, the lack of high resolution, real-time microstructural data meant that the micromechanisms responsible for the lattice changes during the transition from elastic to plastic deformation under shock compression remained unknown.

The experiments in this study, by researchers from Washington State University with support from the Carnegie Institution of Washington, made use of subnanosecond x-ray pulses to record diffraction data from pure and magnesium-doped LiF single crystals shocked along the [100] and [111] orientations. For shock compression of LiF along the [100] direction,elastic-plastic deformation occurs and significant broadening in the diffraction patterns was observed, as shown in Fig. 1. The broadening indicates that these LiF(100) crystals developed substructures with lattice rotations of order 1 degree and a characteristic size for coherently diffracting domains (CDD) ranging from 0.1 to 10 μm. Experiments were also carried out for contrast on LiF crystals elastically compressed along [111]. In this case, the diffraction pattern indicated lattice compression, but did not change in size, indicating the lack of crystal substructure.

In addition, the research group also succeeded in demonstrating that the amount of lattice disorder for shocked LiF along [100] depends on the loading history. Indeed, when magnesium-doped and ultrapure LiF crystals were shocked to the same peak stress, it was found that the broadening was larger for the magnesium-doped LiF crystals than for ultrapure LiF [100]; this can be understood by noting that the magnesium-doped LiF has a large elastic precursor. The ability to resolve microstructural details in shocked crystals is important and was made possible by the synchrotron x-rays.

All of the data was compared with results from simulations using a model consisting of coherently diffracting domains where the lattice orientation and lattice strain are assumed constant within each domain, but vary from domain to domain following a Gaussian distribution. In every instance, the experimental results were in excellent agreement with simulated diffraction patterns.

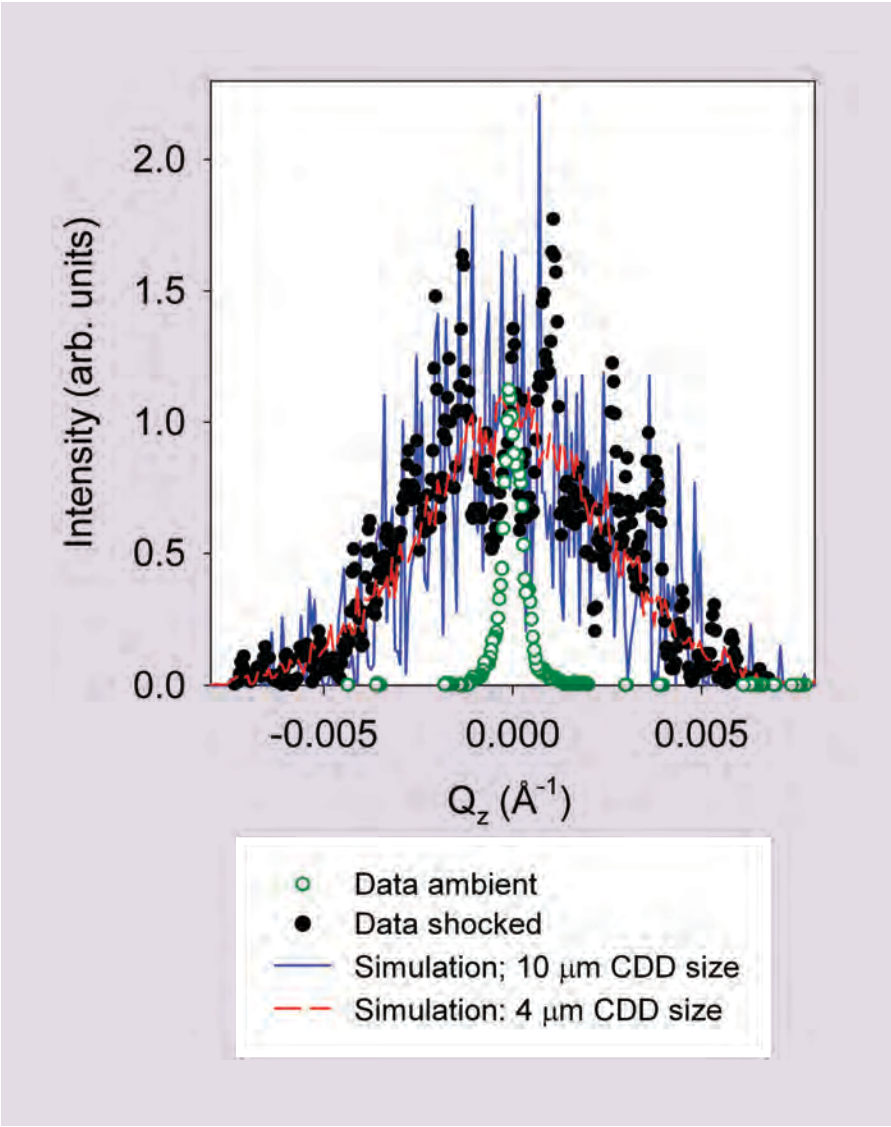

^ *Fig. 1 Diffraction patterns for ambient (white/green disks) and shocked (black disks) LiF samples. The simulation results for coherently diffracting domains of 4 and 10 micrometer size are denoted by dashed and solid lines, respectively. (Copyright © 2009 American Institute of Physics)*

The high-resolution, real-time x-ray diffraction experimental set-up employed at the HP-CAT beamline allowed the researchers to examine how the load history for pure and Mg-doped LiF(100) influence the microstructural changes. This research represents a new paradigm, paving the way for future work in the field of shock compression in crystals.

— Luis Nasser

See > Stefan J. Turneaure[1]*, Y.M. Gupta[1], K. Zimmerman[1], K. Perkins[1], C.S. Yoo[1], and G. Shen[2], "Real-time microstructure of shocked LiF crystals: Use of synchrotron x-rays," J. Appl. Phys. **105**, 053520 (2009). DOI:10.1063/1.3080176

Author affiliations >
[1]Washington State University,
[2]Carnegie Institution of Washington

Correspondence >
*stefant@wsu.edu

> This work was supported primarily by DOE Grant No. DE-FG03-97SF21388. HP-CAT is supported by DOE-BES, DOE-NNSA, NSF, and the W.M. Keck Foundation. Use of the Advanced Photon Source at Argonne National Laboratory was supported by the U.S. Department of Energy, Office of Science, Office of Basic Energy Sciences, under Contract No. DE-AC02-06CH11357.

> 16-ID-D • HP-CAT • Materials science, geoscience, physics • Nuclear resonant scattering, inelastic x-ray scattering, x-ray Raman scattering, x-ray emission spectroscopy • 3.3-cm Undulator A • Accepting general users

Timing it Right

IN SHORT > The pulsed nature of the x-rays from the APS enables a variety of time-resolved research—often involving ultrafast lasers. To perform meaningful time-resolved measurements with the combined system of laser and x-rays it is important to accurately determine their relative timing. Reducing intrinsic response times from several picoseconds to a few femtoseconds, researchers from Argonne National Laboratory used a gas phase technique at XOR beamline 7-ID to temporally reference the two types of ultrafast pulses—hard x-ray and optical—with the use of fluorescence emission. The results produced here provide a way to monitor and diagnose the time-based overlap of infrared laser and hard x-ray pulses. Specifically, as advances occur the technique should also be able to characterize the implementation of picosecond x-ray pulses proposed for the APS Upgrade.

MORE > Understanding the interaction of electromagnetic radiation with matter on an atomic scale is essential for much of the research carried out at the APS. For this reason, these researchers performed a simple cross correlation between hard x-ray and infrared pulses (Fig. 1). Specifically, the researchers concentrated on preparing, or pumping, atoms with ultrafast infrared pulses and probing them with hard x-rays, focusing on core excitations and subsequent fluorescence emissions. The hard x-ray pulses were produced from a synchrotron radiation source, while the infrared pulses were created from a tabletop laser.

The Argonne researchers used the gas phase technique, rather than the traditional x-ray diffraction methods using solid samples, because of its ability to produce quick responses of a few femtoseconds. They combined two ultrafast atomic physics processes. First, optical-field tunnel ionization was applied to a neutral, closed-shell krypton (Kr) atom. The tunnel ionization process—the pump phase—allows electrons from Kr atoms to escape, leaving behind a krypton ion (Kr^+), because their binding barrier is distorted after being subjected to the intense electric field of the laser pulse.

Secondly, the researchers applied x-ray resonant absorption to distinguish unambiguously between the pumped Kr^+ ions and the unpumped Kr atoms. The resonant x-ray fluorescence—resulting from Kr^+—acts as an excellent probe because it is not reabsorbed by the surrounding sample, and external electric fields do not affect it. It is also highly selective to krypton ions because neutral krypton atoms absorb ~40 times fewer x-rays at the resonant x-ray energy (Fig. 1 insert). The combination of the two processes is called a "laser pump/x-ray probe" technique because of the synchronized nature of the pump and probe beams. The scanning of the relative delay time of the two processes is called a "cross correlation" measurement because it reveals whether, and how, they correlate.

The laser pump/x-ray probe measurements used two APS operating modes: 24-bunch and hybrid fill, with different x-ray pulse lengths. XOR beamline 7-ID produces a monochromatized hard x-ray beam (the probe)—which focuses to about 10 × 10 μm^2. An infrared light titanium-sapphire laser, also located at this beamline, was used to produce the pump beam—focused to approximately 100 × 100 μm^2. The infrared laser pulses (~50 fs) are about 1,000 times shorter than the x-ray pulses in either operating mode. The two beams met at a small crossing angle of 1.5°, with the focus inside a vacuum chamber containing neutral krypton gas. Two x-ray fluorescence detectors were positioned perpendicular to the x-ray beam, with 1-mm slits limiting their viewing length to the region of spatial overlap.

As shown in Fig. 1, negative delays mean that the x-ray pulses from the beamline arrived *before* the Ti: sapphire laser pulses generated Kr^+ ions and, thus, resonant fluorescence was not detected. At positive delays, however, the x-ray

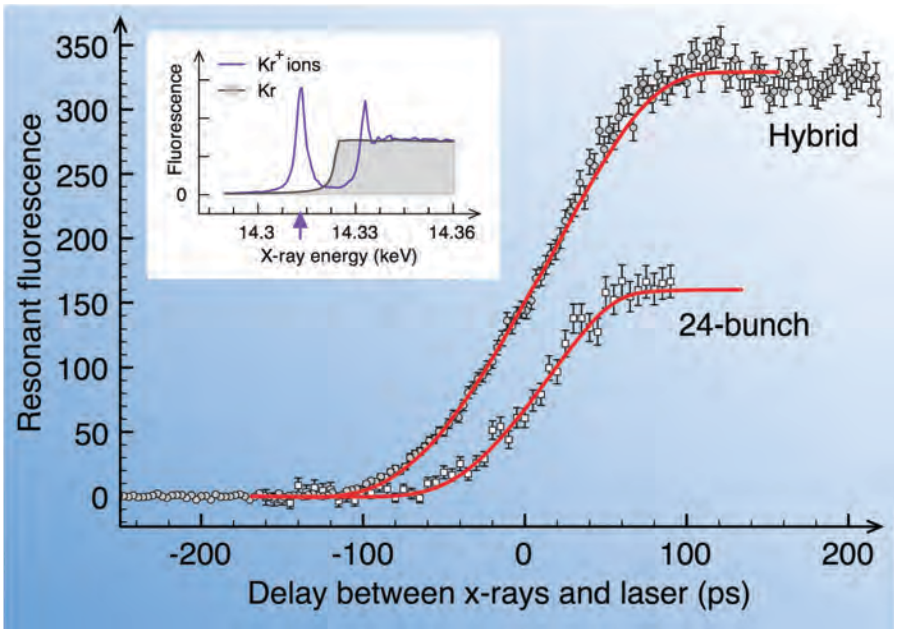

^ *Fig. 1 The cross-correlation data of resonant fluorescence from laser-produced krypton ions as a function of the relative delay between the x-ray and laser pulses for two APS operating modes with different x-ray pulse lengths. Note that the data accumulation time in 24-bunch mode was twice as long as in hybrid fill mode.* ***Insert:*** *Fluorescence signal as a function of incident x-ray energy for neutral Kr atoms (gray line and shading) and for Kr^+ ions (purple line). The arrow indicates the x-ray energy at which the cross correlation measurements were conducted.*

pulses arrived *after* the laser pulses, leading to maximum resonant x-ray absorption with rapid emissions of fluorescence photons. The resonant fluorescence is perceivable for some time after the laser pulse because the ions diffuse out of the interaction region on a time scale much longer than the hard x-ray and infrared laser pulses. The interesting region is the transition from no to maximum fluorescence near zero delay because it provides a diagnostic of the temporal integral of the x-ray pulse. Intrinsically, the technique is capable of a temporal resolution down to a few femtoseconds, but is currently limited by the temporal jitter in the synchronization between laser and x-ray source.

This simple cross-correlation technique may aid future research employing both infrared and hard x-ray pulses because it is nondestructive to the beams and has the ability to drastically reduce response times.

— William Arthur Atkins

See > Bertold Krässig*, Robert W. Dunford, Elliot P. Kanter, Eric C. Landahl§, Steve H. Southworth, and Linda Young, "A simple cross-correlation technique between infrared and hard x-ray pulses," Appl. Phys. Lett. **94**, 171113 (2009). DOI: 10.1063/1.3125256

Author affiliations >
Argonne National Laboratory
§Present address: De Paul University

Correspondence >
*kraessig@anl.gov

> This work was supported by the Argonne Chemical Sciences, Geosciences, and Biosciences divisions, and also in the case of the Advanced Photon Source, the U.S. Department of Energy Office of Science, Office of Basic Energy Sciences, under Contract No. DE-AC02-06CH11357.

> 7-ID • XOR • Atomic physics, chemistry, materials science • Phase contrast imaging, time-resolved x-ray absorption fine structure, time-resolved x-ray scattering • 33-cm Undulator A • Accepting general users

Superconducting Undulators: The Best Route to Bright X-ray Sources above 20 keV

IN SHORT > Increasingly, many experiments with high-energy (>20 keV) x-rays are on systems undergoing dynamic processes. Examples include measuring the strain rate response of composite materials under tension or compression, determination of metastable phases that briefly appear during amorphous to crystalline phase transformations, and response of materials to dynamic loading (e.g., shock waves). Such experiments are inherently "flux hungry" and are often limited by beam intensity. More photons equate to the ability to probe faster time scales and to explore wider parameter spaces, increasing our full understanding of the dynamic processes, both from a basic science point of view, but also toward practical ends that can be used to produce better materials for applications. Users engaged in these types of experimental programs are requesting higher photon fluxes at higher energies.

MORE > The emerging superconducting undulator (SCU) technology potentially outperforms all other technologies in terms of peak magnetic field at small periods (near 1.5 cm), thereby resulting in higher photon brilliances at higher energies. The expected brilliance of superconducting devices is shown and compared with the APS Undulator A (UA) in Fig. 1 [1].

As part of the APS superconducting undulator development project, many short prototype magnetic structures have been built at the APS. After detailed magnetic modeling analysis, refining of the winding geometry, and development of winding techniques, a magnetic structure design was chosen. The core must be potted in epoxy resin to hold the windings firmly; a technique for this epoxy vacuum impregnation was developed in a collaboration with the Technical Division of Fermilab

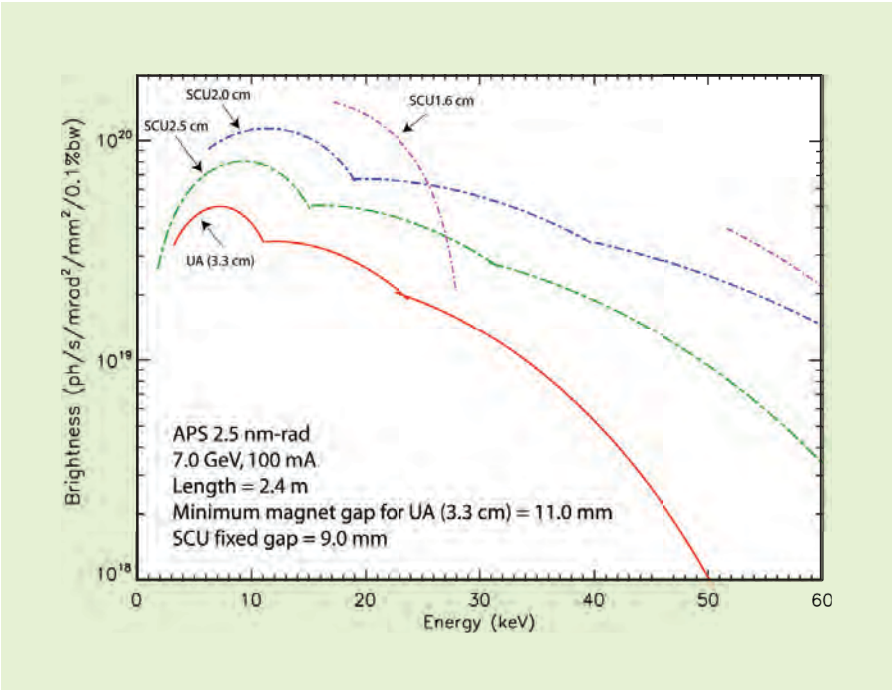

^ *Fig. 1 Tuning curves for Undulator A and some shorter-period SCUs. Note that the shorter periods give higher brightness, especially at higher photon energies. The advantage of SCUs and their stronger field is that the tuning range extends to a lower photon energy for each harmonic, giving the user more flexibility in choice of photon energy. The limited achievable field strength results in gaps in the tuning range like that seen for the 1.6-cm-period SCU. With permanent-magnet undulators, such gaps are wider and persist for period lengths as long as 2.7 cm. The SCU 1.6 cm is five times brighter than the Undulator A at 20 keV.*

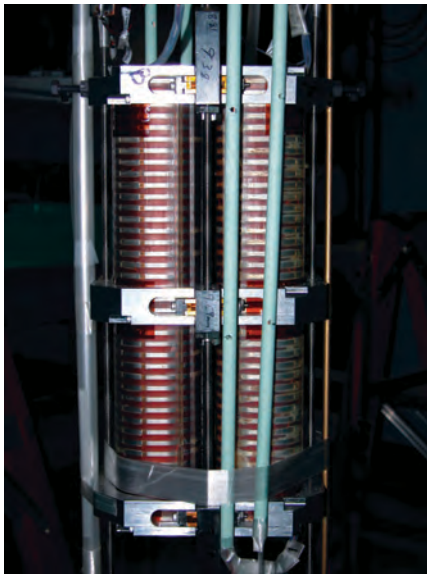

^ *Fig. 2* ***Left:*** *A single SCU core, after winding. The superconductor is wound in the grooves between poles. The current travels in opposite directions in adjacent coil packs.* ***Right:*** *A pair of cores, assembled as for an undulator magnetic structure with a gap between for the beam tube. Here they are ready to go into a vertical dewar for cold testing.*

in Illinois. A 42-pole prototype is shown in Fig. 2, where the left photo is of a single core after winding with superconducting wire. There are grooves between the poles where the wire is placed, and the winding is arranged so the current goes in opposite directions in adjacent winding packs. In order to provide a smooth trajectory entrance into and exit from the undulator, there are fewer windings of the main current coil in the last two grooves at each end. The extra space allows separate windings—which will be connected to separate power supplies—in those end grooves. Those coils will allow for trajectory correction at the ends. The right photo in Fig. 2 is of a pair of cores assembled together, ready for testing in a vertical dewar. The beam will travel through a beam chamber that will fit in the gap between the two cores. For the vertical dewar tests, a guide tube for a Hall probe is inserted instead. The test measurements of the field are very encouraging. The quality of the coil winding is such that, without magnetic field corrections in the body of the undulator, the magnetic field phase error requirement of 8 deg is met, with a 7.1-deg phase error at the current needed for 20-keV photons, and a 3.3-deg phase error at the current for 25 keV. For comparison, today's permanent magnet undulators routinely achieve 4-degrees phase error after tuning. Lower phase errors have their strongest impact on the higher harmonics in the photon spectrum, so for users who want to work at higher energies and higher harmonics, reducing the phase error would be desirable.

Now that a magnetic structure has been successfully tested, the work is focusing on the design of a cryostat that will complete the SCU and result in a device that could be installed on the APS storage ring. A collaboration with the Budker Institute in Novosibirsk is under way. The plan is to complete the undulator and have it ready for installation and testing in the storage ring in two years. After that, the length of the magnetic structure will be increased from the initial 42-pole length (at 1.6-cm period) to about 1.1 m, to achieve a corresponding increase in brilliance. Eventually, after additional R&D on manufacturing and field correction techniques, and construction of a larger test facility, the magnetic length will increase to something closer to the APS-standard 2.4 m.

Contact > Yury Ivanyushenkov (yury@aps.anl.gov), Liz Moog (emoog@aps.anl.gov), and Dean Haeffner (haeffner@aps.anl.gov)

Reference > [1] R. Dejus, M. Jaski, and S.H. Kim, "On-Axis Brilliance and Power of In-Vacuum Undulators for the Advanced Photon Source," ANL/APS/LS-314, formerly Technical Note MD-TN-2009-004.

An Intermediate-Energy X-ray Beamline at the APS

IN SHORT > A new beamline is under construction at APS Sector 29. The IEX collaborative development team (IEX-CDT) beamline will cover the energy range from 0.2 to 2.5 keV, with resolving powers in the range of 5000 to 20,000 in the high-energy end of the spectrum and a spot size of order $\sigma = 2.2\ \mu$m. The beamline will serve two experimental techniques: high-energy, angle-resolved photoemission spectroscopy (ARPES), which is a bulk probe of the low-energy excited states in condensed matter; and resonant soft x-ray scattering (RSXS), which is a direct probe of electronic ordering. ARPES and RSXS complement one another scientifically, are of interest to the same scientific community, and in particular have highly compatible source and beamline technical requirements.

MORE > The application of electron and x-ray spectroscopy in the 0.2- to 2.5-keV energy range has significant potential for advancing our knowledge of condensed matter science by elucidating the low-energy electronic excitations in both materials and artificial structures, which govern most of their physical properties.

The source for this beamline will be an elliptically polarized undulator. This source has the advantage of providing radiation with variable linear polarization and circular polarization. In the circularly polarized mode, studies of magnetic structures and excitations can be facilitated, and in addition, the source does not produce significant harmonics—an important consideration for the experiments to be carried out on the IEX-CDT beamline. The beamline, shown schematically in Fig. 1, will use mirrors to select low-energy x-rays from the undulator. The grating monochromator and the focusing mirrors provide the end stations with high resolving power and small focus.

The x-ray source for this beamline is a 4.8-m-long, 12.5-cm-period, electromagnetic, elliptically polarizing undulator. The device is capable of operating in one of three polarization modes: circular, horizontal linear, and vertical linear. Additionally, the device is capable of operating in quasi-period fashion if needed to enhance harmonic suppression for the beamline optics. The device

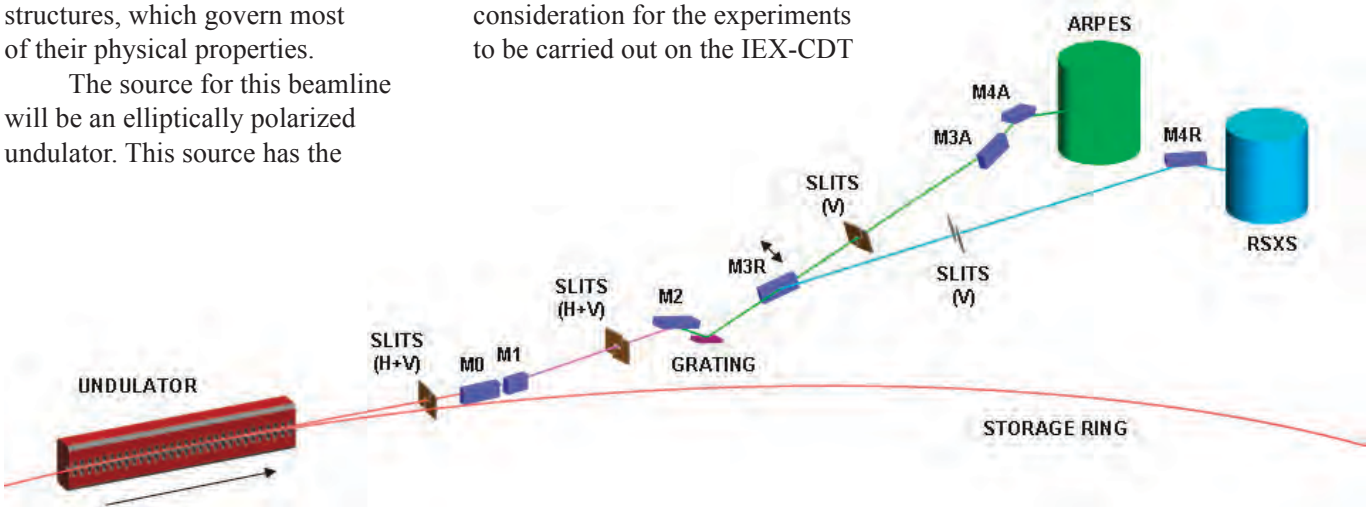

v Fig. 1 Isometric view of key beamline elements for the IEX beamline. M0, M1, and M2 are white-beam mirrors, while M3x and M4x are monochromatic mirrors.

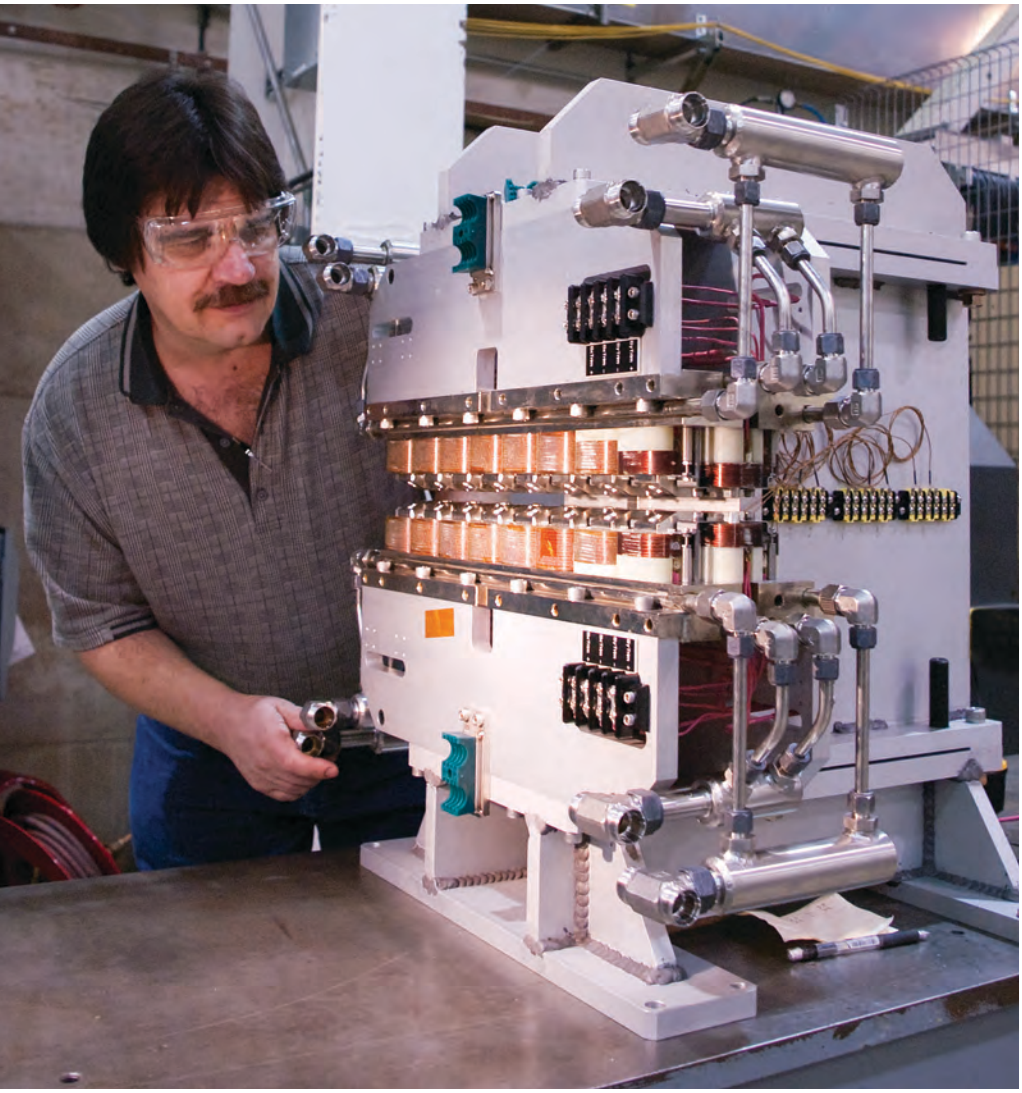

< Fig. 2 Design engineer Mark Jaski (ANL-ASD) working on the prototype 4-period, electromagnetic, elliptically polarizing undulator.

is being designed and built at the APS; a 4-period prototype (Fig. 2) has been fabricated and is undergoing testing at the time of this writing.

The IEX beamline is being designed and constructed by the IEX-CDT group, which consists of principal investigators from the University of Illinois at Chicago, the University of Illinois at Urbana-Champaign, and the University of Michigan together with personnel from the APS. The project is jointly funded by the National Science Foundation and the U.S. Department of Energy (DOE). The beamline will be a national user facility openly available to researchers from across the nation and abroad through the APS General User Program. It will, therefore, contribute critically to this nation's scientific infrastructure. Currently, facilities such as this beamline are only available at the SPring-8 synchrotron in Japan and at the European Synchrotron Radiation Facility in France. A significant advantage of having such a facility at the APS for carrying out cutting-edge experiments is that it will become a valuable resource in training future generations of researchers and educators, who will not be required to use light sources in other countries, as is currently necessary for people engaged in this type of research. This will help to maintain a forefront materials research program in the U.S., particularly in complex materials, which hold much promise for future technologies.

To make the IEX-CDT beamline still more accessible, it is already slated to participate in the the National School on Neutron and X-ray Scattering, which is a collaborative effort of the APS at Argonne and the Spallation Neutron Source (SNS) at Oak Ridge National Laboratory. The school is funded by the DOE and is intended to introduce beginning graduate students to the utilization of national research facilities. The school meets for two weeks every summer and typically includes 30 hours of lectures followed by a series of experiments at both the APS and the SNS. Each year, the school invites approximately 60 students from a wide geographic and demographic distribution. Many past students are now current users of national facilities across the U.S. Through participation in this program, the IEX-CDT beamline will be an active component in training an ethnically and demographically diverse body of students to become the next generation of U.S. scientists.

Contact > Juan Carlos Campuzano (campuzano@anl.gov), George Srajer (srajerg@aps.anl.gov), Mohan Ramanathan (mohan@aps.anl.gov)

A Dedicated Fuel-Spray Beamline at APS 7-BM

IN SHORT > **"The evolution of fuel sprays plays a defining role…in determining both combustion efficiency and the formation of…pollutants. This level of understanding may permit extraordinary new technologies, such as smart fuel injectors…"**

Basic Research Needs for Clean and Efficient Combustion of 21st Century Transportation Fuels. Report from the U.S. Department of Energy Office of Basic Energy Sciences Workshop on Clean and Efficient Combustion of 21st Century Transportation Fuels, October 29-November 1, 2006.

> *Jin Wang (ANL-XSD) in the 7-BM beamline enclosure.*

MORE > High-pressure, high-speed fuel sprays are a critical technology for many applications, including engine fuel-injection systems where the structure and dynamics of the fuel sprays are key to increasing fuel efficiency and reducing pollutants. But because liquid sprays are difficult to image with conventional (optical) techniques, particularly in the region close to the nozzle, quantitative information the structure of these sprays has been elusive. Research on this critical subject has been ongoing at the APS for several years. The primary technique for these investigations has been ultrafast x-radiography carried out mainly at XOR Sector 1 at the APS and at the Cornell High Energy Synchrotron Source, with microsecond x-ray tomography also being employed. Results, which have seen wide circulation in several peer-reviewed journals articles, have yielded information on quantitative fuel mass distribution and high-speed spray and combustion models. Perhaps the most (to date) intriguing result has been capturing the propagation of spray-induced shock waves in a gaseous medium (MacPhee et al., Science **295**[5558], 1261 [2002] and Powell et al., J. Synchrotron Rad. **7**, 356, [2000], Im et al, Phys. Rev. Lett., in press).

The researchers have engaged with an ever-expanding roster of academic, industrial, and federal-lab partners in order to improve injector system design in areas such as better spray definition, better use of air charge, and minimized needle bouncing.

The time has now arrived for the creation of a dedicated, ultrafast-imaging facility on the Sector 7 bend magnet beamline at the APS. This facility will provide a centralized resource for transportation engine technologies, offering high-throughput measurement capabilities for a large user community. The U.S. Department of Energy's Office of Energy Efficiency and Renewable Energy, Office of Vehicle Technologies program made a significant investment in rebuilding the beamline, where two research stations and associated beam transport components were already in place.

The beamline makes available ultrafast (μs) x-radiography, ultrafast (μs) x-tomography, high beam intensity, wide-bandpass mono (10^{13}-10^{14} ph/s, tunable from 6 to 12 keV), and flexible beam size. Instrumentation includes a sagittal focusing double-multilayer monochromator, a harmonics rejection mirror for use with area detectors, a secondary Kirkpatrick-Baez focusing mirror for use with point detectors, modular sample stations, pressurized chambers, unpressurized chambers, and

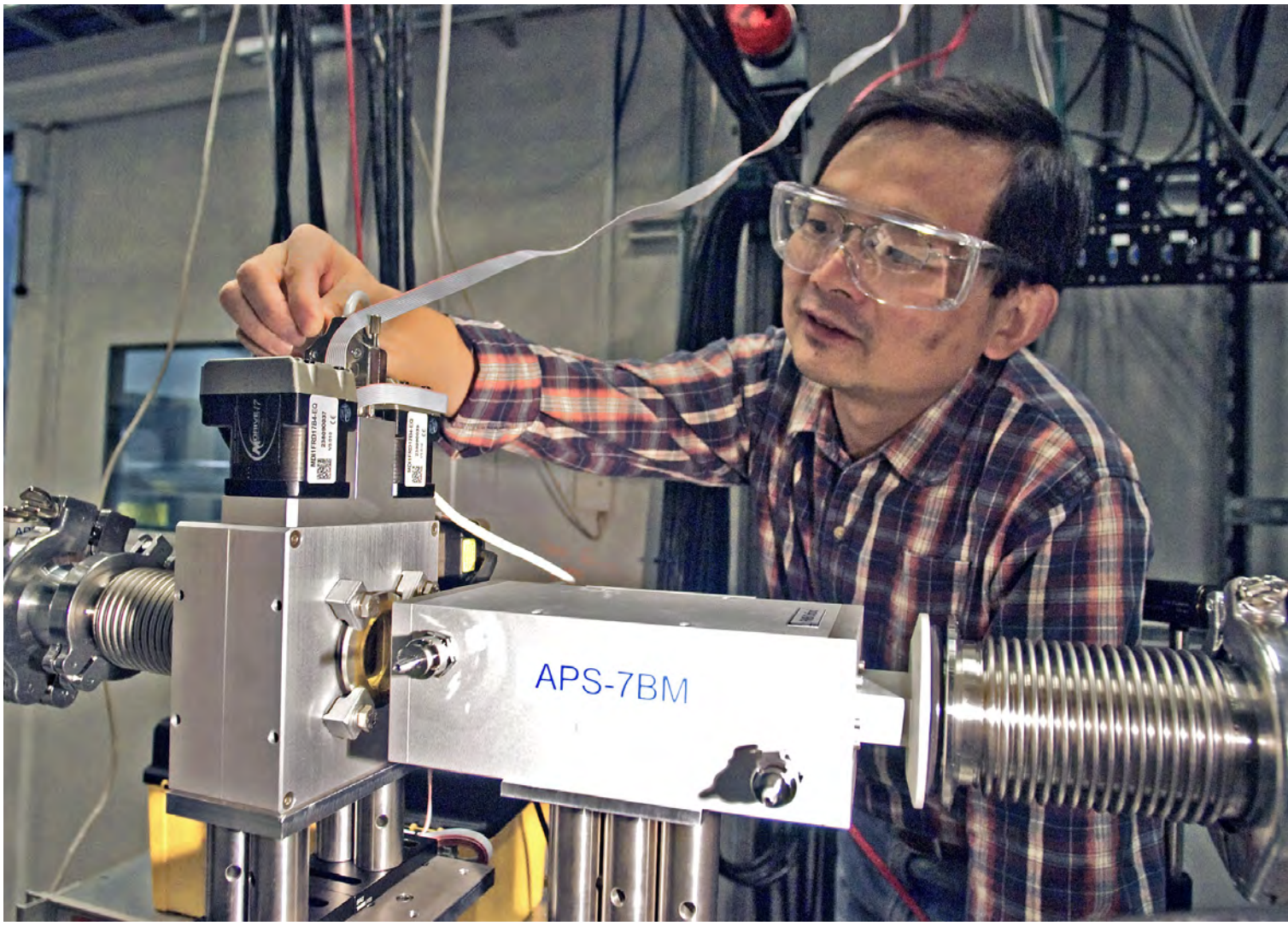

rapid compression machines. Major emphasis is placed on safe operation under high-pressure, high-temperature conditions. Ultrafast area detectors are the coming from Cornell and the APS.

The beamline control system was completed and major x-ray optics components were installed in January 2009. At the time of this writing, the beamline was in its commissioning period and scheduled to be available to general users during user the third user run in 2010. Contact Jin Wang (wangj@aps.anl.gov)

Two Independent Beamlines for SAXS at 12-ID

IN SHORT > The APS Strategic Plan calls for XOR/BESSRC beamline 12-ID to become a dedicated small-angle x-ray scattering (SAXS) facility. For the last seven years, the demand for SAXS beam time by users of 12-ID has consistently exceeded the available time by a factor of two. The current SAXS facility (originally funded from the FY1996 DOE Scientific Facilities Initiative) has steadily grown to now represent 50% of the usage of the 12-ID beamline. With the current instrument configuration oversubscribed, the only way in which the present SAXS community can continue to grow, and new users can take advantage of these new capabilities, is to provide simultaneous operation of two 12-ID experimental stations by adding canted undulators and new beamline optics. This enhancement would provide the APS with a dedicated SAXS beamline to better serve the general user community in a number of areas in materials science, chemistry, and biology. At least half of current 12-ID users are doing bioSAXS.

MORE > The increasing demand for SAXS beam time has been driven by research into the structure and dynamics of nanoscale materials (for which SAXS is an extremely valuable probe), an increased interest in soft matter, and increased usage of the 12-ID SAXS facility for time-dependent structural investigations. General-user experiments have included these areas, as well as the extensive use of the 12-ID SAXS instrumentation for biological research. The more than 350 users who have done experiments on the X-ray Science Division (XSD) Chemical and Materials Science (CMS) Group's SAXS instrument represent more than 42 U.S. universities, 9 national laboratories and government institutions, 6 industrial research laboratories, and researchers from 11 foreign universities and laboratories.

Increasing interest in time-dependent SAXS experiments led the CMS Group to add a pink-light mirror system to the 12-ID beamline. Installed in late FY 2005, this addition has enhanced the flux on sample by over three orders of magnitude, providing new time-resolved experimental opportunities for small-angle scattering experiments. With the development of dedicated instrumentation for anomalous grazing-incidence small-angle x-ray scattering at 12-ID, the beamline will also serve as an important complement to the infrastructure for the Center for Nanoscale Materials at Argonne and further increase the demand for this beamline. This will enable XSD to pursue options such as high-throughput SAXS, which could be used for combinatorial materials studies.

The vacuum chamber for the canted undulators was installed in FY2006 and the canted undulator front end (Fig. 1) has now also been installed. Currently, two undulators are installed inline: a U30S and U33S; in May 2010 they will be canted. In the future the U33S will be replaced with a U27 undulator, which is optimized for

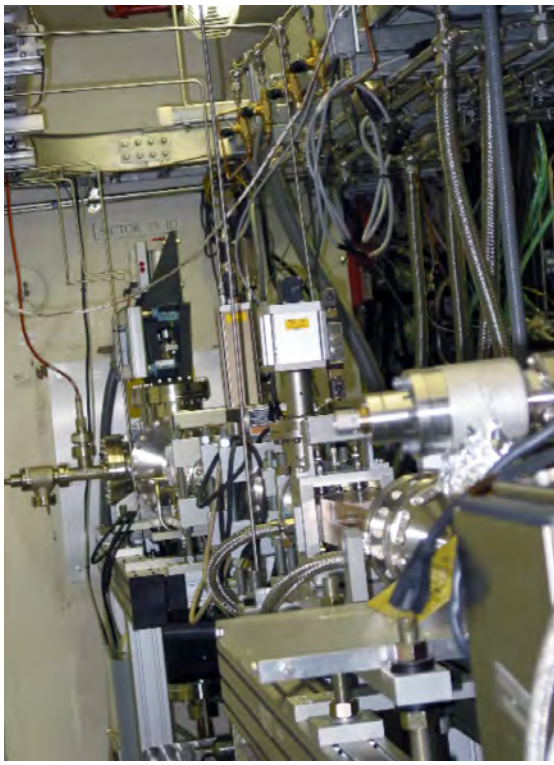

^ *Fig. 1 Canted undulator front end.*

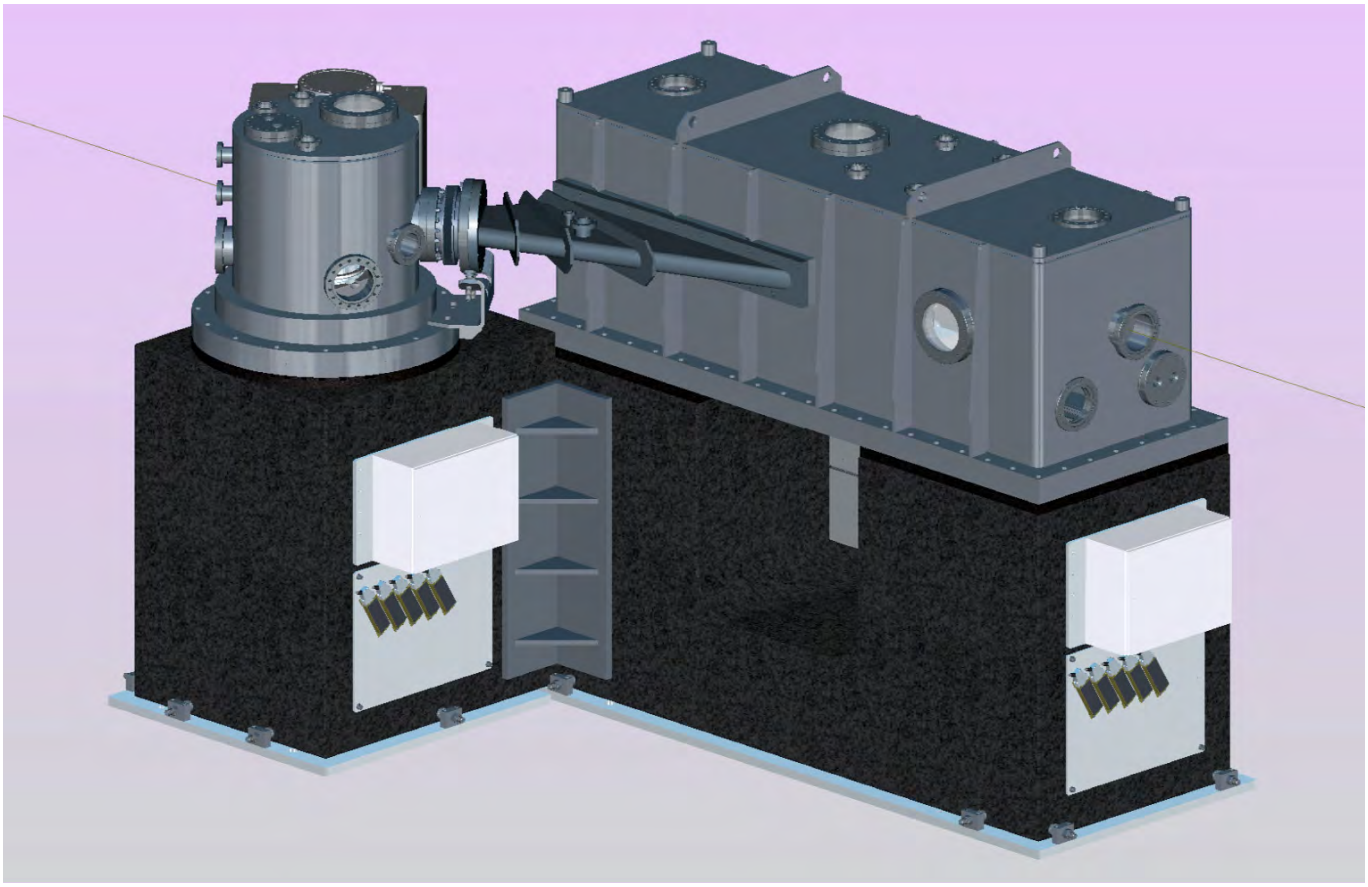

^ *Fig. 2 Conceptual drawing for the large-offset side-bounce monochromator to be used for the 12-ID-B branch beamline.*

the energy range on the 12-ID-B beamline. One of the resulting undulator beamlines will use a more stable version of the current monochromator with an energy range of 4.5 to 35 keV and a mirror system that includes the existing pink-beam mirror. This beam will feed 12-ID-C/D and be used for anomalous, time resolved, grazing incidence SAXS in the C hutch, and surface scattering and metal organic chemical vapor deposition studies in the D hutch. The experiments in the C hutch will use a new mosaic large-area charge-coupled device detector built by XSD.

After canting, the second undulator will feed 12-ID-B as a dedicated SAXS station using a large offset monochromator (870 mm). This monochromator (Fig. 2) will use a cryo-cooled silicon [220] first crystal to provide an energy range of 7.4 – 13.9 keV. A Pilatus large-area detector will be used in conjunction with a large vacuum-scattering chamber where the position of the detector can be changed automatically to access different Q ranges, and a wide-angle detector will be attached permanently to the front of the chamber. A two-dimensional detector with high linearity, dynamic range, stability, and low or no dark current is crucial for SAXS. The Pilatus detector has overwhelming capability in these respects, with a 20-bit dynamic range and no dark current. These detectors will make 12-ID-B a very versatile SAXS beamline.

Monthly meetings are held with the user community to update them on progress as the upgrade of 12-ID moves forward, and give them the opportunity for input. The final installation of beamline components and commissioning is scheduled for the May 2010 shutdown through the 2010-2 run cycle. Randall Winans (rewinans@anl.gov)

The APS User Community

IN SHORT > During 2009, the APS user community continued its relatively steady growth, with the number of unique users by fiscal year demonstrating a sharp increase from FY2008 to FY 2009. Figure 1 shows the number of unique users by fiscal year since the APS began operations, as well as the number of operating beamlines. Figure 2, which shows the number of experiments by fiscal year, also demonstrates steady user community growth, with a sharp increase from FY2008 to 2009.

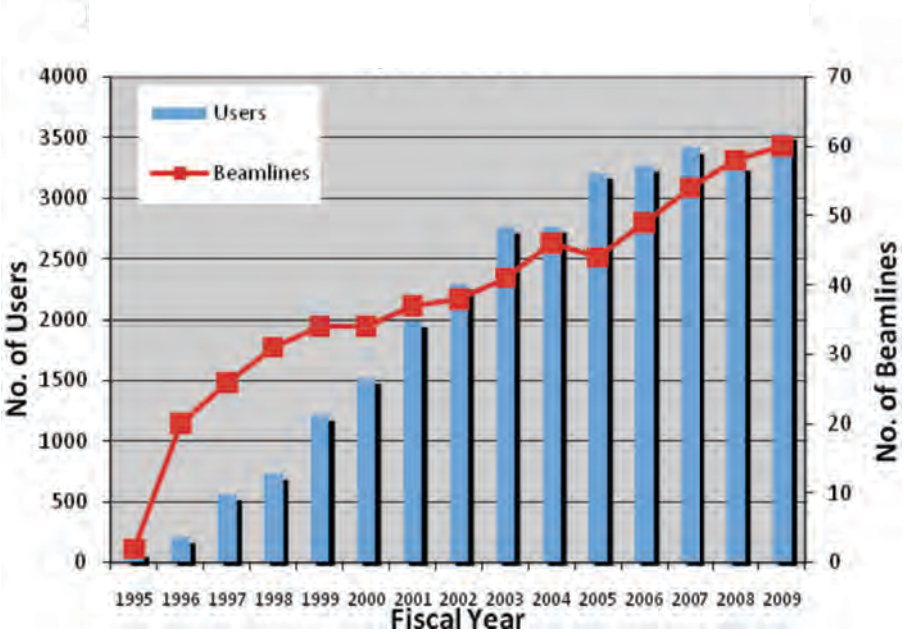

^ *Fig. 1 Number of APS unique users and operating beamlines, by fiscal year.*

MORE > The character of the user community, however, is begining to change. Although the number of on-site unique users is continuing to increase, this increase may be moderated in the future by the number of users choosing to either operate beamlines remotely or mail

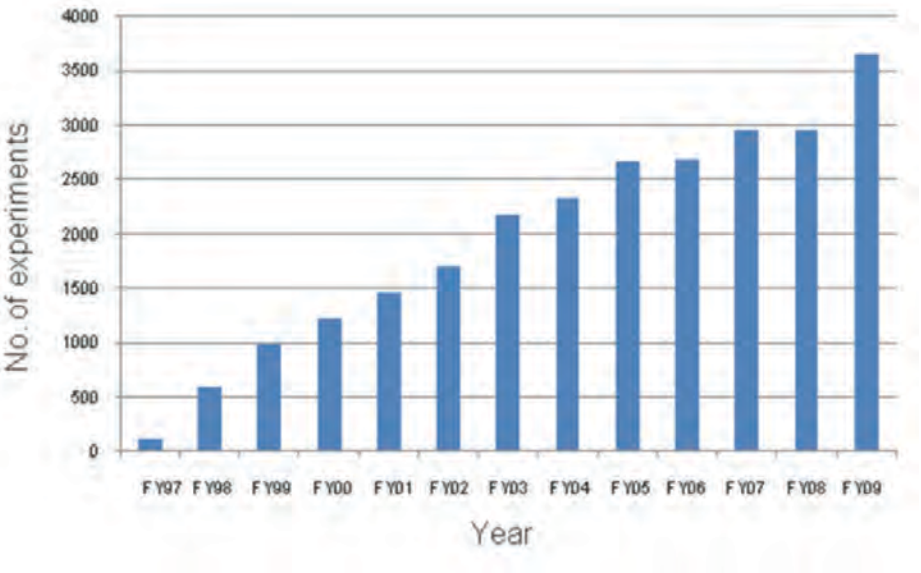

^ *Fig. 2 Number of experiments at the APS, by fiscal year.*

in samples for beamline staff to handle. Figure 3 demonstrates this change over the past three years.

During FY2009, users affiliated with universities continued to constitute our largest community, which has been the case since the APS began user operations. Figure 4 shows the institutional distribution of FY2009 users. Figure 5 shows the distribution by research field, with biology/life sciences once again constituting the majority community.

Demand for general user beam time also increased slightly in 2009, with 3095 beam-time requests (BTRs) submitted (vs. 2900 BTRs in 2008), with an average oversubscription rate across all beamlines during 2009 of 1.7.

Beginning in 2010, all beam time, not just general user time, will be requested through a central beam-time request system. This new system will provide better tracking of beam-time use and permit the APS to respond more quickly to changing user needs and demographics.

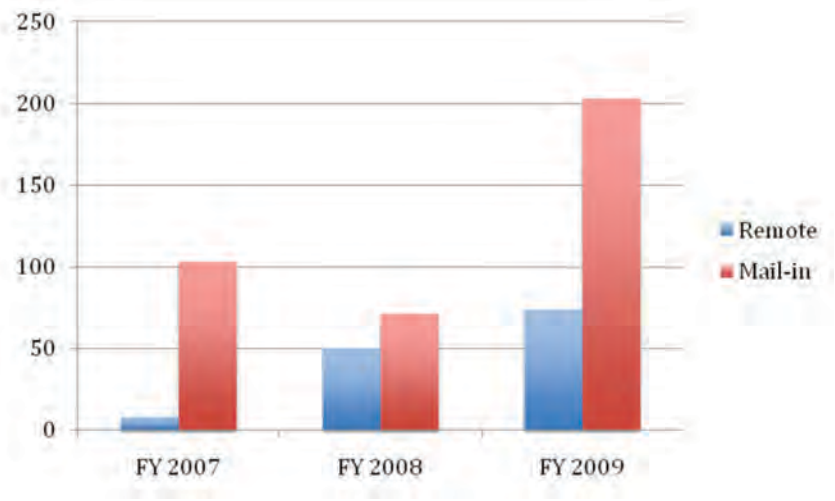

^ *Fig. 3 Number of remote and mail-in users at the APS during the years 2007 through 2009.*

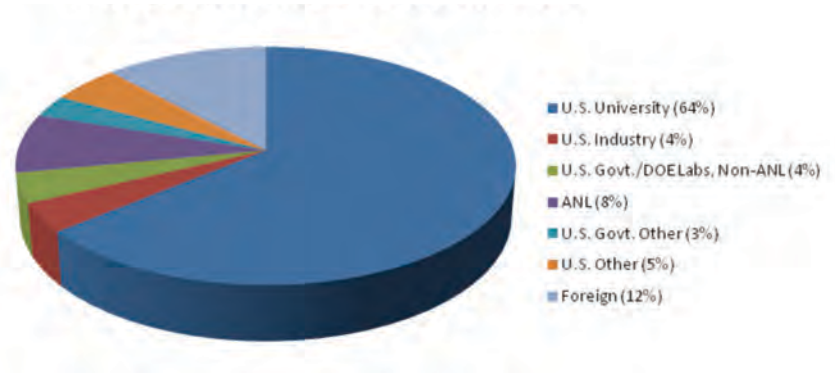

^ *Fig. 4 FY09 APS user distribution by institution.*

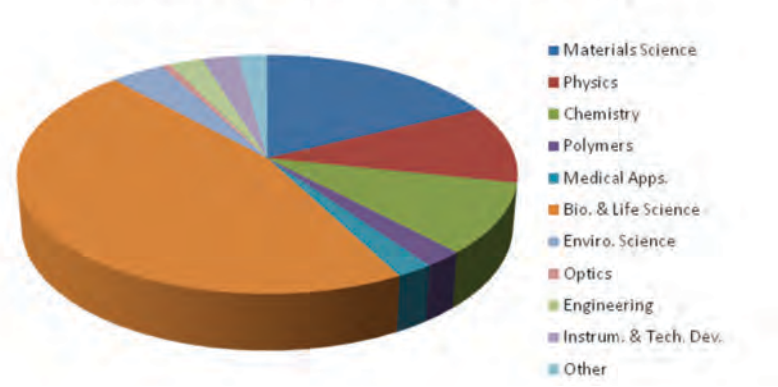

^ *Fig. 5 FY09 APS user distribution by research field.*

User Week 2009

IN SHORT > Although Argonne's 2009 User Week focused primarily on the APS Upgrade, it also included talks on a wide range of research-related topics, and reports from two other Argonne user facilities: the Center for Nanoscale materials (CNM) and the Electron Microscopy Center (EMC) for Materials Research.

MORE > Monday featured scientific highlights and a session on the APS Upgrade proposal. In his opening APS update, Argonne Associate Laboratory Director for Photon Sciences and APS Director Murray Gibson reviewed a broad range of topics, including better-burning fuels, natural solar cells, metal oxide frameworks for hydrogen storage, better batteries, climate change, human health, infrastructure concerns, ancient cultures, high-pressure science, and of course, basic science. Gibson also addressed possible changes to the General User Program to address the expertise of judges on the review panels and to better accommodate industrial proposals.

Pedro Montano of the U.S. Department of Energy (DOE) Office of Science, Office of Basic Energy Sciences (BES) painted a promising picture of upcoming funding for facility operations. New funding (in addition to research funding already designated in facility budgets) will also be available for accelerator and detector research. Montano confirmed that the APS Upgrade is a first priority in new construction for the Office of Science, but cautioned that the project must be designed so that it does not impact ongoing science. He noted that, in terms of the APS Upgrade, the goal is to achieve another 10 to 12 years at top performance, and because beamlines become obsolete earlier than machines do, beamlines must be refreshed during this process. In FY 2008, BES facilities served 10,995 users. The light sources were the highest volume facilities, serving 8,492 users (39% of those at APS). According to Montano, the five BES nanoscience centers are also doing very well; all of them have hit the ground running.

In reports from the CNM and EMC, Stephen Streiffer and Dean Miller (respectively) highlighted current and upcoming capabilities. Streiffer noted that the CNM is discussing the merits of targeting a 5-nm beam size. Miller noted that the Sub-Angstrom Microscopy and Microanalysis Facility is now complete and operational. The EMC has been closely involved in the TEAM project, a multi-laboratory collaboration to develop a transmission electron aberration-corrected microscope. Portions of the new technology are already in use, and the exciting results being obtained with aberration correction were the subject of a Monday afternoon presentation by Bernd Kabius (EMC).

Two other afternoon presentations highlighted recent work at the APS. Janet Smith, (University of Michigan) discussed "Finding Gems in Low-quality Crystalline Proteins with an X-ray Mini-Beam," and Brian Stephenson (Argonne) spoke on "Chemical Switching of Polarization in Ultrathin Ferroelectric $PbTiO_3$ Films."

A special session on the APS Upgrade included a perspective from the APS Scientific Advisory Committee, a detailed review of the science drivers (the result of extensive discussion by 10 science teams), a report on proposed accelerator upgrades, and a summary of the overall vision for how the Upgrade will be structured.

The 2009 Compton Award was presented jointly to Gerhard Grübel, Simon Mochrie, and Mark Sutton (Fig. 1) for their pioneering efforts in x-ray photon correlation spectroscopy (XPCS), which exploits the coherent properties of synchrotron x-rays to study the slow dynamics of condensed matter at short length scales. Each winner spoke briefly on his perspective on the development and applications of XPCS.

Recognition was also provided for student users Naji Sami Husseini (University of Michigan), who gave the student invited talk, and for poster award winners Jonathan D. Emery (Northwestern University), David Kissick (Purdue University), and D.K. Schreiber (Northwestern University).

Tuesday morning was devoted to talks that explored the pressing research questions in the areas of the dynamics of life (Keith Moffat, University of Chicago), materials for energy applications (George Crabtree, Argonne, presenting on behalf of Michelle Buchanan, Oak Ridge

National Laboratory), materials under pressure (Russell Hemley, Carnegie Institution of Washington), and characterization of real-world materials systems (Roger Leach, DuPont). On Tuesday afternoon, the focus turned to new techniques, with overviews of coherent diffraction and x-ray imaging (Keith Nugent, University of Melbourne), x-ray microscopy (Chris Jacobsen, Stony Brook University), metrology and optics (Lahsen Assoufid, Argonne), and ultrafast x-ray spectroscopy (Robert Schoenlein, Lawrence Berkeley National Laboratory). During the morning and afternoon "user visions" sessions, eight users presented their cases for scientific directions for the APS Upgrade.

On Wednesday, users selected from three half-day and three full-day workshops focusing on topics supporting the Upgrade proposal: detectors, optics, nanopositioning, high-speed imaging, imaging of biological systems, and chemical science. Susan Strasser (strasser@aps.anl.gov)

v *Fig. 1 The 2009 Compton Award was presented by (left) APSUO Chair Laurence Lurio (Northern Illinois University) and Argonne Associate Laboratory Director Murray Gibson to (center) Mark Sutton (McGill University), Simon Mochrie (Yale University), and Gerhard Grübel (European Synchrotron Radiation Facility) for their pioneering efforts in x-ray photon correlation spectroscopy, which exploits the coherent properties of synchrotron x-rays to study the slow dynamics of condensed matter at short length scales.*

Beam Stabilization Developments

IN SHORT > As reported in last year's annual report, upgrade work is underway to improve the data acquisition for the broadband (monopulse) rf beam position monitor (bpm) system. By the end of 2009, a total of 5 sectors have been installed in the ring, specifically in sectors 33 through 36 and 38. With parts on hand for three additional sectors, eight sectors will be instrumented by the summer of 2010, with production of components for additional sectors in process. Operationally, these units have already shown their value, allowing rapid diagnosis of unscheduled beam loss events using turn-by-turn data waveforms encompassing a quarter million turns (approx. one second) for each of the 7 channels per sector so instrumented. From an accelerator physics standpoint, this capability provides the potential for some very extensive investigations of beam dynamics supporting new machine optics for the APS upgrade. From a beam stabilization standpoint, this new data acquisition system has an extremely low noise floor (< 100 nm rms) over a relatively wide frequency bandwidth (1-200 Hz), and will allow the long term goal of 0.42 microns rms AC beam stability to be realized. Presently, rms beam motion in this band is about 5 microns horizontally, and 1.6 microns vertically, at insertion device source points.

MORE > In other developments, a prototype high-power hard x-ray beam position monitor is being tested in the sector 35 beam diagnostic insertion device beamline. This device holds the promise of providing long term pointing stability at the level of 500 nanoradians peak-to-peak or better over a one week period. Planned to be located in insertion device beamline front ends as part of the APS upgrade, this device should improve orbit reproducibility and make beamline steering adjustments more precise and predictable. This work has been ongoing for the past few years, and will make use of pin diodes sensing the x-ray flourescence emitted from a cooled Glidcop surface oriented at grazing incidence (Fig. 1). One interesting design feature of the final design will be that all sensors will be outside of vacuum, obviating the need for electrical vacuum feedthroughs while simplifying maintenance and repair; the x-ray fluorescence will be viewed through a large beryllium window located off-axis transversely as shown in the figure. The detector assemblies (not shown) make use of a diode array coupled with pinhole camera apertures to sense motions of the x-ray fluorescence footprint along the inclined glidcop surfaces. An in-air scale model of this design has been installed in beamline 35-ID and has been used to validate the geometry (Fig. 2).

> Fig. 1 Diagram showing the geometry for the high-power grazing-incidence hard x-ray beam position monitor for insertion device beamlines. (Courtesy S.H. Lee, AES-MED)

Coupled with improvements and upgrades to beam position monitoring systems will be an upgrade to the real-time feedback system, including a new high-speed data link transmitting bpm and steering corrector information around the ring. The existing real-time feedback system was designed in the early 1990's and some of the hardware is as much as 15 years old. It operates at a rate of 1534 correction steps per second, but is restricted to use at most 160 bpms and only 38 steering correctors in each plane. In order to achieve 200 Hz closed loop bandwidth taking into account computational and data distribution latencies, a sample rate of between 10 and 20 kHz will be required. In addition, the use of modern network hardware should allow access to all of the more than 500 channels of beam position monitoring (narrowband rf, broadband rf, and bending magnet and insertion device photon bpms). One other goal will be to relocate a significant number (dozens) of "slow" steering correctors to vacuum spool pieces, converting them to "fast" correctors by eliminating the retarding effects of eddy currents

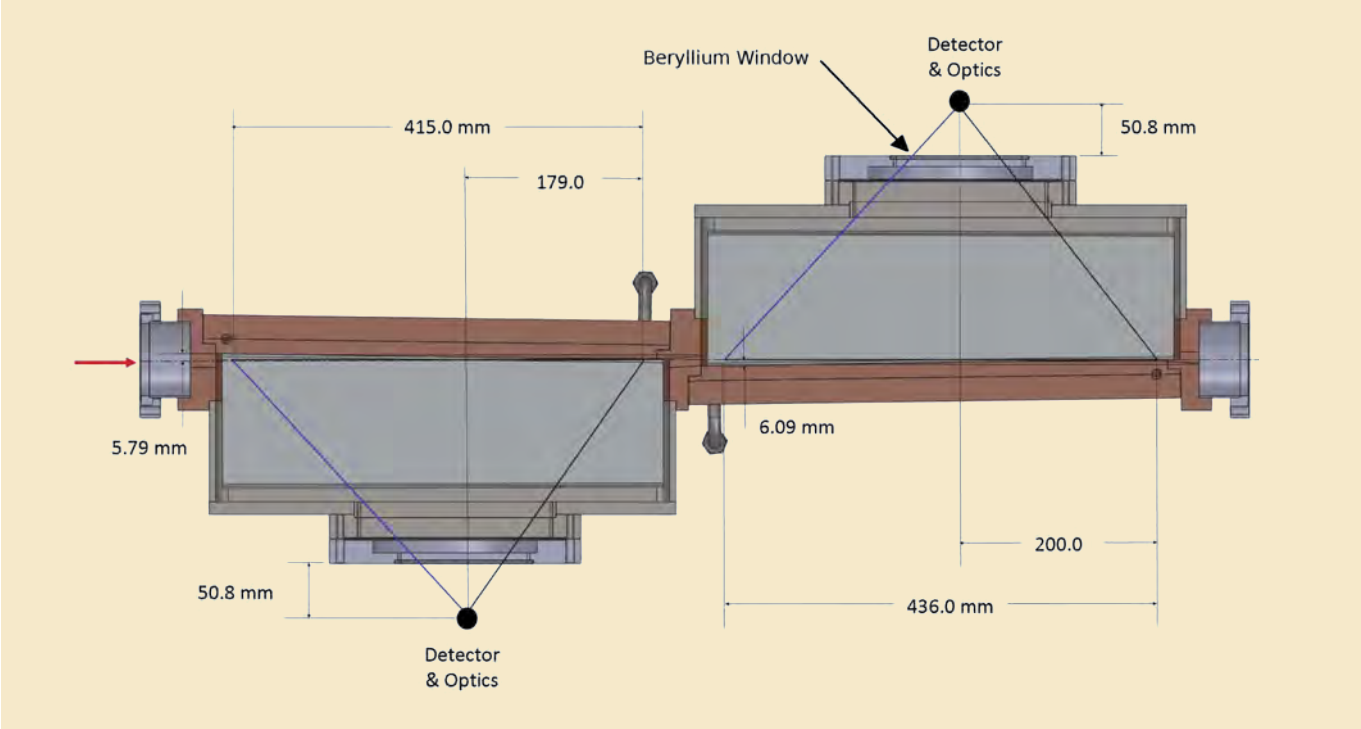

associated with the thick aluminum vacuum chambers. This will provide the ability to compensate noise sources with a finer spatial density, providing more local correction of these sources.

The end result of these developments will be a world-class orbit stabilization system providing AC stability better than half a micron and 200 nanoradians rms in the 1-200 Hz bandwidth, and long term stability at the level of one micron and 500 nanoradians p-p over one-week time periods.

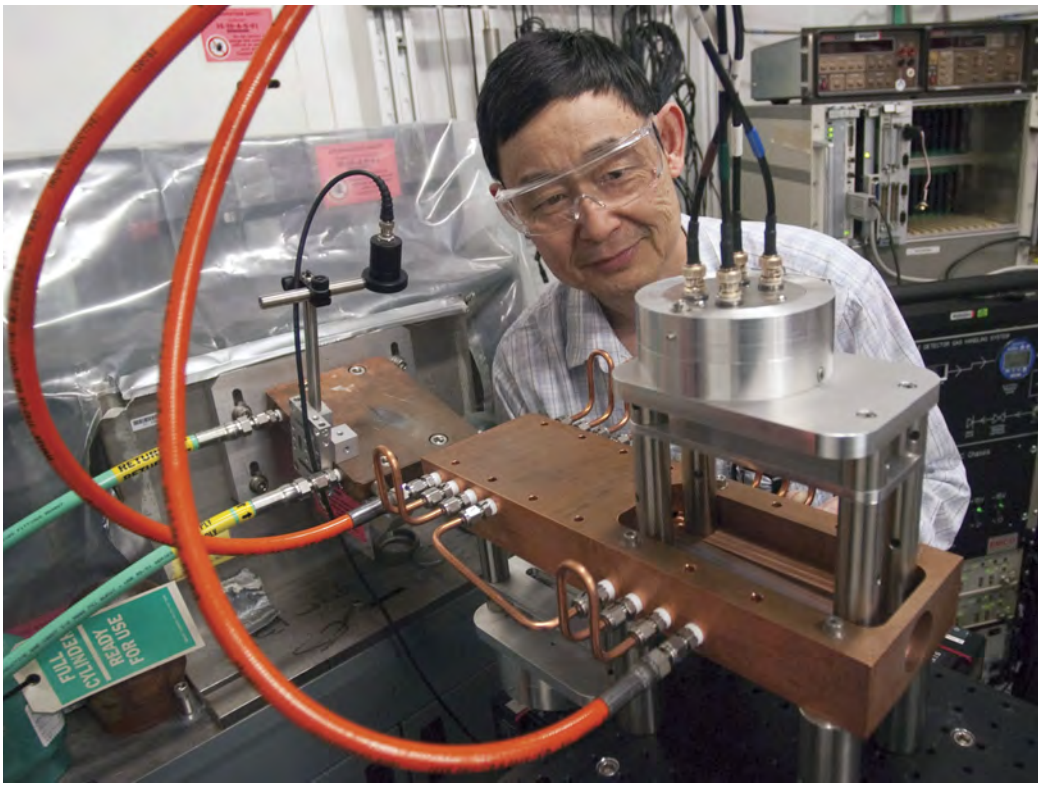

> Fig. 2 Beamline scientist Bingxin Yang (ANL-ASD) with scale model of the grazing incidence insertion device photon bpm at diagnostic beamline 35-ID.

R&D for an X-ray Free-Electron Laser Oscillator

IN SHORT > Research and development on the x-ray free-electron laser oscillator (XFELO) has now progressed significantly further than reported in *APS Science 2008* ("R&D Progress on an X-ray Free-Electron Laser Oscillator," p. 134). The main progress is summarized here.

MORE > 100-fs- Pulse Operation with Relaxed Tolerances

The previous study used an electron beam with 20 A of current in a 1-ps, 0.2-mm-mrad emittance bunch at 7 GeV, which interacted with an undulator of about 3000 periods in an x-ray cavity whose total round-trip reflectivity was 81%. Since the tunable x-ray cavity scheme requires six optical elements (four diamond crystals and two grazing incident mirrors), the reflectivity per each element should be higher than 96.5%. We have studied another parameter regime with relaxed requirements.

We found that when compressing the bunch to 0.1 ps, thereby increasing the current to 100 A, the round-trip reflectivity of 50% is sufficient even with a larger emittance (0.3-mm-mrad) and a smaller number of undulator periods (N_u = 1000) [1]. The requirement on the reflectivity of each element becomes significantly relaxed, such that the reflectivity of each should be higher than 89%. The cavity could be shorter, 50 m rather than 100 m, leading to a relaxed angular stability. Thus, the shorter bunch operation offers improved time resolution with relaxed tolerances. The XFELO parameters with two-pulse-length operation are compared in Table 1.

v *Table 1 Comparison of XFELO parameters with 1-ps and 0.1-ps electron bunches.*

Electron Bunch			
	Energy (GeV)	7.0	
	Energy spread (MeV)	1.4	
	Repetition rate (MHz)	1	
	Length (rms) (ps)	1.0	0.1
	Charge (pC)	50	25
	Current (A)	20	100
	Emittance (mm mrad)	0.2	0.3
Undulator			
	Period length (cm)	1.8	
	Undulator length (m)	57	25
X-ray Cavity			
	Roundtrip reflectivity (%)	81	50
	Reflectivity per element (%)	96.5	89
X-ray Output			
	Peak power (MW)	3.9	3.8
	# Photons/pulse	4×10^9	0.5×10^9
	Pulse length (95% rms) (ps)	0.69	0.084
	$\Delta\omega/\omega$ (95% rms)	1×10^{-7}	6×10^{-7}

Generation of 1-fs Pulses without Fluctuation?

While the narrow bandwidth of the Bragg mirrors precludes the possibility of directly producing femtosecond x-ray pulses using an XFELO, it may be advantageous to use this concept to seed a very short electron beam; an electron beam so prepared could then be extracted from the oscillator region and passed through a short (a couple of gain lengths) undulator section to produce fully coherent, femtosecond x-ray pulses. The femtosecond pulse produced in this scheme will be stable, in contrast to the ultrafast self-amplified spontaneous emission pulses proposed recently [2], which have inherent fluctuations. Extracting and transporting a high-energy beam from the oscillator while maintaining the Å-scale microbunching is challenging and will require careful beam optics design [3].

Diamond Crystal

With the cavity scheme using four crystals, the photon energy can be tuned continuously in a finite spectral region and all spectral regions of interest can be covered by one crystal material working at different Bragg planes. The choice of material is diamond, a crystal with the highest reflectivity and excellent mechanical and chemical properties. The reflectivity of a perfect diamond crystal is predicted to be 98-99% in the hard x-ray region of 5 to 25 keV. The required volume is not large, about $1 \times 1 \times 0.1$ mm^3.

Experiments performed at XOR/IXS beamline 30-ID at the APS have provided the first evidence that diamonds perform in practice close to the theoretical predictions, in terms of reflectivity and energy bandwidth [4]. We have shown that small areas (about 1×1 mm^2) of commercially available, synthetic type IIa diamond crystals can exhibit a high degree of perfection, with the measured spectral width and reflectivity approaching their theoretical values, $\Delta E = 2.9$ meV and $R = 89\%$, respectively. These were measured in Bragg diffraction at normal incidence to the reflecting atomic planes, using hard x-rays with a photon energy of $E = 23.7$ keV. The preliminary selection of near-perfect crystal regions was done using x-ray white beam topography. These data are shown in Fig.1. Note the close correlation of diamond qualities seen in the topograms to the spectral width and reflectivity measurement.

The temperature variation of a lattice parameter of a synthetic diamond crystal (type IIa) was measured using high-energy-resolution x-ray Bragg diffraction in backscattering [5]. By improving the measurement accuracy by two orders of magnitude from previous experiments, we were able to directly probe the linear thermal expansion

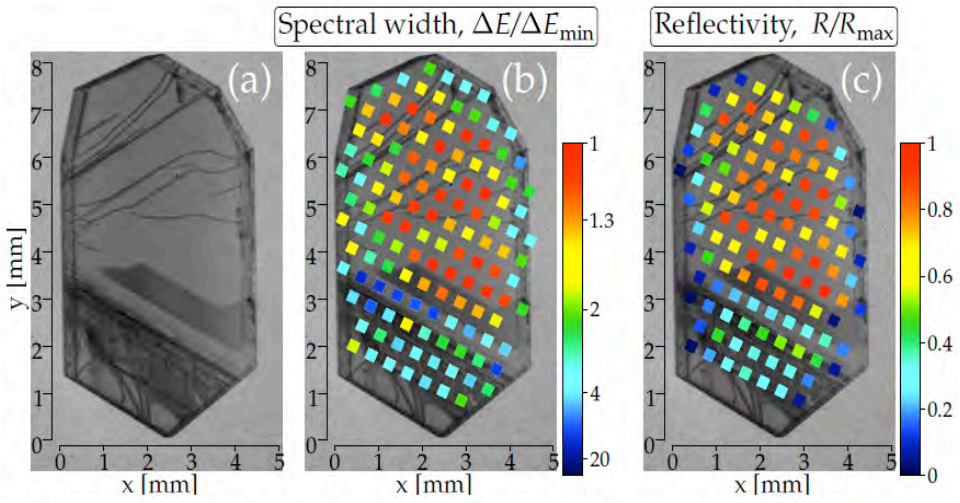

^ *Fig. 1 X-ray images of the sample diamond crystal.* ***(a)*** *White-beam x-ray topogram of the diamond crystal plate in transmission.* ***(b)*** *and* ***(c)*** *Color maps for the relative spectral width, $\Delta E=\Delta E_{min}$* ***(b)****, and the relative peak reflectivity for the (995) Bragg reflection, $R=R_{max}$* ***(c)****, at different points on the diamond crystal, measured with a 23.765-keV x-ray photon beam of 0.7 × 0.7mm^2 cross section. The beam footprint is larger than the pixels on the color maps, and has been reduced in size to allow direct comparison with the underlying white-beam topogram.*

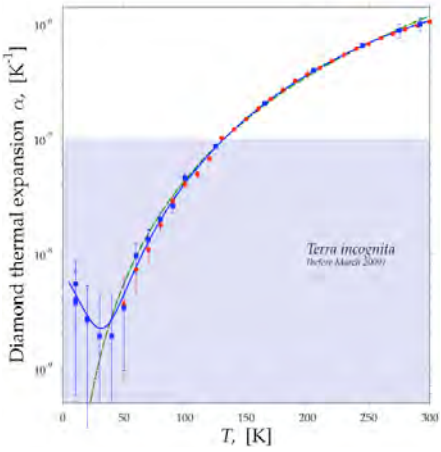

> *Fig. 2 Linear thermal expansion coefficient of diamond, obtained by point-by-point determination from experiment 1 (circles) and from experiment 2 (squares), calculated from the polynomial approximation (solid line) and the Debye model approximation ~T^3 (dashed line). The shaded area represents the region that was inaccessible to previous experiments due to their limited measurement accuracy.*

coefficient at temperatures below 100K, as shown in Fig. 2. The lowest value measured was $2 \times 10^{-9}K^{-1}$ near 30K. It was found that the coefficient deviates from the expected Debye law (T^3) below ~50K, while no negative thermal expansion was observed. When used in conjunction with the known value of the thermal conductivity at low temperatures, this discovery helps pave the way to solving the heat load problem of the x-ray cavity.

A pilot experiment to stabilize crystal angles via a feedback loop based on the null-detection principle was discussed in the previous *APS Science* report. Stabilization within 15 nrad in 1-Hz noise bandwidth was achieved [6]. Further progress for tighter angular stability (10 nm), broader bandwidth (1 kHz), and multi-axes system will be required.

A Test X-ray Cavity

For an integrated test, we will construct the prototype x-ray cavity shown schematically in Fig. 3 [6]. This prototype should be built in an available space at an APS insertion device beamline so that high-brightness x-ray beams can be injected into the cavity. The length of the prototype will be 23-24 m, about one-fourth of the actual x-ray cavity for an XFELO, which will be convenient because in this case, the mirror is smaller than that required for the 100-m cavity. The round-trip path length will be chosen to be either the same as the APS bunch spacing (46 m) for studying the evolution of the single high-intensity mode, or longer by about 1 m to allow for time measurements of x-ray pulses circulating in the cavity. The crystal and mirrors will be aligned with nanoradian-precision angular and submicron-precision high-stiffness linear stages. The stages will be driven by piezo actuators coupled to the feedback system. Room-temperature, as well as cryogenically cooled, optical elements will be tested.

v *Fig. 3 A concept for a test x-ray cavity.*

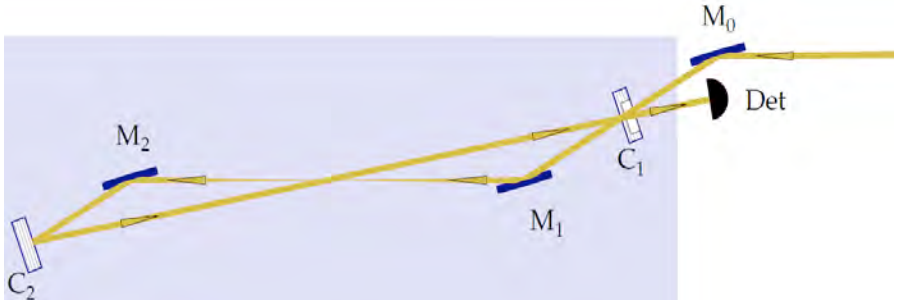

References >

[1] R. Lindberg and K.-J. Kim, to be published

[2] J. Rosenzweig et al., Nucl. Instrum Methods A **593**, 39 (2008).

[3] M. Borland, private communication

[4] Yuri V. Shvyd'ko, Stanislav Stoupin, Alessandro Cunsolo, Ayman H. Said, and Xianrong Huang, Nat. Phys. **6**(3). Published online 17 January 2010. DOI:10.1038/nphys1506

[5] Stanislav Stoupin and Yuri V. Shvyd'ko, Phys. Rev. Lett. **104** (2010)

[6] Stanislav Stoupin, F. Lenkszus, R. Laird, K. Goetze, Yuri V. Shvyd'ko, and K.-J. Kim, submitted to Rev. Sci. Instrum. Methods A.

[7] Yuri V. Shvyd'ko and K.-J. Kim, unpublished

Development of a 352-MHz Solid-State Rf Amplifier

IN SHORT > The Radio Frequency Group of the Accelerator Systems Division has initiated a long-term program to ultimately design and built a solid-state, 200-kW, 352-MHz radio-frequency (rf) amplifier to replace the existing APS klystron-based rf systems. This initiative is being undertaken by the group in order to address the potential long-term unavailability of this product by developing an alternative approach to deal with the issue. The RF Group is progressing toward construction and testing of a 352-MHz/4-kW, CW, solid-state rf amplifier demonstration system to be used to evaluate the practicality of solid-state rf systems for the APS accelerators.

MORE > The group has built and tested several 352-MHz/1-kW CW amplifiers utilizing the Freescale MRF6VP41KHR6 LDMOS rf power transistor, and a high-efficiency cold plate designed to maximize cooling of the transistor die (Fig. 1). Preliminary tests indicate that the design of a 200-kW, solid-state rf power system operating at 352-MHz and utilizing single-package transistor power amplifier devices operating at 1-kW CW is feasible.

A total of four 352-MHz/1-kW amplifiers have been built, two with one-piece copper cold plates and two with carrier/cold-plate construction. The carrier-version amplifiers were constructed with copper and aluminum cold plates to determine any differences in thermal performance.

Two 352-MHz four-port combiners, a standard 1/4λ combiner (Fig. 2) requiring external circulators for isolation, and one Gysel with inherent isolation have been designed to combine the output from four 1-kW amplifiers to produce the 4-kW demonstration system. The 4-kW system will be tested to understand how to improve overall system efficiency, reduce cooling water requirements, and estimate reliability. A 1/4λ combiner was designed in advance of fabrication. Initial tests of the 4-kW system are tentatively scheduled for April 2010. Ali Nassiri (nassiri@aps.anl.gov), and Doug Horan (horan@aps.anl.gov)

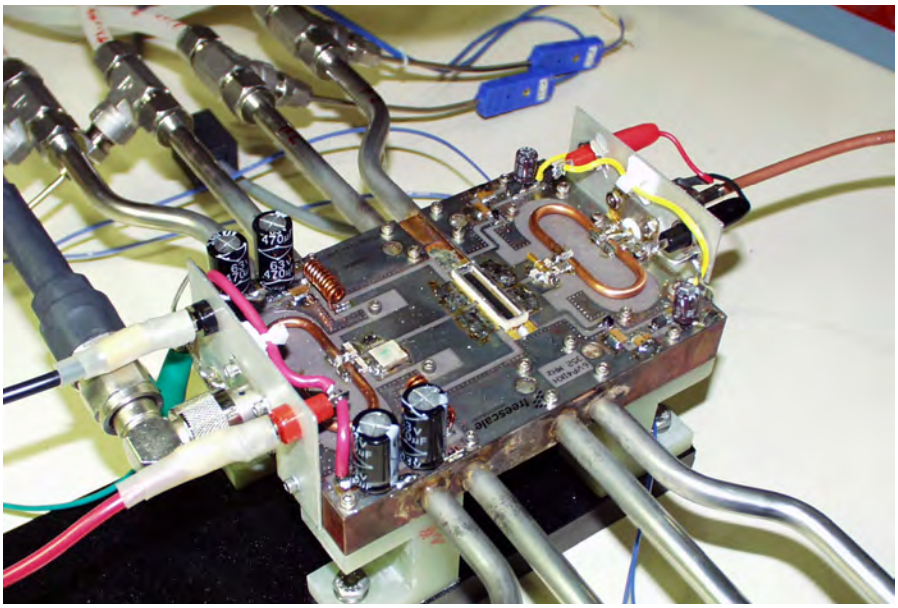

^ *Fig. 1 A 1-kW, 352-MHz test amplifier.*

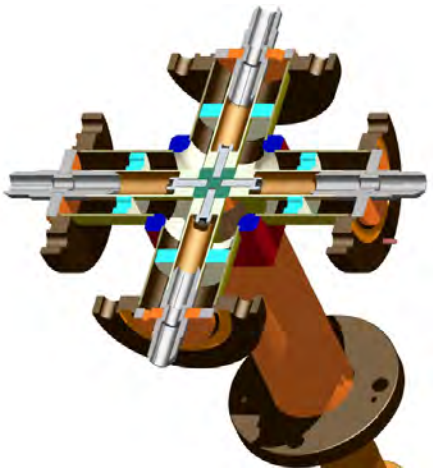

^ *Fig. 2 Cut-away view of a four-way rf combiner.*

Progress on the P0 Feedback Project

IN SHORT > The Advanced Photon Source storage ring has several bunch fill patterns for user operation. The hybrid fill pattern consists of a single bunch with a charge of 16 mA and a bunch train of lower-charge bunches. Due to its high single-bunch charge, beam instabilities exist and are currently compensated for with high chromaticity correction. High chromaticity reduces dynamic aperture, reduces beam lifetime, and generally increases non-linear effects on the storage ring beam. The P0 feedback project was initiated as part of an effort to control beam instability and reduce the chromatic correction for the APS storage ring. An initial system was installed and tested. It has achieved the goal of stabilizing beam and storing beam with high single-bunch charge and balanced chromaticity.

MORE > Figure 1 shows a picture of the main part of the system installed at the Sector 2 storage ring mezzanine, and Figure 2 is a block diagram of the system. The system samples the transverse beam position of each target bunche at a stripline monitor, filters the sampled data to generate the correct drive signal, and sends the drive signal to high-power radio frequency amplifiers that drive the target bunch through a drive stripline. Closed-loop operation of the system generates damping on all target bunches and achieves beam stabilization.

An initial system was installed in 2008 and beam tests were performed. Several system upgrades of the design followed: improvement of the front-end electronics, moving a horizontal stripline to a new high-β_x region, installation of two 500-watt amplifiers, addition of a remote

v *Fig. 1 Main rack of the P0 feedback system.*

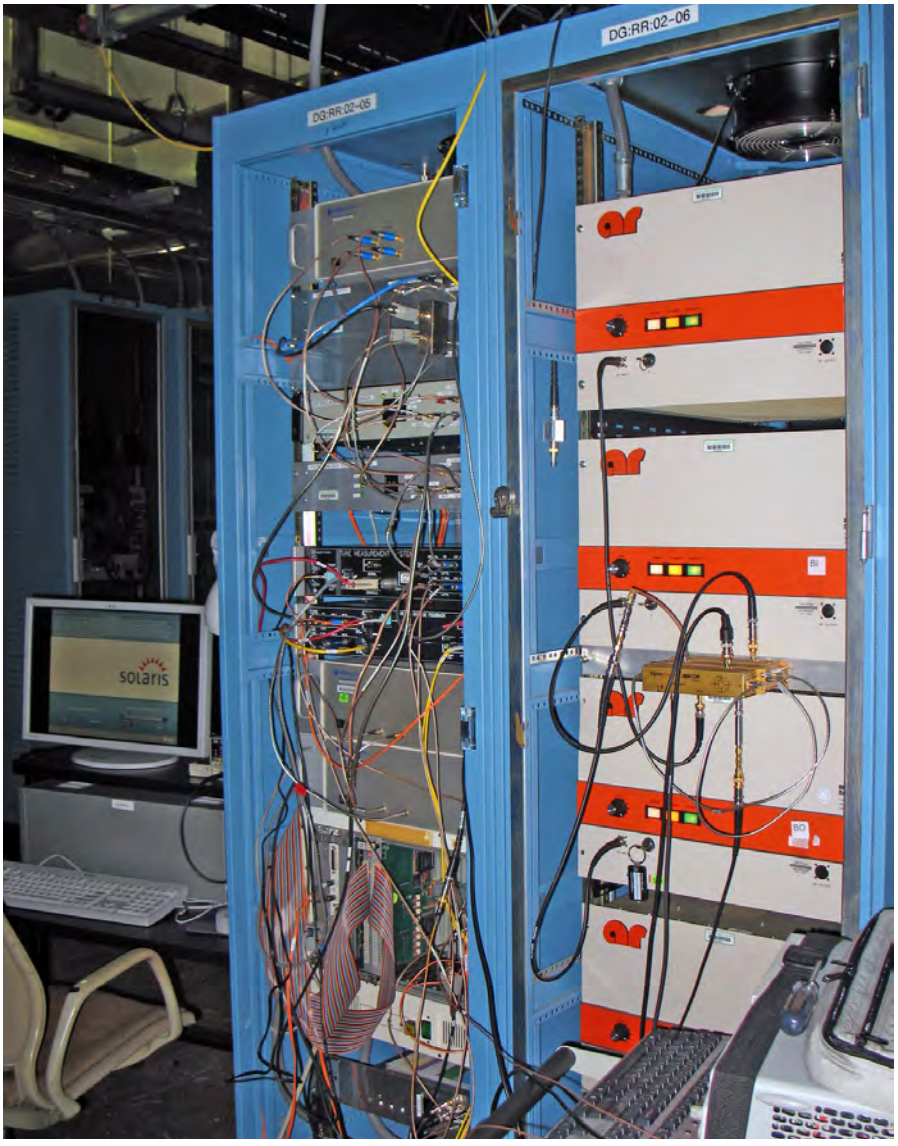

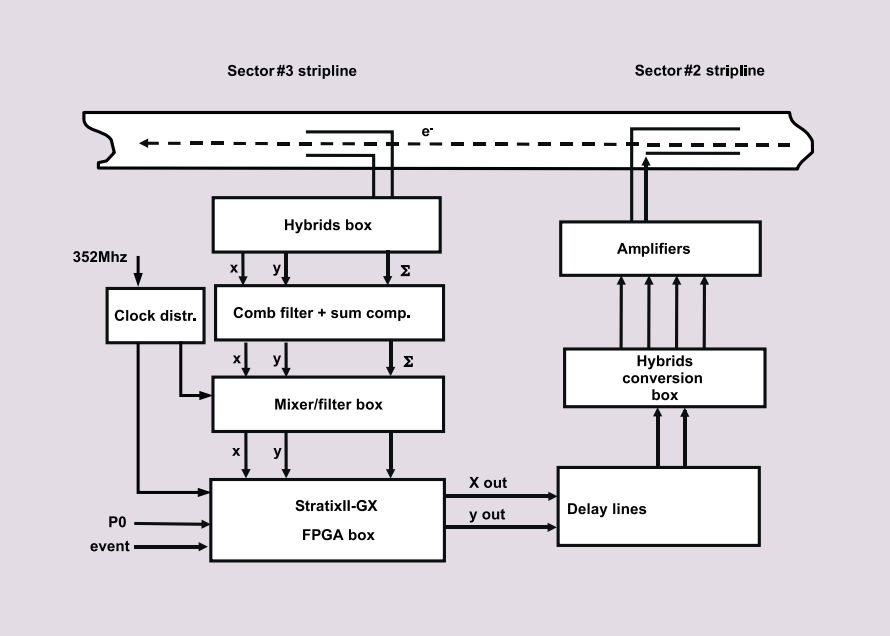

< *Fig. 2 Block diagram of the P0 feedback system.*

The plot shows: (1) Around target charge of 17-mA per bunch a reduction of 2.5 to 3 of chromaticity is achievable. (2) Areas B and C, which were previously not available for operations, are now included by operating with closed feedback loops.

Work is under way to review and implement operation readiness of the system so that a test run period can be conducted during user operations to further optimization and evaluation of the system. Contact: C.Y. Yao (e-mail: cyao@aps.anl.gov)

FPGA slave for horizontal drive, and design of a new two-blade horizontal stripline.

Commissioning of the system continued after the system upgrade. Significant progress was achieved during closed-loop beam tests.

We achieved the first goal of stabilizing standard 24-singlet-pattern beam with reduced chromaticity on November 3, 2009. A 10-mA 24-singlet fill pattern beam was injected and kept in top-up mode with feedback loops closed at reduced chromaticity of 0.5 in the horizontal plane and 2.5 in the vertical plane. Normal operation chromaticity for this fill pattern is around 6 for both planes. We ran in top-up for 2 h and observed an increase of beam life from 8.5 h to 15 h. We did not observe any obvious side effects on either beam emittance or rms beam motion. On December 19 we achieved our second goal of storing beam with high single-bunch charge with reduced chromaticity.

Figure 3 shows the results of a scan experiment, in which beam current stability and accumulation limit were measured while varying x and y chromaticities with the loop open and closed. Region A is the area where we can operate the storage ring with the loops open. Generally, we attempt to operate near the limiting curve for reduced lattice non-linearity. Regions B and C are areas where either vertical or horizontal instabilities are observed with feedback loops open.

v *Fig. 3 Stability and accumulation limits versus chromaticity with and without closing the feedback system loops. The black curve is the accumulation limit when the feedback system is turned on. The green curve is the accumulation limit when the feedback system is turned off. Beam is always stable in region A and has instability in both regions B.*

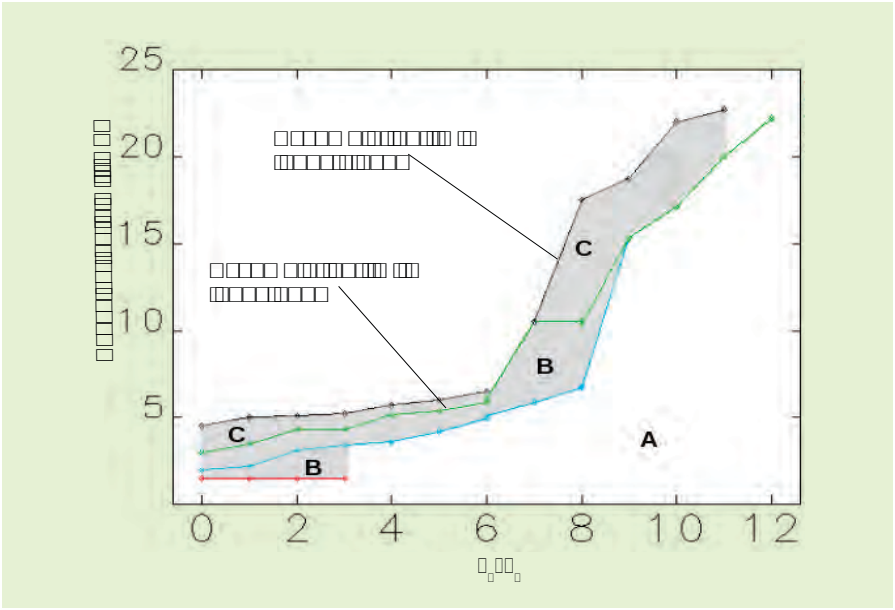

Collaboration with the NSLS-II at Brookhaven National Laboratory

IN SHORT > Vacuum Chambers for the NSLS-II

The National Synchrotron Light Source-II (NSLS-II) at the U.S. Department of Energy's (DOE's) Brookhaven National Laboratory will be a new, 3-GeV, 500-mA storage ring designed to deliver x-rays 10,000 brighter than those available from the current NSLS. Construction of NSLS-II began in 2009; early operations are expected in 2014. The lattice of the NSLS-II storage ring calls for 60 dipole vacuum chambers, 90 multipole vacuum chambers, and 45 straight-section vacuum chambers to contain the electron beam that will orbit around the 792-m ring and the x-ray beams that will be delivered down the facility's 58 beamlines. These vacuum chambers are the subject of a two-year collaboration among Brookhaven and Argonne scientists and engineers that has brought the extensive APS expertise in aluminum vacuum chamber design, fabrication, and commissioning to the service of a sister DOE light source.

MORE > The NSLS-II storage ring vacuum chambers (Fig.1) will be made of extruded aluminum 6063-T5, similar to the chambers used at the APS and based on good experience at the APS with extrusions, the cost of fabrication compared to other methods, the ability to obtain a smooth interior cross section, good thermal conductivity, impedance issues, and ease of *in situ* bake out. Brookhaven engineers adopted designs for their aluminum chambers from existing APS chamber designs, with the assistance of engineers at the APS.

v *Fig. 1 The first prototype NSLS-II dipole vacuum chamber was welded at the APS and sent to Brookhaven for testing and evaluation.*

Accommodating the NSLS-II chamber design required extensive welding development work. The cross sections of the NSLS-II chambers have a different profile than that of the APS chambers, and the NSLS-II multipole and dipole chambers have two completely different cross sections. The new chamber extrusion geometry required new tooling for the 6-in. × 4.63-in. and 6-in × 6-in. flanges to multipole and dipole end adapters. Because most NSLS-II chambers are shorter in length than those used at the APS, a tooling adapter was fabricated so as to not require repositioning of the tail stock tooling on the automated welding machines at the APS. New headstock tooling and tailstock tooling was installed on both welding machines to accommodate the two different cross sections. In addition, new tooling was needed for chamber components, including pumping ports, absorber ports, instrumentation ports, and x-ray exit ports. Because of the number of welding-part computer programs needed, the automated welding machines at the APS were upgraded, quadrupling the amount of part-program storage. Where possible, welding joint profiles and material selection were duplicated from the APS chambers and implemented into the NSLS-II chambers.

Additional APS engineering assistance has been applied to the NSLS-II process water system designs and to R&D for thermal stability of the vacuum system support girders. Contact George Goeppner (gag@aps.anl.gov)

IN SHORT > Nanopositioning

Based on the experiences gained from the nanopositioning system designed at Argonne for the Center for Nanoscale Materials (CNM)/APS multilayer Laue lens (MLL)-based hard x-ray nanoprobe project, a new nanopositioning system is being designed for the NSLS-II Hard X-ray Nanoprobe (HXN) prototype through a Brookhaven/Argonne joint work project. The joint work project was started in September 2009 and is expected to last for three years. Scientists and engineers at the Argonne APS Engineering Support and X-ray Science divisions and the CNM, and their counterparts at the NSLS-II are collaborating on the following important nanopositioning tasks:

- Identifying and solving engineering and technical tasks with the HXN prototype.
- Developing a laser encoding scheme to ensure stability between the sample and the MLL optics.
- Developing a sample holder allowing easy fiducialization of the sample with ancillary pre-alignment microscopes.
- Developing an HXN with adequate vibration properties.
- Solving various engineering challenges that will be encountered during prototype development.

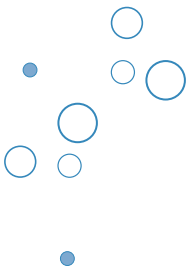

MORE > The design and prototyping activities for the NSLS-II nanopositioning system will also benefit further development of the CNM/APS MLL-based hard x-ray nanoprobe. Contact Deming Shu (shu@aps.anl.gov)

Novel Nanopositioning Stages with a Sub-Centimeter Travel Range

IN SHORT > Recent developments in hard x-ray focusing at the nanometer scale with linear multilayer Laue lenses (MLLs) have demonstrated promising new x-ray optics for focusing to a spot of a few nanometers. In order to use x-ray optics with a nanometer-scale resolution limit, scanning x-ray nanoprobes with corresponding mechanical positioning capabilities must be designed. In particular, positioning stages with both sub-nanometer resolution and a positioning/scanning range of several millimeters are a necessity. The precision ball-bearing or roller-bearing-based stage systems provide large travel range. However, they present difficulties in meeting the required sub-nanometer resolution, high tilting stiffness, and high straightness of trajectory within a single guiding system. It has always been a dream to have a compact, single-flexure stage to cover a large travel range with very high positioning resolution.

MORE > A two-dimensional (2-D) linear flexure stage system designed at the APS features high structure stiffness through the use of a laminar overconstrained weak-link mechanism. This represents a new development in the application of redundantly constrained laminar structures as weak-link mechanisms. Using a photochemical machining process together with lithography techniques, we were able to construct a strain-limited, over-constrained mechanism on thin metal sheets by stacking the thin metal weak-link sheets with alignment-pins, resulting in a solid, complex, laminar weak-link structure with ultrahigh positioning sensitivity and stability. The novelty of this new 2-D linear flexure stages system lies in its fishbone-shaped multiple-parallelogram guiding structure, which performs the function of a high-stiffness, high-precision linear motion guider with sub-centimeter travel range and sub-nanometer positioning resolution.

The 2-D linear flexure stages system comprises two weak-link stages: a vertical weak-link stage, APS T8-31, and a horizontal weak-link stage, T8-32. It is designed to perform a 2-D sub-nanometer resolution scanning function in a 3-mm × 3-mm range for a nanoprobe sample holder with a maximum weight of 5 kg for the MLL test setup. Figure 1 shows a three-dimensional (3-D) model of the APS T8-31/T8-32 2-D weak-link stage.

There are four fishbone-shaped laminar weak-link modules for the T8-31 vertical stage guiding structure. A commercial PZT-based nanopositioning motor, such as the N-214 NEXLINE™ motor made by PI GmbH and Co., provides the driving force for the T8-31. With the N-214 NEXLINE™ motor, the T8-31 weak-link stage has a 10-kg load capacity, 3-mm travel range with 10-nm closed-loop resolution, and sub-nanometer resolution within a 3-μm step. For applications that need a long scanning range with sub-nanometer resolution, a laser encoder with sub-nanometer resolution will be equipped for the stage positioning closed-loop feedback system. A customized stepping-motor-driven linear driver, combined with a PZT actuator, can provide the driving force for sub-nanometer-level, closed-loop resolution in the entire 3-mm travel range.

The horizontal-stage T8-32 consists of three laminar weak-link modules with an inverse "U" configuration for a 5-kg load capacity. As for the vertical stage, there are two options for the stage's driver. With a PI N111 NEXLINE™ motor, the T8-32 stage has 5-nm closed-loop resolution for a 3-mm travel range and sub-nanometer

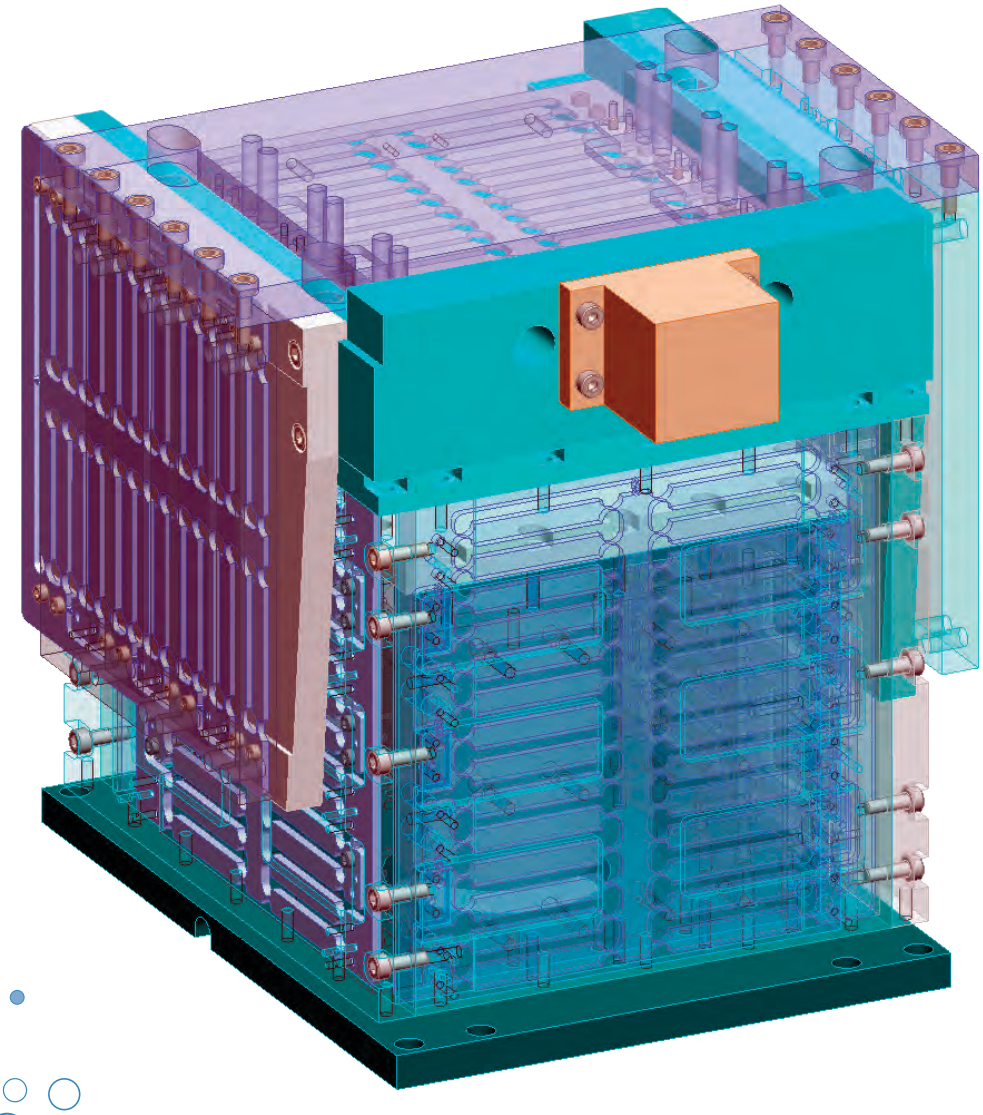

^ *Fig. 1 A 3-D model of the APS T8-31/T8-32 2-D weak-link stage with 3-mm × 3-mm travel range and sub-nanometer positioning resolution.*

resolution within a 0.8-μm step. With a laser encoder system and a customized motor/PZT combined linear driver, the T8-32 stage has sub-nanometer level resolution for the entire 3-mm travel range.

Using a commercial dual-beam laser interferometer system with 0.9-μrad resolution, we tested the vertical stage system's stiffness for all six degrees of freedom. The test results show that, driven by a PI N-214 driver, the T8-31 vertical weak-link stage has a vertical stiffness comparable to a worm-gear-driven precision screw stage in a similarly sized guiding structure using crossed-roller bearings. The straightness of our trajectory test results show that the T8-31 vertical weak-link stage has motion trajectory accuracy better than many commercial motor-driven, linear bearing-guiding vertical stages with a similar structure size. Contact Deming Shu (shu@aps.anl.gov)

See > D. Shu and J. Maser, "Study of precision weak-link stage systems with large travel range and sub-nanometer-scale resolution," to be published in Nucl. Instrum. and Methods A, the AIP Conference Proceedings of the 10th International Conference on Synchrotron Radiation Instrumentation, SRI-2009 (27 September-2 October, 2009, Melbourne, Australia).

Beamline Scheduling System

IN SHORT > When the APS began operations, all beamlines had been designed, funded, built, and were being operated by independent collaborative access teams (CATs). Each CAT was responsible for managing the operations of its own beamlines, including soliciting, reviewing, and scheduling requests for beam time. In early 2002, the Department of Energy, Office of Basic Energy Sciences, which funded several CATs, began to transition this funding to the APS, directing the APS to assume operational responsibilities for these CAT beamlines. As the operation of more and more beamlines was transitioned to the APS, it became clear that centralization of many processes would provide strong benefits to users, as well as to the scientists operating the beamlines. A centralized General User Program (for the submission, review, and allocation of general user beam time) was established in 2003, but individual beamlines continued to manage their own scheduling. As more and more beamlines were commissioned and began operations, the collection of uniform data for various types of reporting and planning became increasingly more difficult.

MORE > During the next few years, the APS began to consider methods for centralized beamline scheduling, eventually appointing a project team to build an entirely new database-based scheduling application. Requirements were gathered in 2008, and a technical review committee was formed comprising several senior beamline scientists. The committee reviewed progress and provided regular feedback to the developers. The software was successfully launched for use in late 2009 for a pilot program involving approximately half of all APS beamlines. The overall schedule for each run cycle can now be viewed in single, zoomable, scrollable chart (Fig. 1).

The application allows each beamline to schedule all types of APS-defined beam time: general user, collaborative access team, beamline staff, and partner user. These beam-time requests may be scheduled in two phases, allowing for reversible tentative scheduling followed by a formal commitment to the experimenters. The beamline staff supporting the incoming experimenters may also be independently scheduled. Fine-grained authorization allows each beamline to control the level of detail visible to the different customers of the application. A variety of guidance, warning, and statistics are provided during the graphical scheduling process. Another popular feature is the automated emails, which provide beamlines the ability to create custom email templates that drive automated email notifications during scheduling.

> Fig. 1 An example of the application "view-all" screen.

The project was a unique challenge for three reasons. Foremost was that many of the processes for scheduling developed over the prior 15 years were largely undocumented. The domain knowledge was distributed among many people, and had to be collected and represented formally. Secondly, supporting the scheduling process graphically proved to be a challenge. Much of what seems simple and intuitive about the act of scheduling is actually quite difficult to support with a simple user interface. This necessitated a more sophisticated application platform, and so the third challenge was evaluating and selecting the technology. The application user interface was built using Adobe Flex, and all business logic is provided as web services built using Java, Spring, Hibernate

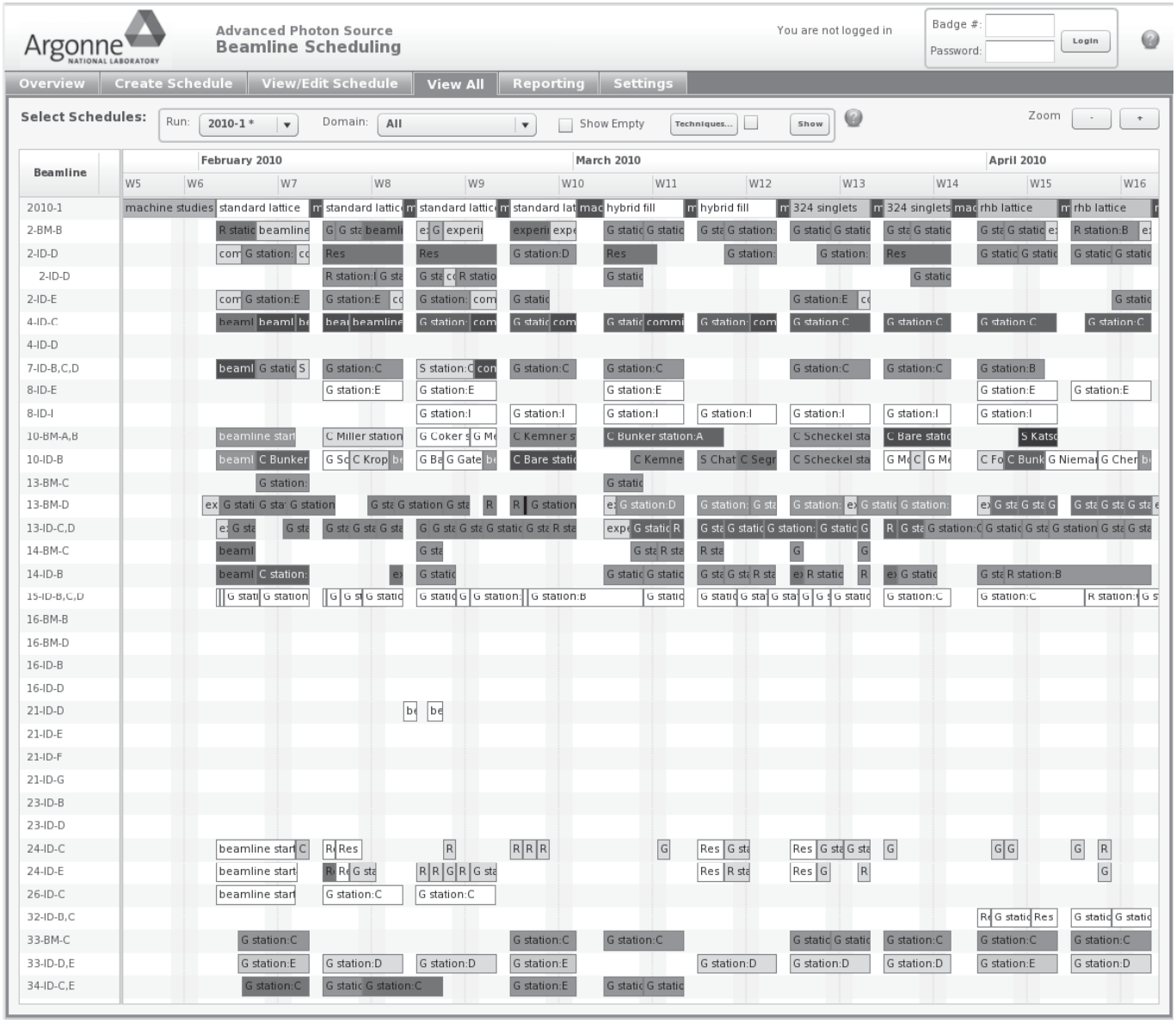

object-relational modeling, and the Oracle database.

Feedback from users has been very positive, with several citing significant expected time savings and the ease-of-use of the user interface. Work still remains, particularly in regard to reporting requirements. The future holds the possibility of integrating scheduling with other systems such as the detector pool, and further integration into a comprehensive scientific workflow management architecture. Contact Claude Saunders (saunders@aps.anl.gov)

A Synthesis of Sustainability and Science

IN SHORT > Sustainable building design is challenging engineers to push the envelope in innovation and adaptation of the latest breakthroughs in scientific research. The Department of Energy (DOE) now requires that a minimum of 15% of all existing DOE buildings meet stringent high-performance and sustainability requirements by 2015. Further, all new buildings with a construction cost in excess of $5 M must meet achieve a "Gold" sustainability rating from the United States Green Building Council.

MORE > Commercial buildings, which include most laboratories, account for 17% of all energy used in the United States and are fertile ground for making a significant impact on the nation's energy use and carbon footprint. Research facilities like the APS can use more than 10 times the energy per square foot than a typical commercial office building. The APS itself has an average power demand of nearly 20 MW, at a cost in excess of $11 million per year. All of this energy is converted to low-grade waste heat in the range of 20 to 35º C, removal of which has relied on a typical combination of mechanical refrigeration and evaporative cooling. Needless to say, the APS has an enormous carbon footprint.

Long before the current DOE sustainability requirements, the APS strove to reduce energy consumption and increase facility sustainability. These efforts included lighting upgrades, improvement in temperature control, increases in system operational efficiencies, and novel techniques in the recovery and reuse of low-grade waste heat.

In the article "Saving Energy for Science" (*APS Science 2008*, pg. 139), we documented a number of the energy efficiency enhancements at the APS that had been completed or were in the planning and construction phase. As of the beginning of 2010 all the energy efficiency improvements outlined in that article will have been completed and become operational. The projected energy savings and improvement in our carbon footprint resulting from the newly completed facility enhancements are projected to provide an annual savings of 33,296 x 10^6 Btu (10 million kW h) with a resulting yearly reduction of 12,269,768 pounds of carbon dioxide (CO^2) 16,576 pounds of nitrogen oxides (NOx), and 35,450 pounds of sulfur dioxide (SO^2). All of this work was completed under Energy Savings and Performance Contracts (ESPC's) requiring no up-front capital expenditure by Argonne. This work was a joint effort of the Argonne APS Engineering Support (AES) and Facilities Management and Services divisions, leveraging the resources and expertise of both. APS has been the beneficiary of a substantial reduction in operating costs, which to date is on the order of $600,000 per year.

The APS has long recognized the need to reclaim the vast amount of waste heat it generates in the production of x-rays. Taking advantage of our cold winter weather, engineers at the AES Division have developed a process of segregating air streams in ventilation systems to isolate and directly heat cold outdoor ventilation air. This is a novel approach that achieves the segregation without additional dedicated air conditioning systems and their associated capital and maintenance costs. Isolating the cold outdoor air stream increases the heat exchange temperature differentials and substantially improves heat transfer with the low-grade waste-heat source, making this a practical and efficient process. Since laboratories require the continuous introduction of large quantities of outdoor air, cold weather conditions provide an opportunity to recycle a portion of our waste heat.

Another feature of laboratories and research facilities is the need to continuously heat space supply air to achieve temperature and humidity conditions required for scientific programs. In order to keep heat transfer surfaces as efficient as possible, and minimize air pressure drops, these reheat coils

require heating-water temperatures well above those of our low-grade waste heat. Past attempts to tap the low-grade heat has resulted in heat transfer coils either dimensionally too large to fit in the available space or with excessive air pressure drops resulting in a substantial increase in fan energy consumption. In response, we have investigated two other approaches to waste-heat recovery; using fuel cell technology for on-site electrical generation with simultaneous heating, and the application of heat pumps that push the envelope of state-of-the-art technology.

In a cooperative effort with the Argonne Chemical Sciences and Engineering Division, AES is participating in the preparation of a proposal for the purchase and installation of a 400-kW stationary fuel cell for the Argonne Center for Nanoscale Materials (CNM) building. This fuel cell will provide electrical power at a lower cost than our utility provider and make available two new sources of usable waste heat; a low-grade source at 60° C and a high-grade source at 120° C. The addition of these two sources to the existing waste-heat recovery system at the CNM would shift all building heating needs strictly to waste heat. The combination of lower electrical generation cost and elimination of the need for heat from the Argonne site steam system would provide sufficient energy cost savings to make the purchase and installation of a stationary fuel cell affordable.

To expand our ability for low-grade heat extraction, AES has prepared a preliminary design for the installation of a heat-recovery chiller at the APS central cooling plant in building 450. Advances in centrifugal chiller technology, along with the expanded capability of the APS temperature control network have allowed us to push the limit on the hot water temperature generated by the chiller. This chiller would operate as a large heat pump capable of providing the simultaneous cooling and heating required by the APS in the spring, summer, and autumn seasons. Approximately 1.8 MW of accelerator and beamline waste heat would be extracted from the deionized process water cooling loop to produce heating water in the range of 65 to 70º C. This water would be used to provide a preheat stage in the APS heating plant. Monitoring heating water demand against outdoor air conditions would allow the APS to adjust the heating system temperatures to take maximum advantage of heat reclaimed from the new chiller. At the same time, a significant part of the DI process water cooling load would be shifted to the heat-recovery chiller, freeing up valuable chiller capacity needed during the summer.

Another large source of energy consumption is the APS lighting system. The existing experiment hall high-intensity discharge (HID) lamps consume approximately 2 million kW h per year with a yearly operating cost of $160,000. Due to the long warm-up time of the lamps, the use of timers or other on/off control devices is not practical. AES is currently investigating the replacement of all HID and other inefficient lighting with state-of-the-art LED lamps. This would not only reduce lighting power usage by nearly 65%, but with the longer life span of light-emitting diode (LED) lamps, the labor for re-lamping the fixtures would be reduced by at least 50%. A mock-up of the new experiment hall LED lighting will be installed in spring 2010 along with LED lighting for one laboratory/office module office

The preliminary estimated cost savings for the three new projects is on the order of $300,000 per year and will be submitted for inclusion in the next Argonne Energy Savings Performance contract scheduled for release at the end of 2010. Implementation of these projects relies on close cooperation among the various Argonne divisions and a continuing commitment to energy efficiency and sustainability. This, coupled with the willingness to push the envelope on emerging technologies should insure the successful completion of these projects and our ability to exceed the current DOE building sustainability goals. Marvin Kirshenbaum (kirshen@aps.anl.gov)

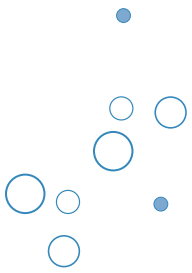

Sector Safety Reviews

IN SHORT > The APS has established a comprehensive user safety program to ensure the safe operation of the facility and a safe environment for its users. A portion of this program is the periodic review of each sector, its associated facilities (office areas, control areas, labs, experiment equipment with engineered safety controls, etc.), and experimental safety program. The review program was started in 1997 as the Independent CAT Safety Assessments. In this peer review program the individual sectors operated by collaborative access teams (CATs) were divided into groups that reviewed each other. The reviews were organized and directed by the APS, with the CATs being part of the review team.

MORE > In 2004 the program was modified to verify that all APS beamline facilities were safe and met APS/Argonne safety standards. In addition, the scope was broadened to include verification of beamline documentation records that are maintained by the APS. The APS took on primary responsibility for organizing and executing the sector reviews. Each APS sector is reviewed through this program on a three-year cycle.

The APS User Safety Officer chairs the review and appoints a review committee that includes the Radiation Safety System Manager, the User Technical Interface, Area Emergency Supervisor, X-ray Science Division ES&H coordinators, and others as appropriate to the sector's programs and facilities. The APS provides suggested topics to be covered in the review.

The sector staff submits an updated safety plan, providing a 20-30 minute summary and status report of the beamline and experiment safety programs, and demonstrating how Integrated Safety Management (ISM) is incorporated into the program. They note any changes in the sector since the last design review. Suggested topics that are covered in the summary include sector safety organization/changes, overview of the sector safety plan and (in subsequent reviews) changes to the plan, changes in management, examples of communication of safety information to sector members and users, standard procedures followed at the beamlines and in the LOM Labs, new procedures, as applicable, the experimental program safety, significant shop activity and shop operational problems and solutions, waste handling complications and resolutions, safety reviews of new instrumentation, management of critical shielding and issues related to PSS and EPS operation, experience with safety planning for beamline commissioning/operations and general experimental work, unique hazards encountered during the past year and their mitigation, reports on safety incidents, follow-up on action items (if any) from the previous review, and lessons learned and good safety practices.

The review committee verifies that the APS has safe operations sector records for the sector on file and that they are consistent with the beamline as-built conditions. Typically, these records include the beamline sector layout, synchrotron and bremsstrahlung ray-traces, shielding component designs (e.g., assembly drawings that show component functionality for shutters, stops, and critical dimensions), personnel safety system operations, shielding designs, the safe-operations envelope for the beamline (e.g., maximum beam current or minimum gap limits), and reports of outstanding items from previous safety inspections. The committee also conducts an inspection of the beamlines, experiment stations, and associated.

The findings of the review are reported to Sector management for correction, comment, or prompt mitigation of identified problems. The report may include notable safety practices found on the beamline, opportunities for safety enhancements, and findings of deficiencies where the beamline operations have not met APS/Argonne standards. The report is entered in the APS Integrated Content Management System and tracked for completion. The number of currently operating beamlines requires that approximately one review is completed every month. Bruce Glagola (glagola@aps.anl.gov)

GeoSoilEnviroCARS (Sector 13) Receives Federal Grants for Canted Undulator Upgrade

IN SHORT > GeoSoilEnviroCARS (GSECARS) at APS Sector 13, which is dedicated to Earth, environmental, and planetary science, has received funding to implement a canted undulator upgrade (Fig. 1). This upgrade will double the available undulator beam time on this highly oversubscribed beamline, and provide new sector capabilities, thereby enhancing the science conducted at the sector.

MORE > The upgrade involves the installation of two undulators, optimized for different energy ranges, in the Sector 13 straight section. The two insertion devices (IDs) are arranged in a canted geometry to provide two independent x-ray sources. The upstream undulator, optimized for lower x-ray energies (2.3-23 keV), will be the source for a sub-micron-resolution, Kirkpatrick-Baez mirror-based, x-ray microprobe in a dedicated enclosure (13-ID-E). This new enclosure will be produced by isolating the upstream one-third of the existing 13-ID-C enclosure with an interior wall installed perpendicular to the beams. A 300-mm horizontal separation between the two undulator beams in the 13-ID-E enclosure will be achieved using dual deflecting mirrors (located in the first optics enclosure, 13-ID-A) on the outboard (13-ID-E) beam. The second of these mirrors will be bendable to allow a horizontal compound-focusing geometry to produce focal spots down to 250 nm for the microprobe. With this single instrument, detailed speciation and compositional research will be conducted on both light elements (as low as sulfur) and heavy elements in systems of geochemical, environmental, and cosmochemical significance. The second undulator will be optimized for higher x-ray energies (5.6-80 keV) to significantly enhance the high-pressure (laser-heated diamond anvil cell and multi-anvil press) and surface and interface scattering (general purpose diffractometer) research programs. Modifications to existing beamline components will be made to allow independent, full-time utilization of the two undulator beams.

Support of the beamline component modifications and additions is being shared equally by three separate federal programs: U.S. Department of Energy–Midscale Instrumentation, U.S. National Science Foundation–Division of Earth Sciences–Instrumentation and Facilities, and the National Aeronautics and Space Administration– Sample Return Laboratory Instruments and Data Analysis. The combined total of these grants is $2.3 M. In addition, a portion of the $5.6 M awarded to the APS under the American Reinvestment and Recovery Act is being used to support the installation of the two new, optimized undulators and required front-end components.

The scientific impact of the GSECARS upgrade will be in high-pressure mineral physics and chemistry, non-crystalline and nano-crystalline materials at high pressure, chemistry of hydrothermal fluids, reactions at mineral-water interfaces, biogeochemistry, flow dynamics of fluids and solids, oxidation states of magmas, and cosmochemistry of extraterrestrial materials. In particular, the ability to access S, Cl, K, and Ca *K*-edges, as well as *K*- and *L*-edges of heavy elements with the sub-micron-resolution microprobe will offer tremendous new scientific opportunities.

An aggressive design, fabrication, and installation timeline is being pursued which will allow this upgrade to be achieved with minimal impact and interruption to the existing user program. Commissioning of the upgraded sector is planned for 2012.

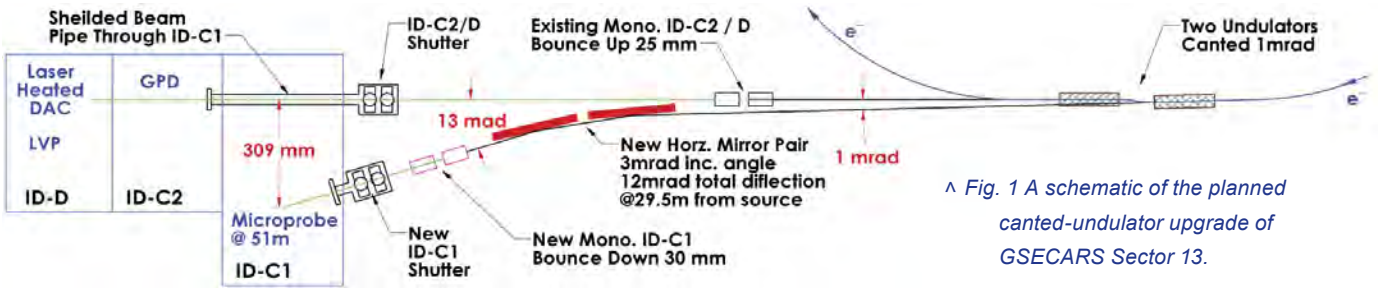

^ *Fig. 1 A schematic of the planned canted-undulator upgrade of GSECARS Sector 13.*

Mitigating Obsolescence

IN SHORT > The APS is now entering its fifteenth year of providing beam to users. During this first decade- and-a-half of operations, the APS has arguably become known for (among other achievements) operating the most reliable accelerator serving a broad user community. APS scientists have enjoyed beam availability greater than 97% since 2002. The mean time between unplanned beam dumps exceeded 50 h (the original goal) in 2004 and has remained well over that number ever since. The rewards of this success contribute to the way in which science is done at our beamlines, which can now accommodate more users in shorter time slots. Thus, even a short accelerator downtime may mean that some very good science simply does not get done. The APS accelerator staff is continually looking for ways to ramp-up their efforts in order to maintain the optimum level of operation.

MORE > The electronics that are relied upon in today's world have an increasingly short lifespan, and the APS is now confronted with the fact that many of the operating systems that were designed nearly 20 years ago (and parts acquired soon thereafter) are no longer available. This is particularly true for the most complex (and therefore most fault prone) systems. Budgets during the last few years have allowed for repairs of known problems, but not for development of new systems to replace those that are aging.

The APS has planned to deal with this through an aggressive program of systems upgrades utilizing capital expenditures, known as Accelerator Improvement Projects. Technical experts have assessed the state of their systems and assigned a risk to each, based on the likelihood of system to failure if no action is taken to address problems, and the impact on the APS if such a failure was to occur. This list of projects is regularly reviewed by APS management and updated as needed. Some of the projects on this list involve straightforward procurements and installation of new hardware; other projects require more complex integration into the APS facility, because the new components are not identical to the obsolete components. In other cases, the replacements do not exist in industry and the overall project will require an extensive R&D program prior to development and implementation. An example of this latter category is the klystrons used in the APS booster and storage ring (Fig 2).

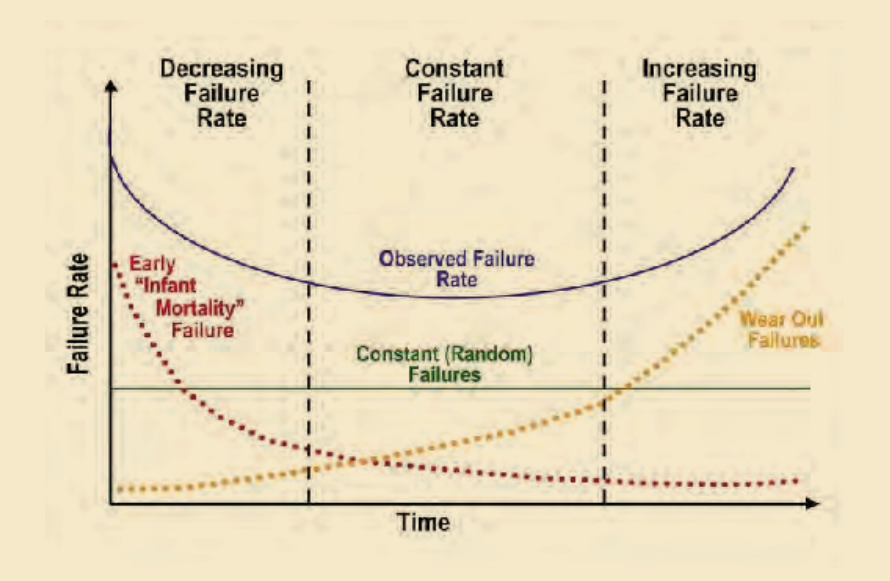

^ *Fig. 1 Evidence based on APS systems maintenance records indicates that some critical systems within the facility are nearing the end of the "Constant Failure Rate" period. Without replacments, the APS will soon enter a period of "Increasing Failure Rate."*

^ *Fig. 2 Chief technician Dave Mayer (ANL-ASD) inspects one of the APS storage ring klystrons. The APS is dependent on three or four of these for operation. At present there is only one vendor, and new units cost $800 K. The APS is undertaking an R&D program to develop a solid-state amplifier, which will eliminate our dependence on these klystrons.*

Examples of other systems needing major obsolescence upgrades are low-level radio-frequency systems, beam monitoring systems, vacuum systems, water systems, computing systems, and storage ring power supply controllers.

We plan to allocate roughly $25M in obsolescence upgrades, spread out over a five-year period. Contact Rod Gerig (rod@aps.anl.gov)

APS Organization Chart

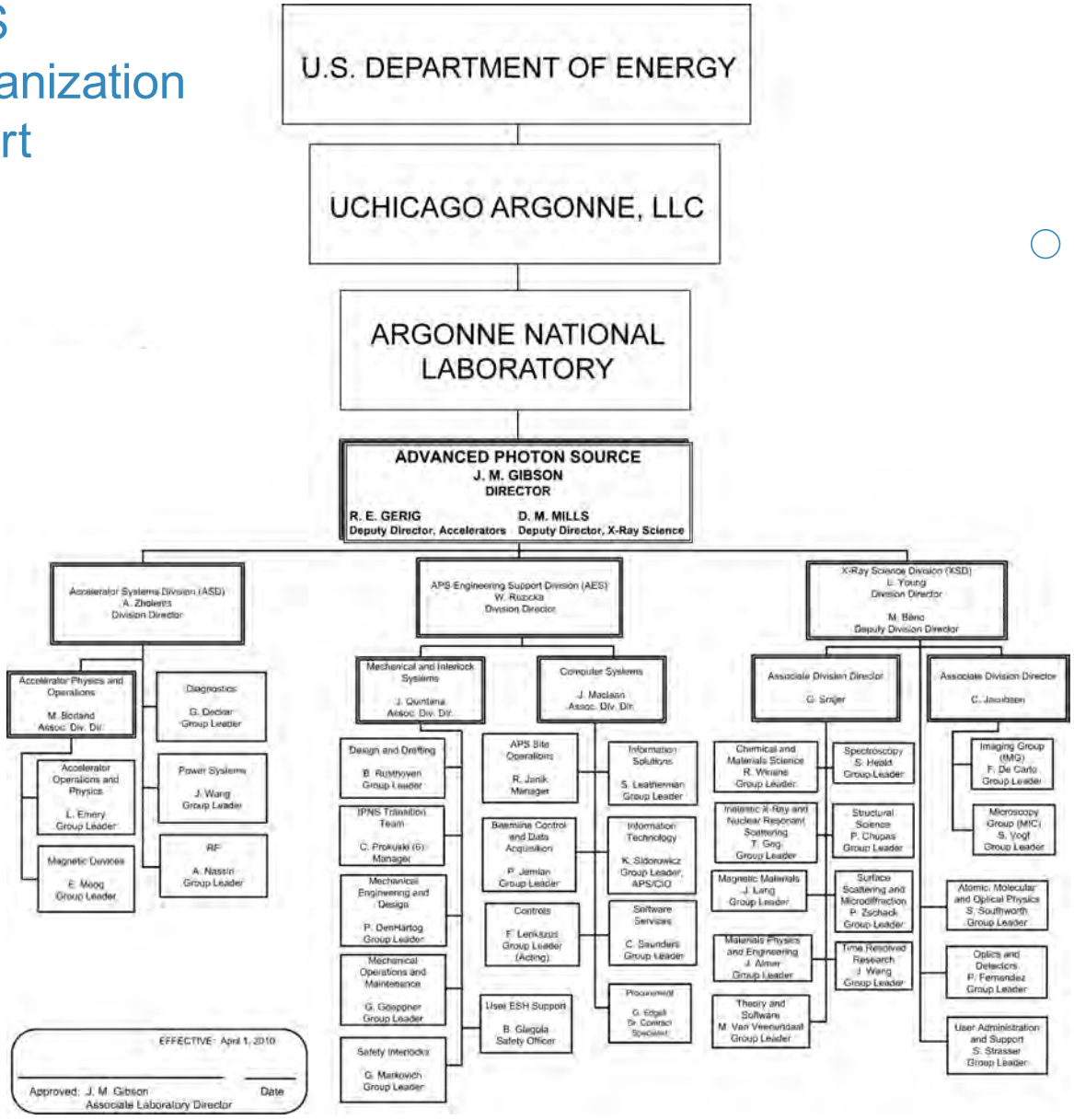

APS Staffing and Funding

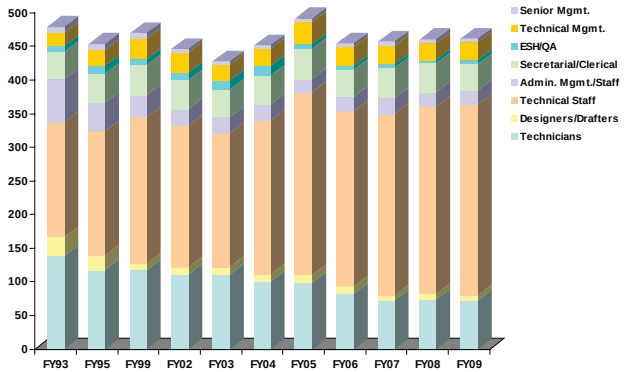

APS Staffing Levels FY93 – FY09

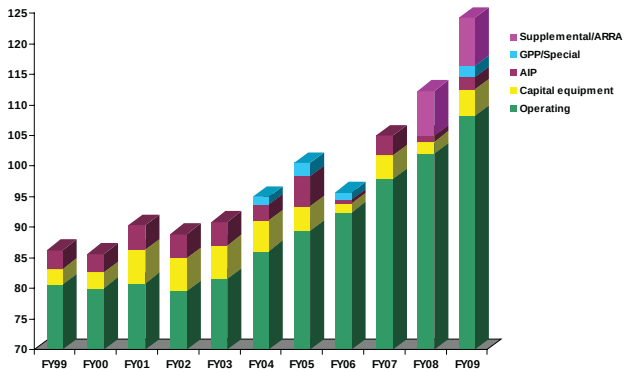

APS Funding Levels FY99 – FY09

Acknowledgments

APS Science Editorial Board:

Cele Abad-Zapatero (University of Illinois at Chicago), Mark A. Beno (ANL-XSD), Paul Fuoss (ANL-MSD), Rodney E. Gerig (ANL-PSC), J. Murray Gibson (ANL-PSC), Efim Gluskin (ANL-ASD), Denis Keane (Northwestern University), Dennis M. Mills, (ANL-PSC), William G. Ruzicka (ANL-AES), George Srajer (ANL-XSD)

The Research Highlights in this report were written by:

William Arthur Atkins (waarc@grics.net)

David Bradley (david@sciencebase.com)

Yvonne Carts-Powell (yvonnecp@verizon.net)

Vic Comello (ANL-TSD, vcomello@anl.gov)

Sandy Field (sfield@fieldscientific.com)

Carol Hart (chart@nasw.org)

Emma Hitt (emma@emmasciencewriter.com)

Philip Koth (philkoth@comcast.net)

Elise LeQuire (cygnete@mindspring.com)

David Lindley (dlindley@nasw.org)

JR Minkel (jrminkel@gmail.com)

Mona A. Mort (monasbox@gmail.com)

Luis Nasser (luis.nasser@gmail.com)

Patricia E. Panatier (pep2@optonline.net)

Mark Wolverton (exetermw@earthlink.net)

Art Direction: MeachamHowellDesign (meachamhowelldesign@yahoo.com)

Design: Daniel F. Sarro (ANL-TSD)

Printing Coordination: Gary Weidner (ANL-TSD)

Photography: Wes P. Agresta and George J. Joch (both ANL-TSD), Richard B. Fenner (ANL-PSC)

Aerial Photograph of the APS: Tigerhill Studio (www.tigerhillstudio.com/)

Contracts, rights and permissions: Jessie L. Skwarek (ANL-PSC)

Project Coordination: APS Scientific Information Services

Our thanks to the corresponding authors who assisted in the preparation of the research highlights, to the users and APS personnel who wrote articles for the report, and our apologies to anyone inadvertently left off this list. To all: your contributions are appreciated.

Argonne NATIONAL LABORATORY

Advanced Photon Source

Argonne National Laboratory
9700 South Cass Avenue
Argonne, IL 60439 USA

www.anl.gov
www.aps.anl.gov

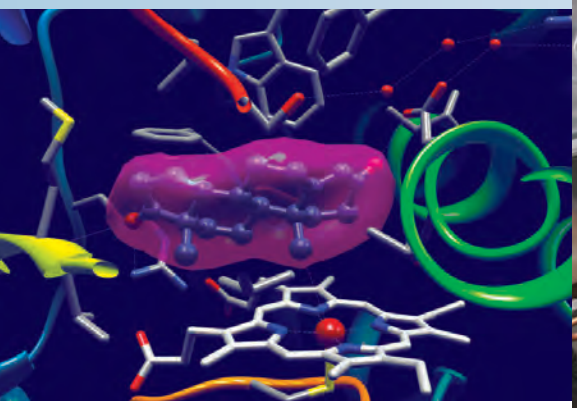

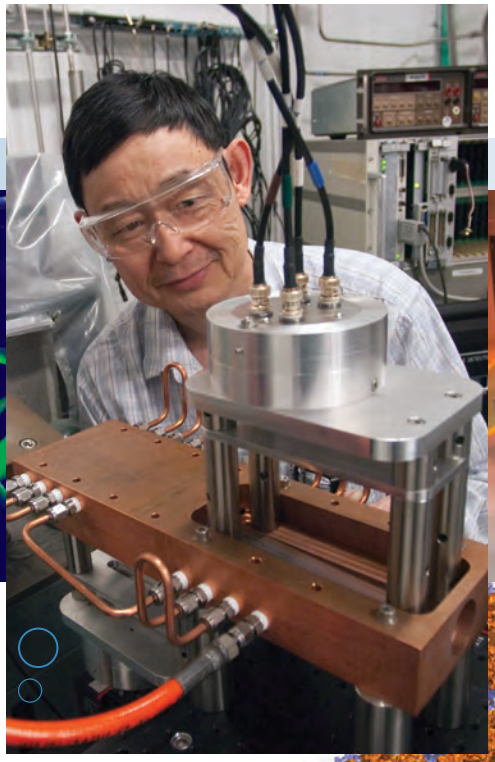

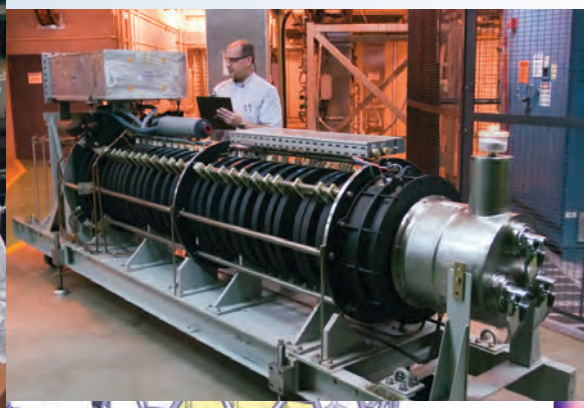

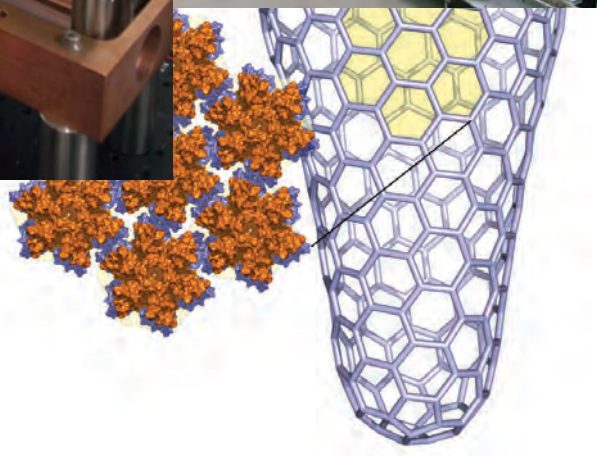

U.S. DEPARTMENT OF ENERGY

Argonne National Laboratory is a U.S. Department of Energy laboratory managed by UChicago Argonne, LLC